Bulgarian Academy of Sciences
Institute of Mathematics and Informatics
Department of Mathematical Modelling
and Numerical Analysis

NUMERICAL MODELLING OF NONLINEAR BOUNDARY VALUE PROBLEMS OF SECOND AND FOURTH ORDER:

APPLICATION IN PHYSICOCHEMISTRY AND BIOLOGY

Galina Stoyanova Lyutskanova–Zhekova

THESIS

for conferring of academic and scientific degree doctor
in professional field 4.5 Mathematics
(Mathematical modelling and application of mathematics)

SUPERVISORS:

Prof. Dr.Sc. Krassimir D. Danov
Corresponding member of the Bulgarian Academy of Sciences

Assoc. Prof. Ph.D. Ivan B. Bazhlekov

September 2022

The Ph.D. thesis considers three applications of boundary value problems in physico-chemistry and biology:

- to calculate the distribution of the electrostatic potentials in two immiscible fluid phases (polar and nonpolar) and in a dielectric spherical colloidal particle, attached to the flat interface between them;
- to compute the drag force, acting on a spherical colloidal particle, which is attached to a flat interface between two incompressible viscous fluids and translates along it with constant velocity;
- to clarify the effect of interfacial rheology (tangential mobility and immobility of interfaces) on the motion of a long bubble in a narrow cylindrical capillary under the simultaneous action of gravity and Poiseuille flow.

The dissertation is written in English on 160 pages and contains 27 figures and a table. It includes an introduction, three chapters, corresponding to the three applications considered, a conclusion, an appendix, and a bibliography of 142 sources. Three supplementary materials are attached to the work, which give information on the topics "Tensors in curvilinear coordinates", "Electrostatics" and "Continuum fluid mechanics".

The research, which is described in the thesis, was conducted in the Ph.D. program "Mathematical modeling and application of mathematics" at the department of Mathematical Modelling and Numerical Analysis in the Institute of Mathematics and Informatics, Bulgarian Academy of Sciences.

The dissertation has been discussed and directed for defense at a meeting of an extended unit to the Department of Mathematical Modeling and Numerical Analysis at IMI-BAS, held on 12.09.2022.

The defense of the dissertation will take place on ..... at ..... in auditorium ..... in IMI-BAS at an public meeting of a scientific jury.

The defense materials are available at the library of IMI-BAS.

Declaration of Originality

I declare that the thesis and the related publications contain original results obtained in collaboration with Prof. Krasimir D. Danov and Prof. Stoyan K. Smoukov. Results obtained, described and/or published by other scientists are duly and in detail cited in the bibliography.

This dissertation has not been applied for obtaining a scientific degree in another higher school, university or scientific institute.

Date: 26.09.2022

Signature: .....
(Galina Zhekova)

Zu dem Mädchen, das alles wissen will.

Acknowledgements

Words cannot express my gratitude to professor Krassimir Danov. This remarkable researcher not only offered me applied problems on which to work but also showed me by example how to do that. I am thankful for all the efforts he put into teaching me and for all the time he gave to answer my questions. When the deadline for submitting the thesis was approaching, he put himself in my shoes and did everything in his power to help me to finish on time. His significant contribution to the text has to be also acknowledged. Not only did he check the entire text for semantic errors, but also he gave me suggestions for the introduction and conclusion. Finally, his directness and practicality stopped me from losing additional time on unimportant tasks. For all this and much more, I will always be indebted to him.

Submitting my Ph.D. thesis on time would not be possible without associate professor Ivan Bazhlekov, who managed to save me no less than two months checking if it is possible to omit the translation of the text in Bulgarian. Also, I would like to express my deep appreciation to him for proofreading the entire text (which is no small task, given the volume) and for his insightful comments on it. Finally, his valuable advice and moral support are highly appreciated

I acknowledge the financial support from the Scientific Research Fund at the Sofia University "St. Kl. Ohridski" under the contracts 80-10-48/22.03.2021, 80-10-215/06.05.2020, 80-10-17/09.04.2019, 80-10-139/25.04.2018, and 80.10-11/2017.

This endeavor would not have been possible without my husband, Deyan, who believed in me even when I did not. For all the compromises he made and for all the times he was there for me, I am deeply indebted to him. I highly appreciate that he, my mother-in-law and my parents gave a considerable amount of their time to enable me to finish the thesis. Also I am grateful to my parents for instilling in me love of learning and hard work. Finally, I thank my relatives, friends, and colleagues for their moral support.

Contents

Chapter 1

Introduction

The classical and new fluid materials have a wide application in the chemical, food and beverage, and pharmaceutical technologies. They are used for a production of emulsions and foams, drugs with a controllable release, detergents, coating formulations, cosmetic products [1.1, 1.2]. Similar systems find applications also in drug delivery, oilfield industry, turbulent drag-reduction applications, medicine, and environmental protection [1.3, 1.4]. The wide applications and the competition between the companies-producers have led to improvements in the properties of the formulations concerning washing action, skin and eye irritation action, stability and durability, biodegradability, tolerance to hard water, etc., and the design of new fluid materials with preliminary defined rheological properties. For these applications, it is required to have a mathematical description of the materials and processes. There are two main approaches for doing that — molecular dynamics, which describes all molecules in a fluid and their interactions, and fluid dynamics, which assumes that the fluid is continuous, i.e. it neglects the spaces between the molecules. Molecular dynamics requires much more computing power, which makes it inapplicable for three-dimensional problems. Due to this fact, we describe the fluids in this work in the frame of fluid dynamics.

In continuous mechanics, fluid motion is based on the mass, momentum and moment, and energy balance equations. For example, the general mass balance equation, which is based on the fact that mass is not created nor destroyed, has the form [1.5]

$$\frac{\partial \rho}{\partial t} + \nabla \cdot \mathbf{v} = 0, \tag{1.1}$$

where t is time, ∇ is the spatial gradient operator, ρ is the mean mass density, and $\mathbf{v}$ is the mass average velocity vector. In most applications, Eq. (1.1) is not sufficient to describe the problem, since the average velocity of the fluid is usually sought. Due to that fact, the general momentum balance equation, which is analog to the Newton second law for continuous medium, is added to the description [1.5, 1.6]:

$$\frac{\partial}{\partial t}(\rho \mathbf{v}) + \nabla \cdot (\rho \mathbf{v}\mathbf{v} - \mathbf{P} - \mathbf{P}_b) = 0, \tag{1.2}$$

where $\mathbf{P}$ is the material stress tensor, and $\mathbf{P}_b$ is the tensor potential of the body force vector f per unit volume, i.e. $\mathbf{f} \equiv \nabla \cdot \mathbf{P}_b$. The force, $\mathbf{f}$, can be known (e.g. the gravity force), or the result from another type of interaction (e.g. the electrostatic force, which is described by the Maxwell electrostatic tensor $\mathbf{P}_b$ [1.7] and becomes a solution of the respective electrostatic

problem). Note that the system (1.1) and (1.2) is not closed for known $\mathbf{P}_b$. In order to close it, additional information about the material stress tensor $\mathbf{P}$, which depends on the type of fluid, is required.

Rheology [1.8] studies the semi-empirical relationships between the material stress tensor $\mathbf{P}$ and other system parameters (constitutive relations), which describe the special properties of the fluids. For example, the constitutive relationship for Newtonian fluids states that there is a linear relationship between stress $\mathbf{T}$ and strain, i.e.

$$\mathbf{T} = -p\mathbf{I} + \left(\xi - \frac{2\eta}{3}\right)(\nabla \cdot \mathbf{v})\mathbf{I} + \eta\left[\nabla\mathbf{v} + (\nabla\mathbf{v})^T\right], \tag{1.3}$$

where p is the pressure and $\mathbf{I}$ is the identity tensor. There are many fluids, which do not obey the Newtonian constitutive law. These fluids are called complex fluids. Examples of complex fluids are some special kinds of magnetic liquids, liquid crystals, blood and biological tissues. For them, the stress tensor, $\mathbf{P}$, is not even symmetric [1.9]. In most cases, $\mathbf{P}$ is a symmetric tensor — there are no micro-moments, acting on the fluid element (a consequence of the angular momentum balance equation). In the case of typical physicochemical applications, the continuum media are incompressible (the fluid density is a constant) and because of the small sizes of the investigated objects, the velocities of motion are so slow that the bulk fluids are Newtonian and the inertia term in Eq. (1.2) is negligible [1.10, 1.11]. The result of these simplifications is the well-known Stokes problem:

$$\nabla \cdot \mathbf{v} = 0,\ \nabla p = \eta\Delta\mathbf{v} + \mathbf{f}, \tag{1.4}$$

where p is the pressure, η is the dynamic shear viscosity, and Δ is the Laplace operator. From the mathematical viewpoint, Eq. (1.4) leads to $\Delta p = 0$ and to the fourth order partial differential equations for the velocity components, $\Delta(\Delta\mathbf{v}) = 0$. In the physicochemical and biological applications, the complex fluids are multicomponent and the distribution of each species follows the diffusion-convection equations with already calculated velocity field.

The main difference between classical hydrodynamics of multicomponent systems and the physicochemical approach is in the physical description of the boundaries between two phases [1.12, 1.13]. In classical hydrodynamics, the boundary is treated as a mathematical dividing surface, while from the physicochemical aspect — it is two-dimensional material continuum, which has all attributes of the material phases (dilatational elasticities and viscosities, 2D pressure called surface tension, surface charge density, etc.). Moreover, depending on the concrete type of the interfaces, two-dimensional continuum can be not fluid — for example, cell membranes, particle-laden interfaces, interfaces with adsorbed surfactants, proteins or polymers, etc. In addition, the three-phase contact lines represent one-dimensional material continuum with special properties (e.g. line tension, line charge density, etc.). The next important difference between three-dimensional phases and interfaces is that one- and two-dimensional phases are very deformable and compressible.

The forces, acting on the material interfaces, are not isotropic. Instead of the classical kinematic boundary conditions, the interfacial stress tensor, σ, obeys the momentum balance equation:

$$\nabla_s \cdot \sigma = \mathbf{n} \cdot < \mathbf{P} + \mathbf{P}_b > \tag{1.5}$$

at the dividing surface, where $\mathbf{n}$ is the unit normal vector, ∇_s is the surface gradient operator, and $< \cdots >$ means the difference between stress and force tensors from both sides of the contiguous 3D phases. Analogous to the volume metrics, semi-empirical laws are needed to

relate the interfacial stress tensor with the physical properties of the 2D continuum media. Note that the whole behavior of the bulk flows depends on the specific properties of the bound and dividing surfaces. For example, the flow over the solid surface (tangentially immobile with no-slip boundary condition) has considerably different properties than that over a free surface (fully mobile interface) at which there is not tangential friction (e.g. pure water/air interface).

The theoretical description of the interfacial rheological laws is quite difficult because of the complex mathematical tasks related to the appearance of deformable surfaces, adjusted volumes, singularities at the three-phase contact lines, etc. [1.14]. Moreover, the molecular dynamic simulations use a large number of molecules or nanoparticles at the interface, which move under the action of intermolecular, electric and drag forces. From the viewpoint of chemical and biological applications [1.14], these problems are deeply related to the two-dimensional ordering and crystallization of particles and proteins. The sizes of nanoparticles, protein molecules and polymers are small so that they are called in the literature colloidal particles to distinguish them from solid particles with sizes larger than 3 μm, which are not Brownian and for them the gravity and the density difference with the fluid are important. Finally, the mathematical description of the shape of interfaces leads additionally not only to the boundary problem but to a more difficult boundary value problem because physically the respective capillary profiles must be closed — the shape of bubbles, drops, red blood cells, etc. are closed and represent only one stable solution of the respective generalized Laplace equations of capillarity [1.15].

The aim of this thesis is to consider three applications of the boundary value problems in the case of linear or strongly nonlinear models of the second or higher orders. The first two of them are related to the properties of colloidal particles, attached to the interfaces. For the computer modeling of the multi-particle problems, fast and precise computer modules for calculation of the forces, acting on an individual colloidal particle are needed. One of them is the calculation of the electro-dipping force, acting on the colloidal particle, accounting for the dielectric constants of all different media. In the literature, this problem is solved in a particular case of one fully conductive phase. The second problem is to calculate the drag force, acting on the individual colloidal particle, which is attached to the interface and translates along it. This problem is solved in the literature, using the two-vorticity-one-velocity formulation but the applied numerical algorithm is slow and the singularity at the three phase contact line is not isolated. The third aim is to clarify the effect of interfacial rheology (tangential mobility and immobility of interfaces) on the motion of long bubble in a narrow cylindrical capillary under simultaneous action of gravity and Poiseuille flow. We must compare our calculations with available experimental data in order to prove their validity and range of applications. In the particular case of very small velocity of motion, the analytical approximations in the literature for the gravity motion and for the pressure-driven motion separately are known as the classical Bretherton problem.

The solutions to the three problems could be used as a part of highly complex procedures. An application of the first problem is to calculate the electro-dipping force at a curved surface, which could be done by computing consecutively the distribution of the electrostatic potentials in the presence of a flat surface; how the electrostatic components of pressure tensor deform the flat surface; the electric field in the presence of the deformed surface; etc. The solution to the second problem could be applied for determining the contact angle of micron particles (finding the contact angle for which the best fit of experimental data for the drag coefficient is obtained) and for solving the two-dimensional crystallization problem (which is transformed to a problem for ordering of many moving particles and for each of

them the drag coefficient is computed). The solution to the third problem could be used to obtain fluid parameters of a long bubble moving in a capillary, using an image of a bubble.

All the described applications require repeated solving of the problems, considered in the present work. In this regard, both the accuracy of the calculations and their speed are of utmost importance. Since implemented computer programs can be used by practitioners, they must run on a laptop or personal computer. Due to these requirements, we use different transformations of the first two problems (related both to the form of the differential equations and to the geometry of the problems), which greatly simplify the problems to be solved and, thus, reduce the computational time. Finally, the general problem of a long bubble in a tube under the action of gravity and Poiseuille flow is solved under the assumption of the small thickness of the film layer. To achieve sufficient accuracy for different values of the parameters, it is necessary to perform not a small number of calculations by hand. Although the numerical methods used to solve the considered problems require an one-time execution of a large number of calculations by hand, we consider that they are consistent with the objectives of the present study, stated above.

The thesis is organized as follows. The respective problems are described in Chapters 2, 3 and 4, which contain an abstract, literature review, a description of the problem, a method for its solution, detail conclusions and cited references. In fact, these chapters correspond to our publications but do not reproduce them directly. The chapters include detailed mathematical calculations and algorithm descriptions, which are not included in the publications due to the restricted volume. The actuality of the considered problems, new elements in their treatments from physicochemical and mathematical aspects, compared to the available results in the literature, and the main strategies for solving the problems are written in Chapter 5, where our claims are summarized in three points. Finally, because of the possible identical references, cited after different chapters, the list of all used references is added. The thesis contains an appendix and three supplementary materials, which give information on the topics “Tensors in curvilinear coordinates”, “Electrostatics” and “Continuum fluid mechanics”.

References

[1.1] S. Ezrahi, E. Tuval, A. Aserin, and N. Garti. Daily applications of systems with wormlike micelles. In R. Zana and E.W. Kaler, editors, *Giant Micelles. Properties and Applications*, pages 515–544. Taylor and Francis, New York, 2007. DOI: 10.1201/9781420007121-18.

[1.2] L. Nicolas-Morgantini. Giant micelles and shampoos. In R. Zana and E.W. Kaler, editors, *Giant Micelles. Properties and Applications*, pages 493–514. Taylor and Francis, New York, 2007. DOI: 10.1201/9781420007121.

[1.3] P.F. Sullivan, M.K.R. Panda, and V. Laffite. Applications of wormlike micelles in oilfield industry. In C.A. Dreiss and Y. Feng, editors, *Wormlike Micelles. Advances in Systems, Characterization and Applications*, pages 330–352. RSC, 2017. DOI: 10.1039/9781782629788-00330.

[1.4] J. Zakin, A. Maxson, T. Saeki, and P. Sullivan. Turbulent drag-reduction applications of surfactant solutions. In C.A. Dreiss and Y. Feng, editors, *Wormlike Micelles. Advances in Systems, Characterization and Applications*, pages 353–378. RSC, 2017. DOI: 10.1039/9781782629788-00353.

[1.5] G.K. Batchelor. *An Introduction of Fluid Mechanics*. Cambridge Univ. Press, London, 1967.

[1.6] L.D. Landau and E.M. Lifshitz. *Fluid Mechanics*. Pergamon Press, Oxford, 1984.

[1.7] L.D. Landau, E.M. Lifshitz, and L.P. Pitaevskii. *Electrodynamics of Continuous Media*. Elsevier Butterworth-Heinemann, Oxford, 2004.

[1.8] H.A. Barnes, J.F. Hutton, and K. Walters. *An Introduction to Rheology*. Elsevier, Amsterdam, 1989.

[1.9] J.C. Slattery. *Momentum, Energy, and Mass Transfer in Continua*. Krieger, Huntington, New York, 1978.

[1.10] V. Levich. *Physicochemical Hydrodynamics*. Prentice-Hall, Englewood Cliffs, New York, 1962.

[1.11] J. Happel and H. Brenner. *Low Reynolds Number Hydrodynamics with Special Applications to Particulate Media*. Prentice-Hall, Englewood Cliffs, New York, 1965.

[1.12] J.C. Slattery. *Interfacial Transport Phenomena*. Springer-Verlag, New York, 1990. DOI: 10.1007/978-0-387-38442-9.

[1.13] D.A. Edwards, H. Brenner, and D.T. Wasan. *Interfacial Transport Processes and Rheology*. Butterworth-Heinemann, Boston, 1991.

[1.14] P. Kralchevsky and K. Nagayama. *Particles at Fluid Interfaces and Membranes: Attachment of Colloid Particles and Proteins to Interfaces and Formation of Two-Dimensional Areas*. Elsevier Science, 2001.

[1.15] R. Finn. *Equilibrium Capillary Surface*. Springer-Verlag, New York, 1986.

Chapter 2

Effect of the ionic strength on the electro-dipping force

In this chapter, we compute the potential distributions, acting on a dielectric particle, attached to the boundary between water and nonpolar fluid. This calculation is important for the characterization of the surface charge density of micron-size objects and their three-phase contact angles [2.1]. The problem was solved semi-analytically, using the Mehler–Fock transformation in the idealized case, when one of the phases has an infinite dielectric permittivity [2.2]. In the current work, we consider the more realistic case of finite dielectric permittivity of the polar phase. Moreover, we propose a numerical method for calculating the distribution of the electrostatic potential in the three phases. An expression for the singularity parameter at the three-phase contact line is analytically derived. In all of the studied cases, the singularity is weaker than that in the simplified case, studied in [2.2]. The obtained results show that: i) the electrostatic potential distribution is close to that in the model case for micron-size particles, large values of the ionic strength and dielectric constant of the polar phase; ii) the force, arising from the electrostatic field in the polar phase, cannot be neglected for small (nano-size) particles and low ionic strengths.

The results, included in this chapter, are published in

- G. Lyutskanova-Zhekova, K. Danov, Effect of Ionic Strength on the Electro-Dipping Force. In Proceedings of the 9th International conference on Numerical Methods and Applications NMA, Borovets, Bulgaria, 20–24 August 2018; Lecture Notes in Computer Science Volume, SJR: 0.427 (2019). DOI: 10.1007/978-3-030-10692-8_49.

2.1 Literature overview

The prediction of the properties of dielectric particles at fluid–fluid interfaces is of a crucial importance for the characterization of a particle monolayer [2.1, 2.3], formation of particle-stabilized emulsions [2.2, 2.4, 2.5] and colloidosomes [2.6, 2.7], which have a wide application in cosmetics [2.4], food industry [2.8], enhanced oil recovery [2.9], biomedical field [2.10], etc.

We consider a particle, which is attached to the boundary between two dielectric fluid phases. In the absence of electrostatic effects, the position of the particle is determined by the contact angle. For electrically charged particles, attached to the water–nonpolar

interface, an electrodipping force occurs [2.11]. It pushes the particle in the direction of the water phase, which has a greater dielectric constant [2.11]. For micron-sized particles, the effect of electric force is more pronounced than that of gravity [2.11]. Moreover, the deformation of the interface around the particle due to gravity is negligible for particles of radius smaller than 2–3 microns [2.1].

In the current work, we model a small particle (of radius less than 2–3 microns), which is attached to the flat interface between water and nonpolar fluid. We assume that there are surface charges at the particle–nonpolar phase (their existence is established due to the electrostatic repulsion between particles at the oil–water interface [2.11, 2.12]). In the idealized case of water phase with infinite dielectric permittivity, this problem was solved semi-analytically, using the Mehler-Fock transformation [2.2]. The effect of an external electric field, applied to the particle, was discussed in [2.13]. Our aim in the present study is to analyze the effect of water phase with a finite value of the dielectric constant and to calculate the distribution of the electrostatic potentials in all the phases. We solve the Laplace equations in complex physical domains, using modified toroidal coordinates. The developed numerical scheme, which is of second-order with respect to space and numerical time, allows fast and precise calculations.

Finding the distribution of the electrostatic potentials in the case of a flat surface is an essential step in order to compute the electrodipping force in the case of a deformed surface. The main idea is the following. First, one computes the distribution of the electrostatic potentials in the presence of flat surface. Second, one calculates how the electrostatic components of pressure tensor affect the surface deformation. The third step is to calculate the electric field in the presence of the deformed surface and so on. This is, in general, a rather complex numerical problem, and so we limit ourselves in the current work to the first step, i.e. to compute the distributions of the electrostatic potentials in the case of flat surface.

The current chapter is structured as follows. We formulate the problem in Sec. 2.2 and nondimensionalize it in Sec. 2.3. In Sec. 2.4, one formulates the problem into modified toroidal coordinates. This formulation transforms the complex geometry of the problem into rectangles. Next, the asymptotic behaviour of the model near the three-phase contact line is investigated in Sec. 2.5. The numerical method and algorithm for finding the potential distributions are presented in Sec. 2.6, while the numerical results are described in Sec. 2.7.

2.2 Mathematical formulation of the problem

A spherical charged dielectric particle of radius R and dielectric constant ε_{p} is attached to the interface between nonpolar (oil, air) and water phases with dielectric constants ε_{n} and ε_{w}, respectively (Fig. 2.1). The particle position is determined by the three-phase contact angle α (see Fig. 2.1) and, therefore, the radius of the three-phase contact line is $r_{\mathrm{c}} = R\sin\alpha$.

There are surface charges at particle–nonpolar phase boundary (their existence is proven in [2.14, 2.15]). In [2.11], Danov and coworkers found out the values of surface charge density for oil-water and air–water interface (in the case of glass particles) are constant (independent of the specific experiment). Thus, in this work, we shall consider surface charges of constant surface charge density σ_{pn} at the particle–nonpolar fluid surface S_{pn}. These charges induce electrostatic potentials φ_{n}, φ_{w} and φ_{p} in the nonpolar phase, in the water phase and in the particle, respectively. The potentials, φ_j, are modelled as solutions of the Laplace equations

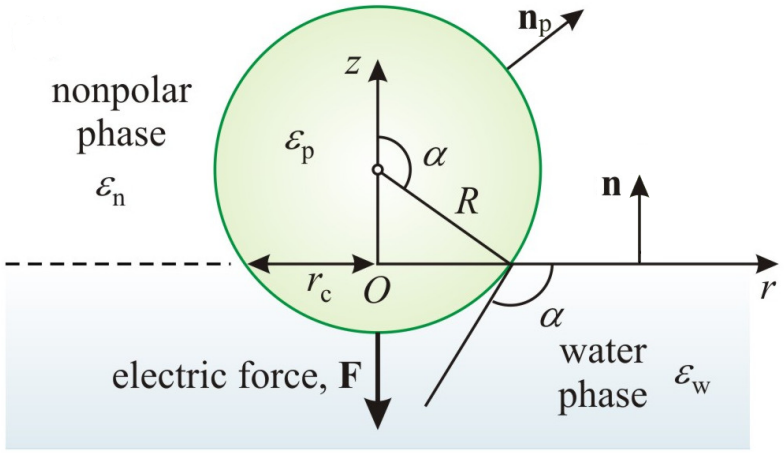

Figure 2.1: Sketch of a particle at the interface between water and nonpolar phases.

(see Supplementary material T, Sect. T.4.1) in the volumes, V_j, i.e.:

$$\nabla^2\varphi_w = 0 \text{ in } V_w,\ \nabla^2\varphi_n = 0 \text{ in } V_n,\ \nabla^2\varphi_p = 0 \text{ in } V_p. \tag{2.1}$$

In order to close the problem, we add boundary conditions at the dividing surfaces. The tangential boundary conditions (see Supplementary material T, Sect. T.5.1) state that all potentials are continuous functions at the dividing boundaries:

$$\varphi_p = \varphi_w \text{ at } S_{pw},\ \varphi_p = \varphi_n \text{ at } S_{pn},\ \varphi_n = \varphi_w \text{ at } S_{nw}, \tag{2.2}$$

where S_{pw} and S_{nw} are the particle–water and nonpolar–water phase boundaries, respectively. At the boundaries between water and dielectric phases, S_{pw} and S_{nw}, there are no adsorbed charges, therefore, the normal boundary conditions (see Supplementary material T, Sect. T.5.2) read

$$\varepsilon_w\mathbf{n}\cdot\nabla\varphi_w = \varepsilon_n\mathbf{n}\cdot\nabla\varphi_n \text{ at } S_{nw}, \tag{2.3}$$

$$\varepsilon_w\mathbf{n}_p\cdot\nabla\varphi_w = \varepsilon_p\mathbf{n}_p\cdot\nabla\varphi_p \text{ at } S_{pw}, \tag{2.4}$$

where $\mathbf{n}_p$ is the outer unit normal vector to the particle surface and $\mathbf{n}$ is the unit normal to S_{nw}, pointing at the nonpolar phase (Fig. 2.1). At the charged part of the particle surface, S_{pn}, we apply the electrostatic normal boundary condition

$$\varepsilon_0\left(\varepsilon_p\mathbf{n}_p\cdot\nabla\varphi_p - \varepsilon_n\mathbf{n}_p\cdot\nabla\varphi_n\right) = \sigma_{pn} \text{ at } S_{pn}, \tag{2.5}$$

where ε_0 is the dielectric permittivity in vacuum. Finally, the electrostatic potentials vanish at infinity. More information about the derivation of the model could be found in Supplementary material T.

2.3 Dimensionless formulation of the problem

It is appropriate to introduce a cylindrical coordinate system $Or\theta z$ with axis of revolution Oz and the radial, vertical and polar coordinates, r, z and θ, respectively, see Fig. 2.1.

Then, for numerical calculations, it is convenient to reformulate the problem (2.1)–(2.5) in a dimensionless form by introducing the following dimensionless operators and variables:

$$\overline{r} = \frac{r}{r_c},\ \overline{z} = \frac{z}{r_c},\ \overline{\nabla} = r_c\nabla,\ \overline{\nabla}^2 = r_c^2\nabla^2,\ \overline{\varphi}_j = \frac{\varphi_j \varepsilon_0 \varepsilon_{\rm n}}{r_{\rm c}\sigma_{\rm pn}},\ j = {\rm p,\ n,\ w} \tag{2.6}$$

and the dielectric ratios[1]

$$\varepsilon_{\rm pn} = \frac{\varepsilon_{\rm p}}{\varepsilon_{\rm n}},\ \varepsilon_{\rm wn} = \frac{\varepsilon_{\rm w}}{\varepsilon_{\rm n}}, \tag{2.7}$$

see Eq. (2.5). By substituting the dimensionless expressions (2.6) and (2.7) in the considered problem, (2.1)–(2.5), we obtain

$$\overline{\nabla}^2\overline{\varphi}_{\rm w} = 0 \text{ in } V_{\rm w},\ \overline{\nabla}^2\overline{\varphi}_{\rm n} = 0 \text{ in } V_{\rm n},\ \overline{\nabla}^2\overline{\varphi}_{\rm p} = 0 \text{ in } V_{\rm p}, \tag{2.8}$$

$$\overline{\varphi}_{\rm n} = \overline{\varphi}_{\rm w},\ \varepsilon_{\rm wn}\mathbf{n}\cdot\overline{\nabla}\overline{\varphi}_{\rm w} = \mathbf{n}\cdot\overline{\nabla}\overline{\varphi}_{\rm n} \text{ at } S_{\rm nw} \tag{2.9}$$

$$\overline{\varphi}_{\rm p} = \overline{\varphi}_{\rm w},\ \varepsilon_{\rm wn}\mathbf{n}_{\rm p}\cdot\overline{\nabla}\overline{\varphi}_{\rm w} = \varepsilon_{\rm pn}\mathbf{n}_{\rm p}\cdot\overline{\nabla}\overline{\varphi}_{\rm p} \text{ at } S_{\rm pw} \tag{2.10}$$

$$\overline{\varphi}_{\rm p} = \overline{\varphi}_{\rm n},\ \varepsilon_{\rm pn}\mathbf{n}_{\rm p}\cdot\overline{\nabla}\overline{\varphi}_{\rm p} - \mathbf{n}_{\rm p}\cdot\overline{\nabla}\overline{\varphi}_{\rm n} = 1 \text{ at } S_{\rm pn}. \tag{2.11}$$

In the next computations, we skip the bars for notation simplicity.

2.4 Formulation of the problem in toroidal coordinates

The problem (2.8)–(2.11) is axissymetric and, therefore, the solution is independent of θ (see Fig. 2.2). Thus, we consider only the half-plane $\theta = 0$. Next, the complex dielectric phases domains (Fig. 2.2) is transformed into rectangles (Fig. 2.3) by introducing modified toroidal coordinates τ and σ:

$$r = \frac{1-\tau^2}{h},\ z = \frac{2\tau\sin\sigma}{h},\ h(\tau,\sigma) = 1+\tau^2-2\tau\cos\sigma, \tag{2.12}$$

see Supplementary material S, Sect. S.5.7. Let us denote the unit vectors of the local basis by $\mathbf{e}_\tau$ and $\mathbf{e}_\sigma$ and the positions of the interfaces are $\sigma = 0$ and $\sigma = 2\pi$ from both sides of $S_{\rm nw}$; $\sigma = \pi - \alpha$ at $S_{\rm pn}$; $\sigma = 2\pi - \alpha$ at $S_{\rm pw}$ (see the definition of σ, Eq. (S.284), and Figs. S.10 and S.11 in the Supplementary Material S).

The axis of revolution corresponds to $\tau = 1$ and the three-phase contact line—to the pole, A_+, where $\tau = 0$ (see Fig. S.9 in the Supplementary Material S). For $\tau = 1$ and $\sigma = 0$, the transformation is singular.

Using the fact that the solution in independent of θ and the formulae for gradient in toroidal coordinates and Laplacian in toroidal coordinates, Eqs. (S.377) and (S.379) in the Supplementary Material S, one obtains

$$\nabla^2\varphi = \frac{h^3}{4\tau\left(1-\tau^2\right)}\frac{\partial}{\partial\tau}\left[\frac{\tau\left(1-\tau^2\right)}{h}\frac{\partial\varphi}{\partial\tau}\right] + \frac{h^3}{4\tau^2}\frac{\partial}{\partial\sigma}\left(\frac{1}{h}\frac{\partial\varphi}{\partial\sigma}\right), \tag{2.13}$$

$$\mathbf{n}_{\rm p}\cdot\nabla\varphi = -\frac{h}{2\tau}\frac{\partial\varphi}{\partial\sigma} \text{ at } S_{\rm pn},\ \mathbf{n}_{\rm p}\cdot\nabla\varphi = \frac{h}{2\tau}\frac{\partial\varphi}{\partial\sigma} \text{ at } S_{\rm pw}, \tag{2.14}$$

$$\mathbf{n}\cdot\nabla\varphi = \frac{h}{2\tau}\frac{\partial\varphi}{\partial\sigma} \text{ at } S_{\rm nw}, \tag{2.15}$$

[1] From physical perspective, it is known that $\varepsilon_{\rm wn} > \varepsilon_{\rm pn}$ and the ratio $\varepsilon_{\rm wn}/\varepsilon_{\rm pn}$ is between 15 and 80.

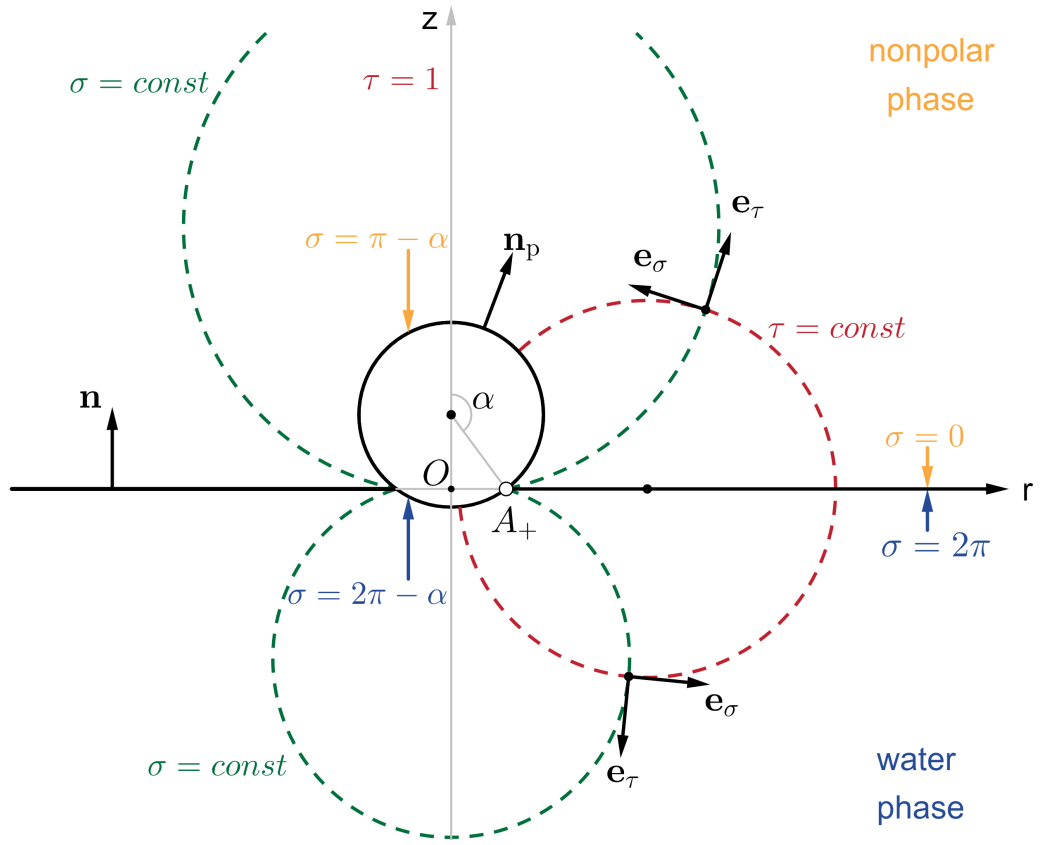

Figure 2.2: A toroidal coordinate system (τ, σ), in which the physical domains are transformed into rectangles.

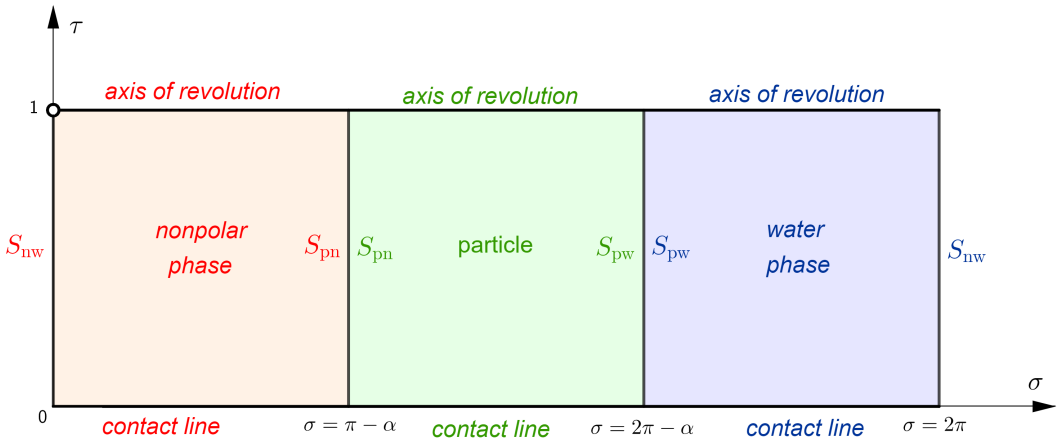

Figure 2.3: Rectangular numerical domain in toroidal coordinates.

see Fig. 2.2. From the latter, we obtain the dimensionless formulation of the considered problem for the electrostatic potentials. In the volumes, we apply the equations (2.8):

$$L_0[\varphi_\mathrm{w}] = 0,\ L_0[\varphi_\mathrm{n}] = 0,\ L_0[\varphi_\mathrm{p}] = 0, \tag{2.16}$$

where the operator L_0 is defined via the formula

$$L_0[\varphi] = \frac{h^3}{4\tau\left(1-\tau^2\right)}\frac{\partial}{\partial\tau}\left[\frac{\tau\left(1-\tau^2\right)}{h}\frac{\partial\varphi}{\partial\tau}\right] + \frac{h^3}{4\tau^2}\frac{\partial}{\partial\sigma}\left(\frac{1}{h}\frac{\partial\varphi}{\partial\sigma}\right), \tag{2.17}$$

see Eq. (2.17). At the dividing boundaries S_nw, S_pw, S_pn, the boundary conditions have the form

$$\varphi_\mathrm{n}|_{\sigma=0} = \varphi_\mathrm{w}|_{\sigma=2\pi},\ \left.\frac{\partial\varphi_\mathrm{n}}{\partial\sigma}\right|_{\sigma=0} = \varepsilon_\mathrm{wn}\left.\frac{\partial\varphi_\mathrm{w}}{\partial\sigma}\right|_{\sigma=2\pi}, \tag{2.18}$$

$$\varphi_\mathrm{p}|_{\sigma=2\pi-\alpha} = \varphi_\mathrm{w}|_{\sigma=2\pi-\alpha},\ \varepsilon_\mathrm{pn}\left.\frac{\partial\varphi_\mathrm{p}}{\partial\sigma}\right|_{\sigma=2\pi-\alpha} = \varepsilon_\mathrm{wn}\left.\frac{\partial\varphi_\mathrm{w}}{\partial\sigma}\right|_{\sigma=2\pi-\alpha}, \tag{2.19}$$

$$\varphi_\mathrm{n}|_{\sigma=\pi-\alpha} = \varphi_\mathrm{p}|_{\sigma=\pi-\alpha},\ \left.\frac{\partial\varphi_\mathrm{n}}{\partial\sigma}\right|_{\sigma=\pi-\alpha} - \varepsilon_\mathrm{pn}\left.\frac{\partial\varphi_\mathrm{p}}{\partial\sigma}\right|_{\sigma=\pi-\alpha} = \frac{2\tau}{h}, \tag{2.20}$$

see Eqs. (2.9)–(2.11). In order to close the problem, we have to add boundary conditions at the axis of revolution and at the three-phase contact line. We assume that the bulk equations holds true at the axis of revolution. Thus, the boundary conditions are obtained by finding the leading order of the equations $L_0[\varphi] = 0$ for $\tau \to 1$, i.e.

$$L_0[\varphi_l] = -\frac{2\tau^2h^2}{4\tau(1-\tau^2)}\frac{\partial\varphi_l}{\partial\tau} + \cdots = -\frac{(2-2\cos\sigma)^2}{4(1-\tau)}\frac{\partial\varphi_l}{\partial\tau} + \cdots = 0,\ l = \mathrm{n,p,w}. \tag{2.21}$$

Then, the following boundary conditions:

$$\left.\frac{\partial\varphi_\mathrm{n}}{\partial\tau}\right|_{\tau=1} = \left.\frac{\partial\varphi_\mathrm{p}}{\partial\tau}\right|_{\tau=1} = \left.\frac{\partial\varphi_\mathrm{w}}{\partial\tau}\right|_{\tau=1} = 0 \tag{2.22}$$

are added at the axis of revolution, $\tau = 1$. From physical viewpoint, these boundary conditions are trivial because of the axial symmetry of the problem.

Due to the fact that the electrostatic potentials are defined up to an additive constant (see Supplementary material T), we could choose instead the potentials to be zero at infinity (one of the boundaries in the Cartesian coordinates), the potentials to be zero at the pole A_+, i.e.

$$\varphi_\mathrm{n} = \varphi_\mathrm{p} = \varphi_\mathrm{w} = 0 \text{ for } \tau = 0. \tag{2.23}$$

In such a way, one obtains a simple boundary condition at the three-phase contact line. Then, the physical electrostatic potential, which has a zero value at infinity, is obtained by subtracting the calculated potential at infinity from φ_l, $l = \mathrm{n},\ \mathrm{p},\ \mathrm{w}$.

2.5 Asymptotic behaviour of the model

The electro-dipping force F_{el} could be computed by integrating the electrostatic pressure p_{el}, exerted at the fluid–fluid interface [2.11], multiplied by the radial coordinate, i.e.:

$$F_{el} = -2\pi\int_{r_c}^{\infty} r\cdot p_{el}(r)dr. \tag{2.24}$$

In [2.11], the following simple semiempirical expression for the electric pressure p_{el}:

$$p_{el} = \frac{A}{(r - r_c)^{1-\eta}\, r^{5+\eta}} \tag{2.25}$$

is obtained, where A and η are constants, $0 < \eta < 1$. Therefore, the integral (2.24) is singular at $r = r_c$ and $0 < \eta < 1$. The type of the singularity is essential in order to obtain high accuracy of the numerical integration.

Due to this fact, we shall investigate the asymptotic behaviour of the model equations in the close vicinity of the three-phase contact line (for $\tau \to 0$) in the current section. In order to do that, we are looking for the solution of the problem (2.16)- (2.20) in the form

$$\varphi_i = \tau^\nu \Phi_i(\sigma) + O\left(\tau^{\nu+1}\right),\ i = \text{n, p, w}. \tag{2.26}$$

Substituting the latter in Eq. (2.17), we obtain

$$\begin{aligned}
\nabla^2 \varphi_i &= \frac{h^3 \nu \Phi_i}{4\tau(1-\tau^2)} \frac{\partial}{\partial \tau}\left[\frac{\tau^\nu\left(1-\tau^2\right)}{h}\right] + \frac{h^3 \tau^\nu}{4\tau^2}\frac{\partial}{\partial \sigma}\left(\frac{1}{h}\frac{\partial \Phi_i}{\partial \sigma}\right) + ... \\
&= \frac{h^3 \nu \Phi_i}{4\tau(1-\tau^2)}\left[\frac{\nu\tau^{\nu-1} - (\nu+2)\tau^{\nu+1}}{h} - \frac{(\tau^\nu - \tau^{\nu+2})(2\tau - 2\cos\sigma)}{h^2}\right] \\
&\qquad + \frac{h^3\tau^{\nu-2}}{4}\left(-\frac{2\tau\sin\sigma}{h^2}\frac{\partial \Phi_i}{\partial \sigma} + \frac{1}{h}\frac{\partial^2 \Phi_i}{\partial \sigma^2}\right) + ... \\
&= \frac{h^2\tau^{\nu-2}}{4}\left\{\frac{\partial^2 \Phi_i}{\partial \sigma^2} + \frac{\nu^2 \Phi_i}{1-\tau^2}\right\} + O(\tau^{\nu-1}),\ i = \text{n, p, w}.
\end{aligned} \tag{2.27}$$

Then, for small values of τ, the leading order problem has the following form

$$\frac{\partial^2 \Phi_i}{\partial \sigma^2} + \nu^2 \Phi_i = 0,\ i = \text{n, p, w}. \tag{2.28}$$

Therefore, the leading order solutions of Eqs. (2.8) for $\tau \to 0$, φ_i^0, are

$$\varphi_i^0 = \tau^\nu \left[A_i^c \cos(\nu\sigma) + A_i^s \sin(\nu\sigma)\right],\ i = \text{n, p, w}, \tag{2.29}$$

where A_i^c and A_i^s are unknown constants, which are found as a solution of system of six linear equations, obtained from the boundary conditions. For computational convenience, we reformulate the boundary conditions (2.18)– (2.20) as follows:

$$\varphi_{\text{n}}|_{\sigma=0} = \varphi_{\text{w}}|_{\sigma=0},\ \left.\frac{\partial \varphi_{\text{n}}}{\partial \sigma}\right|_{\sigma=0} = \varepsilon_{\text{wn}} \left.\frac{\partial \varphi_{\text{w}}}{\partial \sigma}\right|_{\sigma=0}, \tag{2.30}$$

$$\varphi_{\text{n}}|_{\sigma=\pi-\alpha} = \varphi_{\text{p}}|_{\sigma=\pi-\alpha},\ \left.\frac{\partial \varphi_{\text{n}}}{\partial \sigma}\right|_{\sigma=\pi-\alpha} - \varepsilon_{\text{pn}} \left.\frac{\partial \varphi_{\text{p}}}{\partial \sigma}\right|_{\sigma=\pi-\alpha} = \frac{2\tau}{h}, \tag{2.31}$$

$$\varphi_{\text{p}}|_{\sigma=2\pi-\alpha} = \varphi_{\text{w}}|_{\sigma=-\alpha},\ \varepsilon_{\text{pn}} \left.\frac{\partial \varphi_{\text{p}}}{\partial \sigma}\right|_{\sigma=2\pi-\alpha} = \varepsilon_{\text{wn}} \left.\frac{\partial \varphi_{\text{w}}}{\partial \sigma}\right|_{\sigma=-\alpha} \tag{2.32}$$

by considering σ to be in the interval $[-\alpha, 2\pi - \alpha]$ instead of $[0, 2\pi]$. Due to the fact

$0 < \eta < 1$, the leading order boundary conditions acquire the form:

$$\varphi_{\rm n}^0\big|_{\sigma=0} = \varphi_{\rm w}^0\big|_{\sigma=0}\,,\ \left.\frac{\partial\varphi_{\rm n}^0}{\partial\sigma}\right|_{\sigma=0} = \varepsilon_{\rm wn}\left.\frac{\partial\varphi_{\rm w}^0}{\partial\sigma}\right|_{\sigma=0}, \tag{2.33}$$

$$\varphi_{\rm n}^0\big|_{\sigma=\pi-\alpha} = \varphi_{\rm p}^0\big|_{\sigma=\pi-\alpha}\,,\ \left.\frac{\partial\varphi_{\rm n}^0}{\partial\sigma}\right|_{\sigma=\pi-\alpha} = \varepsilon_{\rm pn}\left.\frac{\partial\varphi_{\rm p}^0}{\partial\sigma}\right|_{\sigma=\pi-\alpha}, \tag{2.34}$$

$$\varphi_{\rm p}^0\big|_{\sigma=2\pi-\alpha} = \varphi_{\rm w}^0\big|_{\sigma=-\alpha}\,,\ \varepsilon_{\rm pn}\left.\frac{\partial\varphi_{\rm p}^0}{\partial\sigma}\right|_{\sigma=2\pi-\alpha} = \varepsilon_{\rm wn}\left.\frac{\partial\varphi_{\rm w}^0}{\partial\sigma}\right|_{\sigma=-\alpha}. \tag{2.35}$$

Substituting the general form of the solutions (2.29) in Eq. (2.33), one gets

$$A_{\rm n}^{\rm c} = A_{\rm w}^{\rm c},\ A_{\rm n}^{\rm s} = \varepsilon_{\rm wn}A_{\rm w}^{\rm s}. \tag{2.36}$$

We conclude from Eq. (2.34) that

$$A_{\rm n}^{\rm c}\cos[\nu(\pi-\alpha)] + A_{\rm n}^{\rm s}\sin[\nu(\pi-\alpha)] = A_{\rm p}^{\rm c}\cos[\nu(\pi-\alpha)] + A_{\rm p}^{\rm s}\sin[\nu(\pi-\alpha)], \tag{2.37}$$

$$A_{\rm n}^{\rm c}\sin[\nu(\pi-\alpha)] - A_{\rm n}^{\rm s}\cos[\nu(\pi-\alpha)] = \varepsilon_{\rm pn}\big\{A_{\rm p}^{\rm c}\sin[\nu(\pi-\alpha)] - A_{\rm p}^{\rm s}\cos[\nu(\pi-\alpha)]\big\}. \tag{2.38}$$

One adds Eq. (2.37), multiplied by $\varepsilon_{\rm pn}\cos[\nu(\pi-\alpha)]$, to Eq. (2.38), multiplied by $\sin[\nu(\pi-\alpha)]$ and obtains

$$\begin{aligned}\varepsilon_{\rm pn}A_{\rm p}^{\rm c} &= A_{\rm n}^{\rm c}\left\{\varepsilon_{\rm pn}\cos^2[\nu(\pi-\alpha)] + \sin^2[\nu(\pi-\alpha)]\right\} + \frac{A_{\rm n}^{\rm s}}{2}\left(\varepsilon_{\rm pn}-1\right)\sin[2\nu(\pi-\alpha)]\\ &= \frac{A_{\rm w}^{\rm c}}{2}\left\{\varepsilon_{\rm pn}+1+\left(\varepsilon_{\rm pn}-1\right)\cos[2\nu(\pi-\alpha)]\right\}\\ &\qquad + \frac{\varepsilon_{\rm wn}A_{\rm w}^{\rm s}}{2}\left(\varepsilon_{\rm pn}-1\right)\sin[2\nu(\pi-\alpha)].\end{aligned} \tag{2.39}$$

Multiplying Eq. (2.37) by $\varepsilon_{\rm pn}\sin\left[\nu\left(\pi-\alpha\right)\right]$, Eq. (2.38) by $-\cos\left[\nu\left(\pi-\alpha\right)\right]$ and adding them, one gets

$$\begin{aligned}\varepsilon_{\rm pn}A_{\rm p}^{\rm s} &= \frac{A_{\rm n}^{\rm c}}{2}\left(\varepsilon_{\rm pn}-1\right)\sin[2\nu(\pi-\alpha)] + A_{\rm n}^{\rm s}\left\{\varepsilon_{\rm pn}\sin^2[\nu(\pi-\alpha)] + \cos^2[\nu(\pi-\alpha)]\right\}\\ &= \frac{A_{\rm w}^{\rm c}}{2}\left(\varepsilon_{\rm pn}-1\right)\sin[2\nu(\pi-\alpha)]\\ &\qquad + \frac{\varepsilon_{\rm wn}A_{\rm w}^{\rm s}}{2}\left\{\varepsilon_{\rm pn}+1-\left(\varepsilon_{\rm pn}-1\right)\cos[2\nu(\pi-\alpha)]\right\}.\end{aligned} \tag{2.40}$$

Using Eq. (2.35), we obtain

$$A_{\rm p}^{\rm c}\cos[\nu(2\pi-\alpha)] + A_{\rm p}^{\rm s}\sin[\nu(2\pi-\alpha)] = A_{\rm w}^{\rm c}\cos(\nu\alpha) - A_{\rm w}^{\rm s}\sin(\nu\alpha), \tag{2.41}$$

$$\varepsilon_{\rm pn}\big\{-A_{\rm p}^{\rm c}\sin[\nu(2\pi-\alpha)] + A_{\rm p}^{\rm s}\cos[\nu(2\pi-\alpha)]\big\} = \varepsilon_{\rm wn}\left[A_{\rm w}^{\rm c}\sin(\nu\alpha) + A_{\rm w}^{\rm s}\cos(\nu\alpha)\right]. \tag{2.42}$$

Adding Eq. (2.41), multiplied by $\varepsilon_{\rm pn}\cos[\nu(2\pi-\alpha)]$, and Eq. (2.42), multiplied by $-\sin[\nu(2\pi-$

$\alpha)]$, we conclude that the following equation:

$$\begin{aligned}
\varepsilon_{\mathrm{pn}} A_{\mathrm{p}}^{\mathrm{c}} = \frac{A_{\mathrm{w}}^{\mathrm{c}}}{2}\{\varepsilon_{\mathrm{pn}} \underbrace{2\cos(\nu\alpha)\cos[\nu(2\pi-\alpha)]}_{\cos(2\nu\pi)+\cos[2\nu(\pi-\alpha)]} - \varepsilon_{\mathrm{wn}} \underbrace{2\sin(\nu\alpha)\sin[\nu(2\pi-\alpha)]}_{-\cos(2\nu\pi)+\cos[2\nu(\pi-\alpha)]}\} \\
+ \frac{A_{\mathrm{w}}^{\mathrm{s}}}{2}\{-\varepsilon_{\mathrm{pn}} \underbrace{2\sin(\nu\alpha)\cos[\nu(2\pi-\alpha)]}_{\sin(2\nu\pi)-\sin[2\nu(\pi-\alpha)]} - \varepsilon_{\mathrm{wn}} \underbrace{2\cos(\nu\alpha)\sin[\nu(2\pi-\alpha)]}_{\sin(2\nu\pi)+\sin[2\nu(\pi-\alpha)]}\} \\
= \frac{A_{\mathrm{w}}^{\mathrm{c}}}{2}\left\{(\varepsilon_{\mathrm{pn}}+\varepsilon_{\mathrm{wn}})\cos(2\nu\pi) + (\varepsilon_{\mathrm{pn}}-\varepsilon_{\mathrm{wn}})\cos[2\nu(\pi-\alpha)]\right\} \\
+ \frac{A_{\mathrm{w}}^{\mathrm{s}}}{2}\left\{-(\varepsilon_{\mathrm{pn}}+\varepsilon_{\mathrm{wn}})\sin(2\nu\pi) + (\varepsilon_{\mathrm{pn}}-\varepsilon_{\mathrm{wn}})\sin[2\nu(\pi-\alpha)]\right\}. \qquad (2.43)
\end{aligned}$$

holds true. Analogously, multiplying Eq. (2.41) by $\varepsilon_{\mathrm{pn}}\sin[\nu(2\pi-\alpha)]$, Eq. (2.42) by $\cos[\nu(2\pi-\alpha)]$ and adding them, one gets

$$\begin{aligned}
\varepsilon_{\mathrm{pn}} A_{\mathrm{p}}^{\mathrm{s}} = \frac{A_{\mathrm{w}}^{\mathrm{c}}}{2}\{\varepsilon_{\mathrm{pn}} \underbrace{2\cos(\nu\alpha)\sin[\nu(2\pi-\alpha)]}_{\sin(2\nu\pi)+\sin[2\nu(\pi-\alpha)]} + \varepsilon_{\mathrm{wn}} \underbrace{2\sin(\nu\alpha)\cos[\nu(2\pi-\alpha)]}_{\sin(2\nu\pi)-\sin[2\nu(\pi-\alpha)]}\} \\
+ \frac{A_{\mathrm{w}}^{\mathrm{s}}}{2}\{-\varepsilon_{\mathrm{pn}} \underbrace{2\sin(\nu\alpha)\sin[\nu(2\pi-\alpha)]}_{-\cos(2\nu\pi)+\cos[2\nu(\pi-\alpha)]} + \varepsilon_{\mathrm{wn}} \underbrace{2\cos(\nu\alpha)\cos[\nu(2\pi-\alpha)]}_{\cos(2\nu\pi)+\cos[2\nu(\pi-\alpha)]}\} \\
= \frac{A_{\mathrm{w}}^{\mathrm{c}}}{2}\left\{(\varepsilon_{\mathrm{pn}}+\varepsilon_{\mathrm{wn}})\sin(2\nu\pi) + (\varepsilon_{\mathrm{pn}}-\varepsilon_{\mathrm{wn}})\sin[2\nu(\pi-\alpha)]\right\} \\
+ \frac{A_{\mathrm{w}}^{\mathrm{s}}}{2}\left\{(\varepsilon_{\mathrm{pn}}+\varepsilon_{\mathrm{wn}})\cos(2\nu\pi) - (\varepsilon_{\mathrm{pn}}-\varepsilon_{\mathrm{wn}})\cos[2\nu(\pi-\alpha)]\right\}. \qquad (2.44)
\end{aligned}$$

Using Eqs. (2.39), (2.40), (2.43) and (2.44), we obtain the following system:

$$\begin{aligned}
&\frac{A_{\mathrm{w}}^{\mathrm{c}}}{2}\left\{(\varepsilon_{\mathrm{pn}}+\varepsilon_{\mathrm{wn}})\cos(2\nu\pi) + (1-\varepsilon_{\mathrm{wn}})\cos[2\nu(\pi-\alpha)] - 1 - \varepsilon_{\mathrm{pn}}\right\} \\
&\quad + \frac{A_{\mathrm{w}}^{\mathrm{s}}}{2}\left\{-(\varepsilon_{\mathrm{pn}}+\varepsilon_{\mathrm{wn}})\sin(2\nu\pi) + \varepsilon_{\mathrm{pn}}(1-\varepsilon_{\mathrm{wn}})\sin[2\nu(\pi-\alpha)]\right\} = 0. \qquad (2.45) \\
&\frac{A_{\mathrm{w}}^{\mathrm{c}}}{2}\{(\varepsilon_{\mathrm{pn}}+\varepsilon_{\mathrm{wn}})\sin(2\nu\pi) + (1-\varepsilon_{\mathrm{wn}})\sin[2\nu(\pi-\alpha)]\} \\
&\quad + \frac{A_{\mathrm{w}}^{\mathrm{s}}}{2}\{(\varepsilon_{\mathrm{pn}}+\varepsilon_{\mathrm{wn}})\cos(2\nu\pi) + \varepsilon_{\mathrm{pn}}(\varepsilon_{\mathrm{wn}}-1)\cos[2\nu(\pi-\alpha)] - \varepsilon_{\mathrm{wn}}(1+\varepsilon_{\mathrm{pn}})\} = 0. \qquad (2.46)
\end{aligned}$$

This system has a nontrivial solution, when its determinant is equal to zero, i.e.

$$\begin{aligned}
&(\varepsilon_{\mathrm{pn}}+\varepsilon_{\mathrm{wn}})^2\cos^2(2\nu\pi) + \varepsilon_{\mathrm{pn}}(\varepsilon_{\mathrm{pn}}+\varepsilon_{\mathrm{wn}})(\varepsilon_{\mathrm{wn}}-1)\cos[2\nu(\pi-\alpha)]\cos(2\nu\pi) \\
&\quad - \varepsilon_{\mathrm{wn}}(1+\varepsilon_{\mathrm{pn}})(\varepsilon_{\mathrm{pn}}+\varepsilon_{\mathrm{wn}})\cos(2\nu\pi) \\
&\quad + (1-\varepsilon_{\mathrm{wn}})(\varepsilon_{\mathrm{pn}}+\varepsilon_{\mathrm{wn}})\cos(2\nu\pi)\cos[2\nu(\pi-\alpha)] \\
&\quad - \varepsilon_{\mathrm{pn}}(1-\varepsilon_{\mathrm{wn}})^2\cos^2[2\nu(\pi-\alpha)] - \varepsilon_{\mathrm{wn}}(1-\varepsilon_{\mathrm{wn}})(1+\varepsilon_{\mathrm{pn}})\cos[2\nu(\pi-\alpha)] \\
&\quad - (1+\varepsilon_{\mathrm{pn}})(\varepsilon_{\mathrm{pn}}+\varepsilon_{\mathrm{wn}})\cos(2\nu\pi) - \varepsilon_{\mathrm{pn}}(\varepsilon_{\mathrm{wn}}-1)(1+\varepsilon_{\mathrm{pn}})\cos[2\nu(\pi-\alpha)] \\
&\quad + \varepsilon_{\mathrm{wn}}(1+\varepsilon_{\mathrm{pn}})^2 + (\varepsilon_{\mathrm{pn}}+\varepsilon_{\mathrm{wn}})^2\sin^2(2\nu\pi) - \varepsilon_{\mathrm{pn}}(1-\varepsilon_{\mathrm{wn}})^2\sin^2[2\nu(\pi-\alpha)] \\
&\quad + (1-\varepsilon_{\mathrm{wn}})(\varepsilon_{\mathrm{pn}}+\varepsilon_{\mathrm{wn}})\sin(2\nu\pi)\sin[2\nu(\pi-\alpha)] \\
&\quad - \varepsilon_{\mathrm{pn}}(\varepsilon_{\mathrm{pn}}+\varepsilon_{\mathrm{wn}})(1-\varepsilon_{\mathrm{wn}})\sin[2\nu(\pi-\alpha)]\sin(2\nu\pi) = 0. \qquad (2.47)
\end{aligned}$$

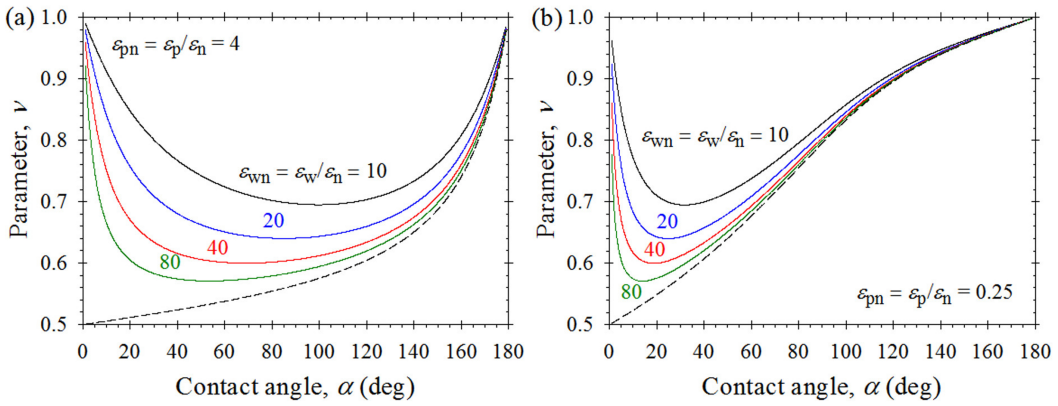

Figure 2.4: Dependence of singularity parameter ν on the contact angle α and ratio $\varepsilon_{\rm wn}$: a) $\varepsilon_{\rm pn} = 4$; b) $\varepsilon_{\rm pn} = 0.25$. Dashed lines show the model case ($\varepsilon_{\rm w} >> \varepsilon_{\rm n}, \varepsilon_{\rm p}$), studied in [2.2].

Eq. (2.47) acquires the form

$$\begin{aligned}
&(\varepsilon_{\rm pn}+\varepsilon_{\rm wn})^2-\varepsilon_{\rm pn}\,(1-\varepsilon_{\rm wn})^2+\varepsilon_{\rm wn}\,(1+\varepsilon_{\rm pn})^2\\
&-(1+\varepsilon_{\rm wn})\,(1+\varepsilon_{\rm pn})\,(\varepsilon_{\rm pn}+\varepsilon_{\rm wn})\underbrace{\cos(2\nu\pi)}_{1-2\sin^2(\nu\pi)}\\
&-(1+\varepsilon_{\rm pn})\,(1-\varepsilon_{\rm wn})\,(\varepsilon_{\rm wn}-\varepsilon_{\rm pn})\underbrace{\cos[2\nu(\pi-\alpha)]}_{2\cos^2[\nu(\pi-\alpha)]-1}\\
&+(1-\varepsilon_{\rm wn})\,(\varepsilon_{\rm pn}+\varepsilon_{\rm wn})\,(1-\varepsilon_{\rm pn})\underbrace{\cos[2\nu\pi-(2\nu\pi-2\nu\alpha)]}_{2\cos^2(\nu\alpha)-1}=0.
\end{aligned}\tag{2.48}$$

Dividing the latter by $2\,(1+\varepsilon_{\rm wn})\,(1+\varepsilon_{\rm pn})\,(\varepsilon_{\rm pn}+\varepsilon_{\rm wn})$, we arrive to the following equation for the singularity parameter ν:

$$\begin{aligned}
&\frac{2\varepsilon_{\rm pn}(1-\varepsilon_{\rm wn})^2}{(1+\varepsilon_{\rm pn})(1+\varepsilon_{\rm wn})(\varepsilon_{\rm pn}+\varepsilon_{\rm wn})}-\sin^2(\nu\pi)=\\
&\frac{(1-\varepsilon_{\rm pn})(1-\varepsilon_{\rm wn})}{(1+\varepsilon_{\rm pn})(1+\varepsilon_{\rm wn})}\cos^2(\nu\alpha)+\frac{(1-\varepsilon_{\rm wn})(\varepsilon_{\rm pn}-\varepsilon_{\rm wn})}{(1+\varepsilon_{\rm wn})(\varepsilon_{\rm pn}+\varepsilon_{\rm wn})}\cos^2\left[\nu(\pi-\alpha)\right].
\end{aligned}\tag{2.49}$$

Equation (2.49) has an infinite number of positive roots for fixed values of the dielectric ratios $\varepsilon_{\rm pn}$ and $\varepsilon_{\rm wn}$ and we are interested in the smallest positive one. It is found for two different ratios $\varepsilon_{\rm pn}$ by applying the bisection method in the interval $[0, 1]$. The results are shown in Fig. 2.4. The following conclusions can be drawn from it. The values of ν increase with the decrease of the ratio between the dielectric constants of water and nonpolar phase, $\varepsilon_{\rm wn}$. This effect is more pronounced for larger values of $\varepsilon_{\rm wn}$ and for smaller values of the contact angle (more hydrophilic particles).

Finally, we consider the limiting case $\varepsilon_{\rm wn} \to +\infty$. For it, one gets

$$\frac{2\varepsilon_{\rm pn}}{1+\varepsilon_{\rm pn}} - \sin^2(\nu\pi) = \frac{\varepsilon_{\rm pn}-1}{\varepsilon_{\rm pn}+1}\cos^2(\nu\alpha) + \cos^2[\nu(\pi-\alpha)], \tag{2.50}$$

$$\frac{2\varepsilon_{\rm pn}}{1+\varepsilon_{\rm pn}} - \frac{1-\cos(2\nu\pi)}{2} = \frac{\varepsilon_{\rm pn}-1}{\varepsilon_{\rm pn}+1} - \frac{\varepsilon_{\rm pn}-1}{\varepsilon_{\rm pn}+1}\sin^2(\nu\alpha) + \frac{1+\cos[2\nu(\pi-\alpha)]}{2}, \tag{2.51}$$

$$\frac{\varepsilon_{\rm pn}-1}{\varepsilon_{\rm pn}+1}\sin^2(\nu\alpha) = \sin(\nu\alpha)\sin[\nu(2\pi-\alpha)] \tag{2.52}$$

$$\sin(\nu\alpha) = 0 \text{ or } \frac{\varepsilon_{\rm pn}-1}{\varepsilon_{\rm pn}+1}\sin(\nu\alpha) - \sin[\nu(2\pi-\alpha)] = 0. \tag{2.53}$$

The smallest positive solution of the first equation is $\pi/\alpha \geq 1$, while that of the second is smaller than 1 due to the following statements:

$$f(0) = 0,\ f'(0) = \frac{\varepsilon_{\rm pn}-1}{\varepsilon_{\rm pn}+1}\alpha - (2\pi-\alpha) = 2(\alpha-\pi) - \frac{2}{\varepsilon_{\rm pn}+1}\alpha < 0, \tag{2.54}$$

$$f(1) = \frac{2\varepsilon_{\rm pn}}{\varepsilon_{\rm pn}+1}\sin\alpha > 0, \tag{2.55}$$

where $f(\eta)$ is

$$f(\eta) = \frac{\varepsilon_{\rm pn}-1}{\varepsilon_{\rm pn}+1}\sin(\nu\alpha) - \sin[\nu(2\pi-\alpha)]. \tag{2.56}$$

Then, we conclude that the value of the singularity parameter ν is a direct consequence of the equation

$$\frac{\varepsilon_{\rm pn}-1}{\varepsilon_{\rm pn}+1}\sin(\nu\alpha) - \sin[\nu(2\pi-\alpha)] = 0, \tag{2.57}$$

which is derived in the model case ($\varepsilon_{\rm wn} \to +\infty$) in [2.2]. Then, the model case, studied in [2.2], follows from Eq. (2.49), when $\varepsilon_{\rm wn} \to +\infty$. The results for the model case are depicted with dashed lines in Fig. 2.4. Note that the singularity in Eq. (2.25) for finite $\varepsilon_{\rm wn}$ is always weaker than that in the model case ($\varepsilon_{\rm wn} \to +\infty$). This result is expected due to the fact that the electrostatic potential on the fluid–fluid interface in the model case is zero.

2.6 Numerical method

2.6.1 Transforming the elliptical problem to parabolic one. D'Yakonov scheme.

Instead of solving the considered elliptical problem, we introduce numerical time t and solve the following parabolic problem:

$$\frac{\partial\varphi_l}{\partial t} = T[\varphi_l] + S[\varphi_l],\ \varphi_l \in V_l,\ 0 < t \leq T,\ l = \text{n, p, w} \tag{2.58}$$

$$\varphi_l(\tau,\sigma,0) = \varphi_{l0}(\tau,\sigma),\ l = \text{n, p, w} \tag{2.59}$$

with applied boundary conditions (2.18)– (2.20), (2.22), (2.23), where $T[.]$ and $S[.]$ are the following operators:

$$S[\varphi] = h\frac{\partial}{\partial\sigma}\left(\frac{1}{h}\frac{\partial\varphi}{\partial\sigma}\right), \tag{2.60}$$

$$T[\varphi] = \frac{h\tau}{1-\tau^2}\frac{\partial}{\partial\tau}\left[\frac{\tau(1-\tau^2)}{h}\frac{\partial\varphi}{\partial\tau}\right], \tag{2.61}$$

which acts in $\tau-$ and in σ-direction, respectively. It is well-known fact that the solution of a parabolic problem with appropriate boundary conditions, applied at the boundaries, approaches the solution of an elliptical problem with the same boundary conditions for $T \to \infty$ regardless of the initial condition. Therefore, we solve the parabolic problem, using the alternating direction implicit method (ADIM) [2.16–2.18], and obtain the sought-out solution for long enough time. The main advantage of this approach is that it could be done computationally efficient — it requires only $O(N^2 \ln N)$ instead of $O(N^3)$ operations compared to the traditional methods for directly solving the elliptic partial differential equations, where N^2 is the number of points for which the solution is computed [2.19].

In order to solve the considered problem, we discretize its rectangular domain by introducing a mesh

$$\omega = \omega_\tau \times (\omega_\mathrm{n} \cup \omega_\mathrm{p} \cup \omega_\mathrm{w}) \times \omega_t, \tag{2.62}$$

where ω_τ, ω_n, ω_p, ω_w and ω_t are defined as

$$\omega_\tau = \{\tau_i = i\delta_\tau,\ \delta_\tau = 1/N,\ i = 0, 1, \cdots, N\}, \tag{2.63}$$

$$\omega_\mathrm{n} = \{\sigma_{\mathrm{n},j} = j\delta_\mathrm{n},\ \delta_\mathrm{n} = (\pi-\alpha)/N_\mathrm{n},\ j = 0, 1, \cdots, N_\mathrm{n}\}, \tag{2.64}$$

$$\omega_\mathrm{p} = \{\sigma_{\mathrm{p},j} = \pi - \alpha + j\delta_\mathrm{p},\ \delta_\mathrm{p} = \pi/N_\mathrm{p},\ j = 0, 1, \cdots, N_\mathrm{p}\}, \tag{2.65}$$

$$\omega_\mathrm{w} = \{\sigma_{\mathrm{w},j} = 2\pi - \alpha,\ j\delta_\mathrm{w},\ \delta_\mathrm{w} = \alpha/N_\mathrm{w},\ j = 0, 1, \cdots, N_\mathrm{w}\}, \tag{2.66}$$

$$\omega_t = \{t_k = k\delta_t,\ \delta_t = T/M,\ k = 0, 1, \cdots, M\}. \tag{2.67}$$

Let us denote the exact solution of the considered problem at a point $(\tau_i, \sigma_{l,j}, t_k)$ by $\varphi_l|_{ij}^k$, l =n, p, w and the approximate one at the same point by $\phi_l|_{ij}^k$, l =n, p, w. Then, we use the Crank-Nicolson method [2.20]:

$$\frac{\varphi_l|_{ij}^{k+1} - \varphi_l|_{ij}^{k}}{\delta_t} = T\left[\varphi_l\right]\Big|_{ij}^{k+1/2} + S\left[\varphi_l\right]\Big|_{ij}^{k+1/2} + O\left(\delta_t^2\right), \tag{2.68}$$

where $T\left[\varphi_l\right]\Big|_{ij}^{k+1/2}$ and $S\left[\varphi_l\right]\Big|_{ij}^{k+1/2}$ denote the values of operators $T[\varphi_l]$ and $S[\varphi_l]$ at a point $(\tau_i, \sigma_{l,j}, t_k + \delta_t/2)$. Taking into account the following second-order approximation formula with a step length δ_x [2.20]:

$$\begin{aligned}\frac{d}{dx}\left(p\frac{du}{dx}\right)\Big|_i &= \frac{1}{\delta_x}\cdot\left[p_{i+1/2}\cdot\frac{u_{i+1}-u_i}{\delta_x} - p_{i-1/2}\cdot\frac{u_i-u_{i-1}}{\delta_x}\right] + O\left(\delta_x^2\right)\\ &= \frac{1}{\delta_x^2}\cdot\left[p_{i+1/2}\left(u_{i+1}-u_i\right) - p_{i-1/2}\left(u_i-u_{i-1}\right)\right] + O\left(\delta_x^2\right),\end{aligned} \tag{2.69}$$

we approximate the differential operators S and T with the difference operators $\tilde{S}$ and $\tilde{T}$ as

follows:

$$\tilde{S}\left[\phi_l|_{ij}^k\right] = \frac{h_{ij}}{\delta_l}\left[\frac{1}{h_{i,j+1/2}}\cdot\frac{\phi_l|_{i,j+1}^k - \phi_l|_{i,j}^k}{\delta_l} - \frac{1}{h_{i,j-1/2}}\cdot\frac{\phi_l|_{i,j}^k - \phi_l|_{i,j-1}^k}{\delta_l}\right], \tag{2.70}$$

$$\tilde{T}\left[\phi_l|_{ij}^k\right] = \frac{h_{ij}\tau_i}{\delta_\tau\left(1-\tau_i^2\right)}\cdot\left[\frac{\tau_{i+1/2}\left(1-\tau_{i+1/2}^2\right)}{h_{i+1/2,j}}\cdot\frac{\phi_l|_{i+1,j}^k - \phi_l|_{i,j}^k}{\delta_\tau}\right.$$
$$\left. - \frac{\tau_{i-1/2}\left(1-\tau_{i-1/2}^2\right)}{h_{i-1/2,j}}\cdot\frac{\phi_l|_{i,j}^k - \phi_l|_{i-1,j}^k}{\delta_\tau}\right] \tag{2.71}$$

for $l =$ n, p, w, where

$$h_{ij} = h(\tau_i, \sigma_{l,j}),\ \tau_{i\pm1/2} = \tau_i \pm \frac{\delta_\tau}{2},\ \sigma_{j\pm1/2} = \sigma_j \pm \frac{\delta_l}{2},\ l = \text{n, p, w}. \tag{2.72}$$

Approximating the differential operators T and S with the difference operators $\tilde{T}$ and $\tilde{S}$, one gets

$$\frac{\varphi_l|_{ij}^{k+1} - \varphi_l|_{ij}^k}{\delta_t} = \tilde{T}\left[\varphi_l|_{ij}^{k+1/2}\right] + \tilde{S}\left[\varphi_l|_{ij}^{k+1/2}\right] + O\left(\delta_t^2 + \delta_l^2 + \delta_\tau^2\right),\ l = \text{n, p, w}. \tag{2.73}$$

The operators at time $t+\delta_t/2$ in the right-hand side of equations (2.73) are replaced by their mean values of the neighboring symmetric time levels, keeping the second-order precision with respect to time:

$$\frac{\varphi_l|_{ij}^{k+1} - \varphi_l|_{ij}^k}{\delta_t} = \frac{1}{2}\left\{\tilde{T}\left[\varphi_l|_{ij}^k\right] + \tilde{T}\left[\varphi_l|_{ij}^{k+1}\right] + \tilde{S}\left[\varphi_l|_{ij}^k\right] + \tilde{S}\left[\varphi_l|_{ij}^{k+1}\right]\right\}$$
$$+ O\left(\delta_t^2 + \delta_l^2 + \delta_\tau^2\right),\ l = \text{n, p, w}. \tag{2.74}$$

Due to the fact that the operators $\tilde{T}$ and $\tilde{S}$ are linear, we conclude that the following equation:

$$\delta\varphi_l|_{ij}^{k+1} - \frac{\delta_t}{2}\tilde{T}\left[\delta\varphi_l|_{ij}^{k+1}\right] - \frac{\delta_t}{2}\tilde{S}\left[\delta\varphi_l|_{ij}^{k+1}\right] = \delta_t\tilde{T}\left[\varphi_l|_{ij}^k\right] + \delta_t\tilde{S}\left[\varphi_l|_{ij}^k\right]$$
$$+ O\left(\delta_t^2 + \delta_l^2 + \delta_\tau^2\right),\ l = \text{n, p, w} \tag{2.75}$$

holds true, where $\delta\varphi_l|_{ij}^{k+1}$ is

$$\delta\varphi_l|_{ij}^{k+1} = \varphi_l|_{ij}^{k+1} - \varphi_l|_{ij}^k,\ l = \text{n, p, w}. \tag{2.76}$$

Then, the left-hand side of Eq. (2.75) is written as a product of two operators

$$\left(U - \frac{\delta_t}{2}\tilde{S}\right)\left(U - \frac{\delta_t}{2}\tilde{T}\right)\left[\delta\varphi_l|_{ij}^{k+1}\right] = \delta_t\tilde{T}\left[\varphi_l|_{ij}^k\right] + \delta_t\tilde{S}\left[\varphi_l|_{ij}^k\right] + O\left(\delta_t^2 + \delta_l^2 + \delta_\tau^2\right), \tag{2.77}$$

where U is the unit operator. Discarding the local truncation error, one obtains the difference scheme:

$$\left(U - \frac{\delta_t}{2}\tilde{S}\right)\left(U - \frac{\delta_t}{2}\tilde{T}\right)\left[\delta\phi_l|_{ij}^{k+1}\right] = \delta_t\tilde{T}\left[\phi_l|_{ij}^k\right] + \delta_t\tilde{S}\left[\phi_l|_{ij}^k\right], \tag{2.78}$$

where $\delta\phi_l|_{ij}^{k+1}$ is defined as follows:

$$\delta\phi_l|_{ij}^{k+1} = \phi_l|_{ij}^{k+1} - \phi_l|_{ij}^{k}\,,\ l = \text{n, p, w.} \tag{2.79}$$

Finally, the process of solving of this system of equations is reduced to the following algorithm. As a first step, one solves the system of equations:

$$\left(U - \frac{\delta_t}{2}\tilde{S}\right)\left[\psi_l|_{ij}^{k+1}\right] = \delta_t\tilde{T}\left[\phi_l|_{ij}^{k}\right] + \delta_t\tilde{S}\left[\phi_l|_{ij}^{k}\right],\ l = \text{n, p, w} \tag{2.80}$$

with appropriate boundary conditions, applied for $\psi_l|_{ij}^{k+1}$. Second, one solves the system of equations:

$$\left(U - \frac{\delta_t}{2}\tilde{T}\right)\left[\delta\phi_l|_{ij}^{k+1}\right] = \psi_l|_{ij}^{k+1}\,,\ l = \text{n, p, w} \tag{2.81}$$

with respective boundary conditions, applied for $\delta\phi_l|_{ij}^{k+1}$ at the three-phase contact line and at the axis of revolution. Finally, $\phi_l|_{ij}^{k+1}$ is obtained, using Eq. (2.79). This method is known in the literature as D'Yakonov scheme. It belongs to the class of alternating direction implicit methods, which reduce the problem of solving a parabolic problem to solving two linear systems with banded matrices in a case of two-dimensional problem [2.18].

In the considered problem, the domain consists of three rectangular subdomains, which are discretized with different steps. In order to apply the method for this problem, we write the equations in the subdomains around dividing boundaries and use the boundary conditions to modify the operators **T** and **S** so that they become valid at the interfaces as well. Thus, the obtained problem in sigma direction is cyclic and has no boundary conditions and the one in tau direction is the one described by Eq. (2.81).

Thus, the sigma problem is cyclic and has no boundary conditions, but for the one on the tau is the original one.

2.6.2 Approximation of the boundary conditions

In order to have a second-order scheme with respect to t, one should take a special care of the form of the boundary conditions. The boundary conditions at the particle surface, at the fluid–fluid interface and at the axis of revolution are obtained by extending the definition of the operators S and T to hold on the dividing boundaries, see Eqs. (2.60), (2.61). The boundary conditions at the three-phase contact line are approximated directly.

At the three-phase contact line

At the three-phase contact line ($\tau = 0$), we apply the following boundary conditions:

$$\phi_l|_{0j}^{k+1} = 0,\ j = \overline{0, N_l},\ k = \overline{0, M-1},\ l = \text{n, p, w,} \tag{2.82}$$

see Eq. (2.23).

At the axis of revolution

The boundary conditions at the axis of revolution are obtained by assuming the validity of the Laplace equations in the close vicinity of the axis of revolution [2.18, 2.21]. Then, one

expands the definitions of the operators T and S, Eqs. (2.60) and (2.61), as follows:

$$\lim_{\tau\to 1} T[\varphi_l] = \lim_{\tau\to 1}\left(\tau\frac{\partial\varphi_l}{\partial\tau} - \frac{2\tau^3}{1-\tau^2}\frac{\partial\varphi_l}{\partial\tau} - \tau^2\frac{\partial\varphi_l}{\partial\tau} + \tau^2\frac{\partial^2\varphi_l}{\partial\tau^2}\right)$$
$$= \lim_{\tau\to 1}\frac{\frac{\partial\varphi_l}{\partial\tau}}{\tau-1} + \left.\frac{\partial^2\varphi_l}{\partial\tau^2}\right|_{\tau=1} = 2\left.\frac{\partial^2\varphi_l}{\partial\tau^2}\right|_{\tau=1}, \tag{2.83}$$

$$\lim_{\tau\to 1} S[\varphi_l] = (1-\cos\sigma)\frac{\partial}{\partial\sigma}\left(\frac{1}{1-\cos\sigma}\cdot\frac{\partial\varphi_l}{\partial\sigma}\right). \tag{2.84}$$

The differential operator S is approximated by difference operator $\tilde{S}$ as follows:

$$\tilde{S}[\phi_l|^k_{Nj}] = \frac{1-\cos\sigma_j}{\delta_\sigma^2}\cdot\left[\frac{\phi_l|^k_{N,j+1} - \phi_l|^k_{N,j}}{1-\cos\sigma_{j+1/2}} - \frac{\phi_l|^k_{N,j} - \phi_l|^k_{N,j-1}}{1-\cos\sigma_{j-1/2}}\right],\ j=\overline{1,N_l-1} \tag{2.85}$$

at $\tau = 1$, see Eq. (2.69). Using the following approximation:

$$u''(x) = \frac{-7u(x) + 8u(x\pm\delta_x) - u(x\pm 2\delta_x)}{2\delta_x^2} \mp \frac{3}{\delta_x}u'(x) + O(\delta_x^2). \tag{2.86}$$

and taking into account the boundary conditions (2.22) and equation (2.83), we conclude

$$\tilde{T}[\phi_l|^k_{Nj}] = \frac{-7\ \phi_l|^k_{Nj} + 8\ \phi_l|^k_{N-1,j} - \phi_l|^k_{N-2,j}}{\delta_\tau^2},\ j=\overline{1,N_l-1}. \tag{2.87}$$

Therefore, we replace the boundary conditions (2.22) with equations (2.81), in which the operators $\tilde{T}$ and $\tilde{S}$ are given by the formulas (2.85) and (2.87). The result is a modified boundary condition in relaxed form.

At the nonpolar–water surface

At the fluid–fluid interface, the form of the operators S and T are simplified as follows:

$$S[\varphi_l] = \frac{\partial^2\varphi_l}{\partial\sigma^2},\ T[\varphi_l] = \frac{\tau(1-\tau)}{1+\tau}\frac{\partial}{\partial\tau}\left[\frac{\tau(1+\tau)}{1-\tau}\frac{\partial\varphi_l}{\partial\tau}\right]. \tag{2.88}$$

The differential operator T is approximated with the difference one $\tilde{T}$ at the internal points of the boundary $S_{\rm nw}$, using the formula

$$\tilde{T}[\phi_{\rm n}|^k_{i0}] = \frac{\tau_i(1-\tau_i)}{\delta_\tau(1+\tau_i)}\cdot\left[\frac{\tau_{i+1/2}(1+\tau_{i+1/2})}{1-\tau_{i+1/2}}\cdot\frac{\phi_{\rm n}|^k_{i+1,0} - \phi_{\rm n}|^k_{i,0}}{\delta_\tau}\right.$$
$$\left. - \frac{\tau_{i-1/2}(1+\tau_{i-1/2})}{1-\tau_{i-1/2}}\cdot\frac{\phi_{\rm n}|^k_{i,0} - \phi_{\rm n}|^k_{i-1,0}}{\delta_\tau}\right]. \tag{2.89}$$

For $\tilde{T}[\phi_{\rm n}|^k_{N0}]$, we use formula (2.87). Next, we shall approximate the operator S at the boundary $S_{\rm pn}$. Using Eqs. (2.86) and (2.88), we obtain the following forms of the operator

S on the both sides of the interface $S_{\rm pn}$:

$$S[\varphi_{\rm n}] = \frac{-7\varphi_{\rm n}(\tau,0)+8\varphi_{\rm n}(\tau,\delta_{\rm n})-\varphi_{\rm n}(\tau,2\delta_{\rm n})}{2\delta_{\rm n}^2} - \frac{3}{\delta_{\rm n}}\cdot\frac{\partial\varphi_{\rm n}}{\partial\sigma}\bigg|_{\sigma=0^+} + O\left(\delta_{\rm n}^2\right), \tag{2.90}$$

$$S[\varphi_{\rm w}] = \frac{-7\varphi_{\rm w}(\tau,2\pi)+8\varphi_{\rm w}(\tau,2\pi-\delta_{\rm w})-\varphi_{\rm w}(\tau,2\pi-2\delta_{\rm w})}{2\delta_{\rm w}^2} + \frac{3}{\delta_{\rm w}}\cdot\frac{\partial\varphi_{\rm w}}{\partial\sigma}\bigg|_{\sigma=2\pi^-} + O\left(\delta_{\rm w}^2\right). \tag{2.91}$$

Multiplying the second equation by $\varepsilon_{\rm wn}\delta_{\rm w}/(\delta_{\rm n}+\varepsilon_{\rm wn}\delta_{\rm w})$, the first one by $\delta_{\rm n}/(\delta_{\rm n}+\varepsilon_{\rm wn}\delta_{\rm w})$ and adding them, we conclude

$$\begin{aligned} S[\varphi_{\rm n}] = {} & \frac{1}{\delta_{\rm n}+\varepsilon_{\rm wn}\delta_{\rm w}}\cdot\frac{-7\varphi_{\rm n}(\tau,0)+8\varphi_{\rm n}(\tau,\delta_{\rm n})-\varphi_{\rm n}(\tau,2\delta_{\rm n})}{2\delta_{\rm n}} \\ & + \frac{\varepsilon_{\rm wn}}{\delta_{\rm n}+\varepsilon_{\rm wn}\delta_{\rm w}}\cdot\frac{-7\varphi_{\rm w}(\tau,2\pi)+8\varphi_{\rm w}(\tau,2\pi-\delta_{\rm w})-\varphi_{\rm w}(\tau,2\pi-2\delta_{\rm w})}{2\delta_{\rm w}} \\ & + \frac{3}{\delta_{\rm n}+\varepsilon_{wn}\delta_{\rm w}}\underbrace{\left[-\frac{\partial\varphi_{\rm n}}{\partial\sigma}\bigg|_{\sigma=0^+} + \varepsilon_{\rm wn}\,\frac{\partial\varphi_{\rm w}}{\partial\sigma}\bigg|_{\sigma=2\pi^-}\right]}_{0\ \text{(see Eq. (2.18))}} + O\left(\delta_{\rm n}^2+\delta_{\rm w}^2\right) = S[\varphi_{\rm w}]. \end{aligned} \tag{2.92}$$

Finally, one gets the following approximation for the differential operator S at the boundary $S_{\rm wn}$:

$$\begin{aligned} \tilde{S}[\,\phi_{\rm n}|_{i0}^k] = {} & \frac{1}{\delta_{\rm n}+\varepsilon_{\rm wn}\delta_{\rm w}}\cdot\frac{-7\,\phi_{\rm n}|_{i0}^k+8\,\phi_{\rm n}|_{i1}^k-\phi_{\rm n}|_{i2}^k}{2\delta_{\rm n}} \\ & + \frac{\varepsilon_{\rm wn}}{\delta_{\rm n}+\varepsilon_{\rm wn}\delta_{\rm w}}\cdot\frac{-7\,\phi_{\rm w}|_{iN_{\rm w}}^k+8\,\phi_{\rm w}|_{i,N_{\rm w}-1}^k-\phi_{\rm w}|_{i,N_{\rm w}-2}^k}{2\delta_{\rm w}} \\ & = \tilde{S}[\,\phi_{\rm w}|_{iN_{\rm w}}^k],\ i=\overline{0,N}. \end{aligned} \tag{2.93}$$

Thus, the second boundary condition in equations (2.18) is replaced by equation (2.80), in which the operators $\tilde{T}$ and $\tilde{S}$ are given by Eqs. (2.89) and (2.93).

At the particle–water surface

The operator T is approximated by $\tilde{T}$, which has the form Eq. (2.71), at the internal nodes of $S_{\rm pn}$ and Eq. (2.87) at the intersection of the $S_{\rm pw}$ and the axis of revolution.

Analogously to the computations for nonpolar–water interface, the operator S is extended in a close vicinity of the dividing surface $S_{\rm pw}$ as follows:

$$S[\varphi_{\rm p}] = \frac{\partial^2\varphi_{\rm p}}{\partial\sigma^2} - \frac{1}{h}\frac{\partial h}{\partial\sigma}\frac{\partial\varphi_{\rm p}}{\partial\sigma} = \frac{\partial^2\varphi_{\rm p}}{\partial\sigma^2} - \frac{2\tau\sin\sigma}{h}\frac{\partial\varphi_{\rm p}}{\partial\sigma}\ \text{at}\ \sigma=\sigma_{\rm pw}-0, \tag{2.94}$$

$$S[\varphi_{\rm w}] = \frac{\partial^2\varphi_{\rm w}}{\partial\sigma^2} - \frac{1}{h}\frac{\partial h}{\partial\sigma}\frac{\partial\varphi_{\rm w}}{\partial\sigma} = \frac{\partial^2\varphi_{\rm w}}{\partial\sigma^2} - \frac{2\tau\sin\sigma}{h}\frac{\partial\varphi_{\rm w}}{\partial\sigma}\ \text{at}\ \sigma=\sigma_{\rm pw}+0, \tag{2.95}$$

where $\sigma_{\rm pw} = 2\pi - \alpha$. Applying the formula (2.86) in the latter, one gets

$$S[\varphi_{\rm p}] = \frac{-7\varphi_{\rm p}(\tau,\sigma_{\rm pw}) + 8\varphi_{\rm p}(\tau,\sigma_{\rm pw}-\delta_{\rm p}) - \varphi_{\rm p}(\tau,\sigma_{\rm pw}-2\delta_{\rm p})}{2\delta_{\rm p}^2} + \left(\frac{3}{\delta_{\rm p}} - \frac{2\tau\sin\sigma_{\rm pw}}{h}\right)\left.\frac{\partial\varphi_{\rm p}}{\partial\sigma}\right|_{\sigma=\sigma_{\rm pw}-0} + O(\delta_{\rm p}^2), \tag{2.96}$$

$$S[\varphi_{\rm w}] = \frac{-7\varphi_{\rm w}(\tau,\sigma_{\rm pw}) + 8\varphi_{\rm w}(\tau,\sigma_{\rm pw}+\delta_{\rm w}) - \varphi_{\rm w}(\tau,\sigma_{\rm pw}+2\delta_{\rm w})}{2\delta_{\rm w}^2} - \left(\frac{3}{\delta_{\rm w}} + \frac{2\tau\sin\sigma_{\rm pw}}{h}\right)\left.\frac{\partial\varphi_{\rm w}}{\partial\sigma}\right|_{\sigma=\sigma_{\rm pw}+0} + O(\delta_{\rm w}^2). \tag{2.97}$$

Next, let the functions $a_{\rm p}(\tau)$ and $a_{\rm w}(\tau)$ are defined as

$$a_{\rm p}(\tau) = \varepsilon_{\rm pn}\left(\frac{3}{\delta_{\rm p}} + \frac{2\tau\sin\alpha}{1+\tau^2-2\tau\cos\alpha}\right)^{-1}, \quad a_{\rm w}(\tau) = \varepsilon_{\rm wn}\left(\frac{3}{\delta_{\rm w}} - \frac{2\tau\sin\alpha}{1+\tau^2-2\tau\cos\alpha}\right)^{-1}. \tag{2.98}$$

Then, adding Eq. (2.96), multiplied by $a_{\rm p}(\tau)/[a_{\rm p}(\tau)+a_{\rm w}(\tau)]$, to Eq. (2.97), multiplied by $a_{\rm w}(\tau)/[a_{\rm p}(\tau)+a_{\rm w}(\tau)]$, we obtain

$$\begin{aligned} S[\varphi_{\rm p}] = {} & \frac{a_{\rm p}(\tau)}{a_{\rm p}(\tau)+a_{\rm w}(\tau)} \cdot \frac{-7\varphi_{\rm p}(\tau,\sigma_{\rm pn}) + 8\varphi_{\rm p}(\tau,\sigma_{\rm pn}-\delta_{\rm p}) - \varphi_{\rm p}(\tau,\sigma_{\rm pn}-2\delta_{\rm p})}{2\delta_{\rm p}^2} \\ & + \frac{a_{\rm w}(\tau)}{a_{\rm p}(\tau)+a_{\rm w}(\tau)} \cdot \frac{-7\varphi_{\rm w}(\tau,\sigma_{\rm pn}) + 8\varphi_{\rm w}(\tau,\sigma_{\rm pn}+\delta_{\rm w}) - \varphi_{\rm w}(\tau,\sigma_{\rm pn}+2\delta_{\rm w})}{2\delta_{\rm w}^2} \\ & + O(\delta_{\rm p}^2+\delta_{\rm w}^2) = S[\varphi_{\rm w}], \end{aligned} \tag{2.99}$$

see Eq. (2.19). Finally, one gets the following approximation:

$$\begin{aligned} \tilde{S}[\,\phi_{\rm p}|_{iN_{\rm p}}^k] = {} & \frac{a_{\rm p}(\tau_i)}{a_{\rm p}(\tau_i)+a_{\rm w}(\tau_i)} \cdot \frac{-7\,\phi_{\rm p}|_{iN_{\rm p}}^k + 8\,\phi_{\rm p}|_{i,N_{\rm p}-1}^k - \phi_{\rm p}|_{i,N_{\rm p}-2}^k}{2\delta_{\rm p}^2} \\ & + \frac{a_{\rm w}(\tau_i)}{a_{\rm p}(\tau_i)+a_{\rm w}(\tau_i)} \cdot \frac{-7\,\phi_{\rm w}|_{i0}^k + 8\,\phi_{\rm w}|_{i1}^k - \phi_{\rm w}|_{i2}^k}{2\delta_{\rm w}^2} = \tilde{S}[\,\phi_{\rm w}|_{i0}^k],\ i=\overline{0,N}. \end{aligned} \tag{2.100}$$

At the particle–nonpolar surface

The operator T is approximated by $\tilde{T}$, which has the form Eq. (2.71) at the internal nodes and Eq. (2.87) at the intersection of the $S_{\rm pn}$ and the axis of revolution.

Analogously to the computations for the nonpolar–water surface, it follows from equations (2.60) and (2.86) that the finite difference representations of the operator S in the close vicinity of the boundary $S_{\rm pn}$ are

$$b_{\rm n}(\tau)S[\varphi_{\rm n}] = \frac{-7\varphi_{\rm n}(\tau,\sigma_{\rm pn}) + 8\varphi_{\rm n}(\tau,\sigma_{\rm pn}-\delta_{\rm n}) - \varphi_{\rm n}(\tau,\sigma_{\rm pn}-2\delta_{\rm n})}{2\delta_{\rm n}^2} b_{\rm n}(\tau) + \left.\frac{\partial\varphi_{\rm n}}{\partial\sigma}\right|_{\sigma=\sigma_{\rm pn}-0} + O(\delta_{\rm n}^2), \tag{2.101}$$

$$b_{\rm p}(\tau)S[\varphi_{\rm p}] = \frac{-7\varphi_{\rm p}(\tau,\sigma_{\rm pn}) + 8\varphi_{\rm p}(\tau,\sigma_{\rm pn}+\delta_{\rm p}) - \varphi_{\rm p}(\tau,\sigma_{\rm pn}+2\delta_{\rm p})}{2\delta_{\rm p}^2} b_{\rm p}(\tau) - \varepsilon_{\rm pn}\left.\frac{\partial\varphi_{\rm p}}{\partial\sigma}\right|_{\sigma=\sigma_{\rm pn}+0} + O(\delta_{\rm p}^2), \tag{2.102}$$

where $\sigma_{\rm pn} := \pi - \alpha$ and the functions $b_{\rm n}(\tau)$ and $b_{\rm p}(\tau)$ are defined as

$$b_{\rm n}(\tau) = \left(\frac{3}{\delta_{\rm n}} - \frac{2\tau \sin\alpha}{1+\tau^2+2\tau\cos\alpha} \right)^{-1}, \; b_{\rm p}(\tau) = \varepsilon_{\rm pn} \left(\frac{3}{\delta_{\rm p}} + \frac{2\tau \sin\alpha}{1+\tau^2+2\tau\cos\alpha} \right)^{-1}. \quad (2.103)$$

The linear combination of equations (2.101) and (2.102) with coefficients $b_{\rm n}/(b_{\rm n}+b_{\rm p})$ and $b_{\rm p}/(b_{\rm n}+b_{\rm p})$ along with the boundary conditions (2.20) leads to the final expression for the finite difference form of the operator S at the boundary $S_{\rm pn}$:

$$\begin{aligned} S[\varphi] = {} & \frac{b_{\rm n}(\tau)}{b_{\rm n}(\tau)+b_{\rm p}(\tau)} \cdot \frac{-7\varphi_{\rm n}(\tau,\sigma_{\rm pn}) + 8\varphi_{\rm n}(\tau,\sigma_{\rm pn}-\delta_{\rm n}) - \varphi_{\rm n}(\tau,\sigma_{\rm pn}-2\delta_{\rm n})}{2\delta_{\rm n}^2} \\ & + \frac{b_{\rm p}(\tau)}{b_{\rm n}(\tau)+b_{\rm p}(\tau)} \cdot \frac{-7\varphi_{\rm p}(\tau,\sigma_{\rm pn}) + 8\varphi_{\rm p}(\tau,\sigma_{\rm pn}+\delta_{\rm p}) - \varphi_{\rm p}(\tau,\sigma_{\rm pn}+2\delta_{\rm p})}{2\delta_{\rm p}^2} \\ & + \frac{1}{b_{\rm n}(\tau)+b_{\rm p}(\tau)} \cdot \frac{2\tau}{h} + O(\delta_{\rm n}^2+\delta_{\rm p}^2). \end{aligned} \quad (2.104)$$

Finally, we approximate the differential operator S at this dividing boundary by

$$\begin{aligned} \tilde{S}[\phi_{\rm n}|_{iN_{\rm n}}^k] = {} & \frac{b_{\rm n}(\tau_i)}{b_{\rm n}(\tau_i)+b_{\rm p}(\tau_i)} \cdot \frac{-7\,\phi_{\rm n}|_{iN_{\rm n}}^k + 8\,\phi_{\rm n}|_{i,N_{\rm n}-1}^k - \phi_{\rm n}|_{i,N_{\rm n}-2}^k}{2\delta_{\rm n}^2} \\ & + \frac{b_{\rm p}(\tau_i)}{b_{\rm n}(\tau_i)+b_{\rm p}(\tau_i)} \cdot \frac{-7\,\phi_{\rm p}|_{i0}^k + 8\,\phi_{\rm p}|_{i1}^k - \phi_{\rm p}|_{i2}^k}{2\delta_{\rm p}^2} \\ & + \frac{1}{b_{\rm n}(\tau_i)+b_{\rm p}(\tau_i)} \cdot \frac{2\tau_i}{1+\tau_i^2+2\tau_i\cos\alpha} = \tilde{S}[\phi_{\rm p}|_{i0}^k], i = \overline{0,N}. \end{aligned} \quad (2.105)$$

At the singularity point

For $\tau = 1$ and $\sigma = 0$, the toroidal transformation is singular. In toroidal coordinates, one reaches the triple point $\tau = 1$ and $\sigma = 0$, using two boundaries: the axis of revolution and the fluid–fluid interface. At the axis of revolution, the definition of the operator S for $\sigma \to 0$ is

$$\begin{aligned} \lim_{\sigma\to 0}(1-\cos\sigma)\frac{\partial}{\partial\sigma}\left(\frac{1}{1-\cos\sigma}\cdot\frac{\partial\varphi_l}{\partial\sigma}\right) &= \lim_{\sigma\to 0}\left[\frac{\partial^2\varphi_l}{\partial\sigma^2} - \frac{\sin\sigma}{1-\cos\sigma}\frac{\partial\varphi_l}{\partial\sigma}\right] \\ &= \left.\frac{\partial^2\varphi_l}{\partial\sigma^2}\right|_{\sigma=0} - \lim_{\sigma\to 0}\frac{\frac{\partial\varphi_l}{\partial\sigma}}{\sin\left(\frac{\sigma}{2}\right)}, \end{aligned} \quad (2.106)$$

see Eq. (2.84). The value of φ_l for $\tau = 1$ and $\sigma = 0$ is a constant due to the fact that the physical value of the potentials at infinity is a constant. Then, we conclude that

$$\left.\frac{\partial\varphi_l}{\partial\sigma}\right|_{\sigma=0} = 0 \quad (2.107)$$

and, therefore,

$$\lim_{\sigma\to 0}(1-\cos\sigma)\frac{\partial}{\partial\sigma}\left(\frac{1}{1-\cos\sigma}\cdot\frac{\partial\varphi_l}{\partial\sigma}\right) = \left.\frac{\partial^2\varphi_l}{\partial\sigma^2}\right|_{\sigma=0} - 2\lim_{\sigma\to 0}\frac{\frac{\partial^2\varphi_l}{\partial\sigma^2}}{\cos\left(\frac{\sigma}{2}\right)} = -\frac{\partial\varphi_l^2}{\partial\sigma^2} \quad (2.108)$$

At the water–nonpolar interface, the definition of the operator T for $\tau \to 1$ is

$$T[\varphi_l] = \lim_{\tau\to 1} \frac{\tau(1-\tau)}{1+\tau}\frac{\partial}{\partial\tau}\left[\frac{\tau(1+\tau)}{1-\tau}\frac{\partial\varphi_l}{\partial\tau}\right] = \lim_{\tau\to 1}\tau\left[\frac{\tau^2-2\tau-1}{\tau^2-1}\frac{\partial\varphi_l}{\partial\tau}+\tau\frac{\partial^2\varphi_l}{\partial\tau^2}\right]$$
$$= \frac{-2}{2}\lim_{\tau\to 1}\frac{\frac{\partial\varphi_l}{\partial\tau}}{\tau-1}+\left.\frac{\partial^2\varphi_l}{\partial\tau^2}\right|_{\tau=1} = 0. \tag{2.109}$$

Then, we use Eq. (2.107) as a boundary condition in the infinity point in σ-direction. Finally, the boundary condition (2.22) is approximated as

$$3\ \phi_{\rm n}|_{N0}^{k+1} - 4\ \phi_{\rm n}|_{N-1,0}^{k+1} + \phi_{\rm n}|_{N-2,0}^{k+1} = 0 \tag{2.110}$$

and Eq. (2.107) — as

$$-3\ \phi_{\rm n}|_{N0}^{k+1} + 4\ \phi_{\rm n}|_{N1}^{k+1} - \phi_{\rm n}|_{N2}^{k+1} = 0, \tag{2.111}$$
$$3\ \phi_{\rm w}|_{NN_{\rm w}}^{k+1} - 4\ \phi_{\rm w}|_{N,N_{\rm w}-1}^{k+1} + \phi_{\rm w}|_{N,N_{\rm w}-2}^{k+1} = 0, \tag{2.112}$$

using the second-order formula [2.22]

$$u'(x) = \pm\frac{3u(x) - 4u(x\mp\delta_x) + u(x\mp 2\delta_x)}{2\delta_x} + O({\delta_x}^2). \tag{2.113}$$

2.6.3 Algorithm

The algorithm for finding the distribution of the electrostatic potentials is presented in Alg. 1. The main idea of algorithm is the following. We solve the problem in the σ direction and obtain the values of $\psi_l|_{ij}^k$, l =n, p, w. Next, the values of the functions $\psi_l|_{ij}^k$, l =n, p, w, at the axis of revolution are obtained. Next, three $\tau-$directional problems are solved and the values $\phi_l|_{ij}^k + 1$, l =n, p, w are obtained. For stopping criterion, an error estimate is used.

Next, we specify the different τ and σ-directional problems that are solved. The σ-directional problem (S) acquires the form:

- At the volumes (Eqs. (2.70) and (2.71)):

$$\left(U-\frac{\delta_t}{2}\tilde{S}\right)\left[\psi_{\rm n}|_{ij}^{k+1}\right] = \delta_t\tilde{S}\left[\phi_{\rm n}|_{ij}^{k}\right] + \delta_t\tilde{T}\left[\phi_{\rm n}|_{ij}^{k}\right],\ j=\overline{1,N_{\rm n}-1}; \tag{2.114}$$
$$\left(U-\frac{\delta_t}{2}\tilde{S}\right)\left[\psi_{\rm p}|_{ij}^{k+1}\right] = \delta_t\tilde{S}\left[\phi_{\rm p}|_{ij}^{k}\right] + \delta_t\tilde{T}\left[\phi_{\rm p}|_{ij}^{k}\right],\ j=\overline{1,N_{\rm p}-1}; \tag{2.115}$$
$$\left(U-\frac{\delta_t}{2}\tilde{S}\right)\left[\psi_{\rm w}|_{ij}^{k+1}\right] = \delta_t\tilde{S}\left[\phi_{\rm w}|_{ij}^{k}\right] + \delta_t\tilde{T}\left[\phi_{\rm w}|_{ij}^{k}\right],\ j=\overline{1,N_{\rm w}-1}; \tag{2.116}$$

- At the nonpolar–water boundary $S_{\rm nw}$ (Eqs. (2.93) and (2.89)):

$$\left(U-\frac{\delta_t}{2}\tilde{S}\right)\left[\psi_{\rm w}|_{iN_{\rm w}}^{k+1}\right] = \delta_t\tilde{S}\left[\phi_{\rm w}|_{iN_{\rm w}}^{k}\right] + \delta_t\tilde{T}\left[\phi_{\rm w}|_{iN_{\rm w}}^{k}\right], \tag{2.117}$$
$$\left(U-\frac{\delta_t}{2}\tilde{S}\right)\left[\psi_{\rm n}|_{i0}^{k+1}\right] = \delta_t\tilde{S}\left[\phi_{\rm n}|_{i0}^{k}\right] + \delta_t\tilde{T}\left[\phi_{\rm n}|_{i0}^{k}\right], \tag{2.118}$$

Algorithm 1 Compute the electrostatic distributions

procedure ComputeDistributions($N, N_\mathrm{n}, N_\mathrm{p}, N_\mathrm{w}, \alpha$)
  Compute the lengths of the steps $\delta_\mathrm{n},\ \delta_\mathrm{p},\ \delta_\mathrm{w},\ \delta_\tau,\ \delta_t$; ▷ (2.63)–(2.67);
  Set the values of $\phi_\mathrm{n},\ \phi_\mathrm{p},\ \phi_\mathrm{w}$ to 0 at the initial moment of time ($k = 0$);

  for $k \leftarrow 0$ to 200 **do**

    for $i \leftarrow 1$ to $N - 1$ **do**
      Solve a σ-directional problem (S) for ψ_w, ψ_n and ψ_p;
    end for

    Solve a σ-directional problem (S_1);

    for $j \leftarrow 1$ to $N_\mathrm{n} - 1$ **do**
      Solve a τ-directional problem (T_n);
    end for

    for $j \leftarrow 1$ to $N_\mathrm{p} - 1$ **do**
      Solve a τ-directional problem (T_p);
    end for

    for $j \leftarrow 1$ to $N_\mathrm{w} - 1$ **do**
      Solve a τ-directional problem (T_w);
    end for

    Compute the values $\phi_\mathrm{n},\ \phi_\mathrm{p},\ \phi_\mathrm{w}$ at the next moment of time; ▷ Eq. (2.79)
  end for
end procedure

- At the particle–nonpolar boundary S_pn (Eqs. (2.105) and (2.71)):

$$\left(U - \frac{\delta_t}{2}\tilde{S}\right)\left[\psi_\mathrm{n}|_{iN_\mathrm{n}}^{k+1}\right] = \delta_t\tilde{S}\left[\phi_\mathrm{n}|_{iN_\mathrm{n}}^{k}\right] + \delta_t\tilde{T}\left[\phi_\mathrm{n}|_{iN_\mathrm{n}}^{k}\right], \tag{2.119}$$

$$\left(U - \frac{\delta_t}{2}\tilde{S}\right)\left[\psi_\mathrm{p}|_{i0}^{k+1}\right] = \delta_t\tilde{S}\left[\phi_\mathrm{p}|_{i0}^{k}\right] + \delta_t\tilde{T}\left[\phi_\mathrm{p}|_{i0}^{k}\right]; \tag{2.120}$$

- At the particle–water boundary S_pw (Eqs. (2.100) and (2.71)):

$$\left(U - \frac{\delta_t}{2}\tilde{S}\right)\left[\psi_\mathrm{p}|_{iN_\mathrm{p}}^{k+1}\right] = \delta_t\tilde{S}\left[\phi_\mathrm{p}|_{iN_\mathrm{p}}^{k}\right] + \delta_t\tilde{T}\left[\phi_\mathrm{p}|_{iN_\mathrm{p}}^{k}\right], \tag{2.121}$$

$$\left(U - \frac{\delta_t}{2}\tilde{S}\right)\left[\psi_\mathrm{w}|_{i0}^{k+1}\right] = \delta_t\tilde{S}\left[\phi_\mathrm{w}|_{i0}^{k}\right] + \delta_t\tilde{T}\left[\phi_\mathrm{w}|_{i0}^{k}\right]; \tag{2.122}$$

The σ-directional problem (S_1), computing the values of the potentials at the axis of revolution $\tau = 1$, is defined as:

- In the volumes (Eqs. (2.70) and (2.87)):

$$\left(U-\frac{\delta_t}{2}\tilde{S}\right)\left[\psi_{\rm n}|_{Nj}^{k+1}\right]=\delta_t\tilde{S}\left[\phi_{\rm n}|_{Nj}^{k}\right]+\delta_t\tilde{T}\left[\phi_{\rm n}|_{Nj}^{k}\right],\ j=\overline{1,N_{\rm n}-1}; \tag{2.123}$$

$$\left(U-\frac{\delta_t}{2}\tilde{S}\right)\left[\psi_{\rm p}|_{Nj}^{k+1}\right]=\delta_t\tilde{S}\left[\phi_{\rm p}|_{Nj}^{k}\right]+\delta_t\tilde{T}\left[\phi_{\rm p}|_{Nj}^{k}\right],\ j=\overline{1,N_{\rm p}-1}; \tag{2.124}$$

$$\left(U-\frac{\delta_t}{2}\tilde{S}\right)\left[\psi_{\rm w}|_{Nj}^{k+1}\right]=\delta_t\tilde{S}\left[\phi_{\rm w}|_{Nj}^{k}\right]+\delta_t\tilde{T}\left[\phi_{\rm w}|_{Nj}^{k}\right],\ j=\overline{1,N_{\rm w}-1}; \tag{2.125}$$

- At $\tau=1$ and $S_{\rm nw}$ (Eq. (2.111) and (2.112)):

$$-3\,\psi_{\rm n}|_{N0}^{k+1}+4\,\psi_{\rm n}|_{N1}^{k+1}-\psi_{\rm n}|_{N2}^{k+1}=0; \tag{2.126}$$

$$3\,\psi_{\rm w}|_{NN_{\rm w}}^{k+1}-4\,\psi_{\rm w}|_{N,N_{\rm w}-1}^{k+1}+\psi_{\rm w}|_{N,N_{\rm w}-2}^{k+1}=0; \tag{2.127}$$

- At $\tau=1$ and $S_{\rm pn}$ (Eqs. (2.105) and (2.87)):

$$\left(U-\frac{\delta_t}{2}\tilde{S}\right)\left[\psi_{\rm n}|_{NN_{\rm n}}^{k+1}\right]=\delta_t\tilde{S}\left[\phi_{\rm n}|_{NN_{\rm n}}^{k}\right]+\delta_t\tilde{T}\left[\phi_{\rm n}|_{NN_{\rm n}}^{k}\right], \tag{2.128}$$

$$\left(U-\frac{\delta_t}{2}\tilde{S}\right)\left[\psi_{\rm p}|_{N0}^{k+1}\right]=\delta_t\tilde{S}\left[\phi_{\rm p}|_{N0}^{k}\right]+\delta_t\tilde{T}\left[\phi_{\rm p}|_{N0}^{k}\right]; \tag{2.129}$$

- At $\tau=1$ and $S_{\rm pw}$ (Eqs. (2.100) and (2.87)):

$$\left(U-\frac{\delta_t}{2}\tilde{S}\right)\left[\psi_{\rm p}|_{NN_{\rm p}}^{k+1}\right]=\delta_t\tilde{S}\left[\phi_{\rm p}|_{NN_{\rm p}}^{k}\right]+\delta_t\tilde{T}\left[\phi_{\rm p}|_{NN_{\rm p}}^{k}\right]; \tag{2.130}$$

$$\left(U-\frac{\delta_t}{2}\tilde{S}\right)\left[\psi_{\rm w}|_{N0}^{k+1}\right]=\delta_t\tilde{S}\left[\phi_{\rm w}|_{N0}^{k}\right]+\delta_t\tilde{T}\left[\phi_{\rm w}|_{N0}^{k}\right]; \tag{2.131}$$

The τ-directional problem ($T_{\rm n}$) has the form:

- At the volumes (Eqs. (2.71)):

$$\left(U-\frac{\delta_t}{2}\tilde{T}\right)\left[\delta\phi_{\rm n}|_{ij}^{k+1}\right]=\psi_{\rm n}|_{ij}^{k+1},\ i=\overline{1,N-1}, \tag{2.132}$$

- At the contact line (Eq. (2.82)):

$$\delta\phi_{\rm n}|_{0j}^{k+1}=0. \tag{2.133}$$

- At the axis of revolution $\tau=1$ and $\sigma\neq 0$ (Eq. (2.87)):

$$\left(U-\frac{\delta_t}{2}\tilde{T}\right)\left[\delta\phi_{\rm n}|_{Nj}^{k+1}\right]=\psi_{\rm n}|_{Nj}^{k+1}, \tag{2.134}$$

- At the infinity point (Eq. (2.110)):

$$3\,\delta\phi_{\rm n}|_{N0}^{k+1}-4\,\delta\phi_{\rm n}|_{N-1,0}^{k+1}+\delta\phi_{\rm n}|_{N-2,0}^{k+1}=0. \tag{2.135}$$

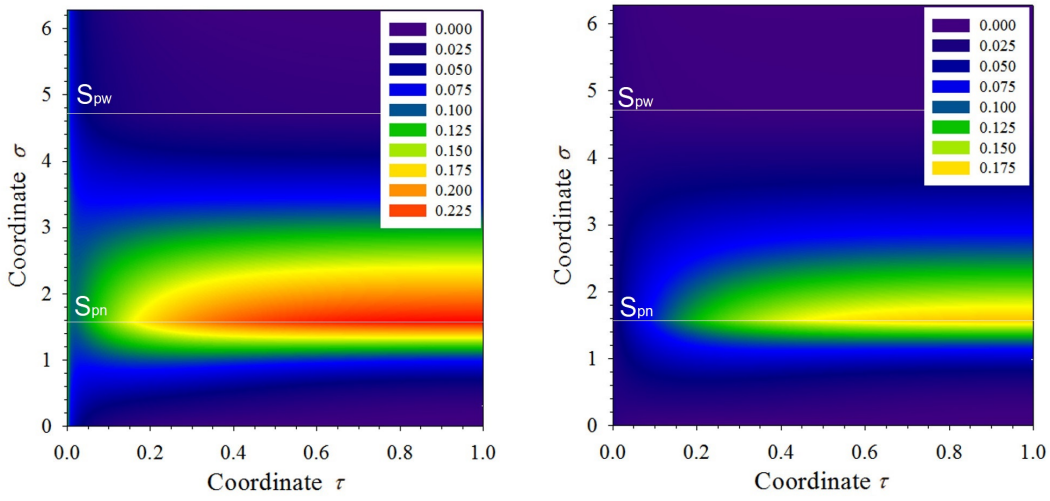

(a) $\varepsilon_{\mathrm{pn}} = 0.874$ and $\varepsilon_{\mathrm{wn}} = 17.2$

(b) $\varepsilon_{\mathrm{pn}} = 2$ and $\varepsilon_{\mathrm{wn}} = 40$

Figure 2.5: Distribution of the electrostatic potentials in numerical domains for contact angle $\alpha = 90°$

Analogously, the τ-directional problem (T_{p}) and (T_{w}) are defined. Note that we solve two linear systems on each time step. Because of the boundary conditions, the considered algorithm reduces the matrix of the linear algebraic system in the τ-direction to a five-diagonal matrix. The respective matrix of the system in the σ-direction is again with five non-zero diagonals, but because of the periodicity of the solution at S_{nw} its first row contains two more elements at the end and the last row contains two more elements at the beginning. We implemented a direct elimination numerical method in order to solve these systems.

Finally, in order to compute the distribution of the electrostatic potentials after long enough time, you need to save only the information in the current and the previous moment of time.

2.7 Numerical results

To achieve good precision of the numerical calculations, we discretize each numerical domain by introducing a 100×100 uniform mesh (see Section 2.6). Due to the fact that the σ-coordinate curve is a circle, which degenerates into the pole A_+ for $\tau \to \infty$ (see Fig. S.9 in the Supplementary material S), then we could work with an uniform mesh over the spacial domain in toroidal coordinates. The time step is chosen to be equal to the minimum of δ_τ, δ_{n}, δ_{p} and δ_{w}. The computation of the potential distributions is fast. The CPU time on a laptop with processor Intel Core i5-4200H is less than a second for any contact angle $\alpha \in (0°, 180°)$ and an 100×100 uniform mesh in each of the domains.

The illustrative figures (Fig. 2.5b and 2.6b) correspond to experimental system parameters $\varepsilon_{\mathrm{pn}} = 2$ and $\varepsilon_{\mathrm{wn}} = 40$ [2.11]. If the oil phase has a larger dielectric constant (for example, castor oil with $\varepsilon_{\mathrm{n}} = 4.54$), then the system parameters are $\varepsilon_{\mathrm{pn}} = 0.874$ and $\varepsilon_{\mathrm{wn}} = 17.2$ (Figs. 2.5a and 2.6a, respectively).

Fig. 2.5 shows the distribution of the physical potentials in the numerical domains

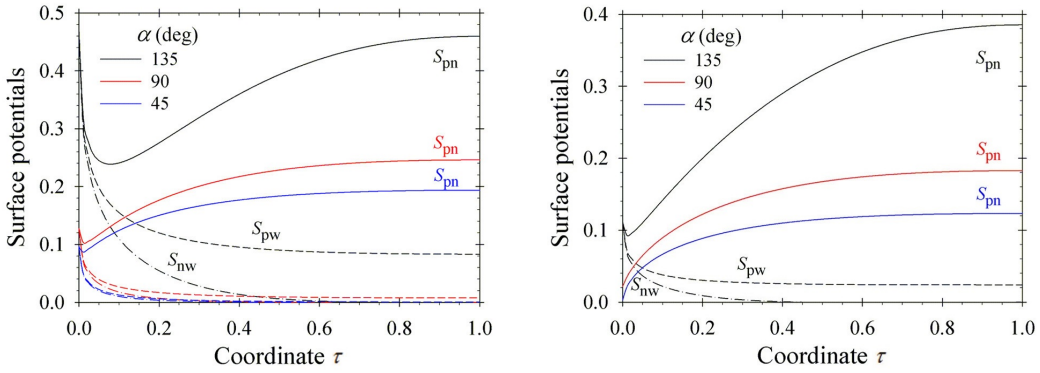

(a) $\varepsilon_{pn} = 0.874$ and $\varepsilon_{wn} = 17.2$ (b) $\varepsilon_{pn} = 2$ and $\varepsilon_{wn} = 40$

Figure 2.6: Distribution of potentials along the interfaces for different values of contact angle α

for three-phase contact angle $\alpha = 90°$. The considerably higher dimensionless potentials are well illustrated for larger values of the dielectric constant of the nonpolar phase. At the coordinate lines, $\sigma = 0$ (S_{nw}) and $\sigma = 3\pi/2$ (S_{pw}), the electrostatic potentials are considerably lower than those at coordinate line $\sigma = \pi/2$ (S_{pn}). As it can be expected, the maxima of the electrostatic potentials are at the cross-section of the particle–nonpolar interface and the axis of revolution. In both cases, the dielectric constant of water is so high that the water phase suppresses the penetration of the electric field in the polar phase.

The calculations in [2.2, 2.11] are performed, assuming zero values of the potentials at the boundaries of the polar fluid. The magnitude of the electro-dipping force decreases if the electrostatic potentials at these boundaries are different than zero. Fig. 2.6 shows the distribution of the surface potentials along the boundaries (solid lines correspond to S_{pn}; dashed lines — to S_{pw}; dot–dashed lines — to S_{nw}). The increase in the three-phase contact angle (more hydrophobic particles) leads to higher potentials because of the more charges, adsorbed at the particle–nonpolar fluid interface. The effect of the water phase becomes more pronounced. It is important to note that the surface potentials at the particle–water boundary are different from zero. Thus, the boundary S_{pw} also contributes to the electro-dipping force. For $\alpha = 45°$ and $\alpha = 90°$ this contribution is small, while for $\alpha = 135°$—it is not negligible. The weak singularities at the three-phase contact line ($\tau = 0$) correspond to those depicted in Fig. 2.4. If the dielectric constant of the particle phase, ε_p, is smaller than that of the nonpolar phase, ε_n, then the electric field penetration inside the particle phase is more effective and the electrostatic potential at boundary S_{pw} is higher.

2.8 Conclusion

The proposed effective numerical algorithm, based on the ADIM, enables us to do fast and precise calculation of the electrostatic distributions, generated from a charged dielectric particle, attached to the nonpolar–water interface. For faster calculations, we transform the complex dielectric phase domains into rectangles, using a modification of the toroidal coordinates. The resulting systems in the respective directions of ADIM are solved, using a

direct elimination method.

The numerical results show the effect of the three-phase contact angle and the dielectric properties of the phases on the induced electric fields and the magnitude of the electro-dipping force. Generally, the decrease of the ratios of the dielectric constants of the particle and nonpolar phase, $\varepsilon_p/\varepsilon_{\mathrm{n}}$, and that of water and nonpolar phase, $\varepsilon_{\mathrm{w}}/\varepsilon_{\mathrm{n}}$, leads to the more pronounced penetration of the electric field and higher surface potentials at the particle–water and nonpolar fluid–water boundaries. The magnitude of the potentials (electro-dipping force) is larger for more hydrophobic particles. The calculations generalize known results — the idealized case of a thin electric double layer in water [2.11], where the dielectric constants of the particle and the nonpolar phase are assumed to be negligible with respect to the constant of water, and the idealized case of water phase with infinite dielectric permittivity [2.2].

References

[2.1] V. Lotito and T. Zambelli. Approaches to self-assembly of colloidal monolayers: A guide to nanotechnologists. *Adv. Colloid Interfac. Sci.*, 246:217–274, 2017. DOI: 10.1016/j.cis.2017.04.003.

[2.2] K. Danov and P. Kralchevsky. Electric forces induced by a charged colloid particle attached to the water–nonpolar fluid interface. *J. Colloid Interface Sci.*, 298(1):213–231, 2006. DOI: 10.1016/j.jcis.2005.12.037.

[2.3] P. Petkov, K. Danov, and P. Kralchevsky. Monolayers of charged particles in a langmuir trough: Could particle aggregation increase the surface pressure? *Journal of Colloid and Interface Science*, 462:223–234, 2015. DOI: 10.1016/j.jcis.2015.09.075.

[2.4] D. Venkataramani, A. Tsulaia, and S. Amin. Fundamentals and applications of particle stabilized emulsions in cosmetic formulations. *Advances in Colloid and Interface Science*, 283:102234, 2020. DOI: 10.1016/j.cis.2020.102234.

[2.5] A. Studart, U. Gonzenbach, I. Akartuna, E. Tervoort, and L. Gauckler. Materials from foams and emulsions stabilized by colloidal particles. *Journal of materials chemistry*, 31:3283–3289, 2007. DOI: 10.1039/B703255B.

[2.6] K. Thompson, M. Williams, and S. Armes. Colloidosomes: Synthesis, properties and applications. *Journal of Colloid and Interface Science*, 447:217–228, 2014. DOI: 10.1016/j.jcis.2014.11.058.

[2.7] M. Hsu, M. Nikolaides, A. Dinsmore, A. Bausch, V. Gordon, X. Chen, J. Hutchinson, D. Weitz, and M. Marquez. Self-assembled shells composed of colloidal particles: fabrication and characterization. *Langmuir*, 21(7):2963–2970, 2005. DOI: 10.1021/la0472394j.

[2.8] E. Dickinson. Food emulsions and foams: Stabilization by particles. *Current Opinion in Colloid & Interface Science*, 15(1):40–49, 2010. DOI: j.cocis.2009.11.001.

[2.9] H. Son, H. Kim, G. Lee, J. Kim, and W. Sung. Enhanced oil recovery using nanoparticle-stabilized oil/water emulsions. *Korean J. Chem. Eng.*, 31:338–342, 2014. DOI: 10.1007/s11814-013-0214-5.

[2.10] Q. Sun, J. Chen, and A. Routh. Coated colloidosomes as novel drug delivery carriers. *Expert Opinion on Drug Delivery*, 16(9):903–906, 2019. DOI: 10.1080/17425247.2019.1652594.

[2.11] K. Danov, P. Kralchevsky, and M. Boneva. Electrodipping force acting on solid particles at a fluid interface. *Langmuir*, 20(15):6139–6151, 2004. DOI: 10.1021/la0497090.

[2.12] T. Horozov, R. Aveyard, B. Binks, and J. Clint. Structure and stability of silica particle monolayers at horizontal and vertical octane-water interfaces. *Langmuir*, 21(16):7405–7412, 2005. DOI: 10.1021/la050923d.

[2.13] K. Danov and P. Kralchevsky. Forces acting on dielectric colloidal spheres at a water/nonpolar fluid interface in an external electric field. 2. charged particles. *Journal of colloid and interface science*, 405:269–277, 2013. DOI: 10.1016/j.jcis.2013.05.015.

[2.14] R. Aveyard, B. Binks, J. Clint, P. Fletcher, T. Horozov, B. Neumann, V. Paunov, J. Annesley, S. Botchway, D. Nees, A. Parker, A. Ward, and A. Burgess. Measurement of long-range repulsive forces between charged particles at an oil-water interface. *Phys. Rev. Lett.*, 88:246102–246106, 2002. DOI: 10.1103/PhysRevLett.88.246102.

[2.15] T. Horozov, R. Aveyard, J. Clint, and B. Binks. Order-disorder transition in monolayers of modified monodisperse silica particles at the octane-water interface. *Langmuir*, 19(7):2822–2829, 2003. DOI: 10.1021/la020858x.

[2.16] Y. D'Yakonov. Difference schemes with a "disintegrating" operator for multidimensional problems. *USSR Computational Mathematics and Mathematical Physics*, 2(4):581–607, 1963. DOI: 10.1016/0041-5553(63)90531-7.

[2.17] N. Yanenko. *The Method of Fractional Steps, the Solution of Problems of Mathematical Physics in Several Variables*. Springer Berlin, Heidelberg, 1971. DOI: 10.1007/978-3-642-65108-3.

[2.18] J. Thomas. *Numerical Partial Differential Equations: Finite Difference Methods*. Springer New York, 1995. DOI: 10.1007/978-1-4899-7278-1.

[2.19] D. Peaceman and J. Rachford. The numerical solution of parabolic and elliptic differential equations. *Journal of the Society for Industrial and Applied Mathematics*, 3(1):28–41, 1955. DOI: 10.1137/0103003.

[2.20] S. Dimova, T. Chernogorova, and A. Jotova. *Numerical methods for partial differential equations (in Bulgarian)*. University of Sofia "St. Kliment Ohridski", 2010.

[2.21] Y.-M. Wang and T. Wang. A compact adi method and its extrapolation for time fractional sub-diffusion equations with nonhomogeneous neumann boundary conditions. *Computers and Mathematics with Applications*, 75(3):721–739, 2018. DOI: 10.1016/j.camwa.2017.10.002.

[2.22] K. Rahul and S. Bhattacharyya. One-sided finite-difference approximations suitable for use with richardson extrapolation. *Journal of Computational Physics*, 219(1):13–20, 2006. DOI: 10.1016/j.jcp.2006.05.035.

Chapter 3

Motion of a spherical particle, attached to the interface between two viscous fluids

In this chapter, we compute the drag force, acting on a particle, attached to the boundary between two viscous fluids. This calculation is important for the production of 2D-ordered micro- and nano-layers, which are applied in the production of solar panels, charge-coupled devices (CCDs) and bio-memory chips. The problem was solved semi-analytically for water–air interface and three-phase contact angle $\alpha \leq 90^\circ$, using the Mehler–Fock transformation [3.1]. We propose a numerical method, based on the gauge formulation of the Stokes equations for two viscous fluids. This method is applicable for calculating the velocity field, the pressure and the drag force coefficient for all values of the three-phase contact angle and the fluid viscosities. The weak singularity of the solutions at the three-phase contact line is studied and the respective phase diagram is drawn. The isolation of the singularity type helps us to construct an efficient second-order numerical scheme, based on the alternating direction implicit method. The problem is solved numerically for different three-phase contact angles and ratios of the fluid viscosities.

The results, included in this chapter, are published in

- G. Lyutskanova-Zhekova, K. Danov, Motion of a Spherical Particle Attached to the Interface Between Two Viscous Fluids, Progress in Industrial Mathematics (2019). DOI: 10.1007/978-3-030-27550-1_12.

3.1 Literature overview

The 2D layers of micro- and nano-particles [3.2, 3.3], attached to interfaces, are related to the production of antireflective surface coverages in solar panels [3.4, 3.5], microlense structures in CCD technologies [3.6] and structures for bioengineering and biosensing applications [3.7, 3.8]. The quality of these layers depends on the values of the contact angle, α, and the mobility of particles at interfaces. For small particles, α is measured from the translational motion of individual particles, attached to fluid–fluid interfaces [3.9].

In the current work, we calculate the drag coefficient of a spherical particle, located at a flat interface between two viscous fluids and moving parallel to it. If one of the fluid phases is air, the problem has a semi-analytical solution in terms of the Mehler–Fock integral transformation [3.1], which is valid only for particles more immersed in the fluid phase ($\alpha \leq 90^\circ$). Analytical approximations for the drag and diffusion coefficient of a spherical particle, attached to a flat interface between two immiscible fluids, are constructed for the case of a vanishing viscosity ratio between the fluid phases [3.10]. The general problem is solved in [3.11], using the two-vorticity-one-velocity formalism. A major drawback of the proposed method in [3.11] is that it is slow and, therefore, it cannot be used in the most of the practical applications.

The aim of the present study is to develop a fast and effective numerical method for calculating the velocity field, the pressure and the drag coefficient in the case of two fluid phases with arbitrary viscosities and three-phase contact angles $0 < \alpha < 180^\circ$. The problem is solved, using similar method to this in [3.11] but we use the gauge approach instead of the two-vorticity-one-velocity formalism. This leads to fast and efficient method for solving the problem.

Solving this problem in an efficient way is an important task due to the following reasons. First, these calculations could be used to determine the contact angle of micron particles. These particles are so small that they do not deform the surface, to which they are attached. Moreover, one could see their movement with a microscope but not them in detail. Therefore, the speed of a micron particle is measured thought experiment and using this information, the particle contact angle is computed. The only way to do that for the time being is by using parametric identification. This method requires repeated calculations of the drag force for different values of the contact angle to obtain the best fit of the experimental data for the drag coefficient. Second, an efficient algorithm for computation of the drag force is needed in order to solve the two-dimensional crystallization problem. This problem is transformed to a problem for ordering of many moving particles, which is solved, using the drag force coefficient for each particle. Moreover, an efficient algorithm is needed because the number of particles is great and they have different contact angles. Due to above presented applications, the solution of the presented above problem is an important task.

The current chapter is structured as follows. We formulate the problem in Sec. 3.2 and nondimensionalize it in Sec. 3.4. In Sec. 3.5, one transforms the problem into a convenient form for numerical modeling. In Sec. 3.6, the asymptotic solutions at the three-phase contact line are found in order to have a good approximation for the drag force, which has a singularity at $\tau = 0$. Finally, the numerical method and algorithm for finding the drag force, and the results are presented in Sec. 3.7.

3.2 Mathematical formulation of the problem

A small spherical particle of radius R is attached to the interface between two infinite incompressible viscous fluids (Fig. 3.1) and moves parallel to the fluid interface with known constant velocity V. The particle position is determined by the three-phase contact angle α, see Fig. 3.1. For small capillary numbers, the perturbations of the dividing surface due to the particle motion are sufficiently small so that the surface is flat. Thus, the three-phase contact line is a circumference of radius $r_c = R \sin \alpha$. Its center is chosen to be an origin of a Cartesian coordinate system with unit basis vectors $\mathbf{e}_x$, $\mathbf{e}_y$, and $\mathbf{e}_z$, where $\mathbf{e}_y$ points at the direction of the particle movement and $\mathbf{e}_z$ is normal to the fluid–fluid interface, pointing at

the upper fluid phase (see Fig. 3.1).

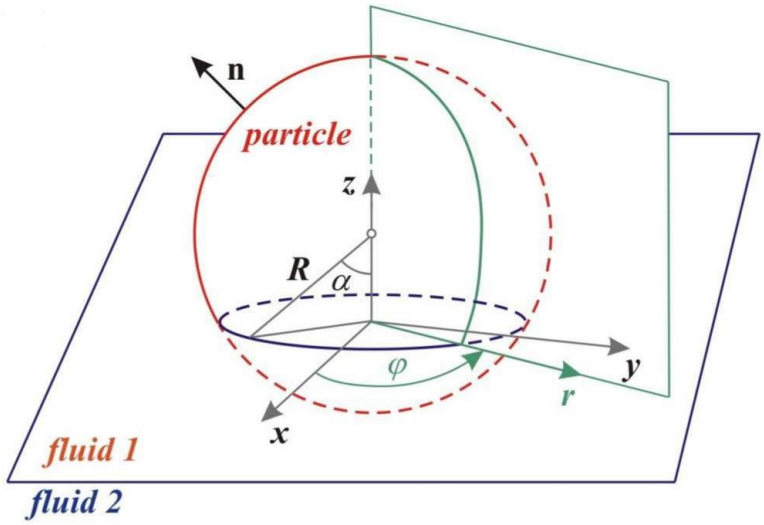

Figure 3.1: Sketch of a spherical particle, attached to the plane interface between two fluids.

The translation of the particle causes the fluid motion, which is assumed to be so slow so that the inertia terms in the Navier–Stokes equations can be neglected. Thus, we describe the sought-out local velocities $\mathbf{v}_m$ for both phases as solutions of the Stokes equations, i.e.

$$\nabla \cdot \mathbf{v}_m = 0, \ m = 1, 2, \tag{3.1}$$

$$\nabla p_m = \eta_m \nabla^2 \mathbf{v}_m, \ m = 1, 2, \tag{3.2}$$

where p_m is the pressure, η_m is the dynamic viscosity, ∇ is the spatial gradient and subscripts "1" and "2" denote the upper and lower phases, respectively.

In order to close the obtained system of partial differential equations, we need to apply the respective boundary conditions. The no-slip boundary conditions at the particle surface, S_p, state

$$\mathbf{v}_m = V\mathbf{e}_y \text{ at } S_\mathrm{p}, \ m = 1, 2, \tag{3.3}$$

see Eq. (U.77) in the Supplementary material U. The kinematic boundary conditions at the non-perturbed interface $z = 0$ are

$$\mathbf{v}_1 = \mathbf{v}_2, \ \mathbf{v}_1 \cdot \mathbf{e}_z = 0, \ \mathbf{v}_2 \cdot \mathbf{e}_z = 0 \text{ at } z = 0, \tag{3.4}$$

see Eqs. (U.79), (U.81) in the Supplementary Material U. The interface is assumed to have no surface elasticity, diffusivity, viscosity, etc., then, the dynamic boundary condition at interface $z = 0$ has the form:

$$\mathbf{e}_z \cdot (\mathbf{T}_1 - \mathbf{T}_2) = \mathbf{0} \text{ at } z = 0, \tag{3.5}$$

where $\mathbf{T}_1$ and $\mathbf{T}_2$ are the bulk stress tensors, see (U.93) in the Supplementary Material U. Taking into account that the fluids are incompressible Newtonian, then the following constitutive relations:

$$\mathbf{T}_m = -p_m \mathbf{I} + \eta_m \left[\nabla \mathbf{v}_m + (\nabla \mathbf{v}_m)^T \right], \ m = 1, 2 \tag{3.6}$$

hold true, see Section U.4 in the Supplementary Material U. Substituting Eqs. (3.6) in the general dynamic boundary condition (3.5), we obtain

$$-p_1 \mathbf{e}_z + \eta_1 \mathbf{e}_z \cdot \left[\nabla \mathbf{v}_1 + (\nabla \mathbf{v}_1)^T \right] = -p_2 \mathbf{e}_z + \eta_2 \mathbf{e}_z \cdot \left[\nabla \mathbf{v}_2 + (\nabla \mathbf{v}_2)^T \right], \tag{3.7}$$

$$-p_1 \mathbf{e}_z + 2\eta_1 \frac{\partial \mathbf{v}_1}{\partial z} = -p_2 \mathbf{e}_z + 2\eta_2 \frac{\partial \mathbf{v}_2}{\partial z} \text{ at } z = 0, \tag{3.8}$$

see Eqs. (S.69), (S.211) in the Supplementary Material S. In order to remove the unknown pressures from the dynamic boundary condition, we take the vector product of Eq. (3.8) with $\mathbf{e}_z$ and obtain

$$\eta_1 \frac{\partial \mathbf{v}_1}{\partial z} \times \mathbf{e}_z = \eta_2 \frac{\partial \mathbf{v}_2}{\partial z} \times \mathbf{e}_z \text{ at } z = 0, \tag{3.9}$$

Finally, the physical values of $\mathbf{v}_m, \ m = 1, 2$, and $p_m, \ m = 1, 2$, vanish at large distances from the particle, i.e.

$$\lim_{\rho \to \infty} \mathbf{v}_m = \mathbf{0}, \ \lim_{\rho \to \infty} p_m = 0, \ m = 1, 2, \tag{3.10}$$

where ρ denotes the length of the radius vector and it is computed as follows:

$$\rho = \sqrt{x^2 + y^2 + z^2}. \tag{3.11}$$

3.3 Exact solution of the problem

Let us introduce a cylindrical coordinate system r, φ, and z with center, coinciding with the center of the three-phase contact line, and unit basis vectors $\mathbf{e}_r$, $\mathbf{e}_\varphi$ and $\mathbf{e}_z$ (see Fig. 3.1). In the considered coordinate system, the exact solution of the Stokes problem (3.1) and (3.2) with boundary conditions (3.3) and (3.10), which describes the movement of a particle in an unbounded fluid m of viscosity η_m, is

$$\begin{aligned} v_{mr}^{st} = {} & \frac{3V}{4} \cdot \frac{R^3 (z - R\cos\alpha)^2 \sin\varphi}{\left[r^2 + (z - R\cos\alpha)^2 \right]^{5/2}} - \frac{3V}{4} \cdot \frac{R (z - R\cos\alpha)^2 \sin\varphi}{\left[r^2 + (z - R\cos\alpha)^2 \right]^{3/2}} \\ & - \frac{V}{2} \cdot \frac{R^3 \sin\varphi}{\left[r^2 + (z - R\cos\alpha)^2 \right]^{3/2}} + \frac{3V}{2} \cdot \frac{R \sin\varphi}{\left[r^2 + (z - R\cos\alpha)^2 \right]^{1/2}}, \ m = 1, 2, \end{aligned} \tag{3.12}$$

$$v_{m\varphi}^{st} = \frac{V}{4} \cdot \frac{R^3 \cos\varphi}{\left[r^2 + (z - R\cos\alpha)^2 \right]^{3/2}} + \frac{3V}{4} \cdot \frac{R \cos\varphi}{\left[r^2 + (z - R\cos\alpha)^2 \right]^{1/2}}, \ m = 1, 2, \tag{3.13}$$

$$v_{mz}^{st} = -\frac{3V}{4} \cdot \frac{R^3 r (z - R\cos\alpha) \sin\varphi}{\left[r^2 + (z - R\cos\alpha)^2 \right]^{5/2}} + \frac{3V}{4} \cdot \frac{R r (z - R\cos\alpha) \sin\varphi}{\left[r^2 + (z - R\cos\alpha)^2 \right]^{3/2}}, \ m = 1, 2, \tag{3.14}$$

$$p_m^{st} = \frac{3V\eta_m}{2R} \cdot \frac{R^2 r \sin\varphi}{\left[r^2 + (z - R\cos\alpha)^2 \right]^{3/2}}, \ m = 1, 2, \tag{3.15}$$

see [3.12]. For three-phase contact angle $\alpha = 90°$, i.e. the center of the coordinate system coincides with the center of the particle, one gets

$$v_{mr}^{st} = -\frac{3V}{4} \cdot \frac{Rz^2 \sin\varphi}{\left(r^2+z^2\right)^{3/2}} \left(1 - \frac{R^2}{r^2+z^2}\right) + \frac{V}{2} \cdot \frac{R\sin\varphi}{\left(r^2+z^2\right)^{1/2}} \left(\frac{1}{3} - \frac{R^2}{r^2+z^2}\right), \tag{3.16}$$

$$v_{m\varphi}^{st} = \frac{V}{4} \cdot \frac{R^3 \cos\varphi}{\left(r^2+z^2\right)^{3/2}} + \frac{3V}{4} \cdot \frac{R\cos\varphi}{\left(r^2+z^2\right)^{1/2}}, \tag{3.17}$$

$$v_{mz}^{st} = -\frac{3V}{4} \cdot \frac{R^3 rz \sin\varphi}{\left(r^2+z^2\right)^{5/2}} + \frac{3V}{4} \cdot \frac{Rrz\sin\varphi}{\left(r^2+z^2\right)^{3/2}}, \tag{3.18}$$

$$p_m^{st} = \frac{3V\eta_m}{2R} \cdot \frac{R^2 r \sin\varphi}{\left(r^2+z^2\right)^{3/2}}, \tag{3.19}$$

for both phases. Note that these equations give the exact solution of our problem both for equal or different viscosities of the fluid phases in the case of $\alpha = 90°$. We shall prove this statement in the next lines. First, the kinematic boundary conditions (3.4) hold true. Second, the dynamic boundary condition (3.9) acquires the form:

$$\eta_1 \left(- \mathbf{e}_\varphi \frac{\partial v_{1r}}{\partial z}\bigg|_{z=0} + \mathbf{e}_r \frac{\partial v_{1\varphi}}{\partial z}\bigg|_{z=0} \right) = \eta_2 \left(-\mathbf{e}_\varphi \frac{\partial v_{2r}}{\partial z}\bigg|_{z=0} + \mathbf{e}_r \frac{\partial v_{2\varphi}}{\partial z}\bigg|_{z=0} \right). \tag{3.20}$$

Due to the facts

$$\frac{\partial v_{mr}}{\partial z}\bigg|_{z=0} = 0, \ \frac{\partial v_{m\varphi}}{\partial z}\bigg|_{z=0} = 0, \ m = 1,2, \tag{3.21}$$

we conclude that the dynamic boundary condition (3.9) holds true.

3.4 Dimensionless formulation of the problem

The dimensionless form of the problem is obtained by introducing the following new variables:

$$\overline{x} = \frac{x}{r_c}, \ \overline{y} = \frac{y}{r_c}, \ \overline{z} = \frac{z}{r_c}, \ \overline{\rho} = \frac{\rho}{r_c}, \ \overline{\nabla} = r_c \nabla, \ \overline{\nabla}^2 = r_c^2 \nabla^2, \tag{3.22}$$

$$\overline{\mathbf{v}}_m = \frac{\mathbf{v}_m}{V}, \ \overline{p}_m = \frac{r_c p_m}{\eta_m V}, \ \mu_m = \frac{\eta_m}{\eta_1 + \eta_2}, \ m = 1,2. \tag{3.23}$$

Then, by substituting Eqs. (3.22) and (3.23) in the considered problem (3.1)– (3.4) and (3.9), we obtain the respective Stokes problem

$$\overline{\nabla} \cdot \overline{\mathbf{v}}_m = 0, \ m = 1,2, \tag{3.24}$$

$$\overline{\nabla} \overline{p}_m = \overline{\nabla}^2 \overline{\mathbf{v}}_m, \ m = 1,2, \tag{3.25}$$

with the following boundary conditions:

- no-slip boundary conditions:

$$\overline{\mathbf{v}}_m = \mathbf{e}_y \text{ at } S_\mathrm{p}, \ m = 1,2; \tag{3.26}$$

- kinematic boundary conditions:

$$\overline{\mathbf{v}}_1 = \overline{\mathbf{v}}_2,\ \overline{\mathbf{v}}_1 \cdot \mathbf{e}_z = 0,\ \overline{\mathbf{v}}_2 \cdot \mathbf{e}_z = 0 \text{ at } \overline{z} = 0; \tag{3.27}$$

- dynamic boundary conditions:

$$\mu_1 \frac{\partial \overline{\mathbf{v}}_1}{\partial \overline{z}} \times \mathbf{e}_z = \mu_2 \frac{\partial \overline{\mathbf{v}}_2}{\partial \overline{z}} \times \mathbf{e}_z \text{ at } \overline{z} = 0; \tag{3.28}$$

- boundary conditions at infinity:

$$\lim_{\overline{\rho} \to \infty} \overline{\mathbf{v}}_m = \mathbf{0},\ \lim_{\overline{\rho} \to \infty} \overline{p}_m = 0,\ m = 1, 2. \tag{3.29}$$

For simplicity of notations, we shall skip the bars in the subsequent computations.

3.5 Transforming the model in a convenient form for numerical modelling

In the current section, we transform the model in a form, which is convenient for numerical modelling (see Fig. 3.2). First, the problem is reformulated, using the gauge method. The main idea of the method is to transform the original system, which consists of six second-order and two first-order partial differential equations, to a system of eight elliptic partial differential equations. Secondly, we simplify the 3D problem to the 2D one, taking into account the fact that the considered problem contains only the first mode with respect to the Fourier transform. Next, the partial differential equations in the system are uncoupled by introducing new variables. Finally, a modification of the toroidal coordinates is used in order to transform the complex geometry of the problem into rectangles.

3.5.1 Gauge formulation of the problem

Solving the Navier–Stokes equations (and in particular the Stokes equations) is not a straight-forward task. In support of this thesis, Langtangen and coworkers [3.13] described the main issues that arise from using a naive approach for this problem and the most common numerical strategies to solve the problem. Generally speaking, the main challenge is to maintain the incompressibility constraint during the iterative processes [3.14]. In order to solve this issue, we use the gauge formulation of the problem [3.15, 3.16], which introduces a vector, $\mathbf{w}_m$, and a scalar, ξ_m, potentials by using the following definition:

$$\mathbf{v}_m = \mathbf{w}_m - \nabla \xi_m,\ m = 1, 2. \tag{3.30}$$

The substitution of the expression for the vector $\mathbf{v}_m$ (3.30) into the continuity equation (3.24) leads to the Poisson equation

$$\nabla^2 \xi_m = \nabla \cdot \mathbf{w}_m,\ m = 1, 2, \tag{3.31}$$

and into the momentum balance equation (3.25) — to the following:

$$\nabla p_m = \nabla^2 \mathbf{v}_m = \nabla^2 \left(\mathbf{w}_m - \nabla \xi_m\right) = \nabla^2 \mathbf{w}_m - \nabla^2 (\nabla \xi_m),\ m = 1, 2, \tag{3.32}$$

$$\nabla^2 \mathbf{w}_m = \nabla (p_m + \nabla^2 \xi_m),\ m = 1, 2. \tag{3.33}$$

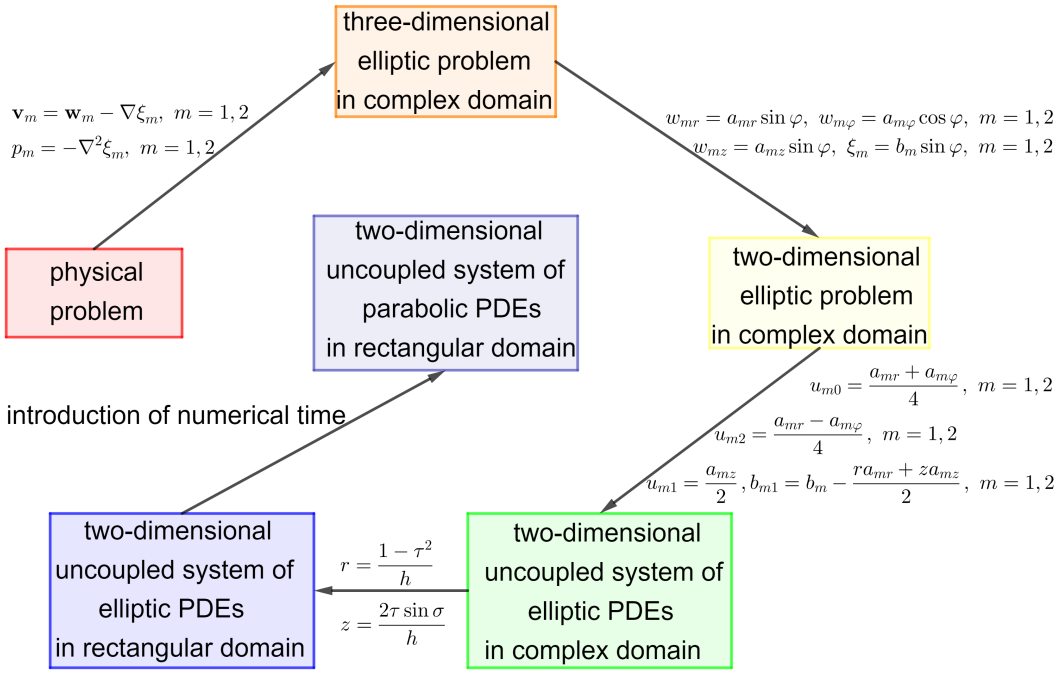

Figure 3.2: Schematic representation of the transformations, which are applied to the considered problem

Taking into account that the definition (3.30) introduces four new variables and gives only three equations between them, one adds the constraint

$$p_m = -\nabla^2\xi_m,\ m = 1,2, \tag{3.34}$$

which leads to a significant simplification of the momentum balance equation:

$$\nabla^2\mathbf{w}_m = 0,\ m = 1,2. \tag{3.35}$$

Thus, the Stokes problem (3.24), (3.25) is reduced to a well-defined system of elliptic partial differential equations (3.31), (3.35). Moreover, the vector equation (3.35) could be solved separately and, then, one could obtain ξ_m from Eq. (3.31). Finally, one obtains $\mathbf{v}_m$ and p_m, using (3.30) and (3.34). The main disadvantage of the gauge method is that the reformulation of the problem increases the number of degrees of freedom and additional self-consistent boundary conditions for the vector and scalar potential have to be added to the problem. In our case, we specify the following additional boundary conditions:

$$\xi_m = 0 \text{ at } S_p,\ m = 1,2, \tag{3.36}$$

$$\xi_1 = \xi_2,\ \mu_1\frac{\partial\xi_1}{\partial z} = \mu_2\frac{\partial\xi_2}{\partial z} \text{ at } z = 0. \tag{3.37}$$

Note that Eq. (3.36) has already been used in the literature [3.15], while Eq. (3.37) is original to our knowledge. Moreover, the boundary conditions match the physical picture and they simplify significantly the form of the kinematic and dynamic boundary conditions

in cylindrical coordinates, see Eqs. (3.44)–(3.45). This formulation of the problem has two important advantages from numerical viewpoint. First, the problem consists of eight elliptic partial differential equations with well-defined boundary conditions. Second, all vector and scalar potentials are regular functions of r and z in the closed numerical domains, including the three-phase contact line. The pressure functions is possible to have weak singularities at the three-phase contact line for some values of the central angles and viscosities, while the vector and scalar potentials do not.

3.5.2 From three-dimensional to two-dimensional problem

Next, we introduce a cylindrical coordinate system r, φ, and z with unit basis vectors $\mathbf{e}_r$, $\mathbf{e}_\varphi$ and $\mathbf{e}_z$ (see Fig. 3.1). In it, the problem in terms of vector and scalar potentials, Eqs. (3.31), (3.35), has the following coordinate form:

$$\frac{1}{r}\frac{\partial}{\partial r}\left(r\frac{\partial w_{mr}}{\partial r}\right)+\frac{1}{r^2}\frac{\partial^2 w_{mr}}{\partial \varphi^2}+\frac{\partial^2 w_{mr}}{\partial z^2}-\frac{2}{r^2}\frac{\partial w_{m\varphi}}{\partial \varphi}-\frac{w_{mr}}{r^2}=0,\ m=1,2, \tag{3.38}$$

$$\frac{1}{r}\frac{\partial}{\partial r}\left(r\frac{\partial w_{m\varphi}}{\partial r}\right)+\frac{1}{r^2}\frac{\partial^2 w_{m\varphi}}{\partial \varphi^2}+\frac{\partial^2 w_{m\varphi}}{\partial z^2}+\frac{2}{r^2}\frac{\partial w_{mr}}{\partial \varphi}-\frac{w_{m\varphi}}{r^2}=0,\ m=1,2, \tag{3.39}$$

$$\frac{1}{r}\frac{\partial}{\partial r}\left(r\frac{\partial w_{mz}}{\partial r}\right)+\frac{1}{r^2}\frac{\partial^2 w_{mz}}{\partial \varphi^2}+\frac{\partial^2 w_{mz}}{\partial z^2}=0,\ m=1,2, \tag{3.40}$$

$$\frac{1}{r}\frac{\partial}{\partial r}\left(r\frac{\partial \xi_m}{\partial r}\right)+\frac{1}{r^2}\frac{\partial^2 \xi_m}{\partial \varphi^2}+\frac{\partial^2 \xi_m}{\partial z^2}=\frac{1}{r}\frac{\partial\left(r w_{mr}\right)}{\partial r}+\frac{1}{r}\frac{\partial w_{m\varphi}}{\partial \varphi}+\frac{\partial w_{mz}}{\partial z},\ m=1,2, \tag{3.41}$$

see Eqs. (S.350)– (S.352) in the Supplementary Material S. Next, we obtain the form of the boundary conditions in cylindrical coordinates as follows:

- **No-slip boundary conditions.** For the no-slip boundary conditions (3.26), one gets

$$\sin\varphi\mathbf{e}_r+\cos\varphi\mathbf{e}_\varphi=\mathbf{v}_m=\mathbf{w}_m-\nabla\xi_m,\ m=1,2, \tag{3.42}$$

  see Eqs. (3.30), (S.342) –(S.344) in the Supplementary Material S. Then, the coordinate form of Eq. (3.42) is

$$w_{mr}-\frac{\partial \xi_m}{\partial r}=\sin\varphi,\ w_{m\varphi}-\frac{1}{r}\frac{\partial \xi_m}{\partial \varphi}=\cos\varphi,\ w_{mz}-\frac{\partial \xi_m}{\partial z}=0,\ m=1,2, \tag{3.43}$$

  see Eq. (S.348) in Supplementary material S.

- **Kinematic boundary conditions.** Using Eq. (3.30), the kinematic boundary condition $\mathbf{v}_1=\mathbf{v}_2$, see Eq. (3.27), acquires the form

$$\mathbf{w}_1-\nabla\xi_1=\mathbf{w}_2-\nabla\xi_2. \tag{3.44}$$

  Then, one gets the form of the kinematic boundary conditions along the r direction:

$$w_{1r}=w_{1r}-\frac{\partial \xi_1}{\partial r}=w_{2r}-\frac{\partial \xi_2}{\partial r}=w_{2r}, \tag{3.45}$$

  see Eq. (3.37). Analogously, the kinematic boundary conditions along the φ- and $z-$ directions acquire the form

$$w_{1\varphi}=w_{2\varphi},\ w_{1z}-\frac{\partial \xi_1}{\partial z}=0,\ w_{2z}-\frac{\partial \xi_2}{\partial z}=0 \text{ at } z=0, \tag{3.46}$$

  see Eq. (3.27).

- **Dynamic boundary conditions.** First, we simplify the expression $\frac{\partial \mathbf{v}_m}{\partial z} \times \mathbf{e}_z$ as follows:

$$\frac{\partial \mathbf{v}_m}{\partial z} \times \mathbf{e}_z = -\frac{\partial v_{mr}}{\partial z}\mathbf{e}_\varphi + \frac{\partial v_{m\varphi}}{\partial z}\mathbf{e}_r$$
$$= -\left(\frac{\partial w_{mr}}{\partial z} - \frac{\partial^2 \xi_m}{\partial r \partial z}\right)\mathbf{e}_\varphi + \left(\frac{\partial w_{m\varphi}}{\partial z} - \frac{1}{r}\frac{\partial^2 \xi_m}{\partial \varphi \partial z}\right)\mathbf{e}_r,\ m = 1, 2, \quad (3.47)$$

see Eqs. (3.30), (S.348). Using Eqs. (3.9), (3.37), (3.47), we obtain the following coordinate form of the dynamic boundary conditions (3.9):

$$\mu_1 \frac{\partial w_{1r}}{\partial z} = \mu_2 \frac{\partial w_{2r}}{\partial z},\ \mu_1 \frac{\partial w_{1\varphi}}{\partial z} = \mu_2 \frac{\partial w_{2\varphi}}{\partial z}. \quad (3.48)$$

- **Boundary conditions at infinity.** From the Stokes solution (3.12)– (3.15), one obtains the following expressions for the dimensionless gauge scalar and vector potentials:

$$w_{mr}^{st} = -\frac{3}{2\sin^3\alpha}\frac{(z-\cot\alpha)^2 \sin\varphi}{[r^2+(z-\cot\alpha)^2]^{5/2}} + \frac{1}{\sin^3\alpha}\frac{\sin\varphi}{[r^2+(z-\cot\alpha)^2]^{3/2}}$$
$$+ \frac{3}{2\sin\alpha}\frac{\sin\varphi}{[r^2+(z-\cot\alpha)^2]^{1/2}}, \quad (3.49)$$
$$w_{m\varphi}^{st} = -\frac{1}{2\sin^3\alpha}\frac{\cos\varphi}{[r^2+(z-\cot\alpha)^2]^{3/2}} + \frac{3}{2\sin\alpha}\frac{\cos\varphi}{[r^2+(z-\cot\alpha)^2]^{1/2}}, \quad (3.50)$$
$$w_{mz}^{st} = \frac{3}{2\sin^3\alpha}\frac{r(z-\cot\alpha)\sin\varphi}{[r^2+(z-\cot\alpha)^2]^{5/2}}, \quad (3.51)$$
$$\xi_m^{st} = \frac{3}{4\sin\alpha}\frac{r\sin\varphi}{[r^2+(z-\cot\alpha)^2]^{1/2}} - \frac{3}{4\sin^3\alpha}\frac{r\sin\varphi}{[r^2+(z-\cot\alpha)^2]^{3/2}} \quad (3.52)$$

for both phases ($m = 1, 2$). Note that the vector potential vanishes at large distances from the particle surface, while the scalar potential has the following finite value:

$$\xi_m^{st} \to \frac{3\sin\varphi}{4\sin\alpha} \text{ at } r \to \infty \text{ and } z = const,\ m = 1, 2. \quad (3.53)$$

- **Additional boundary conditions.** The additional boundary conditions have the same form as Eqs. (3.36), (3.37).

In cylindrical coordinates (r, φ, z), the Fourier expansion of the solution with respect to the polar angle, φ, contains only the first Fourier mode [3.1, 3.11]. Thus, the components of the vector and scalar potentials can be presented as

$$w_{mr} = a_{mr}(r, z)\sin\varphi,\ w_{m\varphi} = a_{m\varphi}(r, z)\cos\varphi,\ m = 1, 2, \quad (3.54)$$
$$w_{mz} = a_{mz}(r, z)\sin\varphi,\ \xi_m = b_m(r, z)\sin\varphi,\ m = 1, 2, \quad (3.55)$$

where a_{mr}, $a_{m\varphi}$, a_{mz} and b_m are the amplitudes of the Fourier modes of the general solution. Therefore, the three-dimensional problem is reduced to the following two-dimensional system

of eight partial differential equations in cylindrical coordinates:

$$\frac{1}{r}\frac{\partial}{\partial r}\left(r\frac{\partial a_{mr}}{\partial r}\right)+\frac{\partial^2 a_{mr}}{\partial z^2}-\frac{2a_{mr}}{r^2}+\frac{2a_{m\varphi}}{r^2}=0,\ m=1,2, \tag{3.56}$$

$$\frac{1}{r}\frac{\partial}{\partial r}\left(r\frac{\partial a_{m\varphi}}{\partial r}\right)+\frac{\partial^2 a_{m\varphi}}{\partial z^2}+\frac{2a_{mr}}{r^2}-\frac{2a_{m\varphi}}{r^2}=0,\ m=1,2, \tag{3.57}$$

$$\frac{1}{r}\frac{\partial}{\partial r}\left(r\frac{\partial a_{mz}}{\partial r}\right)+\frac{\partial^2 a_{mz}}{\partial z^2}-\frac{a_{mz}}{r^2}=0,\ m=1,2, \tag{3.58}$$

$$\frac{1}{r}\frac{\partial}{\partial r}\left(r\frac{\partial b_{m}}{\partial r}\right)+\frac{\partial^2 b_{m}}{\partial z^2}-\frac{b_m}{r^2}=\frac{1}{r}\frac{\partial}{\partial r}(ra_{mr})-\frac{a_{m\varphi}}{r}+\frac{\partial a_{mz}}{\partial z},\ m=1,2. \tag{3.59}$$

The system is closed with the respective boundary conditions for the amplitudes of the first Fourier modes, i.e.

- **Boundary conditions at the particle surface (see Eqs.** (3.43) **and** (3.36)**):**

$$a_{mr}-\frac{\partial b_m}{\partial r}=1,\ a_{mz}-\frac{\partial b_m}{\partial z}=0 \text{ at } S_p,\ m=1,2, \tag{3.60}$$

$$b_m=0,\ a_{m\varphi}=a_{m\varphi}-\frac{b_m}{r}=1 \text{ at } S_p,\ m=1,2; \tag{3.61}$$

- **Kinematic boundary conditions and condition for equality of the scalar potentials at the fluid–fluid interface (see Eqs.** (3.45)**,** (3.46) **and** (3.37)**):**

$$a_{1r}=a_{2r},\ a_{1\varphi}=a_{2\varphi},\ b_1=b_2 \text{ at } z=0, \tag{3.62}$$

$$a_{mz}-\frac{\partial b_m}{\partial z}=0 \text{ at } z=0,\ m=1,2; \tag{3.63}$$

- **Dynamic boundary conditions and condition for the derivatives of the scalar potentials at the fluid–fluid interface (see Eqs.** (3.48) **and** (3.37)**):**

$$\mu_1\frac{\partial a_{1r}}{\partial z}=\mu_2\frac{\partial a_{2r}}{\partial z},\ \mu_1\frac{\partial a_{1\varphi}}{\partial z}=\mu_2\frac{\partial a_{2\varphi}}{\partial z},\ \mu_1\frac{\partial b_1}{\partial z}=\mu_2\frac{\partial b_2}{\partial z} \text{ at } z=0. \tag{3.64}$$

- **Boundary conditions at infinity:** Vector potentials vanish at large distances from the particle surface, while the following relation:

$$b_m^{st}\to\frac{3}{4\sin\alpha} \text{ at } r\to\infty \text{ and } z=const,\ m=1,2. \tag{3.65}$$

  holds for the scalar potentials.

3.5.3 Uncoupling the bulk equations of the problem

From numerical viewpoint, it is convenient to uncouple the bulk equations of the considered PDE system (3.56)–(3.59). Obviously, the third equation in the system, Eq. (3.58), is not related to the others. Next, adding Eqs. (3.56), (3.57), one gets

$$\frac{1}{r}\frac{\partial}{\partial r}\left[r\frac{\partial\left(a_{mr}+a_{m\varphi}\right)}{\partial r}\right]+\frac{\partial^2\left(a_{mr}+a_{m\varphi}\right)}{\partial z^2}=0,\ m=1,2. \tag{3.66}$$

Analogously, subtracting Eq. (3.57) from Eq. (3.56), the following equation

$$\frac{1}{r}\frac{\partial}{\partial r}\left[r\frac{\partial\left(a_{mr}-a_{m\varphi}\right)}{\partial r}\right]+\frac{\partial^2\left(a_{mr}-a_{m\varphi}\right)}{\partial z^2}-\frac{4}{r^2}\left(a_{mr}-a_{m\varphi}\right)=0,\ m=1,2 \tag{3.67}$$

holds true. Next, we shall reformulate Eq. (3.59) in two steps. First, we revise the first two terms of the right hand side of Eq. (3.59) as follows:

$$\begin{aligned}\frac{1}{r}\frac{\partial}{\partial r}(ra_{mr})-\frac{a_{m\varphi}}{r}&=\frac{a_{mr}}{r}-\frac{a_{m\varphi}}{r}+\frac{\partial a_{mr}}{\partial r}=\frac{1}{2}\left[\frac{\partial}{\partial r}\left(r\frac{\partial a_{mr}}{\partial r}\right)+\frac{\partial^2\left(ra_{mr}\right)}{\partial z^2}\right]+\frac{\partial a_{mr}}{\partial r}\\&=\frac{1}{2}\left\{\frac{\partial}{\partial r}\left[\frac{\partial(ra_{mr})}{\partial r}-a_{mr}\right]+\frac{\partial^2\left(ra_{mr}\right)}{\partial z^2}\right\}+\frac{\partial a_{mr}}{\partial r}\\&=\frac{1}{2}\left\{\frac{r}{r}\frac{\partial}{\partial r}\left[\frac{\partial(ra_{mr})}{\partial r}\right]+\frac{\partial^2\left(ra_{mr}\right)}{\partial z^2}\right\}+\frac{1}{2}\frac{\partial a_{mr}}{\partial r}\\&=\frac{1}{2}\left\{\frac{1}{r}\frac{\partial}{\partial r}\left[r\frac{\partial(ra_{mr})}{\partial r}\right]-\frac{1}{r}\frac{\partial(ra_{mr})}{\partial r}+\frac{\partial^2\left(ra_{mr}\right)}{\partial z^2}\right\}+\frac{1}{2}\frac{\partial a_{mr}}{\partial r}\\&=\frac{1}{2}\left\{\frac{1}{r}\frac{\partial}{\partial r}\left[r\frac{\partial(ra_{mr})}{\partial r}\right]+\frac{\partial^2\left(ra_{mr}\right)}{\partial z^2}-\frac{ra_{mr}}{r^2}\right\},\ m=1,2,\end{aligned} \tag{3.68}$$

see Eq. (3.56). Second, we find an appropriate expression for the last term in the right hand side of Eq. (3.59):

$$\begin{aligned}\frac{\partial a_{mz}}{\partial z}&=\frac{z}{2}\left[\frac{1}{r}\frac{\partial}{\partial r}\left(r\frac{\partial a_{mz}}{\partial r}\right)+\frac{\partial^2 a_{mz}}{\partial z^2}-\frac{a_{mz}}{r^2}\right]+\frac{\partial a_{mz}}{\partial z}\\&=\frac{1}{2}\left\{\frac{1}{r}\frac{\partial}{\partial r}\left[r\frac{\partial\left(za_{mz}\right)}{\partial r}\right]+z\frac{\partial^2 a_{mz}}{\partial z^2}-\frac{a_{mz}z}{r^2}\right\}+\frac{\partial a_{mz}}{\partial z}\\&=\frac{1}{2}\left\{\frac{1}{r}\frac{\partial}{\partial r}\left[r\frac{\partial\left(za_{mz}\right)}{\partial r}\right]+\frac{\partial}{\partial z}\left(z\frac{\partial a_{mz}}{\partial z}\right)-\frac{\partial a_{mz}}{\partial z}-\frac{za_{mz}}{r^2}\right\}+\frac{\partial a_{mz}}{\partial z}\\&=\frac{1}{2}\left\{\frac{1}{r}\frac{\partial}{\partial r}\left[r\frac{\partial\left(za_{mz}\right)}{\partial r}\right]+\frac{\partial^2\left(za_{mz}\right)}{\partial z^2}-2\frac{\partial a_{mz}}{\partial z}-\frac{za_{mz}}{r^2}\right\}+\frac{\partial a_{mz}}{\partial z}\\&=\frac{1}{2}\left\{\frac{1}{r}\frac{\partial}{\partial r}\left[r\frac{\partial\left(za_{mz}\right)}{\partial r}\right]+\frac{\partial^2\left(za_{mz}\right)}{\partial z^2}-\frac{za_{mz}}{r^2}\right\},\ m=1,2,\end{aligned} \tag{3.69}$$

using Eq. (3.58). Substituting Eqs. (3.68), (3.69) in (3.59), we obtain

$$\begin{aligned}\frac{1}{r}\frac{\partial}{\partial r}\left[r\frac{\partial}{\partial r}\left(b_m-\frac{ra_{mr}}{2}-\frac{za_{mz}}{2}\right)\right]+\frac{\partial^2}{\partial z^2}\left(b_m-\frac{ra_{mr}}{2}-\frac{za_{mz}}{2}\right)\\-\frac{2b_m-ra_{mr}-za_{mz}}{2r^2}=0,\ m=1,2.\end{aligned} \tag{3.70}$$

Then, instead of solving Eqs. (3.56), (3.57), (3.58) and (3.59) with respect to a_{mr}, $a_{m\varphi}$, a_{mz} and b_m, one could obtain the solution of the problem by solving Eqs. (3.66), (3.67), (3.58) and (3.70) with respect to the following new variables:

$$u_{m0}=\frac{1}{4}(a_{mr}+a_{m\varphi}),\ u_{m1}=\frac{1}{2}a_{mz},\ u_{m2}=\frac{1}{4}(a_{mr}-a_{m\varphi}),\ m=1,2, \tag{3.71}$$

$$b_{m1}=b_m-\frac{1}{2}\left(ra_{mr}+za_{mz}\right),\ m=1,2. \tag{3.72}$$

Using the new variables (3.71) and (3.72), the problem is considerably simplify to the following homogeneous system of uncoupled partial differential equations:

$$L_0[u_{m0}] = 0, L_1[u_{m1}] = 0, L_2[u_{m2}] = 0, L_1[b_{m1}] = 0,\ m = 1, 2, \tag{3.73}$$

where the dimensionless Laplace operators L_n have the following form:

$$L_n[u] = \frac{1}{r}\frac{\partial}{\partial r}\left(r\frac{\partial u}{\partial r}\right) + \frac{\partial^2 u}{\partial z^2} - \frac{n^2 u}{r^2},\ n = 0, 1, 2. \tag{3.74}$$

Using the inverse transformations

$$a_{mr} = 2(u_{m0} + u_{m2}),\ a_{m\varphi} = 2(u_{m0} - u_{m2}),\ a_{mz} = 2u_{m1},\ m = 1, 2, \tag{3.75}$$

$$b_m = b_{m1} + r\,(u_{m0} + u_{m2}) + zu_{m1},\ m = 1, 2, \tag{3.76}$$

one obtains the boundary conditions of the problem in the terms of the new variables:

- **Boundary conditions at the particle surface (see Eqs.** (3.60) **and** (3.61)**):**

$$2\,(u_{m0} + u_{m2}) - \frac{\partial}{\partial r}\left[b_{m1} + r\,(u_{m0} + u_{m2}) + zu_{m1}\right] = 1 \text{ at } S_p,\ m = 1, 2, \tag{3.77}$$

$$2u_{m1} - \frac{\partial}{\partial z}\left[b_{m1} + r\,(u_{m0} + u_{m2}) + zu_{m1}\right] = 0 \text{ at } S_p,\ m = 1, 2, \tag{3.78}$$

$$u_{m0} - u_{m2} = \frac{1}{2},\ b_{m1} + r\,(u_{m0} + u_{m2}) + zu_{m1} = 0 \text{ at } S_p,\ m = 1, 2; \tag{3.79}$$

- **Kinematic boundary conditions and condition for equality of the scalar potentials at the fluid–fluid interface** $z = 0$**.** Substituting Eq. (3.75) in the kinematic boundary conditions (3.62), one obtains

$$u_{10} + u_{12} = u_{20} + u_{22} \text{ at } z = 0, \tag{3.80}$$

$$u_{10} - u_{12} = u_{20} - u_{22} \text{ at } z = 0. \tag{3.81}$$

  Adding Eq. (3.80) to Eq. (3.81) and subtracting Eq. (3.81) from Eq. (3.80), we conclude that

$$u_{10} = u_{20},\ u_{12} = u_{22} \text{ at } z = 0. \tag{3.82}$$

  Next, one obtains the form of the boundary condition $b_1 = b_2$ at $z = 0$:

$$b_{11} + r\,(u_{10} + u_{12}) = b_{21} + r\,(u_{20} + u_{22}) \text{ at } z = 0, \tag{3.83}$$

$$b_{11} = b_{21} \text{ at } z = 0,\ m = 1, 2, . \tag{3.84}$$

  see Eqs. (3.62) and (3.82). Finally, we conclude that the boundary condition Eq. (3.63) is transformed as

$$u_{m1} - \frac{\partial b_{m1}}{\partial z} - r\frac{\partial}{\partial z}\,(u_{m0} + u_{m2}) = 0 \text{ at } z = 0,\ m = 1, 2, \tag{3.85}$$

  using the derivative $\partial b_m/\partial z$ at $z = 0$:

$$\frac{\partial b_m}{\partial z} = \frac{\partial b_{m1}}{\partial z} + r\frac{\partial}{\partial z}\,(u_{m0} + u_{m2}) + u_{m1} \text{ at } z = 0. \tag{3.86}$$

- **Dynamic boundary conditions and condition for the derivatives of the scalar potentials at the fluid–fluid interface.** Analogously to the derivation of the kinematic boundary conditions (3.62), we obtain the following form of the dynamic boundary conditions in the terms of the new variables:

$$\mu_1 \frac{\partial u_{10}}{\partial z} = \mu_2 \frac{\partial u_{20}}{\partial z},\ \mu_1 \frac{\partial u_{12}}{\partial z} = \mu_2 \frac{\partial u_{22}}{\partial z} \text{ at } z = 0. \tag{3.87}$$

Finally, we write the additional condition for the derivatives of scalar potentials in terms of the new variables

$$\mu_1 \frac{\partial b_{11}}{\partial z} + \mu_1 u_{11} = \mu_2 \frac{\partial b_{21}}{\partial z} + \mu_2 u_{21} \text{ at } z = 0, \tag{3.88}$$

see Eqs. (3.87) and (3.86). Using Eqs. (3.75), (3.63) and (3.64), we conclude that

$$2\mu_1 u_{11} = \mu_1 a_{1z} = \mu_1 \frac{\partial b_1}{\partial z} = \mu_2 \frac{\partial b_2}{\partial z} = \mu_2 a_{2z} = 2\mu_2 u_{21} \text{ at } z = 0. \tag{3.89}$$

Then, the boundary condition (3.64) acquires the form:

$$\mu_1 \frac{\partial b_{11}}{\partial z} = \mu_2 \frac{\partial b_{21}}{\partial z} \text{ at } z = 0, \tag{3.90}$$

see Eqs. (3.88) and (3.89).

- **Boundary conditions at infinity:** Potentials vanish at large distances from the particle surface because

$$b_{m1}^{st} = \lim_{r\to\infty} b_{m1} = \lim_{r\to\infty} \left[b_m - \frac{1}{2}\left(\frac{r w_{mr}}{\sin\varphi} + z \frac{w_{mz}}{\sin\varphi} \right) \right] = \frac{3}{4\sin\alpha} - \frac{3}{4\sin\alpha} = 0, \tag{3.91}$$

see Eqs. (3.49), (3.51) and (3.65).

3.5.4 Formulation of the problem in toroidal coordinates

To construct an efficient numerical scheme, the complex geometry of the problem (Fig. 3.3) is transformed into rectangles (Fig. 3.4), introducing modified toroidal coordinates τ and σ as follows:

$$r = \frac{1-\tau^2}{h},\ z = \frac{2\tau \sin\sigma}{h}, \tag{3.92}$$

where $h(\tau, \sigma) = 1 + \tau^2 - 2\tau\cos\sigma$ is the normalized metric coefficient (see Section S.5.5).

The axis of revolution corresponds to $\tau = 1$ and the three-phase contact line — to the pole, A_+, where $\tau = 0$. The position of the fluid–fluid interface in toroidal coordinates is described by the equation $\sigma = 0$, while that of the particle surface — by $\sigma = \alpha_m,\ m = 1, 2$, where α_m is defined as

$$\alpha_m = \begin{cases} \alpha, & \text{at the upper part of the particle,} \\ \alpha - \pi, & \text{at the lower part of the particle.} \end{cases}, \tag{3.93}$$

see Fig. 3.1. The derivatives of the toroidal coordinates with respect to the radial and

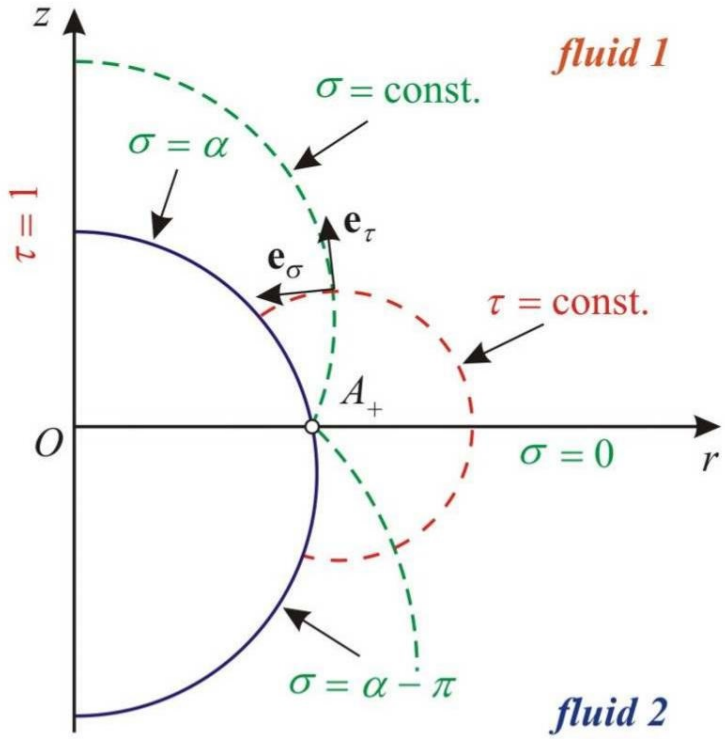

Figure 3.3: Toroidal coordinate τ and σ, which are convenient for numerical calculations. The position of the contact line coincides with the pole, A_+; the fluid-fluid interface corresponds to $\sigma = 0$, the upper particle surface — to $\sigma = \alpha$, and the lower one — to $\sigma = \alpha - \pi$.

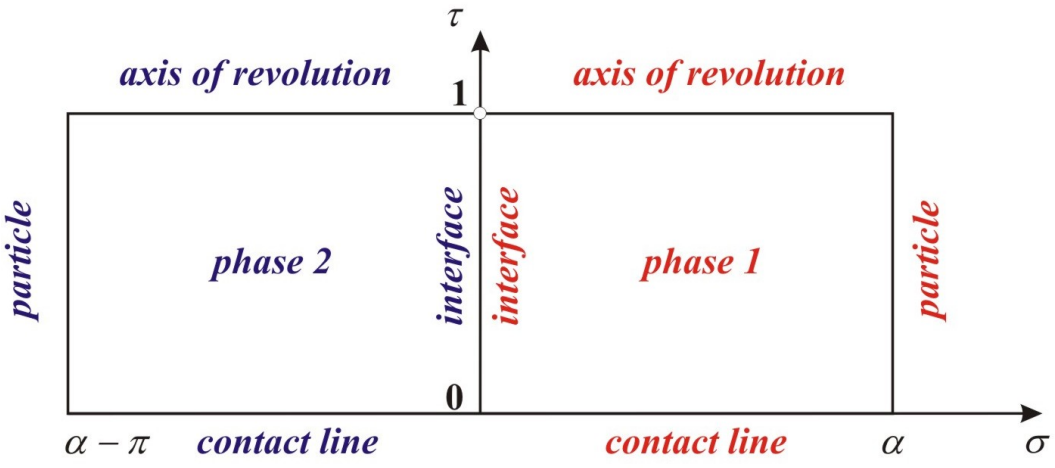

Figure 3.4: Rectangular numerical domain in toroidal coordinates.

vertical coordinates are

$$\frac{\partial\sigma}{\partial r} = -\frac{(1-\tau^2)\sin\sigma}{2\tau}, \qquad \frac{\partial\tau}{\partial r} = \frac{(1+\tau^2)\cos\sigma - 2\tau}{2}, \tag{3.94}$$

$$\frac{\partial\sigma}{\partial z} = \frac{(1+\tau^2)\cos\sigma - 2\tau}{2\tau}, \qquad \frac{\partial\tau}{\partial z} = \frac{(1-\tau^2)\sin\sigma}{2}, \tag{3.95}$$

see Eqs. (S.315)–(S.318) in the Supplementary Material S. Then, we obtain the following expressions for the partial derivatives with respect to r and z:

$$\frac{\partial}{\partial r} = \frac{\partial\sigma}{\partial r}\frac{\partial}{\partial\sigma} + \frac{\partial\tau}{\partial r}\frac{\partial}{\partial\tau} = -\frac{(1-\tau^2)\sin\sigma}{2\tau}\frac{\partial}{\partial\sigma} + \frac{(1+\tau^2)\cos\sigma - 2\tau}{2}\frac{\partial}{\partial\tau}, \tag{3.96}$$

$$\frac{\partial}{\partial z} = \frac{\partial\sigma}{\partial z}\frac{\partial}{\partial\sigma} + \frac{\partial\tau}{\partial z}\frac{\partial}{\partial\tau} = \frac{(1+\tau^2)\cos\sigma - 2\tau}{2\tau}\frac{\partial}{\partial\sigma} + \frac{(1-\tau^2)\sin\sigma}{2}\frac{\partial}{\partial\tau}. \tag{3.97}$$

Substituting the expressions for the vector and scalar potentials (3.54) and (3.55) in the general form for Laplacian in toroidal coordinates, Eq. (S.379), one obtains the following expressions for the Laplace operators, L_n, $(n = 0, 1, 2)$, in toroidal coordinates:

$$L_n[u] = \frac{h^3}{4\tau(1-\tau^2)}\frac{\partial}{\partial\tau}\left[\frac{\tau(1-\tau^2)}{h}\frac{\partial u}{\partial\tau}\right] + \frac{h^3}{4\tau^2}\frac{\partial}{\partial\sigma}\left(\frac{1}{h}\frac{\partial u}{\partial\sigma}\right) - \frac{n^2h^2}{(1-\tau^2)^2}u, \ n = 0, 1, 2. \tag{3.98}$$

The functions in the system of partial differential equations are dependent on each other because of the boundary conditions.

Boundary conditions at the particle surface

Using the fact

$$\begin{aligned}\left.\frac{\partial b_m}{\partial\tau}\right|_{\sigma=\alpha_m} &= \lim_{\Delta\tau\to 0}\frac{b_m(\alpha_m, \tau+\Delta\tau) - b_m(\alpha_m,\tau)}{\Delta\tau} \\ &= \lim_{\Delta\tau\to 0}\frac{0-0}{\Delta\tau} = 0 \text{ at } S_p, \ m = 1, 2,\end{aligned} \tag{3.99}$$

we conclude that the boundary conditions (3.77) and (3.78) in toroidal coordinates have the form:

$$u_{m2} + \frac{\left(1-\tau^2\right)\sin\sigma}{8\tau}\frac{\partial b_m}{\partial\sigma} = 0 \text{ at } S_p, \ m = 1, 2, \tag{3.100}$$

$$u_{m1} - \frac{\left(1+\tau^2\right)\cos\sigma - 2\tau}{4\tau}\frac{\partial b_m}{\partial\sigma} = 0 \text{ at } S_p, \ m = 1, 2, \tag{3.101}$$

see Eq. (3.79). Then, one eliminates $\partial b_m\ \partial\sigma$ from Eq. (3.101) and the boundary condition (3.78) is replaced by the following:

$$2\left[(1+\tau^2)\cos\sigma - 2\tau\right]u_{m2} + \left[(1-\tau^2)\sin\sigma\right]u_{m1} = 0 \text{ at } S_p, \ m = 1, 2. \tag{3.102}$$

In Eq. (3.100), we substitute b_m with the respective expression in toroidal coordinates and obtain

$$u_{m2} + \frac{(1-\tau^2)\sin\sigma}{8\tau}\frac{\partial}{\partial\sigma}\left[b_{m1} + \frac{1-\tau^2}{h}(u_{m0} + u_{m2}) + \frac{2\tau\sin\sigma}{h}u_{m1}\right] = 0. \tag{3.103}$$

Boundary conditions at the fluid–fluid interface

At the fluid–fluid interface ($\sigma = 0$), the partial derivative with respect to z could be simplified considerably as follows:

$$\left.\frac{\partial}{\partial z}\right|_{\sigma=0} = \left.\frac{\partial \sigma}{\partial z}\right|_{\sigma=0} \frac{\partial}{\partial \sigma} + \left.\frac{\partial \tau}{\partial z}\right|_{\sigma=0} \frac{\partial}{\partial \tau} = \frac{(1-\tau)^2}{2\tau} \frac{\partial}{\partial \sigma}, \tag{3.104}$$

see Eq. (3.97). Then, we obtain the form of the boundary condition (3.85) in toroidal coordinates:

$$u_{m1} - \frac{(1-\tau)^2}{2\tau} \frac{\partial b_{m1}}{\partial \sigma} - \frac{1-\tau^2}{1+\tau^2-2\tau} \frac{(1-\tau)^2}{2\tau} \frac{\partial}{\partial \sigma}(u_{m0} + u_{m2}) = 0, \ m = 1, 2 \tag{3.105}$$

at $\sigma = 0$. Moreover, the boundary conditions (3.87) and (3.90) have the form

$$\frac{(1-\tau)^2}{\tau} \left(\mu_1 \frac{\partial u_{12}}{\partial \sigma} - \mu_2 \frac{\partial u_{22}}{\partial \sigma} \right) = 0, \ \frac{(1-\tau)^2}{\tau} \left(\mu_1 \frac{\partial u_{10}}{\partial \sigma} - \mu_2 \frac{\partial u_{20}}{\partial \sigma} \right) = 0, \tag{3.106}$$

$$\frac{(1-\tau)^2}{\tau} \left(\mu_1 \frac{\partial b_{11}}{\partial \sigma} - \mu_2 \frac{\partial b_{21}}{\partial \sigma} \right) = 0. \tag{3.107}$$

Boundary conditions at the axis of revolution

In order to close the problem in the rectangular region, we have to add boundary conditions at the axis of revolution and at the three-phase contact line. At the axis of revolution ($\tau = 1$), it follows from the definitions of the operators (3.98) and the form of the bulk equations (3.73) that the boundary conditions acquire the form

$$\frac{\partial u_{m0}}{\partial \tau} = 0, \ m = 1, 2, \tag{3.108}$$

$$u_{m1} = 0, \ u_{m2} = 0, \ b_{m1} = 0, \ m = 1, 2. \tag{3.109}$$

We shall prove this statement in the next lines. In the case $n \neq 0$, the leading order of the Laplace operator L_n for $\tau \to 1$ is

$$L_n[u] = -\frac{n^2 h^2}{(1-\tau^2)^2} u + \cdots, \ n = 0, 1, 2, \tag{3.110}$$

see Eq. (3.98). Then, taking into account the form of the bulk equations (3.73), we conclude that Eqs. (3.109) hold true. In the case $n = 0$, the leading order of the equation $L_0[u_{m0}] = 0$ for $\tau \to 1$ is

$$L_0[u_{m0}] = -\frac{2\tau^2 h^2}{4\tau(1-\tau^2)} \frac{\partial u_{m0}}{\partial \tau} + \cdots = 0, \ m = 1, 2. \tag{3.111}$$

Then, we obtain Eq. (3.108).

Boundary conditions at the three-phase contact line

In toroidal coordinates, the three phase contact line is a boundary of the numerical domain given by $\tau = 0$ (see Fig. 3.3). Therefore, some boundary conditions have to be added on

it. If we use a similar method to that, presented in the previous section (for the axis of revolution), we obtain

$$\frac{\partial^2 u_{m0}}{\partial \sigma^2} = 0,\ m = 1, 2, \tag{3.112}$$

which is not useful boundary condition. Due to the fact that the point A_+ (with cylindrical coordinates $r = 1,\ z = 0$) lies on the particle surface, we shall use the following two simple boundary conditions:

$$u_{m0} - u_{m2} = \frac{1}{2},\ b_{m1} + u_{m0} + u_{m2} = 0,\ m = 1, 2, \tag{3.113}$$

see equation (3.79). They correspond to the no-slip boundary conditions for the velocity component φ and the additional boundary condition on the particle surface. Therefore, in order to close the problem, we shall obtain boundary conditions for the τ- and σ-velocity components. Expressions for them in terms of velocity components v_{mr} and v_{mz} are presented below:

$$v_{m\tau} = \frac{(1+\tau^2)\cos\sigma - 2\tau}{h} v_{mr} + \frac{(1-\tau^2)\sin\sigma}{h} v_{mz},\ m = 1, 2, \tag{3.114}$$

$$v_{m\sigma} = -\frac{(1-\tau^2)\sin\sigma}{h} v_{mr} + \frac{(1+\tau^2)\cos\sigma - 2\tau}{h} v_{mz},\ m = 1, 2, \tag{3.115}$$

see Eqs. (S.375) and (S.376) in the Supplementary Material S. Therefore, the respective expressions for the vector potential components are

$$\begin{aligned} v_{m\tau} = {} & \frac{(1+\tau^2)\cos\sigma - 2\tau}{h} w_{mr} + \frac{(1-\tau^2)\sin\sigma}{h} w_{mz} \\ & - \frac{(1+\tau^2)\cos\sigma - 2\tau}{h} \frac{\partial \xi_m}{\partial r} - \frac{(1-\tau^2)\sin\sigma}{h} \frac{\partial \xi_m}{\partial z},\ m = 1, 2; \end{aligned} \tag{3.116}$$

$$\begin{aligned} v_{m\sigma} = {} & -\frac{(1-\tau^2)\sin\sigma}{h} w_{mr} + \frac{(1+\tau^2)\cos\sigma - 2\tau}{h} w_{mz} \\ & + \frac{(1-\tau^2)\sin\sigma}{h} \frac{\partial \xi_m}{\partial r} - \frac{(1+\tau^2)\cos\sigma - 2\tau}{h} \frac{\partial \xi_m}{\partial z},\ m = 1, 2, \end{aligned} \tag{3.117}$$

see Eq. (S.348). Next, we simplify the sum of the last two terms in the expression for $v_{m\tau}$ as follows:

$$\begin{aligned} & - \frac{(1+\tau^2)\cos\sigma - 2\tau}{h} \frac{\partial \xi_m}{\partial r} - \frac{(1-\tau^2)\sin\sigma}{h} \frac{\partial \xi_m}{\partial z} \\ & = - \left[\frac{(1+\tau^2)\cos\sigma - 2\tau}{h} \frac{\partial \sigma}{\partial r} + \frac{(1-\tau^2)\sin\sigma}{h} \frac{\partial \sigma}{\partial z} \right] \frac{\partial \xi_m}{\partial \sigma} \\ & \quad - \left[\frac{(1+\tau^2)\cos\sigma - 2\tau}{h} \frac{\partial \tau}{\partial r} + \frac{(1-\tau^2)\sin\sigma}{h} \frac{\partial \tau}{\partial z} \right] \frac{\partial \xi_m}{\partial \tau} \\ & = - \left\{ \frac{\left[(1+\tau^2)\cos\sigma - 2\tau\right]^2}{2h} + \frac{\left[(1-\tau^2)\sin\sigma\right]^2}{2h} \right\} \frac{\partial \xi_m}{\partial \tau} = -\frac{h}{2} \frac{\partial \xi_m}{\partial \tau},\ m = 1, 2 \end{aligned} \tag{3.118}$$

and those — for $v_{m\sigma}$ as follows:

$$\begin{aligned}
&\frac{(1-\tau^2)\sin\sigma}{h}\frac{\partial\xi_m}{\partial r} - \frac{(1+\tau^2)\cos\sigma - 2\tau}{h}\frac{\partial\xi_m}{\partial z} \\
&= + \left[\frac{(1-\tau^2)\sin\sigma}{h}\frac{\partial\sigma}{\partial r} - \frac{(1+\tau^2)\cos\sigma - 2\tau}{h}\frac{\partial\sigma}{\partial z}\right]\frac{\partial\xi_m}{\partial\sigma} \\
&\quad + \left[\frac{(1-\tau^2)\sin\sigma}{h}\frac{\partial\tau}{\partial r} - \frac{(1+\tau^2)\cos\sigma - 2\tau}{h}\frac{\partial\tau}{\partial z}\right]\frac{\partial\xi_m}{\partial\tau} \\
&= -\left\{\frac{\left[(1+\tau^2)\cos\sigma - 2\tau\right]^2}{2h\tau} + \frac{\left[(1-\tau^2)\sin\sigma\right]^2}{2h\tau}\right\}\frac{\partial\xi_m}{\partial\sigma} = -\frac{h}{2\tau}\frac{\partial\xi_m}{\partial\sigma},\ m=1,2, \qquad (3.119)
\end{aligned}$$

see Eqs. (3.94), (3.95) and (S.371). Using Eqs. (3.116)– (3.119), we obtain the following simplified expressions:

$$v_{m\tau} = \frac{(1+\tau^2)\cos\sigma - 2\tau}{h}w_{mr} + \frac{(1-\tau^2)\sin\sigma}{h}w_{mz} - \frac{h}{2}\frac{\partial\xi_m}{\partial\tau},\ m=1,2, \qquad (3.120)$$

$$v_{m\sigma} = -\frac{(1-\tau^2)\sin\sigma}{h}w_{mr} + \frac{(1+\tau^2)\cos\sigma - 2\tau}{h}w_{mz} - \frac{h}{2\tau}\frac{\partial\xi_m}{\partial\sigma},\ m=1,2. \qquad (3.121)$$

These expressions, written for the Fourier modes, are

$$v_{m\tau} = \left[\frac{(1+\tau^2)\cos\sigma - 2\tau}{h}a_{mr} + \frac{(1-\tau^2)\sin\sigma}{h}a_{mz} - \frac{h}{2}\frac{\partial b_m}{\partial\tau}\right]\sin\varphi,\ m=1,2, \qquad (3.122)$$

$$v_{m\sigma} = \left[-\frac{(1-\tau^2)\sin\sigma}{h}a_{mr} + \frac{(1+\tau^2)\cos\sigma - 2\tau}{h}a_{mz} - \frac{h}{2\tau}\frac{\partial b_m}{\partial\sigma}\right]\sin\varphi,\ m=1,2. \qquad (3.123)$$

At the three phase contact line ($\tau = 0$), we get

$$a_{mr}\cos\sigma + a_{mz}\sin\sigma - \frac{1}{2}\frac{\partial b_m}{\partial\tau} = \lim_{\tau\to 0} v_{m\tau} \text{ at } \tau = 0,\ m=1,2, \qquad (3.124)$$

$$-a_{mr}\sin\sigma + a_{mz}\cos\sigma - \frac{1}{2}\frac{\partial^2 b_m}{\partial\sigma\partial\tau} = \lim_{\tau\to 0} v_{m\sigma} \text{ at } \tau = 0,\ m=1,2. \qquad (3.125)$$

Taking into account that the pole A_+ lies at the line $z = 0$, we conclude that the no-slip boundary conditions (3.43) hold true at A_+. Then, Eqs. (3.116) and (3.117) have the form

$$v_{m\tau}|_{\tau=0} = \cos\sigma\left(w_{mr} - \frac{\partial\xi_m}{\partial r}\right) + \sin\sigma\left(w_{mz} - \frac{\partial\xi_m}{\partial z}\right) = \cos\sigma\sin\varphi,\ m=1,2, \qquad (3.126)$$

$$v_{m\sigma}|_{\tau=0} = \cos\sigma\left(w_{mz} - \frac{\partial\xi_m}{\partial z}\right) - \sin\sigma\left(w_{mr} - \frac{\partial\xi_m}{\partial r}\right) = -\sin\sigma\sin\varphi,\ m=1,2 \qquad (3.127)$$

at the three-phase contact line $\tau = 0$. Therefore, we obtain

$$a_{mr}\cos\sigma + a_{mz}\sin\sigma - \frac{1}{2}\frac{\partial b_m}{\partial\tau} = \cos\sigma \text{ at } \tau = 0,\ m=1,2, \qquad (3.128)$$

$$-a_{mr}\sin\sigma + a_{mz}\cos\sigma - \frac{1}{2}\frac{\partial^2 b_m}{\partial\sigma\partial\tau} = -\sin\sigma \text{ at } \tau = 0,\ m=1,2. \qquad (3.129)$$

Using the definitions (3.75) and (3.76), one transforms these conditions to the following ones:

$$[2(u_{m0}+u_{m2})-1]\cos\sigma+2u_{m1}\sin\sigma = \frac{1}{2}\frac{\partial}{\partial\tau}\left[b_{m1}+\frac{1-\tau^2}{h}(u_{m0}+u_{m2})+\frac{2\tau\sin\sigma}{h}u_{m1}\right], \quad (3.130)$$

$$-[2(u_{m0}+u_{m2})-1]\sin\sigma+2u_{m1}\cos\sigma = \frac{1}{2}\frac{\partial^2}{\partial\sigma\partial\tau}\left[b_{m1}+\frac{1-\tau^2}{h}(u_{m0}+u_{m2})+\frac{2\tau\sin\sigma}{h}u_{m1}\right], \quad (3.131)$$

which hold at the three-phase contact line for both phases. Finally, from equations (3.113), we obtain the following two boundary conditions at the three-phase contact line:

$$8u_{m2}\cos\sigma+4u_{m1}\sin\sigma = \frac{\partial}{\partial\tau}\left[b_{m1}+\frac{1-\tau^2}{h}(u_{m0}+u_{m2})+\frac{2\tau\sin\sigma}{h}u_{m1}\right], \quad (3.132)$$

$$-8u_{m2}\sin\sigma+4u_{m1}\cos\sigma = \frac{\partial^2}{\partial\sigma\partial\tau}\left[b_{m1}+\frac{1-\tau^2}{h}(u_{m0}+u_{m2})+\frac{2\tau\sin\sigma}{h}u_{m1}\right] \quad (3.133)$$

for $m=1,2$.

3.5.5 Convenient form for numerical modelling

We solve the following problem:

$$L_0[u_{m0}]=0,\ L_1[u_{m1}]=0,\ L_2[u_{m2}]=0,\ L_1[b_{m1}]=0,\ m=1,2, \quad (3.134)$$

where $L_n[u]$ are defined, using Eq. (3.98). For the first Fourier modes in terms of the new functions, u_{mj} and b_{m1}, (m = 1,2 and j = 0, 1, 2), we apply the following boundary conditions:

- **Boundary conditions at the upper ($\sigma=\alpha$) or at lower part of the particle surface ($\sigma=\alpha-\pi$):**

$$2\left[(1+\tau^2)\cos\sigma-2\tau\right]u_{m2}+\left[(1-\tau^2)\sin\sigma\right]u_{m1}=0,\ m=1,2, \quad (3.135)$$

$$u_{m2}+\frac{(1-\tau^2)\sin\sigma}{8\tau}\frac{\partial b_m}{\partial\sigma}=0,\ m=1,2, \quad (3.136)$$

$$u_{m0}-u_{m2}=\frac{1}{2},\ b_{m1}+\frac{1-\tau^2}{h}(u_{m0}+u_{m2})+\frac{2\tau\sin\sigma}{h}u_{m1}=0,\ m=1,2, \quad (3.137)$$

see Eqs. (3.102), (3.103) and (3.79). In the latter, b_m is defined as follows:

$$b_m(\tau,\sigma)=b_{m1}+\frac{1-\tau^2}{h}(u_{m0}+u_{m2})+\frac{2\tau\sin\sigma}{h}u_{m1},\ m=1,2. \quad (3.138)$$

- **Boundary conditions at the fluid–fluid interface ($\sigma=0,\tau\neq1$):**

$$u_{10}=u_{20},\ u_{12}=u_{22},\ b_{11}=b_{21}, \quad (3.139)$$

$$u_{m1}-\frac{(1-\tau)^2}{2\tau}\frac{\partial b_{m1}}{\partial\sigma}-\frac{1-\tau^2}{2\tau}\frac{\partial}{\partial\sigma}(u_{m0}+u_{m2})=0,\ m=1,2, \quad (3.140)$$

$$\mu_1\frac{\partial u_{10}}{\partial\sigma}=\mu_2\frac{\partial u_{20}}{\partial\sigma},\ \mu_1\frac{\partial u_{12}}{\partial\sigma}=\mu_2\frac{\partial u_{22}}{\partial\sigma},\ \mu_1\frac{\partial b_{11}}{\partial\sigma}=\mu_2\frac{\partial b_{21}}{\partial\sigma}, \quad (3.141)$$

see Eqs. (3.82), (3.84), (3.105)– (3.107);

- **Boundary conditions at the axis of revolution ($\tau = 1$):**

$$\frac{\partial u_{m0}}{\partial \tau} = 0,\ u_{m1} = 0,\ u_{m2} = 0,\ b_{m1} = 0,\ m = 1, 2, \tag{3.142}$$

see Eqs. (3.108) and (3.109);

- **Boundary conditions at the three-phase contact line ($\tau = 0$):**

$$u_{m2} = \frac{1}{8}\left(\frac{\partial b_m}{\partial \tau}\cos\sigma - \frac{\partial^2 b_m}{\partial \sigma \partial \tau}\sin\sigma\right),\ m = 1, 2, \tag{3.143}$$

$$u_{m1} = \frac{1}{4}\left(\frac{\partial b_m}{\partial \tau}\sin\sigma + \frac{\partial^2 b_m}{\partial \sigma \partial \tau}\cos\sigma\right),\ m = 1, 2, \tag{3.144}$$

$$u_{m0} = u_{m2} + \frac{1}{2},\ b_{m1} = -u_{m0} - u_{m2},\ m = 1, 2, \tag{3.145}$$

see Eqs. (3.132), (3.133), (3.113) and (3.138).

- **Boundary conditions at infinity ($\tau = 1,\ \sigma = 0$):**

$$u_{m0}(1, 0) = u_{m1}(1, 0) = u_{m2}(1, 0) = b_{m1}(1, 0) = 0,\ m = 1, 2, \tag{3.146}$$

see Eqs. (3.148) and (3.149).

Note that the boundary conditions of the problem are consistent. More concretely, the following conditions:

$$u_{m0} = \frac{1}{2},\ u_{m1} = 0,\ u_{m2} = 0, b_{m1} = 0,\ m = 1, 2 \tag{3.147}$$

hold at the points $(0, \alpha_m)$. Next, the boundary conditions (3.143) –(3.145) are valid also at the points $(0, \alpha_m),\ m = 1, 2$. Moreover, at the particle surface, they represent the limit of the boundary conditions (3.135)–(3.137) for $\tau \to 0$ and at the fluid-fluid interface, they become limits of the boundary conditions (3.140) for $\tau \to 0$.

Finally, in toroidal coordinates one reaches the triple point $\tau = 1$ and $\sigma = 0$, using two boundaries — the axis of revolution and the fluid-fluid interface. Because of the definition of functions, one has

$$u_{m0} = u_{m1} = u_{m2} = b_{m1} = 0 \text{ at } \tau = 1 \text{ and } \sigma \to 0,\ m = 1, 2, \tag{3.148}$$

$$u_{m0} = u_{m1} = u_{m2} = b_{m1} = 0 \text{ at } \sigma = 0 \text{ and } \tau \to 1,\ m = 1, 2. \tag{3.149}$$

3.6 Asymptotic solutions at the three-phase contact line

The Stokes equations are singular with respect to pressure at the three-phase contact line ($\tau = 0$). Moreover, there is a singularity in the formula for the drag coefficient:

$$\begin{aligned} F_y = -4\pi V R \sin\alpha \left(\eta_1 \int_0^1 \frac{\partial u_{10}}{\partial \sigma} \cdot \frac{1 - \tau^2}{\tau h} d\tau + \eta_2 \int_0^1 \frac{\partial u_{20}}{\partial \sigma} \cdot \frac{1 - \tau^2}{\tau h} d\tau\right) \\ + 2\pi V R \sin\alpha \left[\eta_2 u_{21}(\pi - \alpha) - \eta_1 u_{11}(\pi - \alpha)\right], \end{aligned} \tag{3.150}$$

see Eq. (A.49) in Appendix A. In order to have a good approximation for the drag coefficient, we investigate the asymptotic behaviour of the model in the close vicinity of the three-phase contact line (for $\tau \to 0$).

3.6.1 Toroidal coordinates

In order to do that, we consider the problem (3.56)–(3.64). Using the definition of the modified toroidal coordinates, Eq. (3.92), one obtains the following problem:

$$L_0[a_{mr}] - \frac{2h^2 a_{mr}}{(1-\tau^2)^2} + \frac{2h^2 a_{m\varphi}}{(1-\tau^2)^2} = 0,\ m = 1,2, \tag{3.151}$$

$$L_0[a_{m\varphi}] + \frac{2h^2 a_{mr}}{(1-\tau^2)^2} - \frac{2h^2 a_{m\varphi}}{(1-\tau^2)^2} = 0,\ m = 1,2, \tag{3.152}$$

$$L_0[a_{mz}] - \frac{h^2 a_{mz}}{(1-\tau^2)^2} = 0,\ m = 1,2, \tag{3.153}$$

$$L_0[b_m] - \frac{h^2 b_m}{(1-\tau^2)^2} = \frac{1}{r}\frac{\partial}{\partial r}(r a_{mr}) - \frac{a_{m\varphi}}{r} + \frac{\partial a_{mz}}{\partial z},\ m = 1,2, \tag{3.154}$$

where L_0 has the form (3.98). Using Eqs. (3.93), (3.96), (3.97), (3.104) and the formula

$$\left.\frac{\partial b_m}{\partial \tau}\right|_{\sigma=\alpha_m} = \lim_{\Delta\tau\to 0}\frac{b_m(\tau+\Delta\tau,\alpha_m) - b_m(\tau,\alpha_m)}{\Delta\tau} = 0 \text{ at } S_p,\ m = 1,2, \tag{3.155}$$

we conclude that the problem is closed with the following boundary conditions:

- Boundary conditions at the particle surface:

$$a_{mr} + \frac{\left(1-\tau^2\right)\sin\alpha_m}{2\tau}\cdot\frac{\partial b_m}{\partial\sigma} = 1 \text{ at } S_p,\ m = 1,2, \tag{3.156}$$

$$a_{mz} - \frac{(1+\tau^2)\cos\alpha_m - 2\tau}{2\tau}\cdot\frac{\partial b_m}{\partial\sigma} = 0 \text{ at } S_p,\ m = 1,2, \tag{3.157}$$

$$a_{m\varphi} = 1,\ b_m = 0 \text{ at } S_p,\ m = 1,2. \tag{3.158}$$

- Kinematic boundary conditions and condition for equality of the scalar potentials at the fluid–fluid interface:

$$a_{1r} = a_{2r},\ a_{1\varphi} = a_{2\varphi},\ b_1 = b_2 \text{ at } \sigma = 0, \tag{3.159}$$

$$a_{mz} - \frac{(1-\tau)^2}{2\tau}\cdot\frac{\partial b_m}{\partial\sigma} = 0 \text{ at } \sigma = 0,\ m = 1,2, \tag{3.160}$$

- Dynamic boundary conditions and condition for the derivatives of the scalar potentials at the fluid–fluid interface:

$$\mu_1\frac{\partial b_1}{\partial\sigma} = \mu_2\frac{\partial b_2}{\partial\sigma} \text{ at } \sigma = 0, \tag{3.161}$$

$$\mu_1\frac{\partial a_{1r}}{\partial\sigma} = \mu_2\frac{\partial a_{2r}}{\partial\sigma},\ \mu_1\frac{\partial a_{1\varphi}}{\partial\sigma} = \mu_2\frac{\partial a_{2\varphi}}{\partial\sigma} \text{ at } \sigma = 0, \tag{3.162}$$

3.6.2 Leading order problem

The leading order expansions of Eqs. (3.151)-(3.153) are the same and, then, we are searching for a_{mr}, $a_{m\varphi}$ and a_{mz} in the form:

$$a_{mr} = 1 + \tau^\lambda \overline{a}^0_{mr}(\sigma) + O\left(\tau^{\lambda+1}\right),\ m = 1,2, \tag{3.163}$$

$$a_{m\varphi} = 1 + \tau^\lambda \overline{a}^0_{m\varphi}(\sigma) + O\left(\tau^{\lambda+1}\right),\ m = 1,2, \tag{3.164}$$

$$a_{mz} = \tau^\lambda \overline{a}^0_{mz}(\sigma) + O\left(\tau^{\lambda+1}\right),\ m = 1,2, \tag{3.165}$$

taking into account the boundary conditions (3.156)- (3.158). Substituting these expressions in $L_0[\cdot]$, we obtain the leading order problem:

$$\frac{\partial^2 \overline{a}^0_{mi}}{\partial \sigma^2} + \lambda^2 \overline{a}^0_{mi} = 0,\ m = 1, 2,\ i = r, \varphi, z, \tag{3.166}$$

see Eq. (2.27). Therefore, the leading order expansions of the solutions for a_{mr}, $a_{m\varphi}$ and a_{mz} are

$$a^0_{mr} = 1 + \tau^\lambda \left[A^c_{mr} \cos(\lambda\sigma) + A^s_{mr} \sin(\lambda\sigma)\right],\ m = 1, 2, \tag{3.167}$$

$$a^0_{m\varphi} = 1 + \tau^\lambda \left[A^c_{m\varphi} \cos(\lambda\sigma) + A^s_{m\varphi} \sin(\lambda\sigma)\right],\ m = 1, 2, \tag{3.168}$$

$$a^0_{mz} = \tau^\lambda \left[A^c_{mz} \cos(\lambda\sigma) + A^s_{mz} \sin(\lambda\sigma)\right],\ m = 1, 2, \tag{3.169}$$

where A^c_{mr}, A^s_{mr}, $A^c_{m\varphi}$, $A^s_{m\varphi}$, A^c_{mz} and A^s_{mz} are unknown constants.

Next, we shall find the general leading order solution of Eq. (3.154). In order to do that, we use the relation between the derivatives in cylindrical and in toroidal coordinates

$$\frac{\partial}{\partial r} = \frac{\partial \tau}{\partial r}\frac{\partial}{\partial \tau} + \frac{\partial \sigma}{\partial r}\frac{\partial}{\partial \sigma} = \frac{1}{2}\left(\cos\sigma \frac{\partial}{\partial \tau} - \frac{\sin\sigma}{\tau}\frac{\partial}{\partial \sigma}\right) + \cdots \tag{3.170}$$

$$\frac{\partial}{\partial z} = \frac{\partial \tau}{\partial z}\frac{\partial}{\partial \tau} + \frac{\partial \sigma}{\partial z}\frac{\partial}{\partial \sigma} = \frac{1}{2}\left(\sin\sigma \frac{\partial}{\partial \tau} + \frac{\cos\sigma}{\tau}\frac{\partial}{\partial \sigma}\right) + \cdots, \tag{3.171}$$

see Eqs. (3.96) and (3.97). Using (3.170) and (3.171), the right hand side of Eq. (3.154) is simplified as follows:

$$\begin{aligned}\frac{1}{r}\frac{\partial}{\partial r}(r a_{mr}) - \frac{a_{m\varphi}}{r} + \frac{\partial a_{mz}}{\partial z} &= \frac{1}{2}\left(\frac{a_{mr}}{r} - \frac{a_{m\varphi}}{r} + \frac{\partial a_{mr}}{\partial r} + \frac{\partial a_{mz}}{\partial z}\right) \\ &= \frac{1}{2}\left(\cos\sigma \frac{\partial a_{mr}}{\partial \tau} - \frac{\sin\sigma}{\tau}\frac{\partial a_{mr}}{\partial \sigma} + \sin\sigma \frac{\partial a_{mz}}{\partial \tau} + \frac{\cos\sigma}{\tau}\frac{\partial a_{mz}}{\partial \sigma}\right) + \cdots.\end{aligned} \tag{3.172}$$

Substituting the general solutions for a_{mr} and a_{mz} in the the latter, we obtain

$$\begin{aligned}\cos\sigma \frac{\partial a_{mr}}{\partial \tau} - \frac{\sin\sigma}{\tau}\frac{\partial a_{mr}}{\partial \sigma} &= \lambda\tau^{\lambda-1}\cos\sigma \left[A^c_{mr}\cos(\lambda\sigma) + A^s_{mr}\sin(\lambda\sigma)\right] \\ &\quad - \lambda\tau^{\lambda-1}\sin\sigma \left[-A^c_{mr}\sin(\lambda\sigma) + A^s_{mr}\cos(\lambda\sigma)\right] + O(\tau^\lambda) \\ &= \lambda\tau^{\lambda-1} A^c_{mr}\left[\cos\sigma\cos(\lambda\sigma) + \sin\sigma\sin(\lambda\sigma)\right] \\ &\quad + \lambda\tau^{\lambda-1} A^s_{mr}\left[\sin(\lambda\sigma)\cos\sigma - \sin\sigma\cos(\lambda\sigma)\right] + O(\tau^\lambda) \\ &= \lambda\tau^{\lambda-1}\left\{A^c_{mr}\cos\left[(\lambda-1)\sigma\right] + A^s_{mr}\sin\left[(\lambda-1)\sigma\right]\right\} + O(\tau^\lambda),\end{aligned} \tag{3.173}$$

$$\begin{aligned}\sin\sigma \frac{\partial a_{mz}}{\partial \tau} + \frac{\cos\sigma}{\tau}\frac{\partial a_{mz}}{\partial \sigma} &= \lambda\tau^{\lambda-1}\sin\sigma \left[A^c_{mz}\cos(\lambda\sigma) + A^s_{mz}\sin(\lambda\sigma)\right] \\ &\quad + \lambda\tau^{\lambda-1}\cos\sigma \left[-A^c_{mz}\sin(\lambda\sigma) + A^s_{mz}\cos(\lambda\sigma)\right] + O(\tau^\lambda) \\ &= \lambda\tau^{\lambda-1} A^s_{mz}\left[\sin\sigma\sin(\lambda\sigma) + \cos\sigma\cos(\lambda\sigma)\right] \\ &\quad + \lambda\tau^{\lambda-1} A^c_{mz}\left[\sin\sigma\cos(\lambda\sigma) - \sin(\lambda\sigma)\cos\sigma\right] + O(\tau^\lambda) \\ &= \lambda\tau^{\lambda-1}\left\{A^s_{mz}\cos\left[(\lambda-1)\sigma\right] - A^c_{mz}\sin\left[(\lambda-1)\sigma\right]\right\} + O(\tau^\lambda).\end{aligned} \tag{3.174}$$

Then, Eq. (3.154) has the form

$$L_0[b_m] - \frac{h^2 b_m}{(1-\tau^2)^2} = \frac{1}{2}\lambda\tau^{\lambda-1}\left(A^c_{mr} + A^s_{mz}\right)\cos[(\lambda-1)\sigma] + \frac{1}{2}\lambda\tau^{\lambda-1}(A^s_{mr} - A^c_{mz})\sin[(\lambda-1)\sigma] + O(\tau^{\lambda}),\ m = 1, 2. \tag{3.175}$$

Due to the fact that the right-hand side of the latter is of the order of $\tau^{\lambda-1}$, we are searching for b_m in the form:

$$b_m = \tau^{\lambda+1} b^0_m(\sigma) + O(\tau^{\lambda+2}),\ m = 1, 2. \tag{3.176}$$

Substituting this expression in Eq. (3.175), we obtain the following leading order equation for b^0_m:

$$\frac{1}{4}\left[\frac{\partial^2 b^0_m}{\partial\sigma^2} + (\lambda+1)^2 b^0_m\right] = \frac{\lambda}{2}(A^c_{mr} + A^s_{mz})\cos[(\lambda-1)\sigma] + \frac{\lambda}{2}(A^s_{mr} - A^c_{mz})\sin[(\lambda-1)\sigma],\ m = 1, 2. \tag{3.177}$$

The general solution of the homogeneous equation is

$$B^c_m \cos[(\lambda+1)\sigma] + B^s_m \sin[(\lambda+1)\sigma],\ m = 1, 2, \tag{3.178}$$

where B^c_m and B^s_m are unknown constants. A particular solution of Eq. (3.177) is searched in the form:

$$C_1 \cos[(\lambda-1)\sigma] + C_2 \sin[(\lambda-1)\sigma],\ m = 1, 2. \tag{3.179}$$

Substituting this expression in Eq. (3.177), we obtain

$$C_1\lambda\cos[(\lambda-1)\sigma] + C_2\lambda\sin[(\lambda-1)\sigma] = \frac{\lambda}{2}(A^c_{mr} + A^s_{mz})\cos[(\lambda-1)\sigma] + \frac{\lambda}{2}(A^s_{mr} - A^c_{mz})\sin[(\lambda-1)\sigma],\ m = 1, 2. \tag{3.180}$$

Using the method of undetermined coefficients, one concludes that the particular solution of the problem (3.177) in the form (3.179) is

$$\frac{1}{2}(A^c_{mr} + A^s_{mz})\cos[(\lambda-1)\sigma] + \frac{1}{2}(A^s_{mr} - A^c_{mz})\sin[(\lambda-1)\sigma],\ m = 1, 2. \tag{3.181}$$

Therefore, the leading order expression for b_m, denoted by b^0_m, has the form

$$b^0_m = \tau^{\lambda+1}\left\{B^c_m \cos\left[(\lambda+1)\,\sigma\right] + B^s_m \sin[(\lambda+1)\sigma] + \frac{A^c_{mr} + A^s_{mz}}{2}\cos[(\lambda-1)\sigma] + \frac{A^s_{mr} - A^c_{mz}}{2}\sin[(\lambda-1)\sigma]\right\},\ m = 1, 2. \tag{3.182}$$

Then, we obtain the problem (3.167)– (3.169) and (3.182). In it, there are sixteen unknown constants, which are found, using the following sixteen boundary conditions:

- Boundary conditions at the particle surface:

$$a^0_{mr} + \frac{\sin\alpha_m}{2\tau}\cdot\frac{\partial b^0_m}{\partial\sigma} = 1 \text{ at } S_p,\ m=1,2, \tag{3.183}$$

$$a^0_{mz} - \frac{\cos\alpha_m}{2\tau}\cdot\frac{\partial b^0_m}{\partial\sigma} = 0 \text{ at } S_p,\ m=1,2, \tag{3.184}$$

$$a^0_{m\varphi} = 1,\ b^0_m = 0 \text{ at } S_p,\ m=1,2, \tag{3.185}$$

- Kinematic boundary conditions and condition for equality of the scalar potentials at the fluid–fluid interface:

$$a^0_{1r} = a^0_{2r},\ a^0_{1\varphi} = a^0_{2\varphi},\ b^0_1 = b^0_2 \text{ at } \sigma = 0, \tag{3.186}$$

$$a^0_{mz} - \frac{1}{2\tau}\cdot\frac{\partial b^0_m}{\partial\sigma} = 0 \text{ at } \sigma = 0,\ m=1,2, \tag{3.187}$$

- Dynamic boundary conditions and condition for the derivatives of the scalar potentials at the fluid–fluid interface:

$$\mu_1\frac{\partial b^0_1}{\partial\sigma} = \mu_2\frac{\partial b^0_2}{\partial\sigma} \text{ at } \sigma = 0, \tag{3.188}$$

$$\mu_1\frac{\partial a^0_{1r}}{\partial\sigma} = \mu_2\frac{\partial a^0_{2r}}{\partial\sigma},\ \mu_1\frac{\partial a^0_{1\varphi}}{\partial\sigma} = \mu_2\frac{\partial a^0_{2\varphi}}{\partial\sigma} \text{ at } \sigma = 0, \tag{3.189}$$

3.6.3 Leading order solution for $a^0_{m\varphi}$

Substituting the general solution for $a^0_{m\varphi}$, Eq. (3.168), in the kinematic boundary condition, Eq. (3.186), and in the dynamic boundary condition, Eq. (3.189), we conclude that

$$A^c_{1\varphi} = A^c_{2\varphi}, \tag{3.190}$$

$$\mu_1 A^s_{1\varphi} = \mu_2 A^s_{2\varphi}. \tag{3.191}$$

Let us introduce new constants A^s_φ and A^c_φ, using the following relations:

$$A^c_\varphi = A^c_{1\varphi} = A^c_{2\varphi},\ A^s_{1\varphi} = \mu_2 A^s_\varphi,\ A^s_{2\varphi} = \mu_1 A^s_\varphi. \tag{3.192}$$

Thus, the general solution for $a^0_{m\varphi}$, m=1,2, has the following form:

$$a^0_{m\varphi} = 1 + \tau^\lambda\left[A^c_\varphi\cos(\lambda\sigma) + \mu_{3-m}A^s_\varphi\sin(\lambda\sigma)\right],\ m=1,2. \tag{3.193}$$

Using the no-slip boundary conditions $a^0_{m\varphi} = 1$, Eq. (3.185), at S_p, we conclude that the following equations:

$$A^c_\varphi\cos(\lambda\alpha) + \mu_2 A^s_\varphi\sin(\lambda\alpha) = 0, \tag{3.194}$$

$$A^c_\varphi\cos\left[\lambda(\alpha-\pi)\right] + \mu_1 A^s_\varphi\sin\left[\lambda(\alpha-\pi)\right] = 0 \tag{3.195}$$

hold true. This system has always a trivial solution ($A^c_\varphi = A^s_\varphi = 0$) and it has also non-trivial solutions in case the determinant of the system is 0, i.e.

$$\begin{aligned} 0 = \Delta &= \mu_1\cos(\lambda\alpha)\sin\left[\lambda(\alpha-\pi)\right] - \mu_2\sin(\lambda\alpha)\cos\left[\lambda(\alpha-\pi)\right] \\ &= \mu_1\sin\left[\lambda(2\alpha-\pi)\right] - \sin(\alpha\lambda)\cos\left[\lambda(\alpha-\pi)\right]. \end{aligned} \tag{3.196}$$

This equation describes a class of possible solutions for the singularity parameter λ.

3.6.4 The leading order solutions for a^0_{mr} and a^0_{mz}

Analogously, using the kinematic boundary condition, Eq. (3.186), and the dynamic boundary condition, Eq. (3.189), we conclude that a^0_{mr} has the form

$$a^0_{mr} = 1 + \tau^\lambda \left[A^c_r \cos(\lambda\sigma) + \mu_{3-m} A^s_r \sin(\lambda\sigma)\right],\ m = 1, 2, \tag{3.197}$$

where A^c_r and A^s_r are defined as follows:

$$A^c_r = A^c_{1r} = A^c_{2r},\ A^s_{1r} = \mu_2 A^s_r,\ A^s_{2r} = \mu_1 A^s_r. \tag{3.198}$$

Using the boundary conditions (3.187) and (3.188), the following relation

$$\tau^\lambda \mu_1 A^c_{1z} = \mu_1 a^0_{1z} = \frac{\mu_1}{2\tau}\frac{\partial b^0_1}{\partial z} = \frac{\mu_2}{2\tau}\frac{\partial b^0_2}{\partial z} = \mu_2 a^0_{2z} = \tau^\lambda \mu_2 A^c_{2z} \tag{3.199}$$

is obtained. Then, the general form of a^0_{mz} is

$$a^0_{mz} = \tau^\lambda \left[\mu_{3-m} A^c_z \cos(\lambda\sigma) + A^s_{mz} \sin(\lambda\sigma)\right],\ m = 1, 2, \tag{3.200}$$

where the constant A^c_z satisfies the conditions

$$A^c_{1z} = \mu_2 A^c_z,\ A^c_{2z} = \mu_1 A^c_z. \tag{3.201}$$

The leading order solution for b^0_m

Substituting the expressions for the constants A^c_{mr}, A^s_{mr} and A^c_{mz} in terms of the new constants A^c_r, A^s_r and A^c_z in Eq. (3.182), we get

$$\begin{aligned} b^0_m = \tau^{\lambda+1} \Bigg\{ & B^c_m \cos\left[(\lambda+1)\,\sigma\right] + B^s_m \sin[(\lambda+1)\sigma] + \frac{A^c_r + A^s_{mz}}{2} \cos[(\lambda-1)\sigma] \\ & + \mu_{3-m}\, \frac{A^s_r - A^c_z}{2} \sin[(\lambda-1)\sigma] \Bigg\},\ m = 1, 2. \end{aligned} \tag{3.202}$$

Using the kinematic boundary conditions (3.187) and the general definition of a^0_{mz}, Eqs. (3.200) and (3.201), one concludes that

$$\mu_{3-m} A^c_z - \frac{1}{2}\left[(\lambda+1) B^s_m + \mu_{3-m}(\lambda-1)\frac{A^s_r - A^c_z}{2}\right] = 0,\ m = 1, 2, \tag{3.203}$$

$$\frac{\mu_{3-m}}{2}\left[(1-\lambda) A^s_r + (\lambda+3) A^c_z\right] = B^s_m(\lambda+1),\ m = 1, 2. \tag{3.204}$$

Note that $\lambda > -1$. Therefore, we obtain

$$B^s_m = \frac{\mu_{3-m}}{2(\lambda+1)}\left[(1-\lambda) A^s_r + (\lambda+3) A^c_z\right],\ m = 1, 2. \tag{3.205}$$

Substituting the general form of b^0_m, Eq. (3.202), in the boundary condition $b^0_1(\tau, 0) = b^0_2(\tau, 0)$, Eq. (3.186), we obtain

$$B^c_1 + \frac{A^c_r + A^s_{1z}}{2} = B^c_2 + \frac{A^c_r + A^s_{2z}}{2}. \tag{3.206}$$

Then, it is convenient to introduce a new constant B^c such that

$$B^c = B^c_m + \frac{A^c_r + A^s_{mz}}{2},\ m = 1, 2. \tag{3.207}$$

Therefore, the general form of b^0_m is

$$\begin{aligned} b^0_m = \tau^{\lambda+1} \Bigg\{ & \left(B^c - \frac{A^c_r + A^s_{mz}}{2} \right) \cos\left[(\lambda+1)\,\sigma\right] \\ & + \frac{\mu_{3-m}}{2} \left(A^c_z \frac{\lambda+3}{\lambda+1} - A^s_r \frac{\lambda-1}{\lambda+1} \right) \sin[(\lambda+1)\sigma] \\ & + \frac{A^c_r + A^s_{mz}}{2} \cos[(\lambda-1)\sigma] + \mu_{3-m}\ \frac{A^s_r - A^c_z}{2} \sin[(\lambda-1)\sigma] \Bigg\},\ m = 1, 2. \end{aligned} \tag{3.208}$$

We have already fulfilled the boundary conditions at $\sigma = 0$. Next, the boundary condition (3.184) is replaced by the result from adding Eq. (3.183), multiplied by $\cos\alpha_m$, to (3.184), multiplied by $\sin\alpha_m$, i.e.

$$\cos\alpha_m \cdot a^0_{mr} + \sin\alpha_m \cdot a^0_{mz} = \cos\alpha_m,\ m = 1, 2. \tag{3.209}$$

Substituting obtained expressions for a^0_{mr}, a^0_{mz}, and b^0_m, Eqs. (3.197), (3.200) and (3.202), in the boundary conditions (3.185), (3.209) and (3.183), we get

$$\begin{aligned} & \left(B^c - \frac{A^c_r + A^s_{mz}}{2} \right) \cos\left[(\lambda+1)\,\alpha_m\right] + \frac{\mu_{3-m}}{2} \left(A^c_z \frac{\lambda+3}{\lambda+1} - A^s_r \frac{\lambda-1}{\lambda+1} \right) \sin[(\lambda+1)\alpha_m] \\ & \quad + \frac{A^c_r + A^s_{mz}}{2} \cos[(\lambda-1)\alpha_m] + \mu_{3-m} \frac{A^s_r - A^c_z}{2} \sin[(\lambda-1)\alpha_m] = 0,\ m = 1, 2, \end{aligned} \tag{3.210}$$

$$\begin{aligned} & A^c_r \cos\alpha_m \cos(\lambda\alpha_m) + \mu_{3-m} A^s_r \cos\alpha_m \sin(\lambda\alpha_m) \\ & \quad + \mu_{3-m} A^c_z \sin\alpha_m \cos(\lambda\alpha_m) + A^s_{mz} \sin\alpha_m \sin(\lambda\alpha_m) = 0,\ m = 1, 2, \end{aligned} \tag{3.211}$$

$$\begin{aligned} & 2A^c_r \cos(\lambda\alpha_m) + 2\mu_{3-m} A^s_r \sin(\lambda\alpha_m) \\ & \quad - \left(B^c - \frac{A^c_r + A^s_{mz}}{2} \right) (\lambda+1) \sin\alpha_m \sin\left[(\lambda+1)\,\alpha_m\right] \\ & \quad + \frac{\mu_{3-m}}{2} \left[A^c_z\,(\lambda+3) - A^s_r\,(\lambda-1) \right] \sin\alpha_m \cos[(\lambda+1)\alpha_m] \\ & \quad - \frac{A^c_r + A^s_{mz}}{2} (\lambda-1) \sin\alpha_m \sin[(\lambda-1)\alpha_m] \\ & \quad + \mu_{3-m}(\lambda-1) \frac{A^s_r - A^c_z}{2} \sin\alpha_m \cos[(\lambda-1)\alpha_m] = 0,\ m = 1, 2. \end{aligned} \tag{3.212}$$

The system of equations is simplified, using the redefined constant groups:

$$A^{cs}_{mrz} = A^c_r + A^s_{mz},\ A^+_{rz} = A^s_r + A^c_z,\ A^-_{rz} = A^s_r - A^c_z,\ m = 1, 2. \tag{3.213}$$

Taking into account the definitions (3.213), we simplify Eq. (3.210) as

$$\left(B^c - \frac{A^{cs}_{mrz}}{2}\right)\cos\left[(\lambda+1)\,\alpha_m\right] + \frac{\mu_{3-m}}{2}\left[A^c_z - A^s_r + \frac{2(A^c_z + A^s_r)}{\lambda+1}\right]\sin[(\lambda+1)\alpha_m]$$
$$+ \frac{A^{cs}_{mrz}}{2}\cos[(\lambda-1)\alpha_m] + \mu_{3-m}\frac{A^-_{rz}}{2}\sin[(\lambda-1)\alpha_m] = 0,\ m = 1,2, \tag{3.214}$$

$$B^c\cos\left[(\lambda+1)\,\alpha_m\right] + \frac{\mu_{3-m}A^+_{rz}}{\lambda+1}\sin[(\lambda+1)\alpha_m]$$
$$+ A^{cs}_{mrz}\sin(\lambda\alpha_m)\sin\alpha_m - \mu_{3-m}A^-_{rz}\sin\alpha_m\cos(\lambda\alpha_m) = 0,\ m = 1,2. \tag{3.215}$$

Eq. (3.211) is simplified as

$$A^c_r\left[\cos\alpha_m\cos(\lambda\alpha_m) - \sin\alpha_m\sin(\lambda\alpha_m)\right] + \mu_{3-m}\frac{A^+_{rz} + A^-_{rz}}{2}\cos\alpha_m\sin(\lambda\alpha_m)$$
$$+ \mu_{3-m}\frac{A^+_{rz} - A^-_{rz}}{2}\sin\alpha_m\cos(\lambda\alpha_m) + A^{cs}_{mrz}\sin\alpha_m\sin(\lambda\alpha_m) = 0,\ m = 1,2, \tag{3.216}$$

$$A^c_r\cos\left[(\lambda+1)\alpha_m\right] + \mu_{3-m}\frac{A^+_{rz}}{2}\sin[(\lambda+1)\alpha_m]$$
$$+ \mu_{3-m}\frac{A^-_{rz}}{2}\sin[(\lambda-1)\alpha_m] + A^{cs}_{mrz}\sin\alpha_m\sin(\lambda\alpha_m) = 0,\ m = 1,2. \tag{3.217}$$

In the redefined constant group (3.213), Eqs. (3.212) become

$$2A^c_r\cos(\lambda\alpha_m) + \mu_{3-m}\left(A^+_{rz} + A^-_{rz}\right)\sin(\lambda\alpha_m)$$
$$- \left(B^c - \frac{A^{cs}_{mrz}}{2}\right)(\lambda+1)\sin\alpha_m\sin\left[(\lambda+1)\,\alpha_m\right]$$
$$+ \frac{\mu_{3-m}}{2}\left[\frac{A^+_{rz} - A^-_{rz}}{2}(\lambda+3) - \frac{A^+_{rz} + A^-_{rz}}{2}(\lambda-1)\right]\sin\alpha_m\cos[(\lambda+1)\alpha_m]$$
$$- \frac{A^{cs}_{mrz}}{2}(\lambda-1)\sin\alpha_m\sin[(\lambda-1)\alpha_m]$$
$$+ \mu_{3-m}(\lambda-1)\frac{A^-_{rz}}{2}\sin\alpha_m\cos[(\lambda-1)\alpha_m] = 0,\ m = 1,2, \tag{3.218}$$

$$- B^c(\lambda+1)\sin\alpha_m\sin\left[(\lambda+1)\,\alpha_m\right] + 2A^c_r\cos(\lambda\alpha_m)$$
$$+ \frac{A^{cs}_{mrz}\sin\alpha_m}{2}\left\{\lambda\sin\left[(\lambda+1)\,\alpha_m\right] - \lambda\sin[(\lambda-1)\alpha_m]\right\}$$
$$+ \frac{A^{cs}_{mrz}\sin\alpha_m}{2}\left\{\sin\left[(\lambda+1)\,\alpha_m\right] + \sin[(\lambda-1)\alpha_m]\right\}$$
$$+ \mu_{3-m}A^-_{rz}\sin\alpha_m\left\{\frac{\sin(\lambda\alpha_m)}{\sin\alpha_m} - \frac{\lambda+1}{2}\cos[(\lambda+1)\alpha_m] + \frac{\lambda-1}{2}\cos[(\lambda-1)\alpha_m]\right\}$$
$$+ \mu_{3-m}A^+_{rz}\left\{\sin(\lambda\alpha_m) + \sin\alpha_m\cos[(\lambda+1)\alpha_m]\right\} = 0,\ m = 1,2, \tag{3.219}$$

$$- B^c\sin\left[(\lambda+1)\,\alpha_m\right] + \frac{2A^c_r}{\lambda+1}\frac{\cos(\lambda\alpha_m)}{\sin\alpha_m}$$

$$+\frac{A^{cs}_{mrz}}{\lambda+1}\left[\lambda\sin\alpha_m\cos\left(\lambda\alpha_m\right)+\cos\alpha_m\sin\left(\lambda\alpha_m\right)\right]$$
$$+\frac{\mu_{3-m}A^{-}_{rz}}{\lambda+1}\left\{\frac{\sin(\lambda\alpha_m)}{\sin\alpha_m}+\lambda\sin\alpha_m\sin(\lambda\alpha_m)-\cos\alpha_m\cos(\lambda\alpha_m)\right\}$$
$$+\frac{\mu_{3-m}A^{+}_{rz}}{\lambda+1}\left\{\frac{\sin(\lambda\alpha_m)}{\sin\alpha_m}+\cos[(\lambda+1)\alpha_m]\right\}=0,\ m=1,2. \tag{3.220}$$

Then, we obtain the system

$$B^c\cos\left[(\lambda+1)\,\alpha_m\right]+\frac{\mu_{3-m}A^{+}_{rz}}{\lambda+1}\sin[(\lambda+1)\alpha_m]$$
$$-\mu_{3-m}A^{-}_{rz}\sin\alpha_m\cos(\lambda\alpha_m)+A^{cs}_{mrz}\sin(\lambda\alpha_m)\sin\alpha_m=0,\ m=1,2, \tag{3.221}$$

$$A^c_r\cos\left[(\lambda+1)\alpha_m\right]+\mu_{3-m}\frac{A^{+}_{rz}}{2}\sin[(\lambda+1)\alpha_m]$$
$$+\mu_{3-m}\frac{A^{-}_{rz}}{2}\sin[(\lambda-1)\alpha_m]+A^{cs}_{mrz}\sin\alpha_m\sin(\lambda\alpha_m)=0,\ m=1,2, \tag{3.222}$$

$$-B^c\sin\left[(\lambda+1)\,\alpha_m\right]+\frac{2A^c_r}{\lambda+1}\frac{\cos(\lambda\alpha_m)}{\sin\alpha_m}+\frac{A^{cs}_{mrz}}{\lambda+1}\left[\lambda\sin\alpha_m\cos\left(\lambda\alpha_m\right)+\cos\alpha_m\sin\left(\lambda\alpha_m\right)\right]$$
$$-\frac{\mu_{3-m}A^{-}_{rz}}{\lambda+1}\left\{\cos\alpha_m\cos(\lambda\alpha_m)-\lambda\sin\alpha_m\sin(\lambda\alpha_m)-\frac{\sin(\lambda\alpha_m)}{\sin\alpha_m}\right\}$$
$$+\frac{\mu_{3-m}A^{+}_{rz}}{\lambda+1}\left\{\frac{\sin(\lambda\alpha_m)}{\sin\alpha_m}+\cos[(\lambda+1)\alpha_m]\right\}=0,\ m=1,2. \tag{3.223}$$

In order to eliminate A^{cs}_{mrz}, we subtract Eq. (3.222) from Eq. (3.221) and obtain the equation

$$(B^c-A^c_r)\cos[(\lambda+1)\alpha_m]-\frac{\mu_{3-m}}{2}\left(\frac{\lambda-1}{\lambda+1}A^{+}_{rz}+A^{-}_{rz}\right)\sin[(\lambda+1)\alpha_m]=0 \tag{3.224}$$

for $m=1,2$. Let us denote

$$X_1=B^c-A^c_r,\ X_2=\frac{1}{2}\left(\frac{\lambda-1}{\lambda+1}A^{+}_{rz}+A^{-}_{rz}\right). \tag{3.225}$$

Then, X_1 and X_2 are computed by solving the system

$$X_1\cos[(\lambda+1)\alpha]-\mu_2X_2\sin[(\lambda+1)\alpha]=0, \tag{3.226}$$
$$X_1\cos[(\lambda+1)(\alpha-\pi)]-\mu_1X_2\sin[(\lambda+1)(\alpha-\pi)]=0. \tag{3.227}$$

This system has non-zero solutions in case that the determinant of the system is zero. Therefore, we obtain a second class of solutions for the singularity parameter λ:

$$\mu_1\sin[(\lambda+1)(\alpha-\pi)]\cos[(\lambda+1)\alpha]=\mu_2\sin[(\lambda+1)\alpha]\cos[(\lambda+1)(\alpha-\pi)]. \tag{3.228}$$

The third class of solutions corresponds to $X_1=X_2=0$ and, then, one gets

$$B^c=A^c_r,\ A^{-}_{rz}=-\frac{\lambda-1}{\lambda+1}A^{+}_{rz}. \tag{3.229}$$

By substituting the expressions (3.229) in Eqs. (3.222) and (3.223), the equations are simplified as follows:

$$A_r^c \cos\left[(\lambda+1)\alpha_m\right] + \mu_{3-m}\frac{A_{rz}^+}{\lambda+1}\left\{\sin(\lambda\alpha_m)\cos\alpha_m + \lambda\sin\alpha_m\cos(\lambda\alpha_m)\right\} + A_{mrz}^{cs}\sin\alpha_m\sin(\lambda\alpha_m) = 0,\ m=1,2 \tag{3.230}$$

$$\begin{aligned} &A_r^c\left\{\frac{2\cos(\lambda\alpha_m)}{\sin\alpha_m} - (\lambda+1)\sin[(\lambda+1)\alpha_m]\right\} \\ &+ A_{mrz}^{cs}\left[\lambda\cos(\lambda\alpha_m)\sin\alpha_m + \sin(\lambda\alpha_m)\cos\alpha_m\right] \\ &+ \frac{\mu_{3-m}A_{rz}^+}{\lambda+1}\left[2\lambda\cos(\lambda\alpha_m)\cos\alpha_m - (\lambda^2+1)\sin\alpha_m\sin(\lambda\alpha_m) + \frac{2\sin(\lambda\alpha_m)}{\sin\alpha_m}\right] \\ &= 0,\ m=1,2. \end{aligned} \tag{3.231}$$

From Eqs. (3.230) and (3.231), we eliminate A_{mrz}^{cs} and derive the following system:

$$A_r^c\left[\sin(2\lambda\alpha_m) - \lambda\sin(2\alpha_m)\right] - \frac{\mu_{3-m}A_{rz}^+}{\lambda+1}\left[\cos(2\lambda\alpha_m) - \lambda^2\cos(2\alpha_m) + \lambda^2 - 1\right] = 0 \tag{3.232}$$

for $m = 1, 2$. The explicit form of the system is

$$A_r^c\left[\sin(2\lambda\alpha) - \lambda\sin(2\alpha)\right] = \frac{\mu_2 A_{rz}^+}{\lambda+1}\left[\cos(2\lambda\alpha) - \lambda^2\cos(2\alpha) + \lambda^2 - 1\right], \tag{3.233}$$

$$\begin{aligned} &A_r^c\left\{\sin[2\lambda(\alpha-\pi)] - \lambda\sin[2(\alpha-\pi)]\right\} \\ &\quad = \frac{\mu_1 A_{rz}^+}{\lambda+1}\left\{\cos[2\lambda(\alpha-\pi)] - \lambda^2\cos[2(\alpha-\pi)] + \lambda^2 - 1\right\}. \end{aligned} \tag{3.234}$$

Therefore, third class of possible solutions is

$$\begin{aligned} &\mu_1\left[\sin(2\lambda\alpha) - \lambda\sin(2\alpha)\right]\left\{\cos[2\lambda(\alpha-\pi)] - \lambda^2\cos(2\alpha) + \lambda^2 - 1\right\} \\ &\quad = \mu_2\left\{\sin[2\lambda(\alpha-\pi)] - \lambda\sin(2\alpha)\right\}\left[\cos(2\lambda\alpha) - \lambda^2\cos(2\alpha) + \lambda^2 - 1\right]. \end{aligned} \tag{3.235}$$

From the obtained three classes of solutions (3.196), (3.228) and (3.235) only Eq. (3.235) corresponds to a physical singularity. The other two are result from the fact that we work in gauge formulation.

3.6.5 Results

The semi-analytical results for water–air interface and $\alpha \leq 90°$ [3.1] show that the solutions for the pressure are regular at the three-phase contact line (i.e. the pressure is finite). In the general case, it is possible the functions p_m to have a weak singularity at $\tau = 0$[1] , while local velocities $\mathbf{v}_m$ are finite at $\tau = 0$. The pressure function has a stronger than logarithmic singularity inside the regions, shown in Fig. 3.5, where the singularity parameter $\lambda_p := \lambda - 1$

[1]Pressure is a physical quantity, which is computed as force divided by area on which it acts. Due to the continuous nature of medium, one introduces local pressure, which is defined as a limit of the force divided by the area, when area goes to zero. Practically, whenever there is a contact line, it is possible for the pressure to have a singularity at it (due to the limit in the definition). At the end, it is important for the force, (the integral quantity) to be finite.

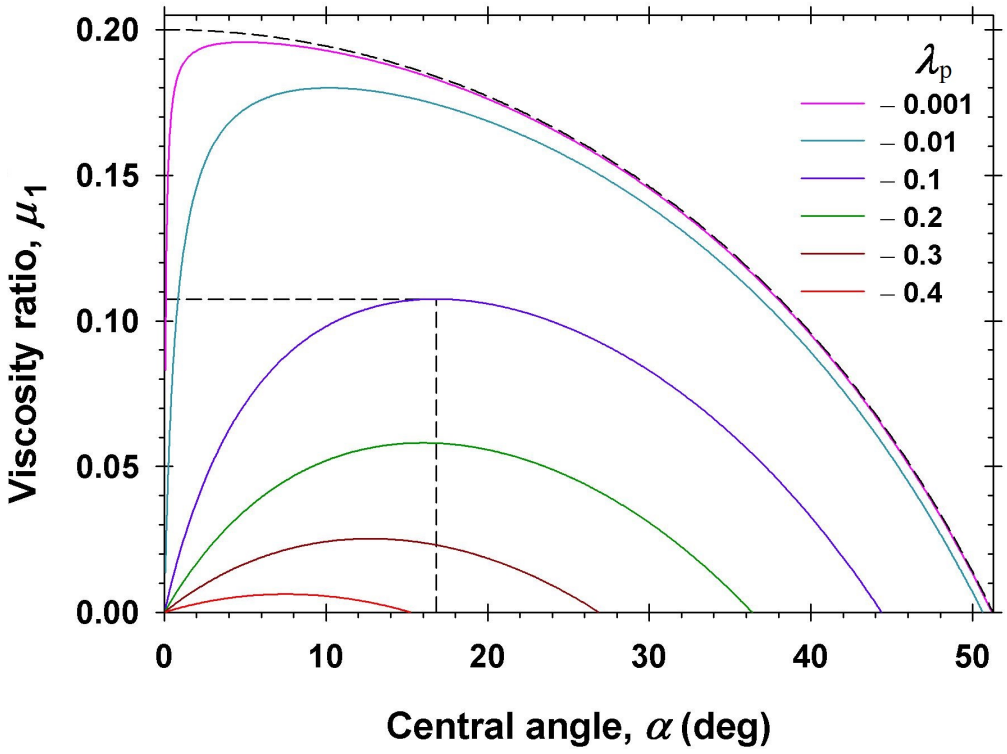

Figure 3.5: Lines with fixed values of the singularity parameter, λ_p

is in the interval $(-0.5, 0)$. Fig. 3.5 shows the dependence of λ_p on the three-phase contact angle, α, and viscosity ratio, μ_1. Because of the symmetry, the picture is analogous replacing μ_1 with μ_2 and α with $\pi - \alpha$. One sees that the pressure singularity becomes stronger with the decrease of viscosity ratio μ_1. For example, the dashed line in Fig. 3.5 shows that if $\mu_1 = 0.1075$, then the strongest singularity of $\lambda_p = -0.1$ takes place for values of the central angle equal to 16.8°. In all the cases $\lambda_p > -0.5$, so the singularity is weak and the integral from the pressure over the particle surface converges (the drag force is finite).

3.7 Numerical method and numerical results

3.7.1 Numerical method

In order to solve the problem (3.134)–(3.10), we introduce numerical time t and seek the stationary solution of the parabolic problem:

$$\frac{\partial \mathbf{u}_m}{\partial t} = T[\mathbf{u}_m] + S[\mathbf{u}_m], \ \mathbf{u}_m \in D_m, \ m = 1, 2, \tag{3.236}$$

$$\mathbf{u}_m(\tau, \sigma, 0) = \mathbf{u}_{m,0}(\tau, \sigma), \ m = 1, 2 \tag{3.237}$$

in the region

$$D_m := \begin{cases} \alpha - \pi < \sigma < 0,\ 0 < \tau < 1,\ 0 < t \le T, & m = 1 \\ 0 < \sigma < \alpha,\ 0 < \tau < 1,\ 0 < t \le T, & m = 2 \end{cases} \tag{3.238}$$

with appropriate boundary conditions imposed, where

$$\mathbf{u}_m = (u_{m0}, u_{m1}, u_{m2}, b_{m1})^T,\ m = 1, 2, \tag{3.239}$$

is a vector of the solutions at the phase m and $S[\cdot]$ and $T[\cdot]$ are the following operators:

$$S[\mathbf{u}_m] = h\frac{\partial}{\partial\sigma}\left(\frac{1}{h}\frac{\partial \mathbf{u}_m}{\partial\sigma}\right),\ T[\mathbf{u}_m] = (T_0[u_{m0}], T_1[u_{m1}], T_2[u_{m2}], T_1[b_{m1}])^T, \tag{3.240}$$

$$T_p[u] = \frac{h\tau}{1-\tau^2}\frac{\partial}{\partial\tau}\left[\frac{\tau(1-\tau^2)}{h}\frac{\partial u}{\partial\tau}\right] - \frac{4p^2\tau^2}{(1-\tau^2)^2}u,\ p = 0, 1, 2, \tag{3.241}$$

which act at $\sigma-$ and $\tau-$direction, respectively. In order to solve the considered problem, we discretize its rectangular domain by introducing a mesh $\omega = \omega_\tau \times (\omega_{\sigma 1} \cup \omega_{\sigma 2}) \times \omega_t$, where ω_τ, ω_t are defined by Eqs. (2.63) and (2.67) and $\omega_{\sigma 1}$ and $\omega_{\sigma 2}$ — as follows:

$$\omega_{\sigma 1} = \{\sigma_j = j\delta_{\sigma 1},\ \delta_{\sigma 1} = \alpha/N_1,\ j = 0, 1, \cdots, N_1\}, \tag{3.242}$$

$$\omega_{\sigma 2} = \{\sigma_j = j\delta_{\sigma 2},\ \delta_{\sigma 2} = (\pi - \alpha)/N_2,\ j = 0, -1, \cdots, -N_2\}. \tag{3.243}$$

Let us denote the exact solution of the considered problem at a point $(\tau_i,\ \sigma_j,\ t_k)$ by

$$\mathbf{u}_1|_{ij}^k = \left(u_{10}|_{ij}^k,\ u_{11}|_{ij}^k,\ u_{12}|_{ij}^k,\ b_{11}|_{ij}^k\right)^T \text{ for } j \ge 0, \tag{3.244}$$

$$\mathbf{u}_2|_{ij}^k = \left(u_{20}|_{ij}^k,\ u_{21}|_{ij}^k,\ u_{22}|_{ij}^k,\ b_{21}|_{ij}^k\right)^T \text{ for } j \le 0 \tag{3.245}$$

and the approximate one — at the same point as

$$\mathbf{Y}_1|_{ij}^k = \left(Y_{10}|_{ij}^k,\ Y_{11}|_{ij}^k,\ Y_{12}|_{ij}^k,\ B_{11}|_{ij}^k\right)^T \text{ for } j \ge 0, \tag{3.246}$$

$$\mathbf{Y}_2|_{ij}^k = \left(Y_{20}|_{ij}^k,\ Y_{21}|_{ij}^k,\ Y_{22}|_{ij}^k,\ B_{21}|_{ij}^k\right)^T \text{ for } j \le 0. \tag{3.247}$$

In order to solve the considered problem, we use the D'Yakonov scheme [3.17–3.19], which is presented in Section 2.6.1. First, we solve a problem in the τ-direction:

$$\left(U - \frac{\delta_t}{2}\tilde{T}\right)\left[\overline{\boldsymbol{Y}}_m|_{ij}^{k+1}\right] = \delta_t\tilde{T}\left[\boldsymbol{Y}_m|_{ij}^k\right] + \delta_t\tilde{S}\left[\boldsymbol{Y}_m|_{ij}^k\right],\ m = 1, 2, \tag{3.248}$$

with boundary conditions, obtained by expanding the operators at the three-phase contact line, at the axis of revolution and at the the fluid–fluid interface. Next, we solve a σ-directional problem

$$\left(U - \frac{\delta_t}{2}\tilde{S}\right)\left[\delta\boldsymbol{Y}_m|_{ij}^{k+1}\right] = \overline{\boldsymbol{Y}}_m|_{ij}^{k+1},\ m = 1, 2, \tag{3.249}$$

with appropriately approximated boundary conditions at the surface of the particle, where $\delta\boldsymbol{Y}_m|_{ij}^{k+1}$ is defined as

$$\delta\boldsymbol{Y}_m|_{ij}^{k+1} = \boldsymbol{Y}_m|_{ij}^{k+1} - \boldsymbol{Y}_m|_{ij}^k,\ m = 1, 2. \tag{3.250}$$

Extension of the operators S and T

As we mention before, we extend the operators T and S at the three-phase contact line, at the axis of revolution and at the fluid–fluid as follows. At the three-phase contact line, one obtains

$$\lim_{\tau\to 0} T_p[u] = 0 \text{ at } \tau = 0,\ s = 0, 1, 2, \tag{3.251}$$

$$\lim_{\tau\to 0} S[u] = \lim_{\tau\to 0}\left(\frac{\partial^2 u}{\partial\sigma^2} - \frac{2\tau\sin\sigma}{h}\frac{\partial u}{\partial\sigma}\right) = \left.\frac{\partial^2 u}{\partial\sigma^2}\right|_{\tau=0}. \tag{3.252}$$

At the axis of revolution, one extends the operators T_0 and S for u_{m0}:

$$T_0[u] = 2\frac{\partial^2 u}{\partial\tau^2} \text{ at } \tau = 1, \tag{3.253}$$

$$S[u] = (1-\cos\sigma)\cdot\frac{\partial}{\partial\sigma}\left(\frac{1}{1-\cos\sigma}\cdot\frac{\partial u}{\partial\sigma}\right) \text{ at } \tau = 1, \tag{3.254}$$

see Eqs. (2.83) and (2.84). For u_{m1}, u_{m2} and b_{m1}, the leading order of the equation $L_p[u] = 0,\ p = 1, 2$, is

$$0 = S[u] + T_p[u] = -\frac{4\tau^2 p^2 u}{(1-\tau^2)^2} + \cdots,\ p = 1, 2 \text{ at } \tau = 1. \tag{3.255}$$

Thus, one gets

$$u_{m1} = u_{m2} = b_{m1} = 0,\ m = 1, 2, \text{ at } \tau = 1. \tag{3.256}$$

Finally, the operators S and T are defined as follows:

$$S[u] = \frac{\partial^2 u}{\partial\sigma^2},\ T_p[u] = \frac{\tau(1-\tau)}{1+\tau}\cdot\frac{\partial}{\partial\tau}\left[\frac{\tau(1+\tau)}{1-\tau}\cdot\frac{\partial u}{\partial\tau}\right] - \frac{4p^2\tau^2 u}{(1-\tau^2)^2}, \tag{3.257}$$

at the fluid–fluid interface, see Eq. (2.88). We derive a relaxed form of the boundary conditions on the fluid–fluid interface. Using formula (2.86), we obtain

$$\begin{aligned}\lim_{\sigma\to 0^+} S[u_{1q}] = \lim_{\sigma\to 0^+}\frac{\partial^2 u_{1q}}{\partial\sigma^2} &= \frac{-7u_{1q}(\tau,0) + 8u_{1q}(\tau,\delta_{\sigma 1}) - u_{1q}(\tau,2\delta_{\sigma 1})}{2\delta_{\sigma 1}^2} \\ &\quad - \frac{3}{\delta_{\sigma 1}}\cdot\left.\frac{\partial u_{1q}}{\partial\sigma}\right|_{\sigma=0^+} + O\left(\delta_{\sigma 1}^2\right);\end{aligned} \tag{3.258}$$

$$\begin{aligned}\lim_{\sigma\to 0^-} S[u_{2q}] = \lim_{\sigma\to 0^-}\frac{\partial^2 u_{2q}}{\partial\sigma^2} &= \frac{-7u_{2q}(\tau,0) + 8u_{2q}(\tau,-\delta_{\sigma 2}) - u_{2q}(\tau,-2\delta_{\sigma 2})}{2\delta_{\sigma 2}^2} \\ &\quad + \frac{3}{\delta_{\sigma 2}}\cdot\left.\frac{\partial u_{2q}}{\partial\sigma}\right|_{\sigma=0^-} + O\left(\delta_{\sigma 2}^2\right).\end{aligned} \tag{3.259}$$

Multiplying the first equation by $\mu_1\delta_{\sigma 1}/(\mu_1\delta_{\sigma 1}+\mu_2\delta_{\sigma 2})$, the second one by $\mu_2\delta_{\sigma 2}/(\mu_1\delta_{\sigma 1}+\mu_2\delta_{\sigma 2})$ and adding them, we conclude that

$$\begin{aligned} S[u_{mq}] = &\frac{\mu_1}{\mu_1\delta_{\sigma 1}+\mu_2\delta_{\sigma 2}}\cdot\frac{-7u_{1q}(\tau,0)+8u_{1q}(\tau,\delta_{\sigma 1})-u_{1q}(\tau,2\delta_{\sigma 1})}{2\delta_{\sigma 1}} \\ &+\frac{\mu_2}{\mu_1\delta_{\sigma 1}+\mu_2\delta_{\sigma 2}}\cdot\frac{-7u_{2q}(\tau,0)+8u_{2q}(\tau,-\delta_{\sigma 2})-u_{2q}(\tau,-2\delta_{\sigma 2})}{2\delta_{\sigma 2}} \\ &+\frac{3}{\mu_1\delta_{\sigma 1}+\mu_2}\underbrace{\left[-\mu_1\left.\frac{\partial u_{1q}}{\partial\sigma}\right|_{\sigma=0^+}+\mu_2\left.\frac{\partial u_{2q}}{\partial\sigma}\right|_{\sigma=0^-}\right]}_{0\text{ (see Eq. (3.141))}}+O\left(\delta_{\sigma 1}^3+\delta_{\sigma 2}^3\right) \end{aligned} \tag{3.260}$$

hold true for $q=0,2$. Analogous computations are valid for b_{m1}. Next, we summarize the obtained results. For $\sigma\in(\alpha-\pi,\alpha)$, the definition of T_p is expanded as follows:

$$T_p[u]=\begin{cases} 0, & \tau=0; \\ \dfrac{h\tau}{1-\tau^2}\dfrac{\partial}{\partial\tau}\left[\dfrac{\tau(1-\tau^2)}{h}\cdot\dfrac{\partial u}{\partial\tau}\right]-\dfrac{4p^2\tau^2u}{(1-\tau^2)^2}, & 0<\tau<1; \\ 2\dfrac{\partial^2u}{\partial\tau^2}, & \tau=1,\ p=0; \\ 0, & \tau=1,\ p=1,2; \end{cases} \tag{3.261}$$

and that for S — as:

$$S[u_{mq}]=\begin{cases} \dfrac{-\mu_1}{\mu_1\delta_{\sigma 1}+\mu_2\delta_{\sigma 2}}\cdot\dfrac{7u_{1q}(\tau,0)-8u_{1q}(\tau,\delta_{\sigma 1})+u_{1q}(\tau,2\delta_{\sigma 1})}{2\delta_{\sigma 1}} & \\ \dfrac{-\mu_2}{\mu_1\delta_{\sigma 1}+\mu_2\delta_{\sigma 2}}\cdot\dfrac{7u_{2q}(\tau,0)-8u_{2q}(\tau,-\delta_{\sigma 2})+u_{2q}(\tau,-2\delta_{\sigma 2})}{2\delta_{\sigma 2}}, & \sigma=0,\ q=0,2; \\ \dfrac{\partial^2u_{mq}}{\partial\sigma^2}, & \tau=0,\ \sigma\neq 0; \\ h\cdot\dfrac{\partial}{\partial\sigma}\left(\dfrac{1}{h}\cdot\dfrac{\partial u_{mq}}{\partial\sigma}\right), & 0<\tau<1,\ \sigma\neq 0; \\ (1-\cos\sigma)\cdot\dfrac{\partial}{\partial\sigma}\left(\dfrac{1}{1-\cos\sigma}\cdot\dfrac{\partial u_{mq}}{\partial\sigma}\right), & \tau=1,\ \sigma\neq 0. \end{cases} \tag{3.262}$$

One obtains analogous definition for $S[b_{m1}]$.

The operators T_p and S are approximated with difference operators $\tilde{S}$ and $\tilde{T}_p$ as follows:

$$\tilde{T}_p[\mathbf{Y}_m|_{ij}^k] = \begin{cases} 0, & i = 0, \\ \dfrac{-7\,\mathbf{Y}_m|_{ij}^k + 8\,\mathbf{Y}_m|_{i-1,j}^k - \mathbf{Y}_m|_{i-2,j}^k}{\delta_\tau^2}, & i = N, \\ & p = 0; \\ 0, & i = N, \\ & p = 1, 2; \\ \dfrac{h_{i,j}\tau_i}{(1-\tau_i^2)\delta_\tau^2} \cdot \left[\dfrac{\tau_{i+1/2}(1-\tau_{i+1/2}^2)}{h_{i+1/2,j}} \cdot \left(\mathbf{Y}_m|_{i+1,j}^k - \mathbf{Y}_m|_{i,j}^k \right) \right. & \\ \qquad \left. - \dfrac{\tau_{i-1/2}(1-\tau_{i-1/2}^2)}{h_{i-1/2,j}} \cdot \left(\mathbf{Y}_m|_{i,j}^k - \mathbf{Y}_m|_{i-1,j}^k \right) \right] & \\ -\dfrac{4p^2\tau_i^2\,\mathbf{Y}_m|_{i,j}^k}{(1-\tau_i^2)^2}, & i \neq 0, N; \end{cases} \tag{3.263}$$

$$\tilde{S}[Y_{mq}|_{ij}^k] = \begin{cases} -\dfrac{\mu_1}{\mu_1\delta_{\sigma 1} + \mu_2\delta_{\sigma 2}} \cdot \dfrac{7\,Y_{1q}|_{i0}^k - 8\,Y_{1q}|_{i1}^k + Y_{1q}|_{i2}^k}{2\delta_{\sigma 1}} & \\ -\dfrac{\mu_2}{\mu_1\delta_{\sigma 1} + \mu_2\delta_{\sigma 2}} \cdot \dfrac{7\,Y_{2q}|_{i0}^k - 8\,Y_{2q}|_{i,-1}^k + Y_{2q}|_{i,-2}^k}{2\delta_{\sigma 2}}, & j = 0, \\ & q = 0, 2; \\ \dfrac{Y_{mq}|_{i,j-1}^k - 2\,Y_{mq}|_{i,j}^k + Y_{mq}|_{i,j+1}^k}{\delta_{\sigma m}^2}, & i = 0, \\ & j \neq N_1, -N_2; \\ \dfrac{1-\cos\sigma_{i,j}}{\delta_{\sigma m}^2} \left[\dfrac{Y_{mq}|_{i,j+1}^k - Y_{mq}|_{i,j}^k}{1-\cos\sigma_{i,j+1/2}} - \dfrac{Y_{mq}|_{i,j}^k - Y_{mq}|_{i,j-1}^k}{1-\cos\sigma_{i,j-1/2}} \right], & i = N, \\ & j \neq 0, N_1, -N_2; \\ \dfrac{h_{ij}}{\delta_{\sigma m}^2} \cdot \left[\dfrac{Y_{mq}|_{i,j+1}^k - Y_{mq}|_{i,j}^k}{h_{i,j+1/2}} - \dfrac{Y_{mq}|_{i,j}^k - Y_{mq}|_{i,j-1}^k}{h_{i,j-1/2}} \right], & i \neq 0, N, \\ & j \neq 0, N_1, -N_2; \end{cases} \tag{3.264}$$

$$\tilde{S}[B_{m1}|_{ij}^k] = \begin{cases} -\dfrac{\mu_1}{\mu_1\delta_{\sigma 1}+\mu_2\delta_{\sigma 2}}\cdot\dfrac{7\,B_{11}|_{i0}^k - 8\,B_{11}|_{i1}^k + B_{11}|_{i2}^k}{2\delta_{\sigma 1}} \\ -\dfrac{\mu_2}{\mu_1\delta_{\sigma 1}+\mu_2\delta_{\sigma 2}}\cdot\dfrac{7\,B_{21}|_{i0}^k - 8\,B_{21}|_{i,-1}^k + B_{21}|_{i,-2}^k}{2\delta_{\sigma 2}}, & j=0, \\ \dfrac{B_{m1}|_{i,j-1}^k - 2\,B_{m1}|_{i,j}^k + B_{m1}|_{i,j+1}^k}{\delta_{\sigma m}^2}, & \begin{array}{l} i=0, \\ j\neq N_1,-N_2; \end{array} \\ \dfrac{1-\cos\sigma_{i,j}}{\delta_{\sigma m}^2}\cdot\left[\dfrac{B_{m1}|_{i,j+1}^k - B_{m1}|_{i,j}^k}{1-\cos\sigma_{i,j+1/2}} - \dfrac{B_{m1}|_{i,j}^k - B_{m1}|_{i,j-1}^k}{1-\cos\sigma_{i,j-1/2}}\right], & \begin{array}{l} i=N, \\ j\neq N_1,-N_2; \end{array} \\ \dfrac{h_{ij}}{\delta_{\sigma m}^2}\cdot\left[\dfrac{B_{m1}|_{i,j+1}^k - B_{m1}|_{i,j}^k}{h_{i,j+1/2}} - \dfrac{B_{m1}|_{i,j}^k - B_{m1}|_{i,j-1}^k}{h_{i,j-1/2}}\right], & \begin{array}{l} i\neq 0,N, \\ j\neq N_1,-N_2. \end{array} \end{cases} \tag{3.265}$$

Approximation of the boundary conditions at the particle surface

Due to the fact that the boundary conditions at the particle surface should be applied for $\delta\mathbf{u}$, we denote the approximation of $\delta\mathbf{u}$ at (τ_i,σ_j,t_k) by

$$\delta\mathbf{Y}_1|_{ij}^k = \left(\delta Y_{10}|_{ij}^k,\ \delta Y_{11}|_{ij}^k,\ \delta Y_{12}|_{ij}^k,\ \delta B_{11}|_{ij}^k\right)^T,\ \text{for } j=\overline{0,N_1}, \tag{3.266}$$

$$\delta\mathbf{Y}_2|_{ij}^k = \left(\delta Y_{20}|_{ij}^k,\ \delta Y_{21}|_{ij}^k,\ \delta Y_{22}|_{ij}^k,\ \delta B_{21}|_{ij}^k\right)^T,\ \text{for } j=\overline{-N_2,0}, \tag{3.267}$$

see Eq. (3.250). Then, the non-zero boundary conditions at the particle surface, see Eqs. (3.137), are presented as follows:

$$\delta Y_{10}|_{iN_1}^{k+1} - \delta Y_{12}|_{iN_1}^{k+1} = \frac{1}{2} - Y_{10}|_{iN_1}^k + Y_{12}|_{iN_1}^k,\ i=\overline{1,N-1}, \tag{3.268}$$

$$\delta Y_{20}|_{i,-N_2}^{k+1} - \delta Y_{22}|_{i,-N_2}^{k+1} = \frac{1}{2} - Y_{20}|_{i,-N_2}^k + Y_{22}|_{i,-N_2}^k,\ i=\overline{1,N-1}. \tag{3.269}$$

For Eq. (3.135), we obtain

$$2\left[\left(1+\tau_i^2\right)\cos\alpha - 2\tau_i\right]\delta Y_{12}|_{iN_1}^{k+1} + \left[\left(1-\tau_i^2\right)\sin\alpha\right]\delta Y_{11}|_{iN_1}^{k+1} = 0,\ i=\overline{1,N-1}, \tag{3.270}$$

$$2\left[\left(1+\tau_i^2\right)\cos\alpha + 2\tau_i\right]\delta Y_{22}|_{i,-N_2}^{k+1} + \left[\left(1-\tau_i^2\right)\sin\alpha\right]\delta Y_{21}|_{i,-N_2}^{k+1} = 0,\ i=\overline{1,N-1}. \tag{3.271}$$

Next, the boundary condition (3.137) is approximated as

$$\delta B_{11}|_{iN_1}^{k+1} + \frac{1-\tau_i^2}{h_{i,N_1}}\left[\delta Y_{10}|_{iN_1}^{k+1} + \delta Y_{12}|_{iN_1}^{k+1}\right] + \frac{2\tau_i\sin\alpha}{h_{i,N_1}}\,\delta Y_{11}|_{i,N_1}^{k+1} = 0, \tag{3.272}$$

$$\delta B_{21}|_{i,-N_2}^{k+1} + \frac{1-\tau_i^2}{h_{i,-N_2}}\left[\delta Y_{20}|_{i,-N_2}^{k+1} + \delta Y_{22}|_{i,-N_2}^{k+1}\right] - \frac{2\tau_i\sin\alpha}{h_{i,-N_2}}\,\delta Y_{21}|_{i,-N_2}^{k+1} = 0 \tag{3.273}$$

for $i = \overline{1, N-1}$. Using the formula [3.20]

$$u'(x) = \pm\frac{3u(x) - 4u(x \mp \delta_x) + u(x \mp 2\delta_x)}{2\delta_x} + O(\delta_x^2), \tag{3.274}$$

we approximate (3.136) for the upper part of the particle surface ($\sigma = \alpha$) as follows:

$$\begin{aligned}
&\delta Y_{12}|_{iN_1}^{k+1} + \frac{\left(1-\tau_i^2\right)\sin\alpha}{16\tau_i\delta_{\sigma 1}} \cdot \Big\{ \delta B_{11}|_{i,N_1-2}^{k+1} - 4\delta B_{11}|_{i,N_1-1}^{k+1} + 3\ \delta B_{11}|_{i,N_1}^{k+1} \\
&\quad + \left(1-\tau_i^2\right)\left[\frac{\delta Y_{10}|_{i,N_1-2}^{k+1}}{h_{i,N_1-2}} - \frac{4\ \delta Y_{10}|_{i,N_1-1}^{k+1}}{h_{i,N_1-1}} + \frac{3\ \delta Y_{10}|_{i,N_1}^{k+1}}{h_{i,N_1}}\right] \\
&\quad + \left(1-\tau_i^2\right)\left[\frac{\delta Y_{12}|_{i,N_1-2}^{k+1}}{h_{i,N_1-2}} - \frac{4\ \delta Y_{12}|_{i,N_1-1}^{k+1}}{h_{i,N_1-1}} + \frac{3\ \delta Y_{12}|_{i,N_1}^{k+1}}{h_{i,N_1}}\right] \\
&\quad + 2\tau_i\left[\frac{\sin\sigma_{N_1-2}}{h_{i,N_1-2}}\ \delta Y_{11}|_{i,N_1-2}^{k+1} - \frac{4\sin\sigma_{N_1-1}}{h_{i,N_1-1}}\ \delta Y_{11}|_{i,N_1-1}^{k+1} + \frac{3\sin\alpha}{h_{i,N_1}}\ \delta Y_{11}|_{i,N_1}^{k+1}\right]\Big\} \\
&\quad = 0,\ i = \overline{1, N-1}
\end{aligned} \tag{3.275}$$

and for the lower part of the particle surface as follows: ($\sigma = \alpha - \pi$)

$$\begin{aligned}
&\delta Y_{22}|_{i,-N_2}^{k+1} + \frac{\left(1-\tau_i^2\right)\sin\alpha}{16\tau_i\delta_{\sigma 2}} \cdot \Big\{ 3\ \delta B_{21}|_{i,-N_2}^{k+1} - 4\delta B_{21}|_{i,1-N_2}^{k+1} + \delta B_{21}|_{i,2-N_2}^{k+1} \\
&\quad + \left(1-\tau_i^2\right)\left[\frac{3\ \delta Y_{20}|_{i,-N_2}^{k+1}}{h_{i,-N_2}} - \frac{4\ \delta Y_{20}|_{i,1-N_2}^{k+1}}{h_{i,1-N_2}} + \frac{\delta Y_{20}|_{i,2-N_2}^{k+1}}{h_{i,2-N_2}}\right] \\
&\quad + \left(1-\tau_i^2\right)\left[\frac{3\ \delta Y_{22}|_{i,-N_2}^{k+1}}{h_{i,-N_2}} - \frac{4\ \delta Y_{22}|_{i,1-N_2}^{k+1}}{h_{i,1-N_2}} + \frac{\delta Y_{22}|_{i,2-N_2}^{k+1}}{h_{i,2-N_2}}\right] \\
&\quad + 2\tau_i\left[-\frac{3\sin\alpha}{h_{i,-N_2}}\ \delta Y_{21}|_{i,-N_2}^{k+1} - \frac{4\sin\sigma_{1-N_2}}{h_{i,1-N_2}}\ \delta Y_{21}|_{i,1-N_2}^{k+1} + \frac{\sin\sigma_{2-N_2}}{h_{i,2-N_2}}\ \delta Y_{21}|_{i,2-N_2}^{k+1}\right]\Big\} \\
&\quad = 0,\ i = \overline{1, N-1}.
\end{aligned} \tag{3.276}$$

Approximation of the boundary conditions at the fluid–fluid interface

At the fluid–fluid interface, the boundary conditions (3.139) are approximated as follows:

$$\delta Y_{10}|_{i0}^{k+1} = \delta Y_{20}|_{i,0}^{k+1},\ \delta Y_{12}|_{i0}^{k+1} = \delta Y_{22}|_{i,0}^{k+1},\ \delta B_{11}|_{i0}^{k+1} = \delta B_{21}|_{i,0}^{k+1},\ i = \overline{1, N-1}, \tag{3.277}$$

Eq. (3.140) for $m = 1$ — as:

$$\begin{aligned}
&\delta Y_{11}|_{i0}^{k+1} + \frac{(1-\tau_i)^2}{4\tau_i\delta_{\sigma 1}}\left[3\ \delta B_{11}|_{i,0}^{k+1} - 4\ \delta B_{11}|_{i,1}^{k+1} + \delta B_{11}|_{i,2}^{k+1}\right] \\
&\quad + \frac{1-\tau_i^2}{4\tau_i\delta_{\sigma 1}}\left[3\ \delta Y_{10}|_{i,0}^{k+1} - 4\ \delta Y_{10}|_{i,1}^{k+1} + \delta Y_{10}|_{i,2}^{k+1}\right] \\
&\quad + \frac{1-\tau_i^2}{4\tau_i\delta_{\sigma 1}}\left[3\ \delta Y_{12}|_{i,0}^{k+1} - 4\ \delta Y_{12}|_{i,1}^{k+1} + \delta Y_{12}|_{i,2}^{k+1}\right] = 0,\ i = \overline{1, N-1}
\end{aligned} \tag{3.278}$$

and Eq. (3.140) for $m = 2$ — as:

$$\begin{aligned}\delta Y_{21}|_{i0}^{k+1} &- \frac{(1-\tau_i)^2}{4\tau_i\delta_{\sigma 2}}\left[\delta B_{21}|_{i,-2}^{k+1} - 4\delta B_{21}|_{i,-1}^{k+1} + 3\ \delta B_{21}|_{i,0}^{k+1}\right] \\ &- \frac{1-\tau_i^2}{4\tau_i\delta_{\sigma 2}}\left[\delta Y_{20}|_{i,-2}^{k+1} - 4\delta Y_{20}|_{i,-1}^{k+1} + 3\ \delta Y_{20}|_{i,0}^{k+1}\right] \\ &- \frac{1-\tau_i^2}{4\tau_i\delta_{\sigma 2}}\left[\delta Y_{22}|_{i,-2}^{k+1} - 4\delta Y_{22}|_{i,-1}^{k+1} + 3\ \delta Y_{22}|_{i,0}^{k+1}\right] = 0,\ i = \overline{1, N-1}, \end{aligned} \tag{3.279}$$

see formula (3.274). The boundary conditions for scalar potentials and dynamic boundary conditions, Eqs. (3.141), are replaced with (3.249), where $\tilde{S}$ is defined, using Eq. (3.264) and (3.265).

Approximation of the boundary conditions at the contact line

In order to approximate the boundary conditions (3.143) and (3.144) at $\tau = 0$, we find the values of the function b_m as follows:

$$b_m|_{ij}^{k+1} = B_{m1}|_{ij}^{k+1} + \frac{1-\tau_i^2}{h_{i,j}}\left(Y_{m0}|_{i,j}^{k+1} + Y_{m2}|_{i,j}^{k+1}\right) + \frac{2\tau_i \sin\sigma_j}{h_{i,j}}\ Y_{m1}|_{i,j}^{k+1} \tag{3.280}$$

for $m = 1, 2$. The derivative $\partial b_m/\partial\tau$ at $\tau = 0$ is approximated as

$$D_\tau b_m|_{0j}^{k+1} = \frac{4\ b_m|_{1j}^{k+1} - b_m|_{2j}^{k+1}}{2\delta_\tau},\ m = 1, 2 \tag{3.281}$$

due to the fact that $b_m|_{0j}^{k+1} = 0$, see (3.145). Next, the approximation of the second mixed partial derivative at $\tau = 0$ — as:

$$D_{\sigma\tau} b_m|_{0j}^{k+1} = \begin{cases} \dfrac{-3\ D_\tau b_2|_{0,-N}^{k+1} + 4\ D_\tau b_2|_{0,-N+1}^{k+1} - D_\tau b_2|_{0,-N+2}^{k+1}}{2\delta_{\sigma 2}}, & \sigma = \alpha - \pi, \\ \dfrac{D_\tau b_2|_{0,j+1}^{k+1} - D_\tau b_2|_{0,j-1}^{k+1}}{2\delta_{\sigma 2}}, & -N_2 < j < 0, \\ \dfrac{D_\tau b_2|_{0,-2}^{k+1} - 4\ D_\tau b_2|_{0,-1}^{k+1} + 3\ D_\tau b_2|_{0,0}^{k+1}}{2\delta_{\sigma 2}}, & \sigma = 0,\ m = 2, \\ \dfrac{-3\ D_\tau b_1|_{0,0}^{k+1} + 4\ D_\tau b_1|_{0,1}^{k+1} - D_\tau b_1|_{0,2}^{k+1}}{2\delta_{\sigma 1}}, & \sigma = 0,\ m = 1, \\ \dfrac{D_\tau b_1|_{0,j+1}^{k+1} - D_\tau b_1|_{0,j-1}^{k+1}}{2\delta_{\sigma 1}}, & 0 < j < N_1, \\ \dfrac{D_\tau b_1|_{0,N-2}^{k+1} - 4\ D_\tau b_1|_{0,N-1}^{k+1} + 3\ D_\tau b_1|_{0,N}^{k+1}}{2\delta_{\sigma 1}}, & \sigma = \alpha. \end{cases} \tag{3.282}$$

Then, the approximations of the boundary condition (3.143) and (3.144) have the form:

$$Y_{m2}|_{0j}^{k+1} = \frac{1}{8}\left(D_\tau b_m|_{0j}^{k+1} \cos\sigma - D_{\sigma\tau} b_m|_{0j}^{k+1} \sin\sigma \right),\ m = 1, 2, \tag{3.283}$$

$$Y_{m1}|_{0j}^{k+1} = \frac{1}{4}\left(D_\tau b_m|_{0j}^{k+1} \sin\sigma + D_{\sigma\tau} b_m|_{0j}^{k+1} \cos\sigma \right),\ m = 1, 2. \tag{3.284}$$

At the contact line ($\tau = 0$), the boundary conditions (3.145) are approximated as

$$\delta Y_{m0}|_{0j}^{k+1} = \frac{1}{2} + Y_{m2}|_{0j}^{k+1},\ j = \overline{-N_2, N_1}, \tag{3.285}$$

$$\delta B_{m1}|_{0j}^{k+1} = -\ Y_{m0}|_{0j}^{k+1} - Y_{m2}|_{0j}^{k+1},\ j = \overline{-N_2, N_1}. \tag{3.286}$$

3.7.2 Algorithm

The algorithm for finding the flow velocities is presented in Algorithm 2. It is analogous to the algorithm for finding the potentials distributions.

Algorithm 2 Compute the velocity fields

procedure ComputeVelocities(N)
  Compute the lengths of the steps $\delta_{\sigma 1},\ \delta_{\sigma 2},\ \delta_\tau,\ \delta_t$; ▷ (2.63), (2.67), (3.242), (3.242);
  $k \to 0$;
  Set the values of $\mathbf{Y}_m,\ m = 1, 2$ to $\mathbf{0}$ for initial moment of time ($k = 0$);

  repeat
    for $j \leftarrow -N_2 + 1$ to -1 **do**
      Solve a τ-directional problem (T2) for $\overline{\mathbf{Y}}_2$;
    end for

    for $j \leftarrow 1$ to $N_1 - 1$ **do**
      Solve a τ-directional problem (T1) for $\overline{\mathbf{Y}}_1$;
    end for

    for $i \leftarrow -N + 1$ to $N - 1$ **do**
      Solve a σ-directional problem (SI) for $\delta\mathbf{Y}_1$ and $\delta\mathbf{Y}_2$;
    end for

    Compute the values of $\delta\mathbf{Y}_m$ at the contact line ▷ Eqs. (3.283)–(3.286)
    Solve a σ-directional problem (S1) for δY_{10} and δY_{20} at the axis of revolution;
    Set the values of δY_{m1}, δY_{m2} and δB_{m1} to 0 at the axis of revolution, $m = 1, 2$;

    Compute the total error $TotalError$ at time k;
    Compute the values $\mathbf{Y}_m,\ m = 1, 2$ at the next moment of time; ▷ Eq. (3.250)
    $k \to k + 1$;
  until ($TotalError > 1$ or $k <= 100000$);
end procedure;

The iteration process stops, when the maximal number of iterations is reached or the following criterion:

$$\left| \frac{Y_{mq}|_{ij}^{k+1} - Y_{mq}|_{ij}^{k}}{\delta_t^3} \right| \approx 1 \tag{3.287}$$

holds true. This criterion is obtained as follows:

$$0 = \left. \frac{\partial u_{mq}}{\partial t} \right|_{\tau_i,\sigma_j}^{t+\delta_t/2} = \frac{Y_{mq}|_{ij}^{k+1} - Y_{mq}|_{ij}^{k}}{\delta_t} - \frac{\delta_t^2}{24} \left. \frac{\partial^3 u_{mq}}{\partial t^3} \right|_{\tau_i,\sigma_j}^{t+\delta_t/2} + O(\delta_t^3). \tag{3.288}$$

Next, we shall specify the different τ and σ-directional problems that are solved. The τ-directional problem (T1) has the form

- At the phase 1:

$$\left(U - \frac{\delta_t}{2}\tilde{T}_0\right) \left[\overline{Y}_{10}|_{ij}^{k+1}\right] = \delta_t \tilde{T}_0 \left[Y_{10}|_{ij}^{k}\right] + \delta_t \tilde{S} \left[Y_{10}|_{ij}^{k}\right], \; i = \overline{1, N-1}, \tag{3.289}$$

$$\left(U - \frac{\delta_t}{2}\tilde{T}_1\right) \left[\overline{Y}_{11}|_{ij}^{k+1}\right] = \delta_t \tilde{T}_1 \left[Y_{11}|_{ij}^{k}\right] + \delta_t \tilde{S} \left[Y_{11}|_{ij}^{k}\right], \; i = \overline{1, N-1}, \tag{3.290}$$

$$\left(U - \frac{\delta_t}{2}\tilde{T}_2\right) \left[\overline{Y}_{12}|_{ij}^{k+1}\right] = \delta_t \tilde{T}_2 \left[Y_{12}|_{ij}^{k}\right] + \delta_t \tilde{S} \left[Y_{12}|_{ij}^{k}\right], \; i = \overline{1, N-1}, \tag{3.291}$$

$$\left(U - \frac{\delta_t}{2}\tilde{T}_1\right) \left[\overline{B}_{11}|_{ij}^{k+1}\right] = \delta_t \tilde{T}_1 \left[B_{11}|_{ij}^{k}\right] + \delta_t \tilde{S} \left[B_{11}|_{ij}^{k}\right], \; i = \overline{1, N-1}; \tag{3.292}$$

- At the contact line:

$$\overline{Y}_{10}|_{0j}^{k+1} = \delta_t \tilde{S} \left[Y_{10}|_{0j}^{k}\right], \tag{3.293}$$

$$\overline{Y}_{11}|_{0j}^{k+1} = \delta_t \tilde{S} \left[Y_{11}|_{0j}^{k}\right], \tag{3.294}$$

$$\overline{Y}_{12}|_{0j}^{k+1} = \delta_t \tilde{S} \left[Y_{12}|_{0j}^{k}\right], \tag{3.295}$$

$$\overline{B}_{11}|_{0j}^{k+1} = \delta_t \tilde{S} \left[B_{11}|_{0j}^{k}\right]; \tag{3.296}$$

- At the axis of revolution:

$$\left(U - \frac{\delta_t}{2}\tilde{T}_0\right) \left[\overline{Y}_{10}|_{Nj}^{k+1}\right] = \delta_t \tilde{T}_0 \left[Y_{10}|_{Nj}^{k}\right] + \delta_t \tilde{S} \left[Y_{m0}|_{Nj}^{k}\right], \tag{3.297}$$

$$\overline{Y}_{11}|_{Nj}^{k+1} = 0, \tag{3.298}$$

$$\overline{Y}_{12}|_{Nj}^{k+1} = 0, \tag{3.299}$$

$$\overline{B}_{11}|_{Nj}^{k+1} = 0; \tag{3.300}$$

Analogously, the problem (T2) is defined. Next, the σ-directional problem for the internal nodes (SI) is written as

- At the phase 1:

$$\left(U-\frac{\delta_t}{2}\tilde{S}\right)\left[\delta Y_{10}|_{ij}^{k+1}\right]=\overline{Y}_{10}|_{ij}^{k+1},\ j=\overline{1,N_1-1}, \tag{3.301}$$

$$\left(U-\frac{\delta_t}{2}\tilde{S}\right)\left[\delta Y_{11}|_{ij}^{k+1}\right]=\overline{Y}_{11}|_{ij}^{k+1},\ j=\overline{1,N_1-1}, \tag{3.302}$$

$$\left(U-\frac{\delta_t}{2}\tilde{S}\right)\left[\delta Y_{12}|_{ij}^{k+1}\right]=\overline{Y}_{12}|_{ij}^{k+1},\ j=\overline{1,N_1-1}, \tag{3.303}$$

$$\left(U-\frac{\delta_t}{2}\tilde{S}\right)\left[\delta B_{11}|_{ij}^{k+1}\right]=\overline{B}_{11}|_{ij}^{k+1},\ j=\overline{1,N_1-1}; \tag{3.304}$$

- At the phase 2:

$$\left(U-\frac{\delta_t}{2}\tilde{S}\right)\left[\delta Y_{20}|_{ij}^{k+1}\right]=\overline{Y}_{20}|_{ij}^{k+1},\ j=\overline{1-N_2,-1}, \tag{3.305}$$

$$\left(U-\frac{\delta_t}{2}\tilde{S}\right)\left[\delta Y_{21}|_{ij}^{k+1}\right]=\overline{Y}_{21}|_{ij}^{k+1},\ j=\overline{1-N_2,-1}, \tag{3.306}$$

$$\left(U-\frac{\delta_t}{2}\tilde{S}\right)\left[\delta Y_{22}|_{ij}^{k+1}\right]=\overline{Y}_{22}|_{ij}^{k+1},\ j=\overline{1-N_2,-1}, \tag{3.307}$$

$$\left(U-\frac{\delta_t}{2}\tilde{S}\right)\left[\delta B_{21}|_{ij}^{k+1}\right]=\overline{B}_{21}|_{ij}^{k+1},\ j=\overline{1-N_2,-1}; \tag{3.308}$$

- At the lower part of the particle, the approximations (3.269), (3.271), (3.273) and (3.276) are used;
- At the interface, we obtain equations (3.249), (3.277)– (3.279) instead of Eqs. (3.141);
- At the upper part of the particle, one uses Eqs. (3.268), (3.270), (3.272), (3.275);

Finally, the problem (S1) is defined as:

- At the phase 1:

$$\left(U-\frac{\delta_t}{2}\tilde{S}\right)\left[\delta Y_{10}|_{Nj}^{k+1}\right]=\overline{Y}_{10}|_{Nj}^{k+1},\ j=\overline{1,N_1-1}; \tag{3.309}$$

- At the phase 2:

$$\left(U-\frac{\delta_t}{2}\tilde{S}\right)\left[\delta Y_{20}|_{N,j}^{k+1}\right]=\overline{Y}_{20}|_{N,j}^{k+1},\ j=\overline{-N_2+1,-1}; \tag{3.310}$$

- At the lower part of the particle surface:

$$\delta Y_{20}|_{N,-N_2}^{k+1}=\frac{1}{2}-Y_{20}|_{N,-N_2}^{k}; \tag{3.311}$$

- At the infinity point:

$$\delta Y_{20}|_{N0}^{k+1}=0,\ \ \delta Y_{10}|_{N0}^{k+1}=0; \tag{3.312}$$

- At the upper part of the particle surface:

$$\delta Y_{10}|_{NN_1}^{k+1} = \frac{1}{2} - Y_{10}|_{NN_1}^{k}\,; \tag{3.313}$$

Note that in order to implement the algorithm, you need the information in the last two moments of time only. Efficient implementation saves only the data in the current and the previous moment of time. In order to compute the drag, we use the formula (A.49), which is derived in Appendix A.

3.7.3 Numerical results

In order to validate the results, we compare the values of the drag coefficient, computed using our method to the semi-analytic results [3.1] for $\alpha \leq 90^\circ$ and fluid–air interface (see Table 3.1). The computations are performed for $\delta_\sigma = 0.017$, $\delta_\tau = 0.05$ and different time steps δ_t. The relative error is less than 1% and the CPU time on a laptop with processor Intel Core i5-4200H is less than 10 s in all studied cases. As it can be expected, the decrease of the grid size decreases the relative error of the drag coefficient. For example, if $\alpha = 15^\circ$ and the rectangular domain is divided by 20×20 then the relative error is 0.16%, while for 30×30—it decreases to 0.017%. The respective CPU time for calculations increases from 4.3s to 11s—it triples by increasing the number of space-discretisation steps by factor of 2.25. Analogous trends hold true for all values of the contact angle.

Table 3.1: Comparison between the calculated values, using the proposed method, and analytic values of the drag force coefficient [3.1].

α (°)	δ_t	CPU time (s)	appr. drag coeff.	exact drag coeff.	Rel. error (%)
15	0.10	2.534	1.4306	1.4374	0.473
30	0.15	7.332	1.4013	1.3392	0.612
60	0.45	7.504	1.2522	1.2509	0.104
75	0.60	5.242	1.1473	1.1370	0.906
90	0.60	8.798	0.9916	1.0000	0.840

Fig. 3.6 shows the pressure distribution for air/water interface and two values of the three-phase contact angle. It is well illustrated that the pressure maximum for $\alpha = 90^\circ$ is at the contact line, while that for $\alpha = 60^\circ$—it is shifted along the particle surface inside the fluid phase. Using the proposed numerical method, it is possible to perform a systematic study for wide ranges of physical parameters. Moreover, the proposed algorithm decreases the computational time from 10 to 1000 times compared to that in the literature. The smallest the contact angle is the fastest the proposed approach is.

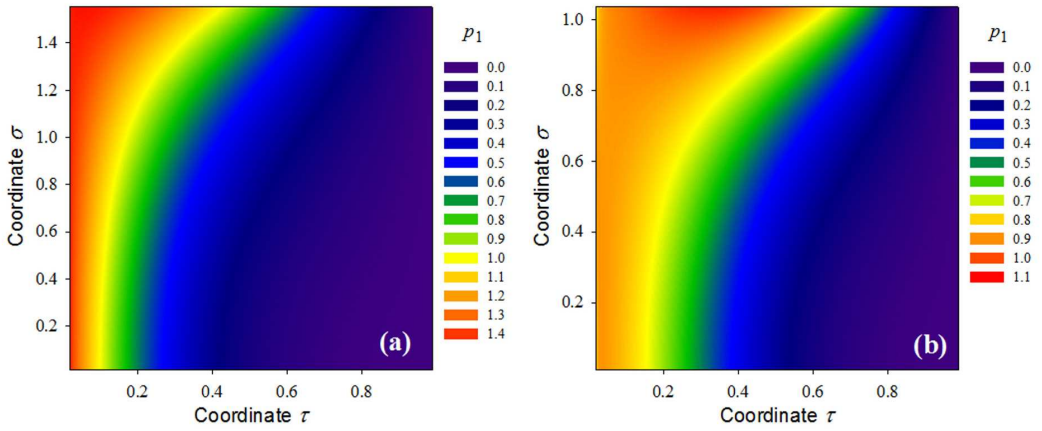

Figure 3.6: Pressure distribution for air/fluid interfaces: **a)** $\alpha = 90°$; **b)** $\alpha = 60°$.

3.8 Conclusion

The hydrodynamic problem for the translation of a spherical particle, attached to a fluid–fluid interface, is simplified using the gauge formulation. The introduction of appropriate functions and toroidal coordinates reduces the three-dimensional Stokes equations to a two-dimensional system of eight homogeneous partial differential equations. The system is coupled because of the complex boundary conditions. The problem is solved, using the efficient alternating direction implicit type second-order numerical scheme and reformulating adequately the boundary conditions. As a result, the method enables us to do fast and precise calculations of all physical parameters (velocity vector and pressure fields, and drag force coefficient). Moreover, the numerical time is reduced from 10 to 1000 times, compared to that in [3.11]. From practical viewpoint, these calculations are introduced as a part of data processing and/or of two-dimensional ordering problems. Thus, the decrease of the computational time becomes an important step to increase the efficiency of complex numerical tasks.

References

[3.1] M. Zabarankin. Asymmetric three-dimensional stokes flows about two fused equal spheres. *Proc. R. Soc. A*, 463(2085):2329–2349, 2007. DOI: 10.1098/rspa.2007.1872.

[3.2] J. Wu and G.-H. Ma. Recent studies of pickering emulsions: Particles make the difference. *Small*, 12(34):4633–4648, 2016. DOI: 10.1002/smll.201600877.

[3.3] H. Jiang, Y. Sheng, and T. Ngai. Pickering emulsions: Versatility of colloidal particles and recent applications. *Current Opinion in Colloid & Interface Science*, 49:1–15, 2020. DOI: 10.1016/j.cocis.2020.04.017.

[3.4] N. Shanmugam, R. Pugazhendhi, R. Elavarasan, K. Pitchandi, and N. Das. Anti-reflective coating materials: A holistic review from pv perspective. *Energies*, 13:2631, 05 2020. DOI: 10.3390/en13102631.

[3.5] K. Baryshnikova, M. Petrov, V. Babicheva, and P. Belov. Plasmonic and silicon spherical nanoparticle anti-reflective coatings. *Scientific Reports*, 6, 08 2015. DOI: 10.1038/srep22136.

[3.6] O. Cayre and V. Paunov. Fabrication of microlens arrays by gel trapping of self-assembled particle monolayers at the decane-water interface. *Journal of Materials Chemistry*, 14, 2004. DOI: 10.1039/b413361g.

[3.7] X. Xing, M. Chen, Y. Gong, Z. Lv, S. Han, and Y. Zhou. Building memory devices from biocomposite electronic material. *Sci Technol Adv Mater.*, 21(1):100–121, 2020. DOI: 10.1080/14686996.2020.1725395.

[3.8] T. Hu, X. Mei, Y. Wang, X. Weng, R. Liang, and M. Wei. Two-dimensional nanomaterials: fascinating materials in biomedical field. *Science Bulletin*, 64(22):1707–1727, 2019. DOI: 10.1016/j.scib.2019.09.021.

[3.9] A. Dani, G. Keiser, M. Yeganeh, and C. Maldarelli. Hydrodynamics of particles at an oil–water interface. *Langmuir*, 31:13290–13302, 2015. DOI:10.1021/acs.langmuir.5b02146.

[3.10] A. Dorr, S. Hardt, H. Masoud, and H. Stone. Drag and diffusion coefficients of a spherical particle attached to a fluid-fluid interface. *J. Fluid Mech.*, 790:607–618, 2016. DOI: 10.1017/jfm.2016.41.

[3.11] K. Danov, R. Dimova, and B. Pouligny. Viscous drag of a solid sphere straddling a spherical or flat surface. *Phys. Fluids*, 12:2711–2722, 2000. DOI: 10.1063/1.1289692.

[3.12] G. Stokes. On the effect of the internal friction of fluids on the motion of pendulums. *Trans. Camb. Phil. Soc.*, 9:8–106, 1851. DOI: 10.1017/CBO9780511702266.002.

[3.13] H. Langtangen, K. Mardal, and R. Winther. Numerical methods for incompressible viscous flow. *Advances in Water Resources*, 25(8):1125–1146, 2002. DOI: 10.1016/S0309-1708(02)00052-0.

[3.14] D. Kwak and C. Kiris. Methods for solving viscous incompressible flow problems. 01 2011. DOI: 10.1007/978-94-007-0193-9_2.

[3.15] W. E and J.-G. Liu. Gauge method for viscous incompressible flows. *Comm. Math. Sci.*, 1(2):317–332, 2003. DOI: 10.4310/CMS.2003.v1.n2.a6.

[3.16] D. Brown, R. Cortez, and M. Minion. Accurate projection methods for the incompressible navier-–stokes equations. *Journal of Computational Physics*, 168(2):464–499, 2001. DOI: 10.1006/jcph.2001.6715.

[3.17] Y. D'Yakonov. Difference schemes with a "disintegrating" operator for multidimensional problems. *USSR Computational Mathematics and Mathematical Physics*, 2(4):581–607, 1963. DOI: 10.1016/0041-5553(63)90531-7.

[3.18] N. Yanenko. *The Method of Fractional Steps, the Solution of Problems of Mathematical Physics in Several Variables*. Springer Berlin, Heidelberg, 1971. DOI: 10.1007/978-3-642-65108-3.

[3.19] J. Thomas. *Numerical Partial Differential Equations: Finite Difference Methods*. Springer New York, 1995. DOI: 10.1007/978-1-4899-7278-1.

[3.20] C. Gerald and P. Wheatley. *Applied numerical analysis*. Pearson College Div, 7 edition, 2004.

Chapter 4

Motion of long bubbles in gravity- and pressure-driven flow through cylindrical capillaries up to moderate capillary numbers

In this chapter, we focus our attention to the motion of long bubbles in gravity- and pressure-driven flows. This problem has a wide range of applications in microfluidics and chemical microprocessing. For the first time, the problem was solved asymptotically for small values of the capillary number by Bretherton in 1961 [4.1]. He computed asymptotic expressions, which describe the dependence of the capillary (Ca) and Bond (Bo) numbers on the system parameters for low axisymmetric bubble velocities, which are valid only in the ranges $0 < Ca < 0.005$ and $0.84 < Bo < 1.04$.

Nowadays, due to the recent advances in technology, there is a renewed interest in the Bretherton problem. We propose a new generalized lubrication approach, which solves the problem in a systemic way. As in the Bretherton solution, the fluid is modeled as Stokes flow but the bubble shape is described, using geometrical considerations and the Young–Laplace equation of capillarity [4.2]. The latter is the main difference between the proposed method and the Bretherton solution, which uses an approximation of the bubble curvature instead. The obtained model consists of six differential equations which are coupled, and appropriate boundary conditions are added in order to close the problem. Assuming that the characteristic thickness of the liquid layer is a small parameter of the considered problem, we obtain not only the zero-order approximation of the hydrodynamic problem in the lubrication approximation, which coincides with the Bretherton solution, but also the first-order approximation. In such a way, the problem is reduced to a boundary value problem, consisting of four ordinary differential equations. The applied initial conditions are computed, using small perturbations around the cylindrical shape of the bubble. The obtained problem is solved numerically to obtain the film thickness, h, between the bubble and the capillary and the dependence of the capillary number on the flow parameters and

magnitude of gravity. The proposed model expands the range of solution applicability 400 and 38 times, respectively ($0 < Ca < 2$ and $0 < Bo < 7.5$). These results are validated with available experimental data. The model simplicity and its transparency give possibility to generalize this approach by including new physicochemical properties of liquids and interfaces.

The results, included in this chapter, are published in

- K. Danov, G. Lyutskanova-Zhekova, S. Smoukov, Motion of long bubbles in gravity- and pressure-driven flow through cylindrical capillaries up to moderate capillary numbers, Physics of fluids **33** (2021), no. 11, IF: 3.521 (2020), Quartile: Q1. DOI: `https://doi.org/10.1063/5.0070619`.

4.1 Literature overview

The transport of bubbles and drops through capillaries and porous media plays an important role in many technological and biological systems: enhanced oil recovery [4.3–4.5]; movement of red blood cells [4.6, 4.7]; pulmonary airway reopeninig [4.8–4.10]; motion of discrete bubbles in porous materials [4.11]; biomechanics and microfluidic devices [4.12–4.14]; circulating fluidized bed (CFB) devices [4.15, 4.16]; etc. In some of these applications (e.g. microfluidics), the dimensionless thickness of the liquid film, h, is an important design parameter and, therefore, it is essential to find an expression for it. In order to do that, two different classes of experimental methods could be used — direct (the film thickness is measured directly) or indirect (the velocity of the bubble is measured directly). Using an indirect experimental method requires to find a relationship between the bubble velocity, other flow parameters and h. One way to do that is by using data fitting techniques. The function type is chosen appropriately, using the data, which is fitted, and some theoretical considerations. The other approach is to use the fluid mechanics and more precisely — the Navier–Stokes equations with appropriate boundary conditions applied. If the film thickness is neglectable with regard to the radius of the tube, the original problem could be significantly simplified, using the lubrication approach. Depending on the applied assumptions, the obtained problem could be simple enough to be solved analytically (analytical approach) or should be solved, using a numerical method (semi-analytical approach). If the film thickness is not neglectable, then the full problem should be solved numerically, using for instance the finite difference, the finite volume or the finite element method.

From experimental and theoretical viewpoint, it is convenient to study two simplified cases of the motion of bubbles: in vertical capillaries, sealed at one end, under the action of gravity; in horizontal tubes through which a fluid is flowing. Important dimensionless parameter, describing the behaviour of these simplified cases, is the capillary number Ca, which is defined as the ratio between the viscous forces and surface tension forces:

$$Ca \equiv \frac{\eta V_b}{\sigma}, \tag{4.1}$$

where η is the liquid dynamic viscosity, V_b is the translational bubble velocity and σ is the surface tension. In case of long bubbles in vertical tubes, one of the most essential parameters is the Bond number Bo (the ratio between the gravitational forces and surfaces tension forces):

$$Bo \equiv \frac{\rho g R^2}{\sigma}, \tag{4.2}$$

while in the case of long bubbles in horizontal tubes, the relative increase of the velocity, W:

$$W \equiv 1 - \frac{V_{pm}}{V_b} \tag{4.3}$$

plays an important role, where g is the gravity acceleration, ρ is the fluid density, R is the capillary radius and V_{pm} is the mean speed of the respective Poiseuille flow. These dimensionless parameters are used in order to find the solution of the two simplified cases. More concretely, a relationship between the dimensionless parameters Ca, $Bo(h)$ and possibly other dimensionless groups is sought out in the case of bubbles in vertical tubes, while a relationship between Ca and $W(h)$ is investigated for bubbles in horizontal capillaries. More complex cases are also considered in the literature. For example, Zukoski [4.17] presented experimental data for the more complex case of incline tubes, studied the influence of tube inclination angle on the rising bubble velocity, and gave qualitative explanations of the flow behavior.

Two of the earliest studies of long bubbles in vertical tubes are conducted by Gibson [4.18] and Barr [4.19]. They noticed that if the Bond number is sufficiently small, then the long bubbles in vertical cylindrical capillaries do not rise at all [4.20]. Systematic experimental dependencies of the Bond number on the capillary number and other dimensionless groups (Reynolds, Froude numbers, etc.) are conducted in [4.21–4.27]. Clanet et al. [4.12] showed experimentally that the Dumitrescu limiting law [4.21], valid in the high-Reynolds-number domain, can be generalized to $V = (8\pi)^{-1/2} (gP)^{1/2}$, where P is the wetted (inside) perimeter of the normal cross-section of cylindrical, rectangular, regular polygons, and toroidal tubes. The semi-analytical and numerical solutions of the respective hydrodynamic problems are reported in the literature [4.28–4.34]. The first analytical result for long rising bubbles at small capillary numbers was derived by Bretherton [4.1]. He solved the hydrodynamic problem in the lubrication approximation for flow in the thin layer between the bubble and the capillary and, then, match the obtained function for the bubble shape with the solution of the Laplace equation around the bubble front. The derived Bretherton dependence reads

$$Bo = 0.842 + 1.25Ca^{2/9} + 2.24Ca^{1/3}, \tag{4.4}$$

which is accurate to within 10% in the region $0.842 < Bo < 1.04$.

The case of long bubbles in horizontal tubes is studied extensively. Firstly, Fairbrother and Stubbs [4.35] pointed out that long bubbles in horizontal cylindrical tubes move faster than the mean speed of the respective Poiseuille flow. Using data fitting techniques, they were able to propose the following relationship between the film thickness h and capillary number Ca:

$$h = 0.5\sqrt{Ca}. \tag{4.5}$$

The latter is valid for $7.5 \times 10^{-5} < Ca < 0.014$. Then, in 1960, Taylor measured the relative increase of the velocity for small and moderate values of the capillary number, $Ca < 2$, [4.36]. The developed new experimental methods [4.16, 4.37–4.44] for the precise measurements of the liquid film thickness and velocity profiles confirm the Taylor experimental data and clarify the physical picture of the bubble shape and surrounding flow behavior. The numerical calculations for small and large Reynolds numbers [4.45–4.56] provide information on the theoretical dependence of W on the system parameters. For example, Langewisch and Buongiorno [4.54] reported numerical results for 125 combinations of capillary numbers ($0.05 < Ca < 2$) and Reynolds numbers (up to 900), which are used therein to construct new empirical correlations. A pioneering theoretical approach was proposed by Bretherton in

[4.1]. He matched the lubrication approximation solution of the hydrodynamic problem for long bubbles with the radius of curvature of the bubble front, corresponding to the capillary radius, and derived the asymptotic expressions:

$$W = 2.68Ca^{2/3},\ h = 1.34Ca^{2/3}, \tag{4.6}$$

which are in error by no more than 10% for small capillary numbers, $Ca < 5.0 \times 10^{-3}$ (more information could be found in Appendix C in [4.57]). In 2000, Aussillous and Quéré [4.39] fitted their and the Taylor experimental data with the following empirical formula:

$$h = \frac{1.34Ca^{2/3}}{1 + 1.34kCa^{2/3}}, \tag{4.7}$$

where $k = 2.5$. In 2014, using the Bretherton approach and matching the lubrication approximation solution with the more realistic radius of curvature of the bubble front, Klaseboer et al. [4.58] derive theoretically Eq. (4.7) with $k = 2.79$ (see Fig. 4.12 below). Balestra et al. reported some more complex and accurate empirical expressions [4.59].

In many applications [4.60, 4.61], the used fluids contain surface active substances (surfactants, polymers, proteins, etc.), which modify the interfacial rheology of bubbles and drops. The effects of soluble and insoluble surfactants on the motion of bubbles, propagating through capillaries, are investigated numerically in [4.62–4.73]. In these numerical studies, the physicochemical properties of the surfactants are modeled below their critical micelle concentrations (CMC), the surface diffusivity and viscosity are neglected, the surfactant solutions are considered as nonionic without added indifferent electrolytes (salts), and the van der Waals, electrostatic and steric interactions are neglected (see [4.74]). As a result, the interfacial rheology is accounted for only through the Marangoni effect. Nevertheless, the numerical calculations have shown that even a trace amount of surfactant leads to immobilization of the interfaces for small and moderate capillary numbers — the fluid interfaces become tangentially immobile. For surfactant concentrations above the CMC, the surfactant adsorption is very fast (in order of microseconds) and the surface tension is constant. Thus, one should expect the measured velocity of the rising bubbles to correspond to the classical observations for bubbles with free surfaces. The recent experiments with nanofluids [4.75–4.77], however, have showed differences of two or three orders of magnitude from these expectations, because of the effects of structural molecular forces. Madec et al. reported the opposite effect in [4.78] — the bubbles rise faster in dense granular suspensions as compared to particle-less liquids of the same effective viscosity. For very low values of Ca, for which the theoretical predictions should be the most precise, the experimental data again deviate considerably from the theory. Typically, these deviations are attributed to impurities of the liquids used but another possible explanation of the breakdown of the Bretherton law can be the wall slippage effect [4.79].

The wide range of different possible physicochemical effects, which affect the motion of long bubbles and drops in tubes, results in a highly complex problem. We need a relatively simple, fast, transparent, and precise method for calculation of bubble shape and translational velocity, which can be generalized by introducing new fluid and/or interfacial properties. In the original Bretherton model [4.1], the hydrodynamic problem in the wetting film close to the wall is solved, using the simplified lubrication approximation for flow in a thin layer, neglecting the tube curvature, which is valid for planar liquid layers only. To extend the validity of this approach, Ratulowski and Chang [4.80] considered the lubrication solution in cylindrical coordinates and Kolb and Cerro [4.81] in tubes of square

cross section, see Sec. 4.5. To avoid the ill-defined procedure of matching [4.1, 4.58] the lubrication approximation solution with the bubble shape at its front, the normal stress boundary condition, written in terms of an arc length of the bubble surface, is used in order to solve the respective boundary value problem [4.80, 4.81] for the thickness of cylindrical film part, h, see Sec. 4.6. This approach [4.80] leads to a good theoretical description of the experimental data for W up to 40 times larger capillary numbers ($Ca < 0.2$) than the applicability region of the Bretherton formula, see Sec. 4.7, but still further improvements are needed to explain the significant deviations at higher capillary numbers.

The effect of buoyancy on the pressure-driven motion of drops and bubbles through cylindrical capillaries is studied experimentally and numerically in the literature [4.82–4.85]. These publications open wide theoretical and experimental areas with practical applications and new physical insights.

In this chapter, we investigate theoretically the effect of buoyancy on the pressure-driven motion of long axisymmetric bubbles with free or tangentially immobile surfaces at small and moderate capillary numbers. Experimental and theoretical investigations [4.82–4.85] show that if the bubble lengths are more than two times greater than the capillary diameters, then well pronounced cylindrical parts in the bubble profiles appear. This criterion is usually used to separate the long bubbles from short ones. The formulation of the problem is described in Sec. 4.2. Then, we nondimensionalize the problem and present a strategy for solving it in Sec. 4.3. In Sec. 4.4, the exact solutions for the cylindrical part of long bubbles are presented. In Sec. 4.5, we obtain the exact solution of the lubrication approximation of the hydrodynamic problem in cylindrical coordinates, accounting for the zero- and first-order approximations (generalized lubrication approximation). These solutions give further insights into the boundary value problem, arising from the normal stress boundary condition, and allow us to solve the problem for the wetting film thickness in the cylindrical part, h, with high accuracy. The method for finding the solution of the boundary value problem is presented in Sec. 4.6. Finally, Sec. 4.7 summarizes our numerical results, comparing them to the available experimental data.

4.2 Mathematical model

Let us consider a cylindrical capillary of radius R, filled with incompressible Newtonian fluid with dynamic viscosity η and density ρ (see Fig. 4.1). Inside the fluid, there is an axisymmetric bubble with an axis of revolution, coinciding with the axis of revolution of the capillary. The bubble moves with velocity V_b, parallel to the tube walls, under the action of the Poiseuille flow (see Appendix U.7) and of gravity with acceleration $\mathbf{g}$. The surface of the bubble is considered to be a fully mobile (the shear stress at the bubble surface is zero) or a tangentially immobile surface (the immobile surface acts as a solid surface). For more information on fully mobile or immobile surfaces, see the schematic presentation of the flow profiles near the bubble in Fig. 4.2.

In the current work, we shall consider the following three cases:

(A) the tube is placed horizontally and only the effect of the Poiseuille flow is considered.

(B) the tube is placed vertically and only the gravitational force is taken into account.

(C) the tube is placed vertically and the simultaneous action of the Poiseuille flow and gravity is considered.

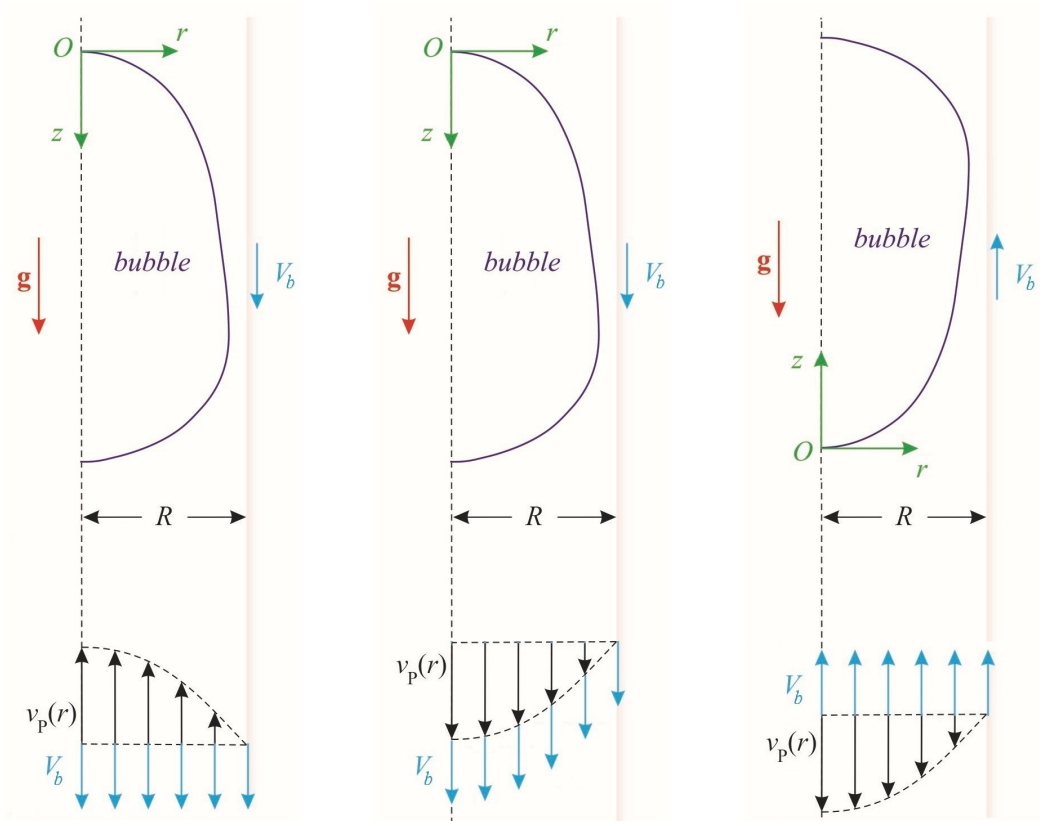

(a) $g_z > 0,\ V_{pm} > 0$ (b) $g_z > 0,\ V_{pm} < 0$ (c) $g_z < 0,\ V_{pm} > 0$

Figure 4.1: An axisymmetric bubble moves in a cylindrical capillary of radius R under the action of gravity and Poiseuille flow.

It is obvious that the cases (A) and (B) are special cases of the case (C). Thus, we derive a mathematical model for the general case (C). In order to do that, we introduce a cylindrical coordinate system (r, φ, z) with a center at the bubble apex and axis of revolution Oz, pointing in a direction, opposite of the bubble motion (see Fig. 4.1). In this coordinate system, the variables are independent of φ because the problem is axisymmetric (the region and the boundary conditions are symmetric with respect to the axis of rotation of the capillary). Therefore, we consider the problem in the $r - z$ plane only. Let us denote, then, the r- and z-components of fluid velocity $\mathbf{v}$ by u and v, and the z-component of the gravity $\mathbf{g}$ by g_z. Another property of this coordinate system is that it is fixed at the bubble apex. This means that the coordinate system translates with a fixed velocity V_b (see Fig. 4.1) and, then, the translational velocity of the bubble is equal to zero and the capillary wall and the whole fluid translate along axis Oz with velocity V_b.

As mentioned previously, a bubble moves in a vertical tube under the simultaneous action of Poiseuille flow and gravity. On one hand, if only the gravity is considered, the bubble moves upwards due to buoyancy. On the other hand, taking into account only the action of Poiseuille flow leads to the conclusion that the bubble moves in the direction of Poiseuille

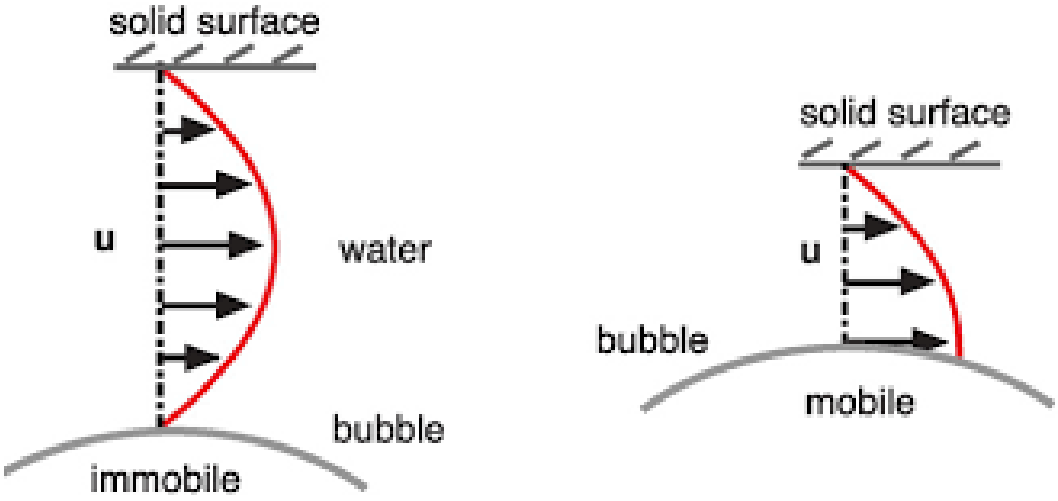

Figure 4.2: Schematic presentation of the flow profiles, depending on the type of the boundary conditions, applied at the bubble surface. A velocity profile for a tangentially immobile surface is shown on the left, while on the right – a profile of a fully mobile surface [4.86].

flow. When both forces act simultaneously on the bubble, there are three main cases, which are shown in Fig. 4.1. Fig. 4.1a illustrates the case when the buoyancy and Poiseuille flow point upwards and the bubble rises. If the forces act in opposite directions, the bubble floats or sinks, depending on which force prevails. If the gravitational force controls the bubble motion ($g_z > 0$), then the mean z-component of the Poiseuille flow velocity, $-V_{pm}$, is positive and the bubble floats (see Fig. 4.1b). Otherwise, gravity acts in the opposite direction of the z-axis ($g_z < 0$) and the bubble sinks, see Fig. 4.1c.

4.2.1 Modelling of the fluid motion

First, we shall describe the motion of the Newtonian fluid. We assume that the flow is so slow that the inertial terms in the Navier–Stokes equations are negligible. Then, the motion of the fluid can be described by Stokes equations

$$\nabla \cdot \mathbf{v} = 0, \tag{4.8}$$

$$\nabla p = \eta \nabla^2 \mathbf{v} + \rho \mathbf{g}, \tag{4.9}$$

where p is the dynamic pressure, see Eqs. (U.73)–(U.74) in the Supplementary material U. For axysymmetric problem in cylindrical coordinates, the system has the following form:

$$\frac{1}{r}\frac{\partial}{\partial r}(ru) + \frac{\partial v}{\partial z} = 0, \tag{4.10}$$

$$\frac{\partial p}{\partial r} = \eta\left[\frac{\partial}{\partial r}\left(\frac{1}{r}\frac{\partial}{\partial r}(ru)\right) + \frac{\partial^2 u}{\partial z^2}\right], \tag{4.11}$$

$$\frac{\partial p}{\partial z} = \eta\left[\frac{1}{r}\frac{\partial}{\partial r}\left(r\frac{\partial v}{\partial r}\right) + \frac{\partial^2 v}{\partial z^2}\right] + \rho g_z, \tag{4.12}$$

see Eqs. (U.101)–(U.103) in the Supplementary Material U.

4.2.2 Boundary conditions

In order to close the system, we add boundary conditions to the problem. More information for their derivation could be found in Section U.6 and for different types of rheological relations — in Section U.4 in the Supplementary material U.

No-slip boundary conditions at the walls of the tube

The fluid is moving with velocity 0 there. Because of the choice of the coordinate system (fixed at the bubble apex), the following boundary conditions:

$$u = 0,\ v = V_b \text{ at } r = R \tag{4.13}$$

are applied, see Eq. (U.77) in the Supplementary Material U.

Inlet/outlet boundary conditions for $|z| \to \infty$

We assume that the fluid flow is Poiseuille at the large distances from the bubble, i.e.

$$u = 0,\ v = V_b + v_p(r) \text{ at } |z| \to \infty, \tag{4.14}$$

where $v_p(r)$ is the axial coordinate of the Poiseuille velocity profile, i.e.

$$v_p(r) = -2V_{pm}\left(1 - \frac{r^2}{R^2}\right), \tag{4.15}$$

see (U.124) in the Supplementary material U. Note that Eq. (4.14) follows from the simple flow rate condition

$$2\int_0^R r\, v(r,z)dr = (V_b - V_{pm})\, R^2 \text{ at } |z| \to \infty. \tag{4.16}$$

Kinematic boundary condition at the bubble surface

The kinematic boundary condition states

$$\mathbf{v} \cdot \mathbf{n} = 0 \text{ at S}, \tag{4.17}$$

where S denotes the surface of the bubble and $\mathbf{n}$ is the unit inward normal to S, see Eq. (U.79) in the Supplementary material U.

Dynamic boundary condition at the bubble surface

For constant surface tension σ, the tangential and normal boundary conditions have the form:

$$\mathbf{n} \cdot (\mathbf{P} - \mathbf{P}_b) \cdot \mathbf{t} = 0 \tag{4.18}$$

and

$$\mathbf{n} \cdot (\mathbf{P} - \mathbf{P}_b) \cdot \mathbf{n} = 2H\sigma, \tag{4.19}$$

where H is the mean curvature of the bubble interface, $\mathbf{P}$ is the flow stress tensor and $\mathbf{P}_b$ is the bubble stress tensor, see Eqs. (U.94)–(U.95) in the Supplementary material U. In order to find the concrete form of the latter, we shall choose the type of rheological relations that

model the fluids in the problem. We assume that the fluid in the bubble is ideal and, then, bubble stress tensor is

$$\mathbf{P}_b = -p_b\mathbf{I}, \tag{4.20}$$

where $\mathbf{I}$ is the identity tensor and p_b is the pressure inside the bubble. The fluid in the tube is assumed to be Newtonian, i.e.

$$\mathbf{P} = -p\mathbf{I} + \eta\left[\nabla\mathbf{v} + (\nabla\mathbf{v})^T\right]. \tag{4.21}$$

Then, the components of the pressure tensor $\mathbf{P}_s := \mathbf{P} - \mathbf{P}_b$ in cylindrical coordinates are

$$P_{s,rr} = p_b - p + 2\eta\frac{\partial u}{\partial r}, \tag{4.22}$$

$$P_{s,rz} = P_{s,zr} = \eta\left(\frac{\partial v}{\partial r} + \frac{\partial u}{\partial z}\right), \tag{4.23}$$

$$P_{s,zz} = p_b - p + 2\eta\frac{\partial v}{\partial z}, \tag{4.24}$$

see Eq. (S.349) in the Supplementary Material S.

4.2.3 Surface parametrization. Normal and tangential boundary conditions

The form of the kinematic and dynamic boundary conditions (4.17)–(4.19) depends on the surface parameterisation of the bubble. Let us denote by r_b and z_b the cylindrical coordinates of the bubble surface and s is the arc length of S, measured from the bubble apex, then the bubble shape is described by $r = r_b(s)$ and $z = z_b(s)$. Using geometric considerations, we conclude that the following differential equations [4.2, 4.87]:

$$\frac{dr_b}{ds} = \cos\theta, \;\; \frac{dz_b}{ds} = \sin\theta, \tag{4.25}$$

model the form of the bubble, where θ is the meniscus running slope angle (see Fig. 4.3). We compute the mean curvature of the bubble surface, H, [4.2, 4.87] as

$$2H = \frac{d\theta}{ds} + \frac{\sin\theta}{r_b} \tag{4.26}$$

and the unit tangential vector $\mathbf{t}$ to the surface S as

$$\mathbf{t} = (\cos\theta, \sin\theta). \tag{4.27}$$

Then, the unit inward normal has the following form:

$$\mathbf{n} = \frac{\frac{d\mathbf{t}}{ds}}{\left|\frac{d\mathbf{t}}{ds}\right|} = (-\sin\theta, \cos\theta). \tag{4.28}$$

Substituting (4.28) in the kinematic boundary condition (4.17), we obtain the form of the kinematic boundary condition

$$v\cos\theta - u\sin\theta = 0 \text{ at } S. \tag{4.29}$$

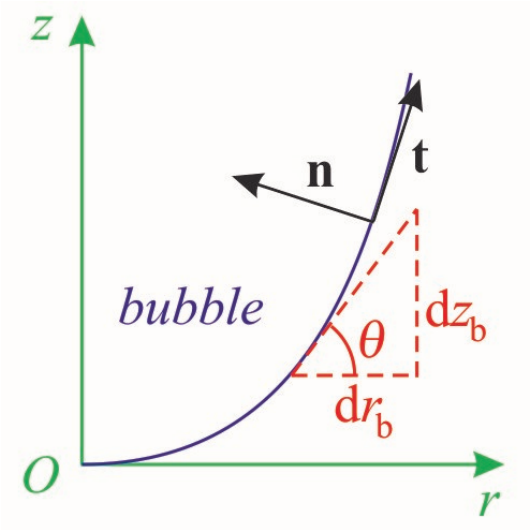

Figure 4.3: Description of the bubble surface: θ is the meniscus running slope angle; $\mathbf{t}$ is the unit tangential vector and $\mathbf{n}$ is the unit inward normal vector to the bubble surface.

Substituting (4.27) and (4.28) in (4.18) and (4.19), we obtain the form of the tangential stress boundary condition

$$\cos(2\theta)\left(\frac{\partial v}{\partial r}+\frac{\partial u}{\partial z}\right)+\sin(2\theta)\left(\frac{\partial v}{\partial z}-\frac{\partial u}{\partial r}\right)=0 \tag{4.30}$$

and the normal stress boundary condition

$$p_b = p - 2\eta\sin^2\theta\left[\cot^2\theta\frac{\partial v}{\partial z}+\frac{\partial u}{\partial r}-\cot\theta\left(\frac{\partial v}{\partial r}+\frac{\partial u}{\partial z}\right)\right]+2H\sigma \tag{4.31}$$

for fully mobile interfaces at the bubble surface S.

In the case of tangentially immobile bubble surface, the kinematic and tangential boundary conditions are replaced by the conditions of the surface solidifation:

$$u=0,\ v=0 \text{ at S}, \tag{4.32}$$

which assume that the surface of the bubble acts as solid. This considerably simplifies the normal stress boundary condition (4.31) to

$$p_b = p + 2H\sigma \text{ at S}. \tag{4.33}$$

Note that the normal stress boundary conditions (4.31) and (4.33) give a relationship between the mean curvature of the bubble, the flow characteristics u, v and p, and the bubble pressure, p_b. The latter means that if one approximates u, v and p at the bubble surface S, it is possible to find the bubble shape as a solution of the system (4.25), (4.26) and (4.31) (in the case of free surface) or (4.25), (4.26) and (4.33) (in a case of immobile surface) with appropriate initial conditions, applied at the bubble apex.

4.2.4 Simple integral flow rate condition as a kinematic boundary condition

For analytical calculations (see Sec. 4.5), it is more convenient to use the simple integral flow rate condition

$$2\int_{r_b}^{R} rv\,(r,z_b)\,dr = (V_b - V_{pm})\,R^2. \tag{4.34}$$

instead of the kinematic boundary condition (4.29). In the next lines, we prove that Eq. (4.34) follows from the kinematic boundary condition. In order to do that, we consider a long bubble in a cylindrical tube (see Fig. 4.4). Next, one introduces the following notation:

- $S_{\overline{z}} = \{(r,\varphi,\overline{z}) \,|\, 0 \le r \le R,\ 0 \le \varphi < 2\pi\}$ or this is the part of the plane $z = \overline{z}$, which is inside the capillary;
- $S_b = \{(r,\varphi,z_b) \,|\, r_b \le r \le R,\ 0 \le \varphi < 2\pi\}$ or this is the part of the plane $z = z_b$, which is inside the capillary and outside the bubble;
- $S_s = \{(R,\varphi,z) \,|\, 0 \le \varphi < 2\pi,\ z_b \le z \le \overline{z}\}$ or this is surrounding surface of the cylinder C with bases S_b and $S_{\overline{z}}$;
- $\overline{S} = \{(r,\varphi,z) \,|\, (r,\varphi,z) \in S,\ z_b \le z < \overline{z}\}$ or this is the part of the bubble surface, which is inside the cylinder C;
- $\mathbf{n}_{\overline{z}}$, $\mathbf{n}_b$ and $\mathbf{n}_s$ are the unit normals to $S_{\overline{z}}$, S_b and S_s, pointing out of the cylinder C, and $\overline{\mathbf{n}}$ is the unit outer normal to the surface $\overline{S}$ (see Fig. 4.4).

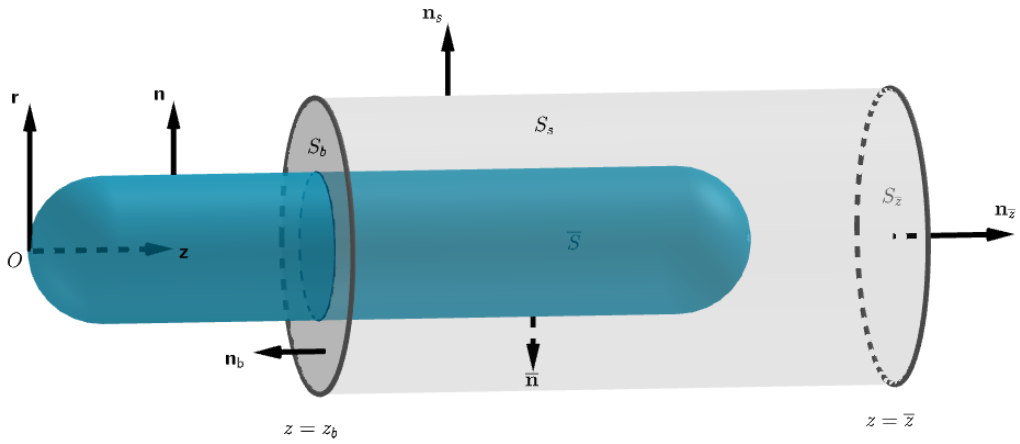

Figure 4.4: Description of the surface $S_f = S_{\overline{z}} \cup S_b \cup S_s \cup \overline{S}$.

Then, using the mass conservation law and the divergence theorem, we obtain

$$\iint_{S_f} \mathbf{n}_f \cdot \mathbf{v} dS = \iiint_{V_f} \nabla \cdot \mathbf{v} dV = \iiint_{V_f} 0 dV = 0, \tag{4.35}$$

where $S_f = S_{\overline{z}} \cup S_b \cup S_s \cup \overline{S}$ is the surface, over which we integrate, $\mathbf{n}_f$ is the unit outer normal to S_f and V_f is the volume, surrounded by S_f. Writing the integral $\iint_{S_f} \mathbf{n}_f \cdot \mathbf{v} dS$ as a sum of four integrals, we obtain consecutively

$$\iint\limits_{S_{\overline{z}}} \mathbf{n}_{\overline{z}} \cdot \mathbf{v} dS + \iint\limits_{S_b} \mathbf{n}_b \cdot \mathbf{v} dS + \iint\limits_{S_s} \mathbf{n}_s \cdot \mathbf{v} dS - \iint\limits_{\overline{S}} \overline{\mathbf{n}} \cdot \mathbf{v} dS = 0. \tag{4.36}$$

We take into account the boundary conditions at the wall of the capillary (4.13) and at the bubble surface (4.17) in the latter and get

$$\iint\limits_{S_{\overline{z}}} v dS - \iint\limits_{S_b} v dS = 0. \tag{4.37}$$

Eq. (4.37) is valid for $\overline{z} \to +\infty$. Using this fact, we obtain

$$\lim_{\overline{z} \to +\infty} \int\limits_0^{2\pi} \int\limits_0^R v\left(r, \overline{z}\right) r dr d\varphi - \int\limits_0^{2\pi} \int\limits_{r_b}^R v\left(r, z_b\right) r dr d\varphi = 0, \tag{4.38}$$

$$2\pi \int\limits_0^R \left[V_b - 2V_{pm} \left(1 - \frac{r^2}{R^2} \right) \right] r dr - 2\pi \int\limits_{r_b}^R v\left(r, z_b\right) r dr d\varphi = 0, \tag{4.39}$$

see Eq. (4.14). Therefore, the following statement:

$$\begin{aligned} \int\limits_{r_b}^R v\left(r, z_b\right) r dr d\varphi &= \frac{V_b R^2}{2} - 2V_{pm} \left(\frac{R^2}{2} - \frac{R^4}{4R^2} \right) \\ &= \frac{R^2 (V_b - V_{pm})}{2} \end{aligned} \tag{4.40}$$

holds true or equivalently (4.34). Note that (4.34) follows from the continuity equation (4.10), the no-slip boundary condition (4.13), the boundary condition at $z \to +\infty$ (4.14) and the kinematic condition (4.17).

Other way to prove (4.34) is by proving that

$$I(z) = \int\limits_{r_b}^R r v(r, z) dr \tag{4.41}$$

is a constant for all points $(r_b, z_b) \in S$. The surface S could be represented as union of non-intersecting surfaces S_k, in which r_b is a function of z. Then, using the continuity equation (4.10), the no-slip boundary condition (4.13) and the kinematic condition (4.29), we obtain

$$\begin{aligned} \frac{\partial I\left(r_b(z), z\right)}{\partial z} &= \frac{\partial I}{\partial r_b} \frac{dr_b}{dz} + \frac{\partial I}{\partial z} = -r_b v\left(r_b, z\right) \cot\theta + \int\limits_{r_b}^R r \frac{\partial v}{\partial z} dr = \\ &= -r_b v\left(r_b, z\right) \cot\theta - \int\limits_{r_b}^R \frac{\partial}{\partial r}\left(ru\right) dr = \\ &= -r_b v\left(r_b, z\right) \frac{\cos\theta}{\sin\theta} - Ru\left(R, z\right) + r_b u\left(r_b, z\right) = 0. \end{aligned} \tag{4.42}$$

The latter holds true for every S_k and then it holds for S. Thus, the integral $\int_{r_b}^{R} rvdr$ is a constant for all points at S. Also if the integral flow rate condition (4.34) holds true, then it follows from (4.42) that the kinematic boundary condition (4.29) also holds true.

4.3 Dimensionless form of the problem and general strategy for solving it.

4.3.1 Dimensionless form in the case of free surfaces

In the case of fully mobile bubble surface, we obtain the Stokes problem (4.10)– (4.12) with applied no-slip boundary conditions at the wall of the capillary (4.13), inlet/outlet boundary condition (4.14), simple flow rate boundary condition (4.34), tangential (4.30) and normal boundary condition (4.31) at the bubble surface S, where S is parametrized by the cylindrical coordinates (r_b, z_b), which fulfill Eq. (4.25), and the mean curvature is computed, using (4.26). Next, the model is non-dimensionalized by introducing the following new dimensionless variables (with bars):

- the radial and axial coordinates are scaled with the capillary radius R

$$\overline{r} = \frac{r}{R},\ \overline{z} = \frac{z}{R}; \tag{4.43}$$

- the arc length, the radial and axial coordinates of the bubble and the mean curvature — with the capillary radius R

$$\overline{r}_b = \frac{r_b}{R},\ \overline{z}_b = \frac{z_b}{R},\ \overline{s} = \frac{s}{R},\ \overline{H} = HR; \tag{4.44}$$

- the velocity components — with the bubble velocity V_b

$$\overline{u} = \frac{u}{V_b},\ \overline{v} = \frac{v}{V_b},\ \overline{v}_p\left(\overline{r}\right) = -2\frac{V_{pm}}{V_b}\left(1-\overline{r}^2\right); \tag{4.45}$$

- the pressure — with $\eta V_b/R$

$$\overline{p}_b = \frac{p_b}{\eta V_b/R},\ \overline{p} = \frac{p}{\eta V_b/R}. \tag{4.46}$$

The effects of buoyancy and capillary forces are measured, using the Bond number, Bo, the capillary numbers, Ca and Ca_{pm}, and the relative increase in the velocity, W:

$$Bo = \frac{\rho g_z R^2}{\sigma},\ Ca = \frac{\eta V_b}{\sigma},\ Ca_{pm} = \frac{\eta V_{pm}}{\sigma},\ W = 1 - \frac{V_{pm}}{V_b}. \tag{4.47}$$

Using the non-dimensional variables, we obtain the dimensionless Stokes problem in cylindrical coordinates:

$$\frac{1}{\overline{r}}\frac{\partial}{\partial\overline{r}}\left(\overline{r}\,\overline{u}\right) + \frac{\partial\overline{v}}{\partial\overline{z}} = 0 \tag{4.48}$$

$$\frac{\partial\overline{p}}{\partial\overline{r}} = \frac{\partial}{\partial\overline{r}}\left[\frac{1}{\overline{r}}\frac{\partial}{\partial\overline{r}}\left(\overline{r}\,\overline{u}\right)\right] + \frac{\partial^2\overline{u}}{\partial\overline{z}^2} \tag{4.49}$$

$$\frac{\partial\overline{p}}{\partial\overline{z}} = \frac{1}{\overline{r}}\frac{\partial}{\partial\overline{r}}\left(\overline{r}\frac{\partial\overline{v}}{\partial\overline{r}}\right) + \frac{\partial^2\overline{v}}{\partial\overline{z}^2} + \frac{Bo}{Ca}, \tag{4.50}$$

see Eqs. (4.10)– (4.12). The following boundary conditions are applied:

- boundary condition at the wall of the capillary

$$\overline{u} = 0,\ \overline{v} = 1 \text{ at } \overline{r} = 1; \tag{4.51}$$

- inlet/outlet boundary conditions for $|\overline{z}| \to \infty$

$$\overline{u} = 0,\ \overline{v} = 1 + \overline{v}_p\left(\overline{r}\right) \text{ at } |\overline{z}| \to \infty; \tag{4.52}$$

- simple flow rate boundary condition

$$2\int\limits_{\overline{r}_b}^{1} \overline{r}\,\overline{v} d\overline{r} = 1 - \frac{V_{pm}}{V_b} = W; \tag{4.53}$$

- tangential stress boundary condition

$$\cos(2\theta)\left(\frac{\partial \overline{v}}{\partial \overline{r}} + \frac{\partial \overline{u}}{\partial \overline{z}}\right) + \sin\left(2\theta\right)\left(\frac{\partial \overline{v}}{\partial \overline{z}} - \frac{\partial \overline{u}}{\partial \overline{r}}\right) = 0 \text{ at } S; \tag{4.54}$$

- normal stress boundary condition

$$\overline{p}_b = \overline{p} - 2\sin^2\theta\left[\cot^2\theta\frac{\partial \overline{v}}{\partial \overline{z}} + \frac{\partial \overline{u}}{\partial \overline{r}} - \cot\theta\left(\frac{\partial \overline{v}}{\partial \overline{r}} + \frac{\partial \overline{u}}{\partial \overline{z}}\right)\right] + \frac{2\overline{H}}{Ca} \text{ at S}, \tag{4.55}$$

where the bubble surface S is computed, using the equations

$$\frac{d\overline{r}_b}{d\overline{s}} = \cos\theta, \tag{4.56}$$

$$\frac{d\overline{z}_b}{d\overline{s}} = \sin\theta, \tag{4.57}$$

$$2\overline{H} = \frac{d\theta}{d\overline{s}} + \frac{\sin\theta}{\overline{r_b}}. \tag{4.58}$$

4.3.2 Dimensionless form in the case of tangentially immobile surfaces

In the case of tangentially immobile bubble surface, we obtain the Stokes problem (4.10)–(4.12) with applied boundary conditions at the wall of the capillary (4.13), for $|z| \to \infty$ (4.14), normal boundary condition (4.33) and boundary condition for surface solidification (4.32) at the bubble surface S. In the non-dimensional variables, the conditions of the surface solidification (4.32) have the following form:

$$\overline{u} = 0,\ \overline{v} = 0 \text{ at S} \tag{4.59}$$

and the normal boundary condition (4.33) reads

$$\overline{p}_b = \overline{p} + \frac{2\overline{H}}{Ca} \text{ at S}. \tag{4.60}$$

In the rest of this chapter, we drop the bars for notational convenience.

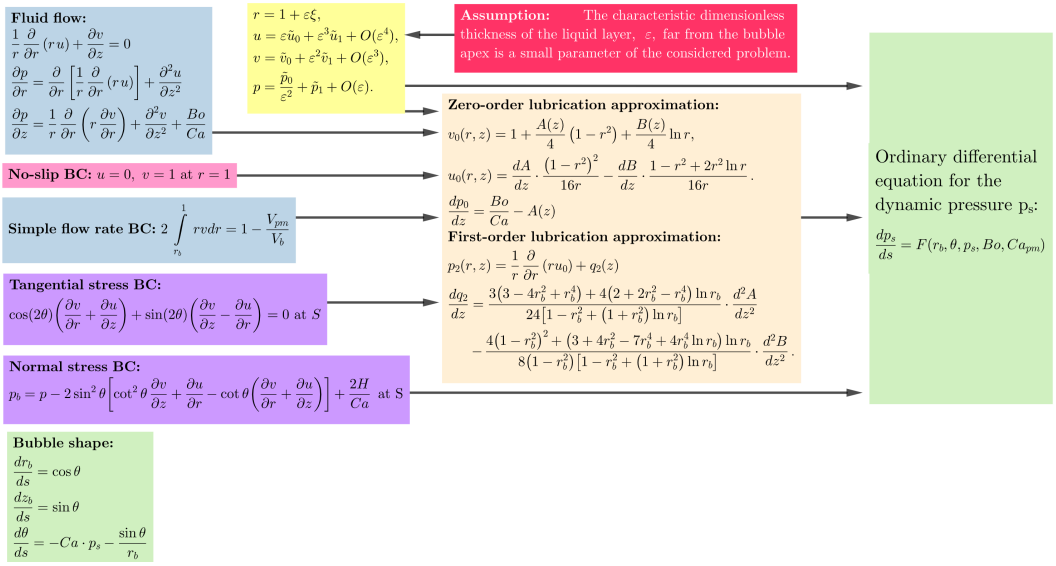

Figure 4.5: Description of the main aspects in the strategy for solving of this problem

4.3.3 General strategy

In this subsection, we describe briefly our strategy for solving this problem. We assume that the characteristic dimensionless thickness of liquid layer, ε, far from the bubble apex is a small parameter of the considered problem and, therefore, rescale the radial coordinate, r, as $r = 1 + \varepsilon\xi$. The expansions in series for the radial and the axial components of the fluid velocity and for the pressure with respect to the small parameter, ε, are sought-out in the following form (4.100)–(4.102). One substitutes the expansions (4.88), (4.100)–(4.102) in the Stokes problem (4.48)– (4.50), closed with the no-slip (4.51), the simple flow rate (4.53) and the tangential boundary condition (4.54) or (4.59). Equating the leading coefficients in each of the equations, we obtain a system of partial differential equations with boundary conditions. Its solution, the zero-order approximations for the flow variables u, v and p, is found analytically. Analogously, one gets the first-order approximations for the flow variables. Next, these approximations are substituted in the normal stress boundary condition and the system (4.196)–(4.199) of four ordinary differential equations for r_b, z_b, θ and the dynamic pressure difference p_s is obtained (see Section 4.6). Further, we find appropriate initial conditions at the cylindrical part of the bubble, using small perturbations around the cylindrical shape of the bubble. Finally, the sought-out film thickness is obtained as a solution of a boundary value problem (additional conditions, ensuring closure of the bubble profile, are added) by using an iterative procedure.

4.4 Exact solution for the cylindrical part of long bubbles

In the case of long bubbles (bubbles with aspect ratios of bubble lengths to capillary diameters greater than 2), a well pronounced cylindrical part of the bubble shape appears.

Let us denote by h the dimensionless thickness of the fluid layer and the respective value of the radial coordinate of the bubble — by $r_c = 1 - h$. In the cylindrical part of the bubble, the Stokes problem (4.48)– (4.50) with boundary conditions (4.51), (4.54), (4.55) in the case of fully mobile surfaces and the Stokes problem (4.48)– (4.50) with boundary conditions (4.51), (4.59), (4.60) in the case of fully immobile surfaces have exact solutions. The obtained Stokes problems are similar to the problem (U.101)– (U.103) with the following differences. First, the problem (4.48)– (4.50) is dimensionless and, secondly, there is an additional term in (4.50), namely Bo/Ca. Due to these facts, we shall be looking for the solution of (4.48)– (4.50) in the form

$$u(r) = 0,\ v(r) = \left(C_{e,1} - \frac{Bo}{Ca}\right)\frac{r^2}{4} + C_{e,2}\ln r + C_{e,3}, \tag{4.61}$$

where $C_{e,1} = \frac{dp}{dz}$, $C_{e,2}$ and $C_{e,3}$ are unknown constants, see Eq. (U.118). Below, we shall consider the cases of free and tangentially immobile surfaces separately.

4.4.1 Free surfaces

The meniscus running slope angle in the cylindrical part of the bubble is $\theta = \frac{\pi}{2}$ and, thus, for fully mobile bubble interface, the tangential boundary condition (4.54) is simplified considerably

$$\left.\frac{\partial v}{\partial r}\right|_{r=r_c} = 0 \tag{4.62}$$

and the normal boundary condition (4.55) has the form

$$p_b = p + \frac{1}{Ca \cdot r_c} \text{ for } r = r_c. \tag{4.63}$$

From the latter, it follows that $C_{e,1} = \frac{dp}{dz} = 0$ for $r = r_c$. Substituting the general solution (4.61) in the no-slip boundary condition (4.51), we obtain

$$C_{e,3} = 1 + \frac{1}{4}\frac{Bo}{Ca} \tag{4.64}$$

or the general solution has the form

$$u(r) = 0,\ v(r) = 1 + \frac{Bo}{4Ca}\left(1 - r^2\right) + C_{e,2}\ln r. \tag{4.65}$$

Using the simplified form of the tangential boundary condition (4.62), we obtain the exact solution for the cylindrical part of a fully mobile bubble surface:

$$v(r) = 1 + \frac{Bo}{4Ca}\left(1 - r^2\right) + \frac{Bo}{2Ca}r_c^2\ln r. \tag{4.66}$$

The substitution of the exact solution, Eqs. (4.66), in the integral flow rate condition, Eq. (4.53), leads to a relationship between the bubble velocity and the physical flow parameters:

$$\begin{aligned} W &= \int_{r_c}^{1}\left[2r + \frac{Bo}{2Ca}\left(r - r^3\right) + \frac{Bo}{Ca}r_c^2 r\ln r\right]dr \\ &= 1 - r_c^2 + \frac{Bo}{8Ca}\left(1 - 2r_c^2 + r_c^4\right) + \frac{Bo}{4Ca}r_c^2\left[r_c^2\left(1 - 2\ln r_c\right) - 1\right] \\ &= 1 - r_c^2 + \frac{Bo}{8Ca}\left(1 - 4r_c^2 + 3r_c^4 - 4r_c^4\ln r_c\right) \end{aligned} \tag{4.67}$$

or equivalently

$$r_c^2 Ca = Ca_{pm} + \frac{Bo}{8}\left(1 - 4r_c^2 + 3r_c^4 - 4r_c^4 \ln r_c\right). \tag{4.68}$$

In the latter, we use the fact

$$\int r \ln r dr = \frac{r^2 \ln r}{2} - \int \frac{r}{2} dr = \frac{r^2}{4}\left(2\ln r - 1\right). \tag{4.69}$$

The substitution of $Ca_{pm} = 0$ in Eq. (4.68) leads to the Goldsmith and Mason formula [4.24] for a bubble, on which only gravity acts. Eq. (4.68) gives an exact relationship between the dimensionless thickness h and capillary number Ca for given values of the physical numbers Bo and Ca_{pm}. In the case of small thicknesses of the cylindrical film layer, $h << 1$, the asymptotic expansion of Eq. (4.68) reads

$$\begin{aligned} Ca &= \frac{Ca_{pm}}{r_c^2} + \frac{Bo}{8}\left(\frac{1}{r_c^2} - 4 + 3r_c^2 - 4r_c^2 \ln r_c\right) \\ &= \left(1 + 2h + 3h^2 + 4h^3\right) Ca_{pm} + \frac{Bo}{8}\left[1 + 2h + 3h^2 + 4h^3\right. \\ &\qquad \left. -4 + 3 - 6h + 3h^2 - 4\left(-h + \frac{3}{2}h^2 - \frac{h^3}{3}\right)\right] + O\left(h^4\right) \\ &= Ca_{pm} + 2Ca_{pm}h + 3Ca_{pm}h^2 + \left(Bo + 6Ca_{pm}\right)\frac{2h^3}{3} + O\left(h^4\right). \end{aligned} \tag{4.70}$$

Due to the fact $Ca \geq 0$, we shall look for additional constraints on the values of Ca_{pm} and Bo. If the bubble is in rest ($Ca = 0$), then Ca_{pm}/Bo can be computed as follows:

$$\frac{Ca_{pm}}{Bo} = -\frac{1}{8}\left(1 - 4r_c^2 + 3r_c^4 - 4r_c^4 \ln r_c\right). \tag{4.71}$$

Otherwise, the capillary number Ca is positive (see Def. 4.47) and it follows

$$Ca_{pm} + \frac{Bo}{8}\left(1 - 4r_c^2 + 3r_c^4 - 4r_c^4 \ln r_c\right) > 0. \tag{4.72}$$

Depending on the sign of Bo, there are two general cases — the Bond number Bo is positive or negative. If the gravity acts along the z-axis ($Bo > 0$), then the following inequality:

$$\frac{Ca_{pm}}{Bo} > -\frac{1}{8}\left(1 - 4r_c^2 + 3r_c^4 - 4r_c^4 \ln r_c\right) \text{ for } Bo > 0 \tag{4.73}$$

holds true and the point $(h, Ca_{pm}/Bo)$ lies above the curve (4.71), corresponding to the bubble at rest (see Fig. 4.6). Moreover, the capillary number Ca_{pm} could be positive (see Fig. 4.1a) or negative (see Fig. 4.1b). In case that $Bo < 0$, then the following inequality:

$$\frac{Ca_{pm}}{Bo} < -\frac{1}{8}\left(1 - 4r_c^2 + 3r_c^4 - 4r_c^4 \ln r_c\right) \text{ for } Bo < 0 \tag{4.74}$$

holds true, the point $(h, Ca_{pm}/Bo)$ is under the curve and the Poiseulle flow acts in direction, opposite of Oz ($Ca_{pm} > 0$), see Fig. 4.6.

This statement follows from the fact that

$$f_1(r_c) := 1 - 4r_c^2 + 3r_c^4 - 4r_c^4 \ln r_c \tag{4.75}$$

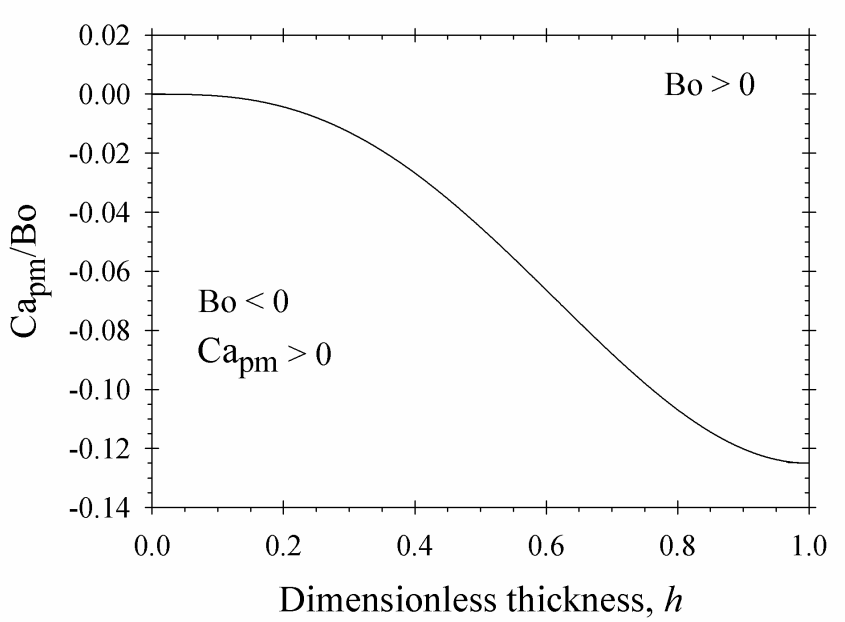

Figure 4.6: Regions of different signs for the Bond number, Bo, depending on the dimensionless wetting film thickness, h, in the case of free surfaces. Solid line corresponds to $Ca = 0$.

is positive for $r_c \in (0,1)$. In order to prove that let us denote by $f_2(r_c)$ the following expression:

$$f_2(r_c) := 1 - r_c^2 + 2r_c^2 \ln r_c. \tag{4.76}$$

Using the fact that $f_2(r_c)$ decreases for $r_c \in (0,1)$ and

$$f_2(r_c) > f_2(1) = 0 \text{ for } r_c \in (0,1), \tag{4.77}$$

we conclude that the function $f_1(r_c)$ decreases for $r_c \in (0,1)$ and, thus,

$$f_1(r_c) > f_1(1) = 0 \text{ for } r_c \in (0,1). \tag{4.78}$$

4.4.2 Tangentially immobile surfaces

In the case of tangentially immobile surfaces, the normal stress boundary condition (4.60) is equivalent to (4.63). Then, by substituting the solution (4.65) in the condition for surface solidification (4.59), the exact solution of the problem in the cylindrical part is obtained in the form:

$$u(r) = 0,\ v(r) = 1 + \frac{Bo}{4Ca}\left(1 - r^2\right) - \left[1 + \frac{Bo}{4Ca}\left(1 - r_c^2\right)\right]\frac{\ln r}{\ln r_c}. \tag{4.79}$$

The relationship between the bubble velocity and the physical flow parameters for tangentially immobile surfaces is obtained as follows:

$$W = \int_{r_c}^{1} \left\{ 2r + \frac{Bo}{2Ca}\left(r - r^3\right) - 2\left[1 + \frac{Bo}{4Ca}\left(1 - r_c^2\right)\right]\frac{r\ln r}{\ln r_c} \right\} dr$$
$$= 1 - r_c^2 + \frac{Bo}{8Ca}\left(1 - 2r_c^2 + r_c^4\right) + \left[1 + \frac{Bo}{4Ca}\left(1 - r_c^2\right)\right]\frac{\left[1 - r_c^2\left(1 - 2\ln r_c\right)\right]}{2\ln r_c}$$
$$= 1 + \frac{1 - r_c^2}{2\ln r_c} + \frac{Bo}{8Ca}\left[1 - r_c^4 + \frac{\left(1 - r_c^2\right)^2}{\ln r_c}\right] \tag{4.80}$$

or equivalently

$$\frac{r_c^2 - 1}{2\ln r_c} Ca = Ca_{pm} + \frac{Bo}{8}\left[1 - r_c^4 + \frac{\left(1 - r_c^2\right)^2}{\ln r_c}\right]. \tag{4.81}$$

Eq. (4.81) gives an exact relationship between the dimensionless thickness h and capillary number Ca for given values of the physical numbers Bo and Ca_{pm} in the case of tangentially immobile surfaces. For a bubble in rest ($Ca = 0$), we obtain

$$\frac{Ca_{pm}}{Bo} = -\frac{1}{8}\left[1 - r_c^4 + \frac{\left(1 - r_c^2\right)^2}{\ln r_c}\right]. \tag{4.82}$$

Otherwise, in the case $Ca > 0$, one gets

$$\frac{Ca_{pm}}{Bo} > -\frac{1}{8}\left[1 - r_c^4 + \frac{\left(1 - r_c^2\right)^2}{\ln r_c}\right] \text{ for } Bo > 0, \tag{4.83}$$

$$\frac{Ca_{pm}}{Bo} < -\frac{1}{8}\left[1 - r_c^4 + \frac{\left(1 - r_c^2\right)^2}{\ln r_c}\right] \text{ for } Bo < 0, \tag{4.84}$$

see Fig. 4.7. In order to investigate the sign of the right hand-side of the latter, we introduce the following function:

$$f_3(r_c) := r_c^2 - 1 - \left(1 + r_c^2\right)\ln r_c. \tag{4.85}$$

It decreases with the increase of r_c for $r_c \in (0, 1)$, see Eq. (4.77). Thus, it follows

$$f_3(r_c) > f_3(1) = 0 \text{ for } r_c \in (0, 1). \tag{4.86}$$

Using the latter, we conclude that the right hand-side of (4.84) is negative and, then, Ca_{pm} is positive in the case of $Bo < 0$ (see Fig. 4.7).

Fig. 4.7 shows the regions of positive capillary numbers, $Ca > 0$, for bubbles with immobile surfaces. If the gravity acts along the z-axis ($Bo > 0$), then the Poiseuille flow in the opposite direction ($Ca_{pm} > 0$) always accelerates the bubble motion. The Poiseuille flow along the z-axis ($Ca_{pm} < 0$) decreases the translational bubble velocity, V_b, and the solid lines in Fig. 4.7 correspond to the bubble in the state of rest. As can be expected, the gravity decelerates the bubble motion for $g_z < 0$ ($Bo < 0$). To ensure the bubble translation with $V_b > 0$, one should apply an intensive enough pressure gradient to have $Ca_{pm} > 0$.

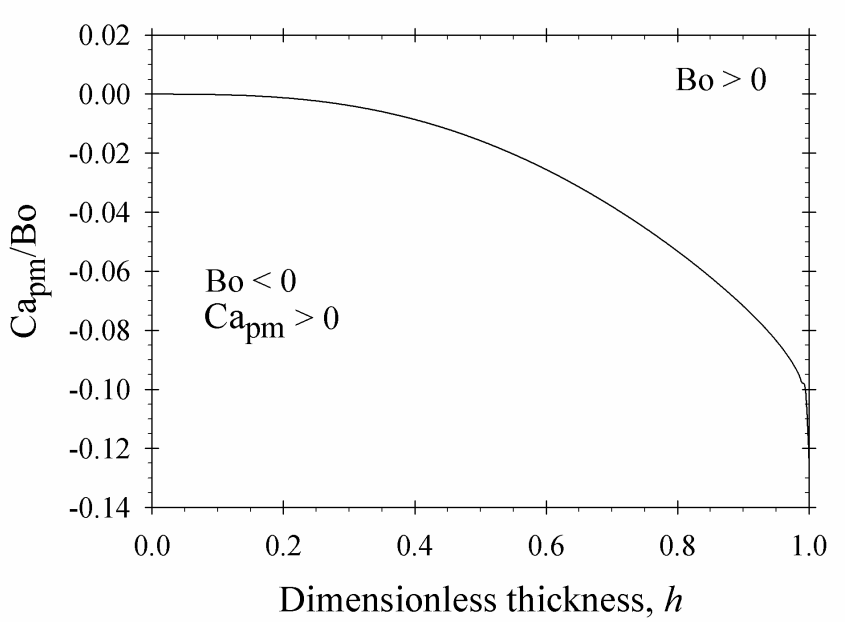

Figure 4.7: Regions of different signs for the Bond number, Bo, depending on the dimensionless wetting film thickness, h, in the case of tangentially immobile surfaces. Solid line corresponds to $Ca = 0$.

In the case of small thicknesses of the cylindrical film layer, $h << 1$, the asymptotic expansion of Eq. (4.81) reads

$$\begin{aligned} Ca &= \frac{2\ln r_c}{(r_c+1)(r_c-1)} Ca_{pm} - \frac{Bo}{4}\left[1 - r_c^2 + \left(1+r_c^2\right)\ln r_c\right] \\ &= \frac{2\left[-h - \frac{h^2}{2} - \frac{h^3}{3} - \frac{h^4}{4} + O\left(h^5\right)\right]}{-2h+h^2} Ca_{pm} \\ &- \frac{Bo}{4}\left\{2h - h^2 + \left(2 - 2h + h^2\right)\left[-h - \frac{h^2}{2} - \frac{h^3}{3} + O\left(h^4\right)\right]\right\} \\ &= \left[1 + h + \frac{5h^2}{6} + \frac{2h^3}{3} + O\left(h^4\right)\right] Ca_{pm} + \frac{h^3}{6} Bo + O(h^4) \\ &= Ca_{pm} + Ca_{pm} h + \frac{5}{6} Ca_{pm} h^2 + \left(Bo + 4Ca_{pm}\right)\frac{h^3}{6} + O\left(h^4\right). \end{aligned} \tag{4.87}$$

One sees that the linear term for free bubble surfaces is 2 times greater than that for immobile interfaces, while that related to the gravity (proportional to h^3) is 4 times greater.

4.5 Generalized lubrication approximation

In the lubrication approximation, one assumes that the partial derivatives in z-direction are smaller than those in the radial direction [4.75, 4.81]. Then, the Stokes problem (4.48),

(4.49) and (4.50) with the no-slip, the simple flow rate and the tangential boundary conditions could be solved analytically. Obtaining the approximations for the flow variables, the normal stress boundary condition is used to calculate the bubble shape, which corresponds to the asymptotic solution of the simplified hydrodynamic problem. Usually one solves only the zero-order approximation in respective reduced Cartesian coordinate system [4.1] or in original cylindrical coordinate system [4.80]. Here, the Stokes equations and boundary conditions are formulated in the lubrication approximation including the zero- and first-order approximations in the following sections. The exact solutions for the zero- and first-order approximations of the velocity and pressure extend the validity of the expressions for the flow parameters and increase the accuracy of obtained results, see Section 4.7.1.

4.5.1 Leading-order problem

We assume that the characteristic dimensionless thickness of liquid layer, ε, far from the bubble apex is a small parameter of the considered problem and, therefore, rescale the radial coordinate, r, as follows:

$$r = 1 + \varepsilon\xi, \tag{4.88}$$

where ξ is the new radial coordinate[1]. Then, the derivatives $\frac{\partial}{\partial r}$ and $\frac{\partial^2}{\partial r^2}$ are computed:

$$\frac{\partial}{\partial r} = \frac{d\xi}{dr}\frac{\partial}{\partial \xi} = \frac{1}{\varepsilon}\frac{\partial}{\partial \xi}, \tag{4.89}$$

$$\frac{\partial^2}{\partial r^2} = \left(\frac{d\xi}{dr}\right)^2 \frac{\partial^2}{\partial \xi^2} = \frac{1}{\varepsilon^2}\frac{\partial^2}{\partial \xi^2}. \tag{4.90}$$

Due to the change of the radial coordinate, it is important to rescale the velocity components, depending on the direction, in which they act. Thus, the radial component u (acting in direction r) is scaled with the small parameter ε and the axial component v (acting in direction z) is scaled with 1:

$$\hat{u} = \frac{u}{\varepsilon},\ \hat{v} = v. \tag{4.91}$$

If we choose different scale for the radial component of the velocity, the mass conservation law would not hold. By substituting (4.91) in (4.48)– (4.50),[2] we obtain the following system:

$$\frac{1}{1+\varepsilon\xi}\frac{\partial}{\partial \xi}(r\hat{u}) + \frac{\partial \hat{v}}{\partial z} = 0, \tag{4.92}$$

$$\frac{\partial p}{\partial \xi} = \frac{\partial}{\partial \xi}\left(\frac{1}{r}\frac{\partial}{\partial \xi}(r\hat{u})\right) + \varepsilon^2\frac{\partial^2 \hat{u}}{\partial z^2}, \tag{4.93}$$

$$\varepsilon^2\frac{\partial p}{\partial z} = \frac{1}{r}\frac{\partial}{\partial \xi}\left(r\frac{\partial \hat{v}}{\partial \xi}\right) + \varepsilon^2\frac{\partial^2 \hat{v}}{\partial z^2} + \varepsilon^2\frac{Bo}{Ca}. \tag{4.94}$$

Next, we shall find an appropriate scale for the pressure p:

$$\hat{p} = \varepsilon^k p, \tag{4.95}$$

[1] We change the variable in such a way in order to "zoom-in" in the thin film region. In it, the new variable ξ is in the range $[-1, 0]$.

[2] Note that system (4.48)– (4.50) is obtained if one finds the dimensionless form of the original problem by introducing new variables $u_0 = u/L,\ v_0 = v/R$ and setting ε to R/L, where u and v are the dimensional radial and axial components of the velocity and L is the length of the bubble. Therefore, the solution of the considered problem for small value of the film thickness corresponds to a long bubble ($L > R$).

using physical considerations. In the current problem, we consider flow, which moves due to the pressure gradient $\frac{\partial p}{\partial z}$ and gravity. The latter means that we cannot neglect the pressure gradient $\frac{\partial p}{\partial z}$ and, therefore, $k \geq 2$, see Eq. (4.94). On the other hand, choosing $k > 2$ leads to the conclusion $\frac{\partial \hat{p}}{\partial \xi} = \frac{\partial \hat{p}}{\partial z} = 0$ or the flow is not moving. Therefore, the appropriate scaling for p is

$$\hat{p} = \varepsilon^2 p. \tag{4.96}$$

Analogously, the term Bo/Ca, which describes the gravitational force, have to be scaled as

$$G = \varepsilon^2 \frac{Bo}{Ca}. \tag{4.97}$$

4.5.2 Iteration formulation of the equations

The solution of hydrodynamic problem could be presented in the approximation form

$$u = u_0 + u_1 + u_2 + \cdots,\ v = v_0 + v_1 + v_2 + \cdots,\ p = p_0 + p_1 + p_2 + \cdots, \tag{4.98}$$

where the subscript "0" denotes the zero-order approximation, "1"—the first correction term, "2"—the second correction term, etc. Taking into account the leading order of the variables $u,\ v,\ p$ (see Sec. 4.5.1), the zero-order approximations, first and second corrections u_k, v_k and p_k are defined by the following expressions:

$$u_k = \varepsilon^{k+1}\tilde{u}_k,\ v_k = \varepsilon^k \tilde{v}_k,\ p_k = \varepsilon^{k-2}\tilde{p}_k. \tag{4.99}$$

Then, the expansions in series for the radial and the axial components of the fluid velocity and for the pressure with respect to the small parameter, ε, are sought-out in the following form:

$$u = \varepsilon\tilde{u}_0 + \varepsilon^2\tilde{u}_1 + \varepsilon^3\tilde{u}_2 + O\left(\varepsilon^4\right), \tag{4.100}$$

$$v = \tilde{v}_0 + \varepsilon\tilde{v}_1 + \varepsilon^2\tilde{v}_2 + O\left(\varepsilon^3\right), \tag{4.101}$$

$$p = \frac{\tilde{p}_0}{\varepsilon^2} + \frac{\tilde{p}_1}{\varepsilon} + \tilde{p}_2 + O\left(\varepsilon\right). \tag{4.102}$$

In terms of the new variables (4.88), (4.100)–(4.102), the Stokes problem (4.48)– (4.50) acquires the following form:

$$\begin{aligned}
&\frac{1}{1+\varepsilon\xi}\,\frac{\partial\left[(1+\varepsilon\xi)\,\tilde{u}_0\right]}{\partial\xi} + \frac{\partial\tilde{v}_0}{\partial z} + \varepsilon\left\{\frac{1}{1+\varepsilon\xi}\frac{\partial\left[(1+\varepsilon\xi)\,\tilde{u}_1\right]}{\partial\xi} + \frac{\partial\tilde{v}_1}{\partial z}\right\} \\
&\qquad + \varepsilon^2\left\{\frac{1}{1+\varepsilon\xi}\frac{\partial\left[(1+\varepsilon\xi)\,\tilde{u}_2\right]}{\partial\xi} + \frac{\partial\tilde{v}_2}{\partial z}\right\} = O\left(\varepsilon^3\right), \qquad (4.103)\\
&\frac{\partial\tilde{p}_0}{\partial\xi} + \varepsilon\frac{\partial\tilde{p}_1}{\partial\xi} + \varepsilon^2\frac{\partial}{\partial\xi}\left\{\tilde{p}_2 - \frac{1}{1+\varepsilon\xi}\frac{\partial\left[(1+\varepsilon\xi)\,\tilde{u}_0\right]}{\partial\xi}\right\} = O\left(\varepsilon^3\right), \qquad (4.104)\\
&\frac{\partial\tilde{p}_0}{\partial z} - \frac{1}{1+\varepsilon\xi}\frac{\partial}{\partial\xi}\left[(1+\varepsilon\xi)\,\frac{\partial\tilde{v}_0}{\partial\xi}\right] - G \\
&\qquad + \varepsilon\left\{\frac{\partial\tilde{p}_1}{\partial z} - \frac{1}{1+\varepsilon\xi}\frac{\partial}{\partial\xi}\left[(1+\varepsilon\xi)\,\frac{\partial\tilde{v}_1}{\partial\xi}\right]\right\} \\
&\qquad + \varepsilon^2\left\{\frac{\partial\tilde{p}_2}{\partial z} - \frac{1}{1+\varepsilon\xi}\frac{\partial}{\partial\xi}\left[(1+\varepsilon\xi)\,\frac{\partial\tilde{v}_2}{\partial\xi}\right] - \frac{\partial^2\tilde{v}_0}{\partial z^2}\right\} = O\left(\varepsilon^3\right). \qquad (4.105)
\end{aligned}$$

Note that we keep the original form of the operators, acting in the radial direction, in the system (4.104)–(4.105) for computational convenience.

Next, we shall find the asymptotic expansions of the boundary conditions. Firstly, the asymptotic expansion of the no-slip boundary conditions (4.51) has the following form:

$$\tilde{u}_0 + \varepsilon\tilde{u}_1 + \varepsilon^2\tilde{u}_2 = O\left(\varepsilon^3\right),\ \tilde{v}_0 + \varepsilon\tilde{v}_1 + \varepsilon^2\tilde{v}_2 = 1 + O\left(\varepsilon^3\right) \text{ at r=1.} \tag{4.106}$$

Analogously, the asymptotic expansion of the simple flow rate condition (4.53) is

$$\int_{r_b}^{1} r\tilde{v}_0 dr + \varepsilon\int_{r_b}^{1} r\tilde{v}_1 dr + \varepsilon^2\int_{r_b}^{1} r\tilde{v}_2 dr = \frac{W}{2} + O\left(\varepsilon^3\right). \tag{4.107}$$

Surface parametrization in the new variables

The other boundary conditions depend on the parametrization of the bubble surface. Hence, the radial coordinate of the bubble profile, r_b, is rescaled similarly to Eq. (4.88):

$$r_b = 1 + \varepsilon\xi_b. \tag{4.108}$$

In order to compute the expressions for the tangential and normal boundary conditions, we express $\cot\theta$ in terms of ε:

$$\cot\theta = \frac{\cos\theta}{\sin\theta} = \frac{dr_b}{dz_b} = \varepsilon\frac{d\xi_b}{dz}. \tag{4.109}$$

Using the latter, we find the asymptotic expansions of $\sin^2\theta$ and $\cos^2\theta$:

$$\sin^2\theta = \frac{1}{1+\cot^2\theta} = \frac{1}{1+\varepsilon^2\left(\frac{d\xi_b}{dz}\right)^2} = 1 - \left(\frac{d\xi_b}{dz}\right)^2\varepsilon^2 + O\left(\varepsilon^3\right), \tag{4.110}$$

$$\cos^2\theta = 1 - \sin^2\theta = \left(\frac{d\xi_b}{dz}\right)^2\varepsilon^2 + O\left(\varepsilon^3\right). \tag{4.111}$$

Tangential boundary condition in the new variables

The expansion in series of the condition for surface solidification (4.59) has the following form:

$$\tilde{u}_0 + \varepsilon\tilde{u}_1 + \varepsilon^2\tilde{u}_2 = O\left(\varepsilon^3\right),\ \tilde{v}_0 + \varepsilon\tilde{v}_1 + \varepsilon^2\tilde{v}_2 = O\left(\varepsilon^3\right) \text{ at S,} \tag{4.112}$$

while the expansion — of the tangential stress boundary condition in the case of free surfaces (4.54) reads

$$\frac{\partial\tilde{v}_0}{\partial\xi} + \varepsilon\frac{\partial\tilde{v}_1}{\partial\xi} + \varepsilon^2\left[\frac{\partial\tilde{u}_0}{\partial z} + \frac{\partial\tilde{v}_2}{\partial\xi} - 2\frac{d\xi_b}{dz}\left(\frac{\partial\tilde{v}_0}{\partial z} - \frac{\partial\tilde{u}_0}{\partial\xi}\right)\right] = O\left(\varepsilon^3\right) \text{ at S.} \tag{4.113}$$

The latter is obtained as follows. Firstly, we substitute Eq. (4.88) in Eq. (4.54) and get

$$\cos(2\theta)\left(\frac{1}{\varepsilon}\frac{\partial v}{\partial\xi} + \frac{\partial u}{\partial z}\right) + \sin(2\theta)\left(\frac{\partial v}{\partial z} - \frac{1}{\varepsilon}\frac{\partial u}{\partial\xi}\right) = 0 \text{ at S.} \tag{4.114}$$

Multiplying the latter by ε, we obtain

$$\left(2\cos^2\theta - 1\right)\left(\varepsilon\frac{\partial u}{\partial z} + \frac{\partial v}{\partial\xi}\right) + 2\sin^2\theta\cot\theta\left(\varepsilon\frac{\partial v}{\partial z} - \frac{\partial u}{\partial\xi}\right) = 0. \tag{4.115}$$

Substituting the asymptotic expansions (4.100)–(4.101), (4.109)–(4.111) in Eq. (4.115), one gets

$$\left[2\left(\varepsilon\frac{d\xi_b}{dz}\right)^2-1\right]\cdot\left[\varepsilon^2\frac{\partial\tilde{u}_0}{\partial z}+\frac{\partial}{\partial\xi}\left(\tilde{v}_0+\varepsilon\tilde{v}_1+\varepsilon^2\tilde{v}_2\right)\right] + 2\varepsilon^2\frac{d\xi_b}{dz}\left(\frac{\partial\tilde{v}_0}{\partial z}-\frac{\partial\tilde{u}_0}{\partial\xi}\right)=O\left(\varepsilon^3\right)\ \text{at S} \tag{4.116}$$

or equivalently

$$\frac{\partial\tilde{v}_0}{\partial\xi}+\varepsilon\frac{\partial\tilde{v}_1}{\partial\xi}+\varepsilon^2\left[\frac{\partial\tilde{u}_0}{\partial z}+\frac{\partial\tilde{v}_2}{\partial\xi}-2\frac{d\xi_b}{dz}\left(\frac{\partial\tilde{v}_0}{\partial z}-\frac{\partial\tilde{u}_0}{\partial\xi}\right)-2\left(\frac{d\xi_b}{dz}\right)^2\frac{\partial\tilde{v}_0}{\partial\xi}\right]=O(\varepsilon^3)\ \text{at S}. \tag{4.117}$$

From the latter, it follows that

$$\frac{\partial\tilde{v}_0}{\partial\xi}=0\ \text{at S}. \tag{4.118}$$

Thus, we obtain Eq. (4.113).

Normal boundary condition in the new variables

In terms of the new variables (4.100)–(4.102), the expansion in series of the normal stress boundary condition acquires the following form:

$$p_b=p_0+p_1+p_2+\frac{2H}{Ca}+O\left(\varepsilon\right)\ \text{at S} \tag{4.119}$$

in the case of immobile surfaces, see Eq. (4.60), and

$$p_b=p_0+p_1+p_2+\frac{2H}{Ca}-2\frac{\partial u_0}{\partial r}+O\left(\varepsilon\right)\ \text{at S} \tag{4.120}$$

in the case of free surfaces, see Eq. (4.55). In the next lines, we shall prove that equation (4.120) holds true. In order to do that, we substitute Eq. (4.88) in Eq. (4.55) and obtain

$$p_b=p+\frac{2H}{Ca}-2\sin^2\theta\left[\frac{1}{\varepsilon}\frac{\partial u}{\partial\xi}+\cot^2\theta\frac{\partial v}{\partial z}-\cot\theta\left(\frac{1}{\varepsilon}\frac{\partial v}{\partial\xi}+\frac{\partial u}{\partial z}\right)\right]\ \text{at S}. \tag{4.121}$$

Using Eq. (4.102), the latter acquires the form

$$\varepsilon^2p_b=\tilde{p}_0+\varepsilon\tilde{p}_1+\varepsilon^2\left(\tilde{p}_2+\frac{2H}{Ca}\right) - 2\varepsilon\sin^2\theta\left[\frac{\partial u}{\partial\xi}+\varepsilon\cot^2\theta\frac{\partial v}{\partial z}-\cot\theta\left(\frac{\partial v}{\partial\xi}+\varepsilon\frac{\partial u}{\partial z}\right)\right]\ \text{at S}. \tag{4.122}$$

Substituting the asymptotic expansions (4.100)–(4.101), (4.110) in (4.122), one concludes

$$\varepsilon^2p_b=\tilde{p}_0+\varepsilon\tilde{p}_1+\varepsilon^2\left(\tilde{p}_2+\frac{2H}{Ca}\right)-2\varepsilon\left[1+O(\varepsilon^2)\right]\left(\varepsilon\frac{\partial\tilde{u}_0}{\partial\xi}-\varepsilon\frac{d\xi_b}{dz}\frac{\partial\tilde{v}_0}{\partial\xi}\right)+O(\varepsilon^3)\ \text{at S}. \tag{4.123}$$

From the latter and Eq. (4.118), it follows

$$\varepsilon^2p_b=\tilde{p}_0+\varepsilon\tilde{p}_1+\varepsilon^2\left(\tilde{p}_2+\frac{2H}{Ca}-2\frac{\partial\tilde{u}_0}{\partial\xi}\right)+O\left(\varepsilon^3\right)\ \text{at S}, \tag{4.124}$$

which is equivalent to Eq. (4.120), see Eq. (4.99).

4.5.3 Zero-order approximations $u_0,\ v_0,\ p_0$

The zero-order approximation of the Stokes problem (4.103)– (4.105) is

$$\frac{1}{1+\varepsilon\xi}\frac{\partial\left[(1+\varepsilon\xi)\,\tilde{u}_0\right]}{\partial\xi}+\frac{\partial\tilde{v}_0}{\partial z}=0, \tag{4.125}$$

$$\frac{\partial\tilde{p}_0}{\partial\xi}=0, \tag{4.126}$$

$$\frac{\partial\tilde{p}_0}{\partial z}-G-\frac{1}{1+\varepsilon\xi}\frac{\partial}{\partial\xi}\left[(1+\varepsilon\xi)\,\frac{\partial\tilde{v}_0}{\partial\xi}\right]=0. \tag{4.127}$$

It is more convenient to solve this problem in its original notation. Changing the variables back to the original ones $r,\ u_0,\ v_0,\ p_0$, we obtain the problem

$$\frac{1}{r}\frac{\partial}{\partial r}\left(ru_0\right)+\frac{\partial v_0}{\partial z}=0, \tag{4.128}$$

$$\frac{\partial p_0}{\partial r}=0, \tag{4.129}$$

$$\frac{\partial p_0}{\partial z}-\frac{1}{r}\frac{\partial}{\partial r}\left(r\frac{\partial v_0}{\partial r}\right)-\frac{Bo}{Ca}=0. \tag{4.130}$$

The zero-order approximations of the boundary conditions in the original variables are listed below:

- the no-slip boundary conditions at the wall:

$$u_0=0,\ v_0=1 \text{ at r=1;} \tag{4.131}$$

- simple flow rate condition[3]:

$$\int_{r_b}^{1} rv_0dr=\frac{W}{2}; \tag{4.132}$$

- the tangential stress boundary condition in case of immobile surfaces:

$$u_0=0,\ v_0=0 \text{ at S} \tag{4.133}$$

  or in case of free surfaces:

$$\frac{\partial v_0}{\partial r}=0 \text{ at S.} \tag{4.134}$$

From (4.129), it is obvious that $p_0=p_0(z)$. Then, using Eq. (4.130), the general form of the velocity along the z-axis v_0 is obtained

$$v_0(r,z)=\left(\frac{dp_0}{dz}-\frac{Bo}{Ca}\right)\frac{r^2}{4}+P_0(z)\ln r+Q_0(z), \tag{4.135}$$

[3]Note that the simple flow rate condition is more convenient to use for analytical computations than the kinematic boundary condition. The main reason is that the kinematic boundary conditions in lubrication approximation gives a relationship between the zero-order approximations u_i and v_i, while using the simple flow rate condition, we could obtain directly an expression for the unknown v_i.

where $P_0(z)$ and $Q_0(z)$ are unknown functions of z, see Eq. (4.61). Substituting the latter in the no-slip boundary condition (4.131), we obtain

$$Q_0(z) = 1 - \frac{1}{4}\left(\frac{dp_0}{dz} - \frac{Bo}{Ca}\right). \tag{4.136}$$

Hence, an expression for $v_0(r,z)$ in the form

$$v_0(r,z) = 1 - \frac{1}{4}\left(\frac{dp_0}{dz} - \frac{Bo}{Ca}\right)\left(1-r^2\right) + P_0(z)\ln r. \tag{4.137}$$

is derived. In order to find $P_0(z)$, we substitute the latter in the flow rate condition (4.132) and obtain consecutively:

$$\begin{aligned}\frac{W}{2} &= \int_{r_b}^{1}\left[r - \frac{1}{4}\left(\frac{dp_0}{dz} - \frac{Bo}{Ca}\right)\left(r-r^3\right) + P_0(z) r\ln r\right]dr \\ &= \frac{1-r_b^2}{2} - \frac{1}{16}\left(\frac{dp_0}{dz} - \frac{Bo}{Ca}\right)\left(1-2r_b^2+r_b^4\right) \\ &\qquad - \frac{P_0(z)}{4}\left(1-r_b^2+2r_b^2\ln r_b\right).\end{aligned} \tag{4.138}$$

In the latter, we used (4.69). Expressing $P_0(z)$ from (4.138), one concludes that

$$P_0(z) = \frac{8\left(1-r_b^2-W\right) - \left(\frac{dp_0}{dz} - \frac{Bo}{Ca}\right)\left(1-r_b^2\right)^2}{4\left(1-r_b^2+2r_b^2\ln r_b\right)}. \tag{4.139}$$

holds true. Then, $v_0(r,z)$ acquires the form:

$$v_0(r,z) = 1 + \frac{A}{4}\left(1-r^2\right) + \frac{B}{4}\ln r, \tag{4.140}$$

where the functions $A(z)$ and $B(z)$ are given by the following definitions:

$$A(z) = \frac{Bo}{Ca} - \frac{dp_0}{dz},\ B(z) = \frac{A\left(1-r_b^2\right)^2 - 8\left(W-1+r_b^2\right)}{1-r_b^2+2r_b^2\ln r_b}. \tag{4.141}$$

By integrating the continuity equation (4.128) and using (4.69), u_0 could be computed as follows:

$$\begin{aligned}u_0 &= -\frac{1}{r}\int r\frac{\partial v_0}{\partial z}dr = \frac{1}{4r}\frac{dA}{dz}\int\left(r^3-r\right)dr - \frac{1}{4r}\frac{dB}{dz}\int r\ln r dr \\ &= \frac{1}{16}\left[\frac{dA}{dz}\left(r^3-2r\right) - \frac{dB}{dz}r\left(2\ln r - 1\right)\right] + \frac{R_0(z)}{r}.\end{aligned} \tag{4.142}$$

In order to find the unknown function $R_0(z)$, we substitute the obtained result in the no-slip boundary condition (4.131) and get the following expressions for $R_0(z)$:

$$R_0(z) = \frac{1}{16}\left(\frac{dA}{dz} - \frac{dB}{dz}\right) \tag{4.143}$$

and, thus, u_0 has the form

$$u_0(r,z) = \frac{dA}{dz}\cdot\frac{\left(1-r^2\right)^2}{16r} - \frac{dB}{dz}\cdot\frac{1-r^2+2r^2\ln r}{16r}. \tag{4.144}$$

Immobile surfaces

In this case, the velocity at the bubble surface is equal to zero, see Eq. (4.133). Using Eqs. (4.133), (4.140) and (4.141), we obtain

$$0 = v_0(r_b) = 1 + \frac{A}{4}\left(1 - r_b^2\right) + \frac{A\left(1 - r_b^2\right)^2 - 8\left(W - 1 + r_b^2\right)}{4\left(1 - r_b^2 + 2r_b^2 \ln r_b\right)} \ln r_b. \tag{4.145}$$

By expressing $A(z)$ from the latter and substituting it in (4.141), we calculate the derivative of pressure function p_0:

$$\frac{dp_0}{dz} - \frac{Bo}{Ca} = -A(z) = \frac{4\left[1 - r_b^2 + 2\left(1 - W\right)\ln r_b\right]}{\left(1 - r_b^2\right)\left[1 - r_b^2 + \left(1 + r_b^2\right)\ln r_b\right]}. \tag{4.146}$$

The substitution of the obtained expression, Eq. (4.146), for the function $A(z)$ in the definition of function $B(z)$, Eq. (4.141), gives an explicit formula for the function $B(z)$

$$B(z) = -\frac{4\left(2W - 1 + r_b^2\right)}{1 - r_b^2 + \left(1 + r_b^2\right)\ln r_b}. \tag{4.147}$$

Free surfaces

In this case, substituting Eq. (4.140) in the zero-order tangential stress boundary condition (4.134), one obtains

$$0 = \left.\frac{\partial v_0}{\partial r}\right|_{r=r_b} = -\frac{2A\,r_b}{4} + \frac{A\left(1 - r_b^2\right)^2 - 8\left(W - 1 + r_b^2\right)}{4r_b\left(1 - r_b^2 + 2r_b^2 \ln r_b\right)}. \tag{4.148}$$

Analogously to the computation in the case of immobile surfaces, we obtain the following differential equation:

$$\frac{dp_0}{dz} - \frac{Bo}{Ca} = -A(z) = \frac{8\left(1 - r_b^2 - W\right)}{1 - 4r_b^2 + 3r_b^4 - 4r_b^4 \ln r_b} \tag{4.149}$$

by expressing $A(z)$ from Eq. (4.148). The respective expression for function $B(z)$ follows from equations (4.141) and (4.149):

$$B(z) = \frac{16r_b^2\left(W - 1 + r_b^2\right)}{1 - 4r_b^2 + 3r_b^4 - 4r_b^4 \ln r_b}. \tag{4.150}$$

4.5.4 First correction terms $u_1,\ v_1,\ p_1$

The first correction terms of the Stokes problem (4.103)– (4.105) are obtained similarly to the zero-order approximation, see Eqs. (4.128)– (4.130). The only difference between the the computations is that the term Bo/Ca is missing from Eq. (4.130) in the first correction term. Thus, the general form of v_1 is

$$v_1(r, z) = \frac{dp_1}{dz}\frac{r^2}{4} + P_1(z)\ln r + Q_1(z), \tag{4.151}$$

where $P_1(z)$ and $Q_1(z)$ are unknown functions of z, see Eq. (4.135). In order to find the unknown functions, we find the first correction terms of the boundary conditions:

- the no-slip boundary conditions at the wall:

$$u_1 = 0,\ v_1 = 0 \text{ at r=1;} \tag{4.152}$$

- simple flow rate condition:

$$\int_{r_b}^{1} r v_1 dr = 0; \tag{4.153}$$

- the tangential stress boundary condition in case of immobile surfaces:

$$u_1 = 0,\ v_1 = 0 \text{ at S} \tag{4.154}$$

or in case of free surfaces:

$$\frac{\partial v_1}{\partial r} = 0 \text{ at S.} \tag{4.155}$$

Substituting (4.151) in the no-slip boundary condition (4.152), we obtain the following expression for $Q_1(z)$:

$$Q_1(z) = -\frac{1}{4}\frac{dp_1}{dz} \tag{4.156}$$

and then $v_1(r,z)$ acquires the form

$$v_1(r,z) = -\frac{1}{4}\frac{dp_1}{dz}\left(1-r^2\right) + P_1(z)\ln r. \tag{4.157}$$

Analogously to finding $P_0(z)$, we substitute (4.157) in the flow rate condition (4.153) and obtain

$$0 = -\frac{1}{16}\frac{dp_1}{dz}\left(1-r_b^2\right)^2 - \frac{P_1(z)}{4}\left(1-r_b^2+2r_b^2\ln r_b\right), \tag{4.158}$$

$$P_1(z) = -\frac{\left(1-r_b^2\right)^2}{4\left(1-r_b^2+2r_b^2\ln r_b\right)}\cdot\frac{dp_1}{dz}. \tag{4.159}$$

Then, $v_1(r,z)$ acquires the form

$$v_1(r,z) = \frac{A_1}{4}\left(1-r^2\right) + \frac{B_1}{4}\ln r, \tag{4.160}$$

where the functions $A_1(z)$ and $B_1(z)$ are given by the following definition:

$$A_1(z) = -\frac{dp_1}{dz},\ B_1(z) = \frac{A_1\left(1-r_b^2\right)^2}{1-r_b^2+2r_b^2\ln r_b}. \tag{4.161}$$

Analogously to the zero-order approximation, we obtain the following expression for u_1:

$$u_1(r,z) = \frac{dA_1}{dz}\cdot\frac{\left(1-r^2\right)^2}{16r} - \frac{dB_1}{dz}\cdot\frac{1-r^2+2r^2\ln r}{16r}. \tag{4.162}$$

Immobile surfaces

In case of immobile surfaces, the velocity at the bubble surface is equal to zero, i.e

$$0 = v_1(r_b) = \frac{A_1}{4}\left(1 - r_b^2\right) + \frac{A_1\left(1 - r_b^2\right)^2}{4\left(1 - r_b^2 + 2r_b^2 \ln r_b\right)} \ln r_b. \tag{4.163}$$

The latter holds true for all points (r_b, z_b) on the bubble surface and, thus, $A_1 \equiv 0$. From Eq. (4.161), it follows that $B_1 \equiv 0$ and, therefore,

$$u_1 = v_1 \equiv 0. \tag{4.164}$$

Using equation (4.161) and (4.164), we obtain the following differential equation:

$$\frac{dp_1}{dz} = 0, \tag{4.165}$$

which could be solved directly.

Free surfaces

In the case of free surfaces, substituting general solution (4.160) in the first-order tangential stress boundary condition (4.155), one obtains

$$0 = \left.\frac{\partial v_1}{\partial r}\right|_{r=r_b} = -\frac{A_1 r_b}{2} + \frac{A_1\left(1 - r_b^2\right)^2}{4r_b\left(1 - r_b^2 + 2r_b^2 \ln r_b\right)}. \tag{4.166}$$

Using similar reasoning to the previous case, one concludes that Eqs. (4.164) and (4.165) hold also for free surfaces.

4.5.5 Second correction terms $u_2,\ v_2,\ p_2$

The second correction terms are obtained by solving the Stokes problem (4.103), (4.104) and (4.105)

$$\frac{1}{1+\varepsilon\xi}\frac{\partial\left[(1+\varepsilon\xi)\,\tilde{u}_2\right]}{\partial\xi} + \frac{\partial\tilde{v}_2}{\partial z} = 0, \tag{4.167}$$

$$\frac{\partial}{\partial\xi}\left\{\tilde{p}_2 - \frac{1}{1+\varepsilon\xi}\frac{\partial\left[(1+\varepsilon\xi)\,\tilde{u}_0\right]}{\partial\xi}\right\} = 0, \tag{4.168}$$

$$\frac{\partial\tilde{p}_2}{\partial z} - \frac{1}{1+\varepsilon\xi}\frac{\partial}{\partial\xi}\left[(1+\varepsilon\xi)\,\frac{\partial\tilde{v}_2}{\partial\xi}\right] - \frac{\partial^2\tilde{v}_0}{\partial z^2} = 0. \tag{4.169}$$

As we said, it is more convenient to solve this problem in its original variables, i.e. $r,\ u_2,\ v_2,\ p_2$. Using them, we obtain the problem

$$\frac{1}{r}\frac{\partial(ru_2)}{\partial r} + \frac{\partial v_2}{\partial z} = 0, \tag{4.170}$$

$$\frac{\partial}{\partial r}\left[p_2 - \frac{1}{r}\frac{\partial(ru_0)}{\partial r}\right] = 0, \tag{4.171}$$

$$\frac{\partial p_2}{\partial z} - \frac{1}{r}\frac{\partial}{\partial r}\left(r\frac{\partial v_2}{\partial r}\right) - \frac{\partial^2 v_0}{\partial z^2} = 0. \tag{4.172}$$

In order to close the system, we add the second correction terms of the boundary conditions, i.e.

- the no-slip boundary conditions at the wall:

$$u_2 = 0,\ v_2 = 0 \text{ at r=1;} \tag{4.173}$$

- simple flow rate condition:

$$\int_{r_b}^{1} r v_2 dr = 0; \tag{4.174}$$

- the tangential stress boundary condition in case of immobile surfaces:

$$u_2 = 0,\ v_2 = 0 \text{ at S} \tag{4.175}$$

or in case of free surfaces:

$$\frac{\partial u_0}{\partial z} + \frac{\partial v_2}{\partial r} - 2\frac{dr_b}{dz}\left(\frac{\partial v_0}{\partial z} - \frac{\partial u_0}{\partial r}\right) = 0 \text{ at S;} \tag{4.176}$$

By integrating Eq. (4.171) with respect to r, we obtain

$$p_2(r,z) = \frac{1}{r}\frac{\partial}{\partial r}(r u_0) + q_2(z), \tag{4.177}$$

where $q_2(z)$ is unknown function of z. Using the continuity equation (4.128), one gets the following expression for p_2:

$$p_2(r,z) = q_2(z) - \frac{\partial v_0}{\partial z}. \tag{4.178}$$

Taking into account Eqs. (4.140), (4.172), (4.178), we obtain consecutively

$$\begin{aligned}\frac{1}{r}\frac{\partial}{\partial r}\left(r\frac{\partial v_2}{\partial r}\right) &= \frac{\partial p_2}{\partial z} - \frac{\partial^2 v_0}{\partial z^2} = \frac{dq_2}{dz} - 2\frac{\partial^2 v_0}{\partial z^2} \\ &= \frac{dq_2}{dz} - \frac{1}{2}\frac{d^2A}{dz^2}\left(1 - r^2\right) - \frac{1}{2}\frac{d^2B}{dz^2}\ln r.\end{aligned} \tag{4.179}$$

In order to find an expression for v_2, we integrate the latter with respect to r twice

$$\frac{\partial}{\partial r}\left(r\frac{\partial v_2}{\partial r}\right) = \frac{dq_2}{dz}r - \frac{1}{2}\frac{d^2A}{dz^2}\left(r - r^3\right) - \frac{1}{2}\frac{d^2B}{dz^2}r\ln r, \tag{4.180}$$

$$\frac{\partial v_2}{\partial r} = \frac{dq_2}{dz}\frac{r}{2} - \frac{1}{8}\frac{d^2A}{dz^2}\left(2r - r^3\right) - \frac{1}{8}\frac{d^2B}{dz^2}\left(2r\ln r - r\right) + \frac{C(z)}{r} \tag{4.181}$$

and finally obtain

$$\begin{aligned}v_2 = {} & \frac{dq_2}{dz}\frac{r^2}{4} + \frac{1}{32}\frac{d^2A}{dz^2}\left(r^4 - 4r^2\right) - \frac{1}{8}\frac{d^2B}{dz^2}\left(r^2\ln r - r^2\right) \\ & + C(z)\ln r + Q_2(z),\end{aligned} \tag{4.182}$$

where $C(z)$ and $Q_2(z)$ are unknown functions of z, see Eq. (4.69). In order to find $Q_2(z)$, one substitutes (4.182) in the no-slip boundary condition (4.173) and gets the following expression for Q_2:

$$Q_2(z) = -\frac{1}{4}\frac{dq_2}{dz} + \frac{3}{32}\frac{d^2A}{dz^2} - \frac{1}{8}\frac{d^2B}{dz^2}. \tag{4.183}$$

Using the latter, an expression for v_2 is obtained

$$v_2 = \frac{1}{4}\frac{dq_2}{dz}\left(r^2-1\right) + \frac{1}{32}\frac{d^2A}{dz^2}\left(r^4-4r^2+3\right) - \frac{1}{8}\frac{d^2B}{dz^2}\left(1-r^2+r^2\ln r\right) + C(z)\ln r. \tag{4.184}$$

Substituting the general form of v_2, Eq. (4.184), in the simple flow rate condition (4.174), we get

$$\begin{aligned} 0 &= \left\{\frac{1}{16}\frac{dq_2}{dz}\left(r^2-1\right)^2 + \frac{1}{32}\frac{d^2A}{dz^2}\left(\frac{r^6}{6}-r^4+\frac{3r^2}{2}\right)\right. \\ &\left. -\frac{1}{8}\frac{d^2B}{dz^2}\left[\frac{r^2}{2}-\frac{r^4}{4}+\frac{r^4}{16}\left(4\ln r-1\right)\right] + \frac{C(z)r^2}{4}\left(2\ln r-1\right)\right\}\Bigg|_{r=r_b}^{1} \\ &= -\frac{1}{16}\frac{dq_2}{dz}\left(r_b^2-1\right)^2 - \frac{1}{192}\frac{d^2A}{dz^2}\left[r_b^6-6r_b^4+9r_b^2-4\right] \\ &+ \frac{1}{128}\frac{d^2B}{dz^2}\left(8r_b^2-5r_b^4+4r_b^4\ln r_b-3\right) \\ &- \frac{C(z)}{4}\left(1-r_b^2+2r_b^2\ln r_b\right). \end{aligned} \tag{4.185}$$

In the latter, we used

$$\begin{aligned} \int r^k \ln r dr &= \frac{1}{k+1}\int \ln r d\left(r^{k+1}\right) = \frac{1}{k+1}\left(r^{k+1}\ln r - \int r^k dr\right) \\ &= \frac{r^{k+1}}{(k+1)^2}\left[(k+1)\ln r - 1\right], \end{aligned} \tag{4.186}$$

which is valid for $k \neq -1$. Expressing $C(z)$ from equation (4.185), one obtains

$$\begin{aligned} C(z) = &-\frac{\left(1-r_b^2\right)^2}{4\left(1-r_b^2+2r_b^2\ln r_b\right)}\cdot\frac{dq_2}{dz} + \frac{\left(1-r_b^2\right)^2\left(4-r_b^2\right)}{48\left(1-r_b^2+2r_b^2\ln r_b\right)}\cdot\frac{d^2A}{dz^2} \\ &- \frac{3-8r_b^2+5r_b^4-4r_b^4\ln r_b}{32\left(1-r_b^2+2r_b^2\ln r_b\right)}\cdot\frac{d^2B}{dz^2}. \end{aligned} \tag{4.187}$$

Immobile surfaces.

In case of immobile surfaces, the velocity at the bubble surface is equal to zero, i.e. $v_2\left(r_b\right) = 0$ (see Eq. (4.175)):

$$\begin{aligned} 0 = v_2\left(r_b\right) = &\frac{1}{4}\frac{dq_2}{dz}\left[r_b^2-1-\frac{\left(1-r_b^2\right)^2}{1-r_b^2+2r_b^2\ln r_b}\ln r_b\right] \\ &- \frac{d^2A}{dz^2}\left[\frac{-r_b^4+4r_b^2-3}{32} - \frac{\left(1-r_b^2\right)^2\left(4-r_b^2\right)}{48\left(1-r_b^2+2r_b^2\ln r_b\right)}\ln r_b\right] \\ &- \frac{1}{8}\frac{d^2B}{dz^2}\left[1-r_b^2+r_b^2\ln r_b + \frac{3-8r_b^2+5r_b^4-4r_b^4\ln r_b}{4\left(1-r_b^2+2r_b^2\ln r_b\right)}\ln r_b\right]. \end{aligned} \tag{4.188}$$

or equivalently

$$\frac{dq_2}{dz} = \frac{3\left(3-4r_b^2+r_b^4\right)+4\left(2+2r_b^2-r_b^4\right)\ln r_b}{24\left[1-r_b^2+\left(1+r_b^2\right)\ln r_b\right]}\cdot\frac{d^2A}{dz^2} - \frac{4\left(1-r_b^2\right)^2+\left(3+4r_b^2-7r_b^4+4r_b^4\ln r_b\right)\ln r_b}{8\left(1-r_b^2\right)\left[1-r_b^2+\left(1+r_b^2\right)\ln r_b\right]}\cdot\frac{d^2B}{dz^2}. \tag{4.189}$$

Free surfaces.

The tangential stress boundary condition in case of free surfaces, Eq. (4.176), written for v_2 reads:

$$\frac{\partial v_2}{\partial r} = 2\frac{dr_b}{dz}\left(\frac{\partial v_0}{\partial z}-\frac{\partial u_0}{\partial r}\right)-\frac{\partial u_0}{\partial z} \text{ at S.} \tag{4.190}$$

The substitution of the zero-order solutions (4.140) and (4.144), the general solution (4.184) and the expression for $C(z)$, Eq. (4.187), in the latter leads to the respective differential equation for q_2:

$$\begin{aligned}\frac{dq_2}{dz} = {} & \frac{7-30r_b^2+33r_b^4-10r_b^6+6r_b^2\left(1-6r_b^2+3r_b^4\right)\ln r_b}{12\left(1-4r_b^2+3r_b^4-4r_b^4\ln r_b\right)}\cdot\frac{d^2A}{dz^2} \\ & - \frac{5-16r_b^2+11r_b^4+4r_b^2\left(4-7r_b^2\right)\ln r_b+24r_b^4\ln^2 r_b}{8\left(1-4r_b^2+3r_b^4-4r_b^4\ln r_b\right)}\cdot\frac{d^2B}{dz^2} \\ & + \frac{\left(1-r_b^2+2r_b^2\ln r_b\right)}{2r_b\left(1-4r_b^2+3r_b^4-4r_b^4\ln r_b\right)}\left[\left(r_b^2-1\right)\left(1+7r_b^2\right)\cdot\frac{dA}{dz}\right. \\ & \left.+\left(1-r_b^2-6r_b^2\ln r_b\right)\cdot\frac{dB}{dz}\right]\cdot\frac{dr_b}{dz} \text{ at S.}\end{aligned} \tag{4.191}$$

The obtained solutions of the hydrodynamic problem in the generalized lubrication approximation are used to solve the boundary value problem for the bubble shape, using the Ratulowski and Chang approach [4.80].

4.6 Boundary value problem, modeling the shape of long bubbles

4.6.1 General formulation

As we mentioned before, if approximations of u, v and p at bubble surface S are obtained, then the bubble shape in the case of free surfaces could be found as a solution of the system (4.55)–(4.58) with appropriate initial conditions, applied at the bubble apex. In section 4.5, we found approximations of u, v and p at bubble surface S in the case of small thickness of the liquid layer, ε. Then, an approximation of the normal stress boundary condition (4.55) could be obtained in the form

$$p_b = p_0 + p_1 + q_2 - \frac{\partial v_0}{\partial z} - 2\frac{\partial u_0}{\partial r} + \frac{2H}{Ca} \text{ at S} \tag{4.192}$$

by substituting Eq. (4.178) in Eq. (4.120) and neglecting the terms of higher order. We have already computed expressions for u_0, Eq. (4.144), and v_0 at S, Eq. (4.140). But, in order

to find expressions for p_0 and q_2, one shall solve additionally differential equations, whose right-hand side depends on r_b and, therefore, are coupled with the rest of the equations in the problem, see Eqs. (4.149) and (4.191). As p_0 and q_2 depend only on the z-coordinate, then at the bubble surface, $z = z_b(s)$, p_0 and q_2 are functions of the arc length of the bubble surface s. Using this fact, we differentiate Eq. (4.192) with respect to s:

$$-\frac{1}{Ca}\frac{d(2H)}{ds} = \frac{dp_0}{ds} + \frac{dq_2}{ds} - \frac{d}{ds}\left(\frac{\partial v_0}{\partial z} + 2\frac{\partial u_0}{\partial r}\right) \text{ at S} \tag{4.193}$$

and substitute the obtained expressions for u_0, v_0, dp_0/ds and dq_2/ds in the right-hand side of the latter in order to reduce the number of equations in the system. Then one could solve the system (4.56)– (4.58), (4.193) instead of the problem (4.55)–(4.58) in case of free surfaces. For tangentially immobile surfaces, Eq. (4.193) is replaced with

$$-\frac{1}{Ca}\frac{d(2H)}{ds} = \frac{dp_0}{ds} + \frac{dq_2}{ds} - \frac{d}{ds}\left(\frac{\partial v_0}{\partial z}\right) \text{ at S.} \tag{4.194}$$

A minor issue in Eqs. (4.193) and (4.194) is that the notation $d(2H)/ds$ is not really convenient. Moreover, the variables, which are usually used in the fluid dynamics models, are the flow velocity, pressure and density. Thus, we introduce the dimensionless pressure difference function, $p_s(s)$, which accounts for the dynamic pressure contribution at the bubble surface, and we shall exclude the mean curvature H from Eqs. (4.58), (4.193) and (4.194). In order to do that, the non-dimensionalized Young–Laplace equation of capillary is used

$$2H = -Ca\, p_s, \tag{4.195}$$

which gives a relationship between the dynamic pressure difference, the mean curvature of the bubble and the surface tension[4], see [4.2, 4.87]. Thus, the following nonlinear system of four ordinary differential equations for the bubble shape:

$$\frac{dr_b}{ds} = \cos\theta, \tag{4.196}$$

$$\frac{dz_b}{ds} = \sin\theta, \tag{4.197}$$

$$\frac{d\theta}{ds} = -Ca\, p_s - \frac{\sin\theta}{r_b}, \tag{4.198}$$

$$\frac{dp_s}{ds} = F\left(r_b, \theta, p_s, Bo, Ca_{pm}\right), \tag{4.199}$$

is obtained, where F is the right hand-side of Eqs. (4.193) or (4.194), see Eqs. (4.56) – (4.58), (4.193)– (4.195). In the next subsections, we shall find the concrete form of the function F in the case of free surfaces or tangentially immobile surfaces.

[4]The dimensional Young–Laplace equation of capillarity has the form $2H\,\sigma = -p_s$. Its dimensionless form is obtained by using Eqs. (4.44), (4.46)–(4.47).

Concrete form of F in the case of tangentially immobile interfaces

In case of tangentially immobile surfaces, we obtain the following expression for the function F:

$$\frac{dp_s}{ds} = \frac{dp_0}{dz}\sin\theta + \left(\frac{dq_2}{dz} - \frac{\partial^2 v_0}{\partial z^2}\right)\sin\theta - \frac{\partial}{\partial r}\left(\frac{\partial v_0}{\partial z}\right)\cos\theta \text{ at S}, \tag{4.200}$$

see Eqs. (4.194), (4.196)–(4.197). From Eqs. (4.140), (4.144), (4.189), it follows that the derivatives $\frac{dq_2}{dz}$, $\frac{\partial^2 v_0}{\partial z^2}$ and $\frac{\partial^2 v_0}{\partial r \partial z}$ have the following form:

$$\frac{dq_2}{dz} = q_{A2}\cdot\frac{d^2A}{dz^2} + q_{B2}\cdot\frac{d^2B}{dz^2} \text{ at S}, \tag{4.201}$$

$$\frac{\partial^2 v_0}{\partial z^2} = \frac{1-r_b^2}{4}\cdot\frac{d^2A}{dz^2} + \frac{\ln r_b}{4}\cdot\frac{d^2B}{dz^2} \text{ at S}, \tag{4.202}$$

$$\frac{\partial^2 u_0}{\partial r \partial z} = -\frac{r_b}{2}\cdot\frac{dA}{dz} + \frac{1}{4r_b}\cdot\frac{dB}{dz} \text{ at S}, \tag{4.203}$$

where q_{A2} and q_{B2} are the coefficients in front of $\frac{d^2A}{dz^2}$ and $\frac{d^2B}{dz^2}$ in Eq. (4.189). The explicit expressions for the first and second derivatives of $A(z)$ and $B(z)$ with respect to z are given below:

$$\frac{dA}{dz} = \frac{dA}{dr_b}\cot\theta, \frac{dB}{dz} = \frac{dB}{dr_b}\cot\theta, \tag{4.204}$$

$$\begin{aligned}\frac{d^2A}{dz^2} &= \frac{d}{dz}\left(\frac{dA}{dr_b}\cot\theta\right) = \frac{d^2A}{dr_b^2}\cot\theta + \frac{dA}{dr_b}\frac{d\left(\cot\theta\right)}{dz} \\ &= \frac{d^2A}{dr_b^2}\cot^2\theta - \frac{dA}{dr_b}\frac{1}{\sin^3\theta}\frac{d\theta}{ds},\end{aligned} \tag{4.205}$$

$$\frac{d^2B}{dz^2} = \frac{d^2B}{dr_b^2}\cot^2\theta - \frac{dB}{dr_b}\frac{1}{\sin^3\theta}\frac{d\theta}{ds}, \tag{4.206}$$

see Eq. (4.196), (4.197). Substituting Eqs. (4.201)–(4.206) in Eq. (4.200), we obtain

$$F = -\frac{a_s(r_b)}{Ca}\sin\theta - \frac{b_s(r_b)}{\sin^2\theta}\frac{d\theta}{ds} + c_s(r_b)\frac{\cos^2\theta}{\sin\theta}, \tag{4.207}$$

where

$$a_s\left(r_b\right) = -Ca\frac{dp_0}{dz}, \tag{4.208}$$

$$b_s\left(r_b\right) = \left(q_{A2} - \frac{1-r_b^2}{4}\right)\frac{dA}{dr_b} + \left(q_{B2} - \frac{\ln r_b}{4}\right)\frac{dB}{dr_b}, \tag{4.209}$$

$$\begin{aligned}c_s\left(r_b\right) = &\left(q_{A2} - \frac{1-r_b^2}{4}\right)\frac{d^2A}{dr_b^2} + \frac{r_b}{2}\frac{dA}{dr_b} \\ &+ \left(q_{B2} - \frac{\ln r_b}{4}\right)\frac{d^2B}{dr_b^2} - \frac{1}{4r_b}\frac{dB}{dr_b}.\end{aligned} \tag{4.210}$$

After lengthy computations, we obtain the exact form of the functions $a_s\left(r_b\right)$, $b_s\left(r_b\right)$ and $c_s\left(r_b\right)$

$$a_s\left(r_b\right) = -\frac{4\left[\left(1-r_b^2\right)Ca + 2Ca_{pm}\ln r_b\right]}{\left(1-r_b^2\right)\left[1-r_b^2+\left(1+r_b^2\right)\ln r_b\right]} - Bo; \tag{4.211}$$

$$
\begin{aligned}
b_s(r_b) = & \frac{\left(1-r_b^2\right)^2 - 2\left(1-W\right)\left(1-r_b^2+2r_b^2\ln r_b\right)}{6r_b\left(1-r_b^2\right)^2\left[1-r_b^2+\left(1+r_b^2\right)\ln r_b\right]^3} \\
& \times \Big[3\left(5r_b^2-3\right)\left(1-r_b^2\right)^2 \\
& + \left(-13+14r_b^2+23r_b^4\right)\left(1-r_b^2\right)\ln r_b \\
& + 2\left(-3+5r_b^2+5r_b^4+5r_b^6\right)\ln^2 r_b\Big]; \qquad (4.212) \\
c_s(r_b) = & \frac{1}{6r_b^2\left[1-r_b^2+\left(1+r_b^2\right)\ln r_b\right]^4}\cdot\Big\{21\left(1+r_b^2\right)\left(1-r_b^2\right)^3 \\
& + 12\left(3+11r_b^2+3r_b^4\right)\left(1-r_b^2\right)^2\ln r_b \\
& + \left(25+131r_b^2+25r_b^4\right)\left(1-r_b^2\right)\ln^2 r_b \\
& + \left(6+52r_b^2+28r_b^4+52r_b^6+6r_b^8\right)\ln^3 r_b \\
& + \frac{2\left(W-1\right)}{\left(1-r_b^2\right)^3}\cdot\Big[3\left(7-12r_b^2+13r_b^4\right)\left(1-r_b^2\right)^4 \\
& + 2\left(18+7r_b^2+4r_b^4+67r_b^6\right)\left(1-r_b^2\right)^3\ln r_b \\
& + \left(25+14r_b^2+228r_b^4+122r_b^6+187r_b^8\right)\left(1-r_b^2\right)^2\ln^2 r_b \\
& + 2\left(3-2r_b^2+86r_b^4+168r_b^6+71r_b^8+58r_b^{10}\right)\left(1-r_b^2\right)\ln^3 r_b \\
& - 4r_b^2(3-21r_b^2-12r_b^4-52r_b^6-7r_b^8-7r_b^{10})\ln^4 r_b\Big]\Big\}. \qquad (4.213)
\end{aligned}
$$

The function $a_s(r_b)$ corresponds to the zero-order solution and the value of $a_s(r_c)$ is equal to zero at the cylindrical part, $r_b = r_c$, see Eq. (4.81). Using Eq. (4.81) twice, the derivative of a_s at the cylindrical part of the bubble, $a_s'(r_c)$, is computed as follows:

$$
\begin{aligned}
a_s'(r_c) = & \frac{-4\left(-2Car_c+2Ca_{pm}\dfrac{1}{r_c}\right)}{\left(1-r_c^2\right)\left[1-r_c^2+\left(1+r_c^2\right)\ln r_c\right]} \\
& - \frac{4\left[\left(1-r_c^2\right)Ca+2Ca_{pm}\ln r_c\right]\left(1-4r_c^2+3r_c^4-4r_c^4\ln r_c\right)}{\left(1-r_c^2\right)^2\left[1-r_c^2+\left(1+r_c^2\right)\ln r_c\right]^2} \\
= & \frac{8\left(r_c^2Ca-Ca_{pm}\right)-Bo\left(1-4r_c^2+3r_c^4-4r_c^4\ln r_c\right)}{r_c\left(1-r_c^2\right)\left[1-r_c^2+\left(1+r_c^2\right)\ln r_c\right]} \\
= & -\frac{\left(1-r_c^2+2r_c^2\ln r_c\right)\left[8Ca_{pm}+Bo\left(1-r_c^2\right)^2\right]}{r_c\left(1-r_c^2\right)^2\left[1-r_c^2+\left(1+r_c^2\right)\ln r_c\right]}. \qquad (4.214)
\end{aligned}
$$

Concrete form of F in case of free surfaces

In case of free surfaces, we obtain the following expression for the function F:

$$
\frac{dp_s}{ds} = \frac{dp_0}{dz}\sin\theta + \left(\frac{dq_2}{dz} - \frac{\partial^2 v_0}{\partial z^2} - 2\frac{\partial^2 u_0}{\partial z\partial r}\right)\sin\theta - \left(\frac{\partial^2 v_0}{\partial r\partial z} + 2\frac{\partial^2 u_0}{\partial r^2}\right)\cos\theta \text{ at S}, \qquad (4.215)
$$

see Eqs. (4.193), (4.196), (4.197). Using Eqs. (4.140), (4.144), (4.191), we obtain

$$
\frac{dq_2}{dz} = q_{A2}\cdot\frac{d^2A}{dz^2} + q_{B2}\cdot\frac{d^2B}{dz^2} + \left(q_{A1}\frac{dA}{dz} + q_{B1}\frac{dB}{dz}\right)\cot\theta, \qquad (4.216)
$$

$$\frac{\partial^2 u_0}{\partial z \partial r} = \frac{\left(1-r_b^2\right)\left(-1-3r_b^2\right)}{16r_b^2} \cdot \frac{d^2A}{dz^2} - \frac{r_b^2 - 1 + 2r_b^2 \ln r_b}{16r_b^2} \cdot \frac{d^2B}{dz^2}, \tag{4.217}$$

$$\frac{\partial^2 u_0}{\partial r^2} = \frac{1+3r_b^4}{8r_b^3} \cdot \frac{dA}{dz} + \frac{-1-r_b^2}{8r_b^3} \cdot \frac{dB}{dz}, \tag{4.218}$$

where q_{1A}, q_{1B}, q_{2A}, q_{2B} are the coefficients in front of $\frac{dA}{dz}\frac{dr_b}{dz}$, $\frac{dB}{dz}\frac{dr_b}{dz}$, $\frac{d^2A}{dz^2}$, $\frac{d^2B}{dz^2}$ in Eq. (4.191), respectively. The explicit expression for the derivative of p_s with respect to s has the general form (4.207), where the functions $a_s(r_b)$, $b_s(r_b)$ and $c_s(r_b)$ are computed as

$$a_s(r_b) = -Ca\frac{dp_0}{dz}, \tag{4.219}$$

$$b_s(r_b) = \left(q_{A2} + \frac{1-r_b^4}{8r_b^2}\right)\frac{dA}{dr_b} + \left(q_{B2} + \frac{r_b^2-1}{8r_b^2}\right)\frac{dB}{dr_b}, \tag{4.220}$$

$$\begin{aligned} c_s(r_b) = &\left(q_{A2} + \frac{1-r_b^4}{8r_b^2}\right)\frac{d^2A}{dr_b^2} + \left(q_{B2} + \frac{r_b^2-1}{8r_b^2}\right)\frac{d^2B}{dr_b^2} \\ &+ \left(q_{A1} - \frac{1+r_b^4}{4r_b^3}\right)\frac{dA}{dr_b} + \left(q_{B1} + \frac{1}{4r_b^3}\right)\frac{dB}{dr_b}, \end{aligned} \tag{4.221}$$

see Eqs. (4.202)–(4.206), (4.216)–(4.218). After lengthy computations, we obtain the exact form of the functions $a_s(r_b)$, $b_s(r_b)$ and $c_s(r_b)$

$$a_s(r_b) = -\frac{8\left(Ca_{pm} - r_b^2 Ca\right)}{1 - 4r_b^2 + 3r_b^4 - 4r_b^4 \ln r_b} - Bo; \tag{4.222}$$

$$\begin{aligned} b_s(r_b) = &\frac{2}{3r_b\left(1-4r_b^2+3r_b^4-4r_b^4\ln r_b\right)^3} \\ &\times \Big\{ \left(3 - 4r_b^2 - 44r_b^4 + 88r_b^6 - 67r_b^8\right)\left(1-r_b^2\right)^2 \\ &+ 4r_b^4\left(3 - 49r_b^2 + 53r_b^4 - 31r_b^6\right)\left(1-r_b^2\right)\ln r_b \\ &- 96r_b^8\left(3 - 3r_b^2 + r_b^4\right)\ln^2 r_b \\ &+ 2(W-1)\cdot\Big[\left(3 + 4r_b^2 - 77r_b^4 + 82r_b^6\right)\left(1-r_b^2\right)^2 \\ &\quad + 4r_b^2\left(3 - 7r_b^2 - 79r_b^4 + 95r_b^6\right)\left(1-r_b^2\right)\ln r_b \\ &\quad - 24r_b^6\left(3 + 18r_b^2 - 23r_b^4\right)\ln^2 r_b - 288r_b^{10}\ln^3 r_b\Big]\Big\}; \end{aligned} \tag{4.223}$$

$$\begin{aligned} c_s(r_b) = &\frac{2}{3r_b^2\left(1-4r_b^2+3r_b^4-4r_b^4\ln r_b\right)^4} \\ &\times \Big\{ \left(-3 + 53r_b^2 - 168r_b^4 - 4r_b^6 - 141r_b^8 + 407r_b^{10}\right)\left(1-r_b^2\right)^3 \\ &+ 8r_b^4\left(18 - 105r_b^2 - 70r_b^4 + 71r_b^6 + 98r_b^8\right)\left(1-r_b^2\right)^2\ln r_b \\ &+ 48r_b^8\left(-25 - 27r_b^2 + 3r_b^4 + 21r_b^6\right)\left(1-r_b^2\right)\ln^2 r_b \\ &+ 384r_b^{12}\left(-9 + 3r_b^2 + r_b^4\right)\ln^3 r_b \\ &- 2(W-1)\cdot\Big[\left(3 - 73r_b^2 + 235r_b^4 + 205r_b^6 - 490r_b^8\right)\left(1-r_b^2\right)^3 \\ &\quad - 12r_b^2\left(1 + 17r_b^2 - 134r_b^4 - 43r_b^6 + 187r_b^8\right)\left(1-r_b^2\right)^2\ln r_b \\ &\quad - 8r_b^6\left(15 - 451r_b^2 - 109r_b^4 + 533r_b^6\right)\left(1-r_b^2\right)\ln^2 r_b \\ &\quad + 576r_b^{10}\left(6 + r_b^2 - 6r_b^4\right)\ln^3 r_b - 1152r_b^{14}\ln^4 r_b\Big]\Big\}. \end{aligned} \tag{4.224}$$

As it should be, $a_s(r_c) = 0$ in the cylindrical part of the bubble shape, see Eq. (4.68). The derivative $a_s'(r_c)$ has the following form:

$$\begin{aligned} a_s'(r_c) &= \frac{16Ca\, r_c}{1 - 4r_c^2 + 3r_c^4 - 4r_c^4 \ln r_c} \\ &\quad + \frac{8\left(Ca_{pm} - r_c^2 Ca\right)\left(-8r_c - 8r_c^3 - 16r_c^3 \ln r_c\right)}{\left(1 - 4r_c^2 + 3r_c^4 - 4r_c^4 \ln r_c\right)^2} \\ &= \frac{8r_c\left[2Ca + Bo\left(1 - r_c^2 + 2r_c^2 \ln r_c\right)\right]}{1 - 4r_c^2 + 3r_c^4 - 4r_c^4 \ln r_c} \\ &= \frac{2\left[8Ca_{pm} + Bo\left(1 - r_c^4 + 4r_c^4 \ln r_c\right)\right]}{r_c\left(1 - 4r_c^2 + 3r_c^4 - 4r_c^4 \ln r_c\right)}. \end{aligned} \tag{4.225}$$

4.6.2 Initial conditions

In order to close the system (4.196)–(4.199), we shall add four initial conditions for the four unknowns in the system $r_b,\ z_b,\ \theta$ and p_s. The most natural choice for the initial point is the bubble apex. Thus, we could add the following initial conditions for the variables $r_b,\ z_b,\ \theta$:

$$r_b(0) = z_b(0) = \theta(0) = 0, \tag{4.226}$$

but the initial condition for p_s at the bubble apex is not clear. Because of that, we shall find appropriate initial conditions at the cylindrical part of the bubble. But before focusing on that, we shall investigate the system (4.196)–(4.199) in detail. First, it is obvious that Eq. (4.197) is not coupled with the rest of the system. This means that the system (4.196), (4.198), (4.199) could be solved and, then, the axial coordinate of bubble surface z_b could be found, using numerical integration of Eq. (4.197). Second, changing the initial conditions for z_b leads to translation of the bubble[5]. Thus, we set the initial condition for z_b to $z_b(s_{in}) = z_{in}$, where z_{in} does not depend on the values of the rest of the initial conditions.

In the next lines, we find appropriate initial conditions for the rest of the variables, i.e. r_b, θ, p_s. In order to do that, we write the system (4.196), (4.198), (4.199) in vector form:

$$\frac{d\mathbf{u}}{ds} = \mathcal{F}(\mathbf{u}) \tag{4.232}$$

where

$$\mathbf{u} = \left(r_b,\ \theta,\ p_s\right)^T, \tag{4.233}$$

$$\mathcal{F}(\mathbf{u}) = \left(\cos\theta,\ -Ca\, p_s - \frac{\sin\theta}{r_b},\ F\left(r_b, \theta, p_s, Bo, Ca_{pm}\right)\right)^T. \tag{4.234}$$

[5] Let us denote by $z_{b,k}$ the solution of the Cauchy problem:

$$\frac{dz_{b,k}}{ds} = \sin\theta, \tag{4.227}$$

$$z_{b,k}(s_{in}) = z_{k,0}, \tag{4.228}$$

where θ is a known function and $z_{k,0}$ are known constants. Then, one obtains

$$\frac{d}{ds}(z_{b,2} - z_{b,1}) = 0, \tag{4.229}$$

$$(z_{b,2} - z_{b,1})\big|_{s=s_{in}} = z_{2,0} - z_{1,0}. \tag{4.230}$$

The solution of the latter is

$$z_{b,2} - z_{b,1} = z_{2,0} - z_{1,0}. \tag{4.231}$$

Thus, changing the initial conditions in the problem leads to translation of the bubble.

In the latter, the transpose of $\mathbf{u}$ is denoted by $\mathbf{u}^T$ and the function F has the following form:

$$F = -\frac{a_s\left(r_b\right)}{Ca}\sin\theta + \frac{b_s\left(r_b\right)}{\sin^2\theta}\left(Ca\,p_s + \frac{\sin\theta}{r_b}\right) + c_s\left(r_b\right)\frac{\cos^2\theta}{\sin\theta}, \tag{4.235}$$

see Eqs. (4.200) and (4.198). It is obvious that the considered system of equations (4.232) has a constant solution

$$\mathbf{u}_0 = \left(r_c,\ \frac{\pi}{2},\ -\frac{1}{Ca\,r_c}\right)^T \tag{4.236}$$

at the cylindrical part of the bubble ($\mathcal{F}(\mathbf{u}_0) = \mathbf{0}$). Then, the expressions for initial conditions at the cylindrical part of the bubble are derived, considering small perturbations $\mathbf{u}_1 = \left(r_{b,1},\ \theta_1,\ p_{s,1}\right)^T$ around the cylindrical shape, i.e.:

$$\mathbf{u} = \mathbf{u}_0 + \mathbf{u}_1. \tag{4.237}$$

Let us fix the initial condition for $r_{b,1}$, i.e.

$$r_{b,1}(s_{in}) = -\delta, \tag{4.238}$$

where $0 < \delta << 1$. In the next lines, we shall derive appropriate expressions for the other conditions in terms of δ. In order to do that, the system (4.232) is linearized around the exact solution $\mathbf{u}_0$, i.e.

$$\frac{d\mathbf{u}_1}{ds} = \mathcal{F}(\mathbf{u}_0) + \nabla\mathcal{F}(\mathbf{u}_0)\mathbf{u}_1 = \nabla\mathcal{F}(\mathbf{u}_0)\mathbf{u}_1, \tag{4.239}$$

where ∇ is the gradient operator and it has the following explicit form:

$$\nabla\mathcal{F}(\mathbf{u}_0) = \begin{pmatrix} 0 & -1 & 0 \\ \frac{1}{r_c^2} & 0 & -Ca \\ -\frac{a_s'(r_c)}{Ca} - \frac{b_s(r_c)}{r_c^2} & 0 & Ca\,b_s(r_c) \end{pmatrix}. \tag{4.240}$$

Thus, the linear form of the studied system of equations (4.196), (4.198), (4.199) reads

$$\frac{dr_{b,1}}{ds} = -\theta_1, \tag{4.241}$$

$$\frac{d\theta_1}{ds} = \frac{r_{b,1}}{r_c^2} - Ca\,p_{s,1}, \tag{4.242}$$

$$\frac{dp_{s,1}}{ds} = -\frac{a_s'(r_c)}{Ca}r_{b,1} - b_s(r_c)\frac{d\theta_1}{ds}. \tag{4.243}$$

Let us recall, that our aim is to find appropriate initial conditions at the cylindrical part of the bubble. At it, the bubble shape is described well by the the zero-order approximation and, thus, it is unnecessary to use the correction terms in the linearized system (see Section 4.5). Then, we can neglect $b_s(r_c)$, which comes from the second-order correction term, see Eqs. (4.192) and (4.219). Therefore, we obtain the following system:

$$\frac{dr_{b,1}}{ds} = -\theta_1, \tag{4.244}$$

$$\frac{d\theta_1}{ds} = \frac{r_{b,1}}{r_c^2} - Ca\,p_{s,1}, \tag{4.245}$$

$$\frac{dp_{s,1}}{ds} = -\frac{a_s'(r_c)}{Ca}r_{b,1} \tag{4.246}$$

Expressing θ_1 from Eq. (4.244) and substituting it in Eq. (4.245), we obtain

$$p_{s,1} = \frac{1}{Ca}\left(\frac{r_{b,1}}{r_c^2} + \frac{d^2 r_{b,1}}{ds^2}\right). \tag{4.247}$$

Using Eqs. (4.246), (4.247), one gets

$$\frac{1}{Ca}\left(\frac{1}{r_c^2}\frac{dr_{b,1}}{ds} + \frac{d^3 r_{b,1}}{ds^3}\right) = -\frac{a_s'(r_c)}{Ca} r_{b,1}, \tag{4.248}$$

$$r_c^3 \frac{d^3 r_{b,1}}{ds^3} + r_c \frac{dr_{b,1}}{ds} + a r_{b,1} = 0, \tag{4.249}$$

where a is computed as follows:

$$a = r_c^3 a_s'(r_c) = \frac{2r_c^2\left[8Ca_{pm} + Bo\left(1 - r_c^4 + 4r_c^4 \ln r_c\right)\right]}{1 - 4r_c^2 + 3r_c^4 - 4r_c^4 \ln r_c} \tag{4.250}$$

for free surfaces and

$$a = \frac{r_c^2\left(1 - r_c^2 + 2r_c^2 \ln r_c\right)\left[8Ca_{pm} + Bo\left(1 - r_c^2\right)^2\right]}{\left(1 - r_c^2\right)^2\left[r_c^2 - 1 - (1 + r_c^2)\ln r_c\right]} \tag{4.251}$$

for tangentially immobile surfaces, see Eqs. (4.214) and (4.225). Eq. (4.249) is a third-order homogeneous differential equation and it has an exact solution. In order to find it, we compute its characteristic polynomial equation

$$(\lambda r_c)^3 + \lambda r_c + a = 0, \tag{4.252}$$

Due to the fact that the polynomial in Eq. (4.252) is increasing in $(-\infty, +\infty)$, the cubic equation has three solutions — one real λ_1 and two conjugate complex numbers $\lambda_2, \lambda_3 = a_2 \pm i a_3$. The real root could be calculated, using the formula

$$\lambda_1 r_c = \left[\left(\frac{a^2}{4} + \frac{1}{27}\right)^{1/2} - \frac{a}{2}\right]^{1/3} - \left[\left(\frac{a^2}{4} + \frac{1}{27}\right)^{1/2} + \frac{a}{2}\right]^{1/3}. \tag{4.253}$$

Then, the general solution of Eq. (4.249) has the form

$$r_{b,1}(s) = C_{i,1} e^{\lambda_1 s} + C_{i,2} e^{a_2 s}\cos(a_3 s) + C_{i,3} e^{a_2 s}\sin(a_3 s), \tag{4.254}$$

where $C_{i,1}$, $C_{i,2}$ and $C_{i,3}$ are unknown constants. There are two general cases for the solution, depending on the signs of λ_1 and a_2. If $a < 0$, then Eq. (4.252) has one positive real root and two conjugate complex roots with negative real part[6]. We are looking for small perturbations of the solutions at the cylindrical part of the bubble, then $C_{i,1} = 0$ (Otherwise, $\lim_{s\to-\infty} r_{b,1}(s) = -\infty$). Then, the obtained solution is a non-physical one —

[6]Using Vieta's formulae, we obtain

$$\lambda_1 + \lambda_2 + \lambda_3 = \lambda_1 + 2a_2 = 0, \tag{4.255}$$

$$\lambda_1\lambda_2\lambda_3 = \lambda_1\left(a_2^2 + a_3^2\right) = -\frac{a}{r_c^3}. \tag{4.256}$$

If $a < 0$, then it follows from Eq. (4.256) that $\lambda_1 > 0$ ($0 < r_c < 1$). Using Eq. (4.255), we conclude $a_2 < 0$.

the capillary surface is periodic with an increasing amplitude for $s < s_{in}$. If $a > 0$, then Eq. (4.252) has one negative real root and two conjugate complex roots with positive real part. Due to the fact that we are looking for small perturbations of the solution, we conclude that $C_{i,2} = C_{i,3} = 0$ and the solution has the form

$$r_{b,1}(s) = C_{i,1} e^{\lambda_1 s}. \tag{4.257}$$

Using (4.238), we obtain

$$r_{b,1}(s) = -\delta\, e^{\lambda_1 (s - s_{in})}. \tag{4.258}$$

Substituting the latter in Eqs. (4.244) and (4.247), one gets

$$\theta_1 = -\frac{d}{ds}\left[-\delta e^{-\lambda_1 (s_{in} - s)}\right] = \lambda \delta e^{-\lambda_1 (s_{in} - s)}, \tag{4.259}$$

$$p_{s,1} = \frac{1}{Ca}\left[\frac{-\delta e^{-\lambda_1 (s_{in} - s)}}{r_c^2} - \lambda_1^2 \delta e^{-\lambda_1 (s_{in} - s)}\right]. \tag{4.260}$$

Thus, the initial conditions for the boundary value problem in the case of long bubbles acquire the form

$$r_b(s_{in}) = r_c - \delta,\ z_b(s_{in}) = z_{in}, \tag{4.261}$$

$$\theta(s_{in}) = \frac{\pi}{2} + \lambda\delta,\ p_s(s_{in}) = -\frac{1}{Ca\, r_c} - \left(\lambda^2 + \frac{1}{r_c^2}\right)\frac{\delta}{Ca}, \tag{4.262}$$

where $\lambda := \lambda_1$ is the negative root of equation (4.252) and it is computed via the formula (4.253), see Eqs. (4.237), (4.238), (4.259), (4.260).

4.6.3 Regions of validity of parameters

As we derive in the previous section, long bubbles appear only if $a > 0$. In the next lines, we shall find constraints for the ratio $\frac{Ca_{pm}}{Bo}$ in order long bubbles to appear.

Free surfaces

The expression for a in the case of free surfaces is given in Eq. (4.250). From the condition $a > 0$, we conclude that

$$8Ca_{pm} + Bo\left(1 - 4r_c^4 + 4r_c^4 \ln r_c\right) > 0 \text{ for } r_c \in (0, 1), \tag{4.263}$$

see Eqs. (4.78), (4.250). Moreover, if $a = 0$, it follows

$$\frac{Ca_{pm}}{Bo} = -\frac{1 - 4r_c^4 + 4r_c^4 \ln r_c}{8} \text{ for } Bo \neq 0. \tag{4.264}$$

For $Bo > 0$, the condition $a > 0$ is equivalent to

$$\frac{Ca_{pm}}{Bo} > -\frac{1 - 4r_c^4 + 4r_c^4 \ln r_c}{8} \tag{4.265}$$

and for $Bo > 0$ — to

$$\frac{Ca_{pm}}{Bo} < -\frac{1 - 4r_c^4 + 4r_c^4 \ln r_c}{8}. \tag{4.266}$$

Taking into account the conditions (4.73)–(4.74) and the following inequality:

$$-\frac{1-4r_c^4+4r_c^4\ln r_c}{8} < -\frac{1-4r_c^2+3r_c^4-4r_c^4\ln r_c}{8} \text{ for } r_c \in (0,1) \tag{4.267}$$

one obtains the regions of possible solutions of the considered problem in the case of free surfaces, see Fig. 4.8. If a long bubble appears and gravity acts along the z-axis ($Bo > 0$), then the point with coordinates h and Ca_{pm}/Bo lies above the curve (4.71), which corresponds to a bubble at rest (see Figs. 4.6 and 4.8). In the case that gravity acts against the z-axis ($Bo < 0$), a long bubbles appear only if the point $(h, Ca_{pm}/Bo)$ is under the curve (4.264) (see Fig. 4.8). For values of the parameters, which correspond to points, lying between the curves (4.71) and (4.264), there is no solution of the problem.

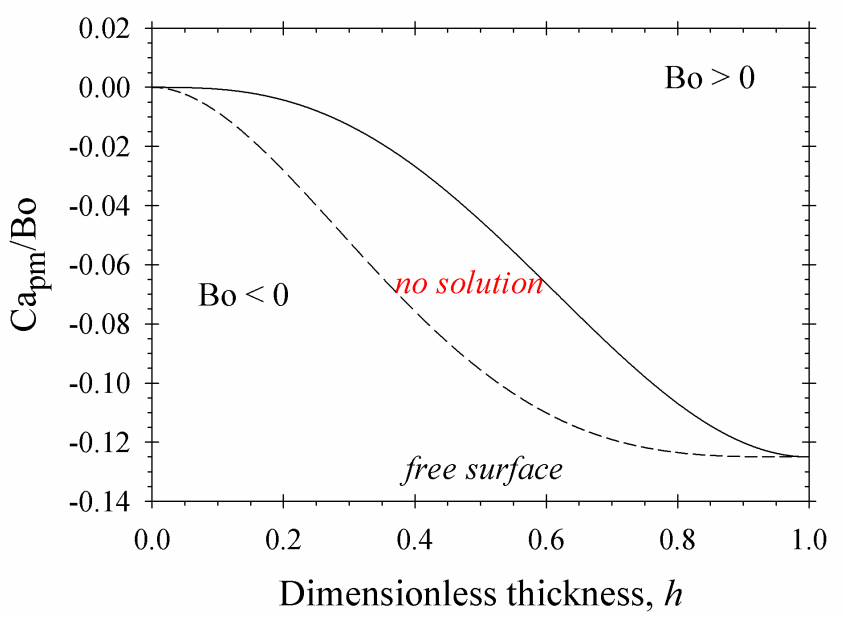

Figure 4.8: Regions of physical parameters for possible elongated bubble profiles for $g_z > 0$ ($Bo > 0$) and $g_z < 0$ ($Bo < 0$) as functions of Ca_{pm} and dimensionless wetting film thickness h in the case of free surfaces. Solid lines correspond to $Ca = 0$ and dashed lines to $a = 0$.

Immobile surfaces

The expression for a in the case of tangentially immobile surfaces is given in Eq. (4.251). The condition $a > 0$ is equivalent to the following inequality:

$$8Ca_{pm} + Bo\left(1-r_c^2\right)^2 > 0, \tag{4.268}$$

see Eq. (4.78). The curve

$$\frac{Ca_{pm}}{Bo} = -\frac{\left(1-r_c^2\right)^2}{8} \tag{4.269}$$

corresponds to $a = 0$. Taking into account conditions (4.83)–(4.84) and the following inequality:

$$-\frac{\left(1-r_c^2\right)^2}{8} < -\frac{1}{8}\left[1 - r_c^4 + \frac{\left(1-r_c^2\right)^2}{\ln r_c}\right] \quad \text{for } 0 < r_c < 1, \tag{4.270}$$

one obtains the regions of the possible solutions (see Fig. 4.9). If the gravity acts along the z-axis ($Bo > 0$), then a long bubble appears only if the point $(h, Ca_{pm}/Bo)$ lies above the curve (4.82), which corresponds to $Ca = 0$. For $Bo < 0$, the existence of the long bubble for particular values of h and Ca_{pm}/Bo is verified if and only if the point $(h, Ca_{pm}/Bo)$ lies under the curve (4.269).

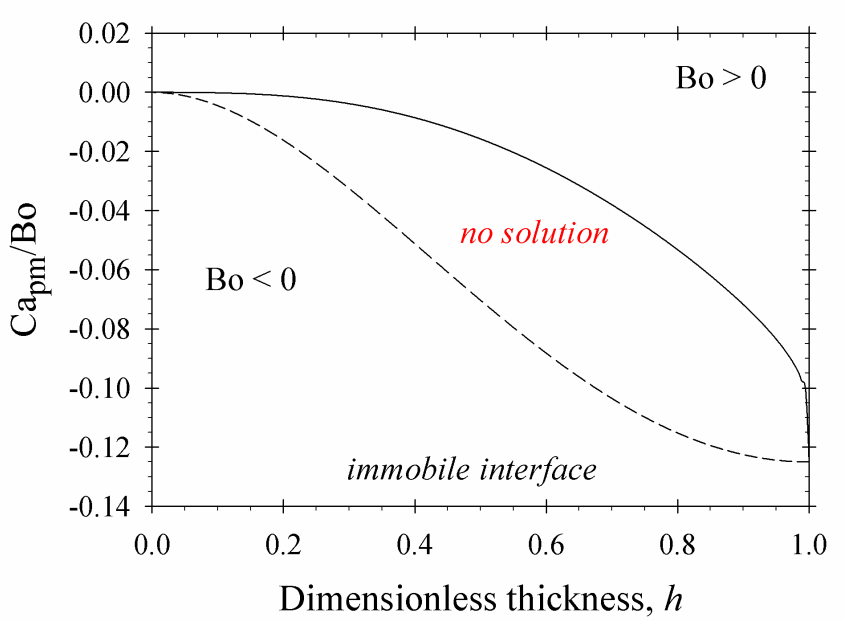

Figure 4.9: Regions of physical parameters for possible elongated bubble profiles for $g_z > 0$ ($Bo > 0$) and $g_z < 0$ ($Bo < 0$) as functions of Ca_{pm} and dimensionless wetting film thickness h in the case of tangentially immobile surfaces. Solid lines correspond to $Ca = 0$ and dashed lines to $a = 0$.

4.6.4 Algorithm for finding the bubble shape

Generally speaking, the system (4.196)–(4.199) models the form of a drop for a given pressure distribution along the bubble surface. The solutions depend on the initial conditions and describe different types of possible capillary profiles: open capillary curves, curves with loops, etc. We are not interested in all solutions of this problem but in that, which corresponds to a closed bubble profile and, therefore, satisfies the natural boundary conditions at the bubble apex, see Eq. (4.226). Indeed, if one defines a tentative value of h, then the radial coordinate is $r_c = 1 - h$ and the capillary number is calculated as $Ca = Ca\,(Bo, Ca_{pm}, r_c)$ from Eqs. (4.68) or (4.81). Hence, for given physical parameters Bo and Ca_{pm}, the system of equations (4.196)–(4.199) with the initial conditions, given by Eq. (4.261) and (4.262),

has a numerical solution, which corresponds to an elongated bubble only for one thickness of the fluid layer in the cylindrical part, h.

Before focusing on finding the dimensionless thickness of the liquid film, h, we shall describe briefly how to solve the considered problem for fixed value of h. First, it can be noticed easily that there is a singularity in the third and the forth equations, (4.198) and (4.199), for $s = 0$. The singularity in the third equation is removed easily due to the following computations:

$$\begin{aligned}\left.\frac{d\theta}{ds}\right|_{s=0} &= -Cap_s(0) - \lim_{s\to 0}\frac{\sin\theta}{r_b} \\ &= -Cap_s(0) - \lim_{s\to 0}\frac{\cos\theta\frac{d\theta}{ds}}{\frac{dr_b}{ds}} = -Cap_s(0) - \left.\frac{d\theta}{ds}\right|_{s=0}. \end{aligned} \tag{4.271}$$

From the latter, it follows that

$$\left.\frac{d\theta}{ds}\right|_{s=0} = -\frac{Cap_s(0)}{2}. \tag{4.272}$$

The singularity at the right hand side in the fourth equation in not removable due to the fact

$$\lim_{r_b\to 0} F(r_b, \theta, p_s, Bo, Ca_{pm}) = +\infty. \tag{4.273}$$

This result comes from the inaccuracy of the approximation and is not physical phenomena. Due to this fact, we write the function F as follows:

$$F = -\frac{a_s(r_b)}{Ca}\sin\theta - \frac{b_s(r_b)}{\sin^3\theta}\sin\theta\frac{d\theta}{ds} + \frac{c_s(r_b)\cos^2\theta}{\sin^2\theta}\sin\theta, \tag{4.274}$$

see Eq. (4.207). In the latter, we shall set $\sin\theta = 1$ in the denominators, i.e.

$$F_1 = -\frac{a_s(r_b)}{Ca}\sin\theta - b_s(r_b)\sin\theta\frac{d\theta}{ds} + c_s(r_b)\cos^2\theta\sin\theta. \tag{4.275}$$

This approximation, obviously, holds in the cylindrical part of the bubble. Moreover, the closer we get to the apex of the bubble, the capillary pressure becomes more pronounced and inaccuracies in solving the hydrodynamic problem effect the solution weakly. Due to this fact, the approximation F_1 is appropriate to use for arbitrary value of θ.

The algorithm for solving the considered problem for fixed value of h in the case of free surfaces is briefly described in Alg. 3. The main idea of algorithm is pretty straightforward. We compute the radius of the cylindrical part of the bubble r_c, the capillary number Ca and the parameter a. By using this information, one finds the only negative root of the polynomial (4.252) and use it to find the initial conditions. Finally, we solve the considered problem, using the tenth-order Runge-Kutta method with fixed step.

The results from running this procedure for $Bo = 2$ and $Ca_{pm} = 0$ and for $Bo = 0$ and $Ca_{pm} = 0.5$ in the case of free surfaces are illustrated in Fig. 4.10. For $Bo = 2$ and $Ca_{pm} = 0$, the capillary curve has a loop for $h = 0.1$, the calculated profile is open for $h = 0.2$, and only for $h = 0.1617$, one obtains the real bubble shape (Fig. 4.10a). In the second case, for $h = 0.26$ and $h = 0.29$, the capillary profiles are open and the physical solution is obtained for $h = 0.2752$ (Fig. 4.10b). For all combinations of Bo and Ca_{pm} (see Sec. 4.7), the behavior of capillary profiles is similar to this, illustrated in Fig. 4.7.

Algorithm 3 Compute the bubble profile in the case of free surfaces for fixed h

procedure ComputeBubbleProfile(Bo, Ca_{pm}, h)
  $r_c \leftarrow 1 - h$;
  $Ca \leftarrow Ca(Bo, Ca_{pm}, r_c)$; ▷ Eq. (4.68)
  $W \leftarrow 1 - Ca_{pm}/Ca$;
  $a = a(Bo, Ca_{pm}, r_c)$; ▷ Eq. (4.250)
  $\lambda_1 = \lambda_1(a)$; ▷ Eq. (4.253)
  $\delta \leftarrow 0.00001$;
  $initialConditions \leftarrow initialConditions(Ca, r_c, \delta, \lambda_1)$; ▷ Eqs. (4.261), (4.262)
  $step \leftarrow -0.0001$;

  procedure RHS(r_b, z_b, θ, p_s)
    if $r_b \geq 0.001$ **then**
      return $\left\{\cos\theta, \sin\theta, -Cap_s - \dfrac{\sin\theta}{r_b}, F_1(r_b, \theta, p_s, Ca, Ca_{pm}, W)\right\}$; ▷ (4.275)
    else
      return $\left\{\cos\theta, \sin\theta, -\dfrac{Cap_s}{2}, 0\right\}$ ▷ (4.273) ;
    end if;
  end procedure;

  $RungeKutta17(step, RHS, initialConditions)$;
end procedure;

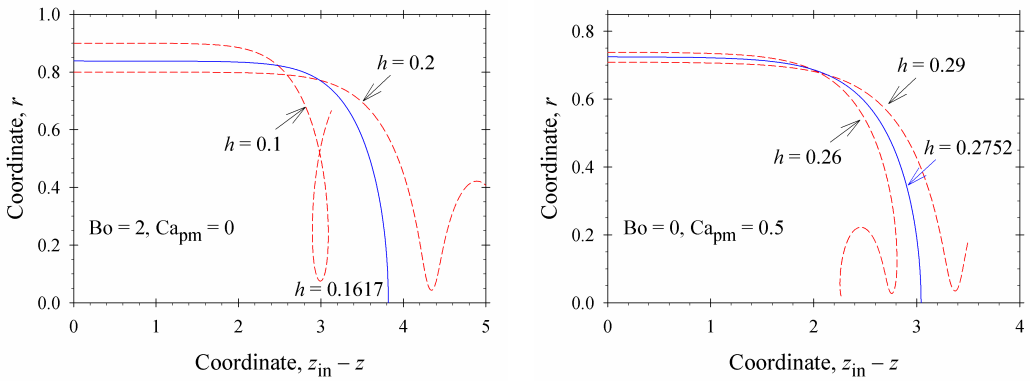

(a) $Bo = 2$, $Ca_{pm} = 0$. (b) $Bo = 0$, $Ca_{pm} = 0.5$.

Figure 4.10: Calculated capillary profiles for three different values of the dimensionless layer thickness, h, in the case of free bubble surfaces.

Next, we shall focus our attention on finding the unique value of h, for which the profile closes (for given values of Bo and Ca_{pm}). In order to do that, first, we shall state the criteria for stopping the Runge–Kutta method in the case that the profile does not close for the current value of h. We use the following stopping criteria:

- $r_{b,next} > r_{b,current}$;

- $z_{b,next} > z_{b,current}$;
- $\theta_{next} > \theta_{current}$,

where the suffix "next" denotes the next computed approximation and the suffix "current" — the current one. Using these criteria, we obtain a sequence of bubble profiles for different values of h. The next step is to investigate how far from closing are these profiles. In order to do that, we introduce a new function $ComputeDist(Bo, Ca_{pm}, h)$, which computes the distance between the end of the profile and the abscissa for given values of Bo, Ca_{pm} and h. Having all this in mind, we are ready to present an algorithm for finding the dimensionless thickness h (see Alg. 4). The main idea of the algorithm is to start with initial guess for h. Then, we obtain the distance from the end of the bubble profile to the abscissa, using the function $ComputeDist$, for the bubble profiles, which have dimensionless thicknesses h, $h(1 - precision)$ and $h(1 + precision)$. Comparing the obtained results, the next value of h is chosen to be that one, for which the distance between the end of profile and the abscissa is the smallest. The algorithm continues, while we cannot find "better" value for h. Then, the precision is set higher. In the current implementation (see Alg.4), the value of h is computed with precision of 0.001%.

Values of the dimensionless thickness h for the closed profiles, depicted in Fig. 4.10, are computed, using Alg. 4.

Algorithm 4 Compute the value of the dimensionless thickness h

```
1:  procedure FindFilmThickness(Bo, Ca_pm)
2:      h ← 0.33;
3:      precision ← 0.1;
4:
5:      for i ← 1 to 5 do
6:          lastRb ← ComputeDist(Bo, Ca_pm, h);
7:          lastRbL ← ComputeDist(Bo, Ca_pm, h(1 − precision));
8:          lastRbU ← ComputeDist(Bo, Ca_pm, h(1 + precision));
9:
10:         while min(lastRb, lastRbL, lastRbU) ≠ lastRb do
11:             if min(lastRbL, lastRbU) == lastRbL then
12:                 h ← h(1 − precision);
13:             else
14:                 h ← h(1 + precision);
15:             end if
16:
17:             lastRb ← min(lastRbL, lastRbU);
18:             lastRbL ← ComputeDist(Bo, Ca_pm, h(1 − precision));
19:             lastRbU ← ComputeDist(Bo, Ca_pm, h(1 + precision));
20:         end while
21:
22:         precision ← precision/10;
23:     end for
24: end procedure
```

4.7 Numerical results

For fixed physical parameters in the regions of possible solutions (Figs. 4.8 and 4.9), the system of equations (4.196), (4.197), (4.198) and (4.199) with initial conditions (4.261) and (4.262) is solved numerically, using the explicit tenth-order Runge-Kutta method [4.88]. In all numerical calculations, the values of the amplitude δ in Eqs. (4.261) and (4.262) is 10^{-5} and the numerical step in the arc length of the bubble surface is 10^{-4}. For given parameters Bo and Ca_{pm}, the dimensionless thickness, h, is varied to obtain the physical bubble shape, see Fig. 4.10.

4.7.1 Comparison with experimental data

Fig. 4.11 shows experimental data [4.24] (symbols) for the capillary numbers and dimensionless layer thicknesses of long rising bubbles in capillaries as functions of the Bond numbers. The authors used pure substances to ensure a constant value of the surface tension. The calculations for free surfaces (solid blue lines) describe the experimental data for all studied values of the Bond number ($Bo \leq 7.5$) excellently. The Bretherton asymptotic formulae (dashed lines in Fig. 4.11) give good results for low values of capillary number, $Ca < 3.2 \times 10^{-4}$. Using our approach, the validity of theoretical calculations is experimentally confirmed for $Ca < 0.3$.

The comparisons between the capillary numbers and dimensionless layer thicknesses, calculated for tangentially immobile or free interfaces, are shown in Fig. 4.11. It is well illustrated that the bubble translational velocity decreases and the film thickness, h, increases in the presence of surface-active substances, which generally lead to immobilization of interfaces.

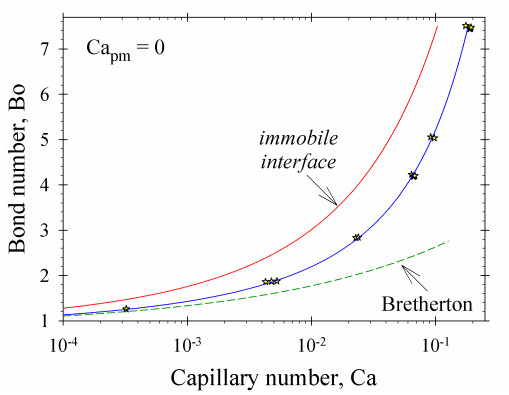

(a) The Bond number, Bo, vs the capillary number, Ca.

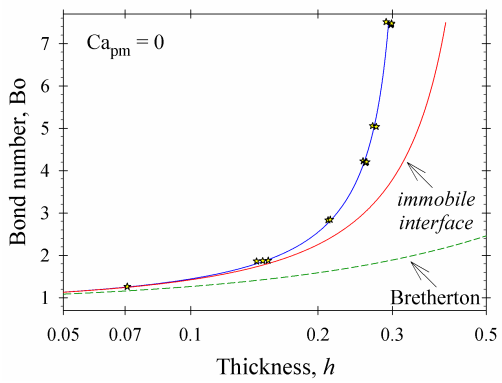

(b) The Bond number, Bo vs dimensionless layer thickness, h.

Figure 4.11: Comparison between experimental data for rising bubble [4.24] (symbols) and the theoretical calculations.

In the case of motion of long bubbles under the action only of the Poiseuille flow ($Bo = 0$), the comparison between experimental data and numerical calculations are shown in Fig. 4.12. The original Bretherton asymptotic solution [4.1] (dashed lines) describes experimental data with accuracy of 10% for low values of the capillary numbers $Ca < 5 \times 10^{-3}$. The extended

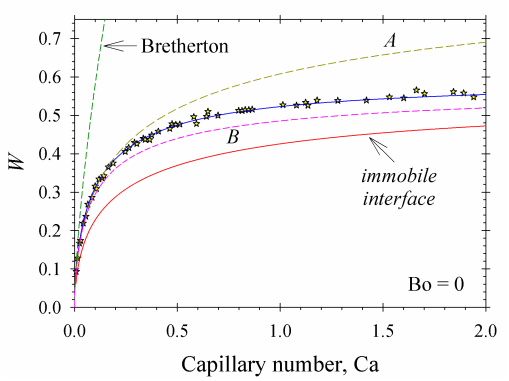

(a) The relative increase of the velocity, W, vs the capillary number, Ca, [4.36], [4.39].

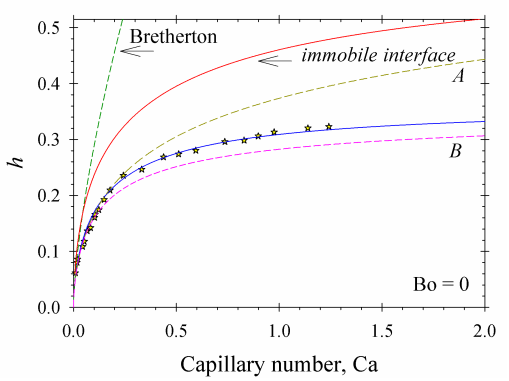

(b) The film thickness, h, vs the capillary number, Ca, [4.39].

Figure 4.12: Comparison between experimental data [4.36], [4.39] (symbols) for Taylor bubbles and the theoretical calculations. Solid line — generalized lubrication approximation; A-line — model, based on the zero-order lubrication approximation [4.80]; B-line — extended Bretherton model [4.58].

Bretherton model [4.58] (B line) gives acceptable results for $Ca < 0.1$ — the predicted parameter W and dimensionless film thickness h are systematically lower than experimental ones for larger values of the capillary number. The model, based on the zero-order lubrication approximation [4.80] (A line), describes well the experimental data for $Ca < 0.2$ but the calculated values of W and h considerably increase for the case where $Ca > 0.2$. The use of the generalized lubrication approximation, which accounts also for the first-order lubrication approximation, leads to an excellent description of experimental data for $Ca < 2.0$, see the blue solid lines in Fig. 4.12 for free surfaces.

The numerical calculations and experimental observations show that there is no pronounced difference between soluble and insoluble surfactants with respect to the film thickness, h, for $Ca < 2.0$ — the calculated and measured values of h are systematically larger than those, corresponding to bubbles in pure liquids [4.72]. These results correlate with the calculated dependencies $W(Ca)$ and $h(Ca)$ in the case of tangentially immobile interfaces (see Fig. 4.12). For fixed mean velocity V_{pm} of the Poiseuille flow (fixed values of Ca_{pm}), the enlarged viscous friction with tangentially immobile interfaces leads to the translation bubble velocity, V_b, closer to V_{pm} and respectively, to lower values of W (Fig. 4.12a). The increased viscous friction gives rise to the dynamic pressure in the liquid film and the translational bubble motion takes place for thicker cylindrical parts of the liquid films, h (Fig. 4.12b).

Fig. 4.13 shows the effect of the mean velocity of the Poiseuille flow, V_{pm}, on the increasing velocity of long bubbles, V_b, for a fixed Bond number, $Bo = 4.6$. The experimental data [4.83] (symbols) are close to the theoretical calculations for bubbles with free surfaces. The calculated dependence V_b/V_{pm} on Ca_{pm} for tangentially immobile interfaces predicts lower values of the relative velocity. At small Ca_{pm}, there is a large effect of interfacial rheology (free vs tangentially immobile interfaces) on the relative translational velocity of bubbles. The small deviations of the experimental data from the calculated theoretical line in the case of bubbles with free surfaces are likely due to trace amounts of surface-active contaminations in the working fluid [4.83].

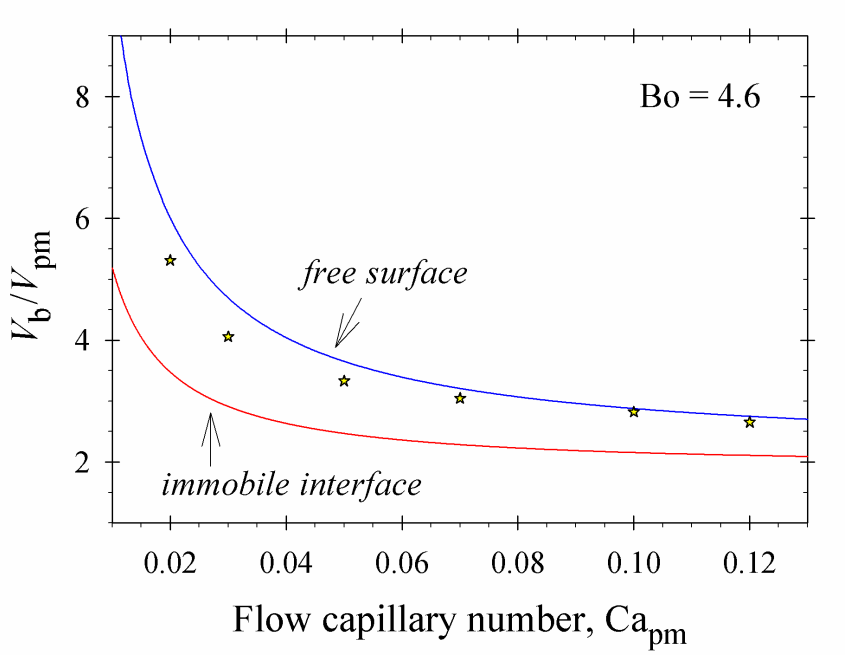

Figure 4.13: Comparison between experimental data [4.83] (symbols) for relative velocity $V_b/V_{pm} > 0$ vs Ca_{pm} of long bubbles for fixed Bond number, $Bo = 4.6$, with the theoretical calculation for fully mobile and immobile interfaces.

4.7.2 Simultaneous action of the Poiseuille flow and gravity

In the literature, there are no systematic experimental data for the long bubble motion under simultaneous action of the Poiseuille flow and gravity (like those illustrated in Fig. 4.13). Figs. 4.8 and 4.9 show that one distinguishes two general cases. The first one corresponds to $Bo > 0$, when the Poiseuille flow with $Ca_{pm} > 0$ accelerates and that with $Ca_{pm} < 0$ decelerates the bubble motion. The experimental data in Fig. 4.13 correspond to $Bo > 0$ and $Ca_{pm} > 0$. Fig. 4.14 summarizes the numerical results for the effect of the Poiseuille flow on the bubble translational velocity and respective thickness of cylindrical film layer for positive values of the Bond number and different models for surfaces (fully mobile and tangentially immobile).

Fig. 4.11 illustrates that for $Ca_{pm} = 0$, the gravity should be sufficiently high to ensure $Bo > 0.842$ in order to have a motion of long bubbles. Figs. 4.14a and 4.14c show that the threshold value of Bo increases with the increase of the absolute value of Ca_{pm} for $Ca_{pm} < 0$. Moreover for tangentially immobile interfaces, these values of Bo are considerably greater. If the both forces act in one direction ($Ca_{pm} > 0$), then the bubble moves and $Ca > 0$ even for $Bo = 0$ (see Fig. 4.12). With the increase of gravity effect (Bo number), the calculated curves for a given Ca_{pm} become closer to that, corresponding to $Ca_{pm} = 0$ and the effect of Poiseuille flow becomes less pronounced.

The greater values of the threshold Bond number for $Ca_{pm} < 0$ are interrelated with the increase of the thicknesses of wetting films in cylindrical parts (Figs. 4.14b and 4.14d). Oppositely for $Ca_{pm} > 0$, very thin cylindrical liquid layers can be realized. As it can

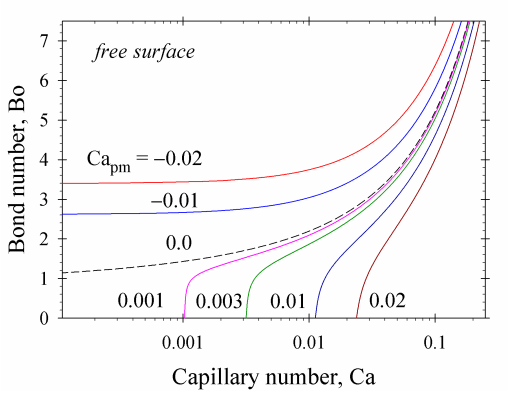

(a) The Bond number, Bo, vs the capillary number, Ca, for free surfaces.

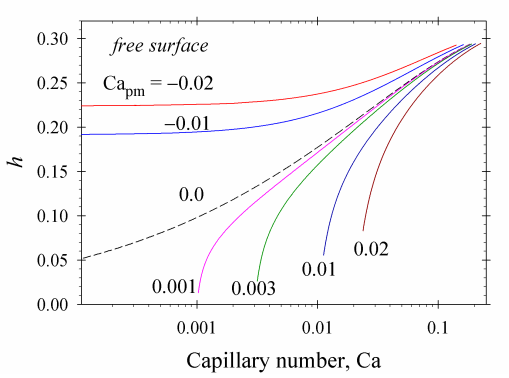

(b) The film thickness, h, vs the capillary number, Ca, for free surfaces.

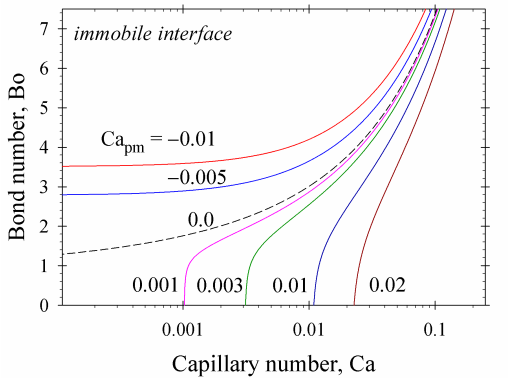

(c) The Bond number, Bo, vs the capillary number, Ca, for tangentially immobile interfaces.

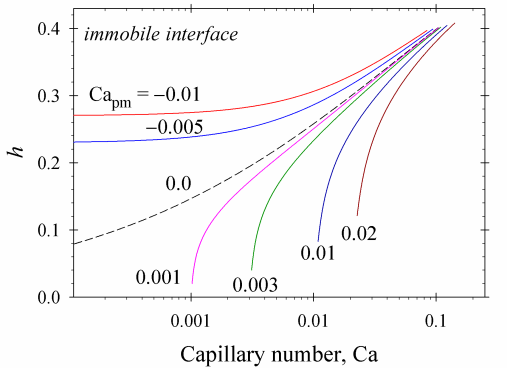

(d) The film thickness, h, vs the capillary number, Ca, for tangentially immobile interfaces.

Figure 4.14: Effect of the Poiseuille flow on the bubble translational velocity and respective thickness of cylindrical film layer.

be expected, the films for tangentially immobile interfaces are thicker than those for fully mobile surfaces.

The second general case is when the gravity decelerates the bubble motion ($Bo < 0$ and $Ca_{pm} > 0$, see Figs. 4.8 and 4.9). The numerical results for the dependence of Ca_{pm} and h on the capillary number, Ca, for both types of bubble interfaces are summarized in Fig. 4.15 for a wide range of Bond numbers, $Bo < 0$. It is well illustrated that with the increase of the magnitudes of Bond number, $|Bo|$, in order to have the same translational velocities of bubbles (for given values of Ca), one need to apply more intensive Poiseuille flows (Figs. 4.15a and 4.15c). Nevertheless, the effect of gravity is relatively weak. For example, the decrease of Bo from 0 to -45 for $Ca = 1$ increases Ca_{pm}: 1.62 times for free surfaces; 1.50 times for immobile interfaces. The values of Ca_{pm}, needed to ensure a given capillary number, are greater for bubbles with tangentially immobile interfaces.

The calculated respective thicknesses h are given in Figs. 4.15b and 4.15d. The increase of the magnitudes of Bond number, $|Bo|$, leads to the decrease of the thicknesses of the

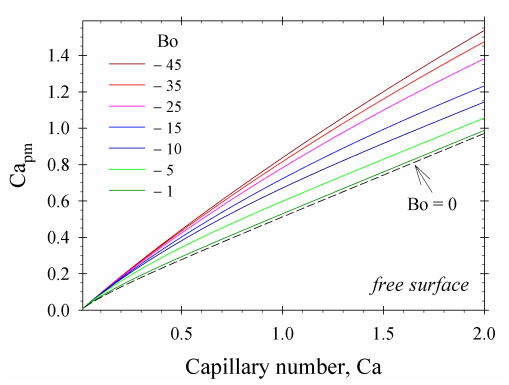

(a) The capillary number, Ca_{pm}, vs the capillary number, Ca, for free surface model.

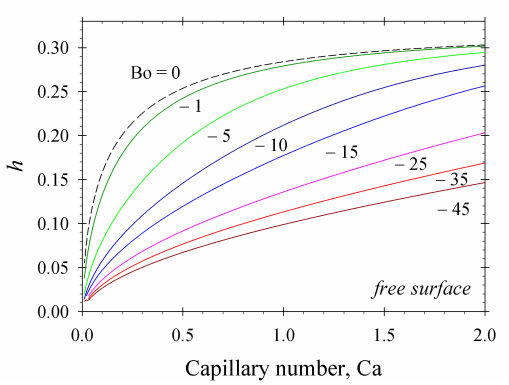

(b) The dimensionless film thickness, h, vs the capillary number, Ca, for free surface model.

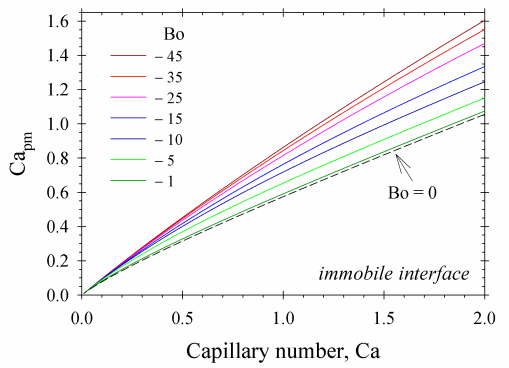

(c) The capillary number, Ca_{pm}, vs the capillary number, Ca, for tangentially immobile surfaces.

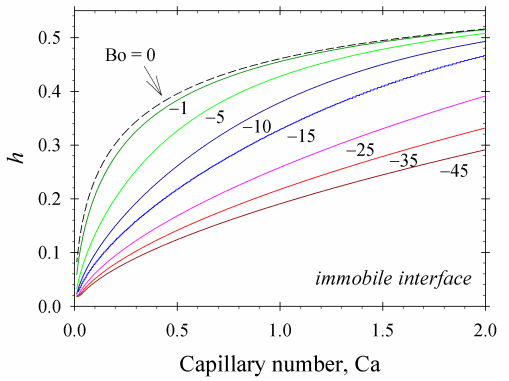

(d) The film thickness, h, vs the capillary number, Ca, for tangentially immobile surfaces.

Figure 4.15: Effect of gravity on the bubble translational velocity and on the thickness of cylindrical film layer, h, in the presence of Poiseuille flow.

wetting cylindrical films. Note that the effect of Bo on h is more pronounced. Indeed, the decrease of Bo from 0 to -45 for $Ca = 1$ decreases h: from 0.284 to 0.0988, that is 2.88 times for free surfaces; from 0.461 to 0.1914, that is 2.41 times for immobile interfaces. The bubbles with tangentially immobile interfaces move with the same translational velocity as those with free surfaces under the action of more intensive Poiseuille flows and with thicker wetting films in their cylindrical parts.

4.8 Conclusion

Most of the research reported numerically or experimentally the motion of drops and bubbles through capillaries in the pressure-driven flow or under the action of gravity separately. The interplay of the two effects is not described systematically [4.82, 4.83]. In addition, the physicochemical properties of liquids and interfaces have been restricted to the Marangoni

effect and bulk diffusivity of soluble and insoluble surfactants, even though small changes in parameters, such as Gibbs elasticity, surface diffusivity and viscosity can change considerably the translational velocity of drops and bubbles. The validity of the asymptotic Bretherton expressions [4.1] has been extended for capillary numbers up to 0.2 in the case of pressure-driven flows [4.39, 4.58]. The various physicochemical properties of investigated systems need a simple and transparent approach for modeling the bubble motion, which is valid for moderate capillary and Bond numbers, and can be generalized by introducing complex interfacial rheology and intermolecular forces.

We studied the motion of long axisymmetric bubbles with free and tangentially immobile interfaces through capillaries, based on the exact solution of the hydrodynamic problem in cylindrical coordinate system in the frame of the generalized lubrication approximation, keeping the zero-order terms [4.80] and the first-order terms. As a result the expressions for the fluid velocity and dynamic pressure are calculated for an arbitrary shape of the bubble. These quantities are substituted in the normal stress boundary condition to obtain the boundary value problem in terms of an arc length for the bubble shape. Diagrams for the necessary conditions for the appearance of long bubbles are constructed (Figs. 4.8 and 4.9). The implemented method allows fast and precise calculation of the dependence of the capillary number and the wetting film thickness in the cylindrical part on the system parameters.

The comparisons with available experiments (Figs. 4.11, 4.12, and 4.13) show the validity of the proposed approach for moderate capillary, Ca, and Bond, Bo, numbers, $Ca < 2$ and $Bo < 7.5$. When the pressure-driven flow hinders the rising of bubbles, the gravity should be sufficiently high to ensure bubble motion (Fig. 4.14). A very low applied pressure gradient in the opposite direction of bubble translation leads to bubble motion and the Bretherton condition ($Bo > 0.842$) does not take a place. When the gravity opposes the pressure-driven bubble motion (Fig. 4.15), the translational velocity decreases for high absolute values of the Bond number. Generally, in the case of tangentially immobile interfaces, the translational velocity, V_b, is lower and the wetting film thickness, h, is higher than those, predicted for free bubble surfaces at given fixed system parameters.

Experimental and theoretical extension of this work could include the effect of surfactants with concentrations above the critical micelle concentration and the motion of long bubbles in nanofluids [4.75, 4.76].

References

[4.1] F. Bretherton. The motion of long bubbles in tubes. *J. Fluid Mech.*, 10(2):166–188, 1961. DOI: 10.1017/S0022112061000160.

[4.2] M. Hoorfar and A. Neumann. Recent progress in axisymmetric drop shape analysis (ADSA). *Adv. Colloid Interfac. Sci.*, 121(1):25–49, 2006. DOI: 10.1016/j.cis.2006.06.001.

[4.3] T. Tran, M. Ahmad, P. Neogi, and B. Bai. A single pore model for displacement of heavy crude oil with carbon dioxide. *SPE J.*, 21(03):0864—-0872, 2016. DOI: 10.2118/178425-PA.

[4.4] P. Grassia. Motion of an oil droplet through a capillary with charged surfaces. *J. Fluid Mech.*, 866:721–758, 2019. DOI: 10.1017/jfm.2019.126.

[4.5] T. Majeed, M. Kamal, X. Zhou, and T. Solling. A review of foam stabilizers for enhanced oil recovery. *Energy Fuels*, 35(7):5594–5612, 2021. DOI: 10.1021/acs.energyfuels.1c00035.

[4.6] D. Halpern and T. Secomb. The squeezing of red blood cells through capillaries with near-minimal diameters. *J. Fluid Mech.*, 203:381–400, 1989. DOI: 10.1017/S0022112089001503.

[4.7] T. Savin, M. Bandi, and L. Mahadevan. Pressure-driven occlusive flow of a confined red blood cell. *Soft Matter*, 12(2):562–573, 2016. DOI: 10.1039/C5SM01282A.

[4.8] D. Gaver, D. Halpern, O. Jensen, and J. Grotberg. The steady motion of a semi-infinite bubble through a flexible-walled channel. *J. Fluid Mech.*, 319:25–65, 1996. DOI: 10.1017/S0022112096007240.

[4.9] M. Heil. The Bretherton problem in elastic-walled channels: finite Reynolds number effects. In A. King and Y. Shikhmurzaev, editors, *IUTAM symposium on free surface flows. Fluid mechanics and its application*, volume 62, pages 113–120, Dordrecht, 2001. Springer. DOI: 10.1007/978-94-010-0796-2_14.

[4.10] C. Baroud, S. Tsikata, and M. Heil. The propagation of low viscosity fingers into fluid-filled branching network. *J. Fluid Mech.*, 546:285–294, 2006. DOI: 10.1017/S0022112005007287.

[4.11] J. Stark and M. Manga. The motion of long bubbles in a network of tubes. *Transport in Porous Media*, 40:201–218, 2000. DOI: 10.1023/A:1006697532629.

[4.12] C. Clanet, P. Heraud, and G. Searby. On the motion of bubbles in vertical tubes of arbitrary cross-sections: some complements to the Dumitrescu–Taylor problem. *J. Fluid Mech.*, 519:359–376, 2004. DOI: 10.1017/S0022112004001296.

[4.13] D. Picchi, A. Ullmann, N. Brauner, and P. Poesio. Motion of a confined bubble in a shear-thinning liquid. *J. Fluid Mech.*, 918:A7, 2021. DOI: 10.1017/jfm.2021.321.

[4.14] C. Chao, X. Jin, and X. Fan. Evolution of thin-liquid films surrounding bubbles in microfluidics and their impact on the pressure drop and fluid movement. *Langmuir*, 36(49):15102–15111, 2020. DOI: 10.1021/acs.langmuir.0c02679.

[4.15] M. Kreutzer, F. Kapteijn, J. Moulijn, C. Kleijn, and J. Heiszwolf. Inertial and interfacial effects on pressure drop of taylor flow in capillaries. *AIChE J.*, 51(9):2428–2440, 2005. DOI: 10.1002/aic.10495.

[4.16] B. Wang, B. Ke, B. Chen, R. Li, and R. Tian. A technical review of research progress on thin liquid film thickness. *Exp. Comput. Multiph. Flow*, 2:199–211, 2020. DOI: 10.1007/s42757-019-0051-9.

[4.17] E. Zukoski. Influence of the viscosity, surface tension, and inclination angle on motion of long bubbles in closed tubes. *J. Fluid Mech.*, 25(4):821–837, 1966. DOI: 10.1017/S0022112066000442.

[4.18] A. Gibson. LXXXIV. On the motion of long air-bubbles in a vertical tube. *Lond. Edinb. Dubl. Phil. Mag.*, 26(156):952–965, 1913. DOI: 10.1080/14786441308635043.

[4.19] G. Barr. XXXI. The air-bubble viscometer. *Lond. Edinb. Dubl. Phil. Mag.*, 1(2):395–405, 1926. DOI: 10.1080/14786442608633640.

[4.20] C. Lamstaes and J. Eggers. Arrested bubble rise in a narrow tube. *J. Stat. Phys.*, 167(3):656–682, 2017. DOI: 10.1007/s10955-016-1559-z.

[4.21] D. T. Dumitrescu. Strömung an einer Luftblase im senkrechten Rohr. *Z. Angew. Math. Mech.*, 23(3):139–149, 1943. DOI: 10.1002/zamm.19430230303.

[4.22] R. Davies and G. Taylor. The mechanics of large bubbles rising through extended liquids and through liquids in tubes. *Proc. R. Soc. Lond. A*, 200:375–390, 1950. DOI: 10.1098/rspa.1950.0023.

[4.23] T. Harmathy. Velocity of large drops and bubbles in media of infinite or restricted extent. *AIChE J.*, 6(2):281–288, 1960. DOI: 10.1002/aic.690060222.

[4.24] H. Goldsmith and S. Mason. The movement of single large bubbles in closed vertical tubes. *J. Fluid Mech.*, 14(1):42–58, 1962. DOI: 10.1017/S0022112062001068.

[4.25] E. White and R. Beardmore. The velocity of rise of single cylindrical air bubbles through liquids contained in vertical tubes. *Chem. Eng. Sci.*, 17:351–361, 1962. DOI: 10.1016/0009-2509(62)80036-0.

[4.26] R. van Hout, A. Gulitski, D. Barnea, and L. Shemer. Experimental investigation of the velocity field induced by a Taylor bubble rising in stagnant water. *Int. J. Multiphas. Flow*, 28(4):579–596, 2002. DOI: 10.1016/S0301-9322(01)00082-9.

[4.27] W. Dhaouadi and J. Kolinski. Bretherton's buoyant bubble. *Phys. Rev. Fluids*, 4(12):123601–123611, 2019. DOI: 10.1103/PhysRevFluids.4.123601.

[4.28] K. Bendiksen. On the motion of long bubbles in vertical tubes. *Int. J. Multiphas. Flow*, 11(6):797–812, 1985. DOI: 10.1016/0301-9322(85)90025-4.

[4.29] Z.-S. Mao and A. Dukler. The motion of Taylor bubbles in vertical tubes – II. Experimental data and simulations for laminar and turbulent flow. *Chem. Eng. Sci.*, 46(8):2055–2064, 1991. DOI: 10.1016/0009-2509(91)80164-T.

[4.30] J. Bugg, K. Mack, and K. Rezkallah. A numerical model of Taylor bubbles rising through stagnant liquids in vertical tubes. *Int. J. Multiphas. Flow*, 24(2):271–281, 1998. DOI: 10.1016/S0301-9322(97)00047-5.

[4.31] J. Bugg and G. Saad. The velocity field around a Taylor bubble rising in a stagnant viscous fluid: numerical and experimental results. *Int. J. Multiphas. Flow*, 28(5):791–803, 2002. DOI: 10.1016/S0301-9322(02)00002-2.

[4.32] R. Azadi and D. Nobes. Local flow dynamics in the motion of slug bubbles in a flowing mini square channels. *Int. J. Heat Mass Transf.*, 178:121588, 2021. DOI: 10.1016/j.ijheatmasstransfer.2021.121588.

[4.33] Z. Li, L. Wang, J. Li, and H. Chen. Drainage and lubrication film around stuck bubbles in vertical capillaries. *Appl. Phys. Lett.*, 115:111601, 2019. DOI: 10.1063/1.5112055.

[4.34] A. Morgado, J. Miranda, J. Araújo, and J. Campos. Review on vertical gas-liquid slug flow. *Int. J. Multiphas. Flow*, 85:348–368, 2016. DOI: 10.1016/j.ijmultiphaseflow.2016.07.002.

[4.35] F. Fairbrother and A. Stubbs. 119. Studies in electro-endosmosis. Part VI. The bubble-tube method of measurement. *J. Chem. Soc.*, (0):527–529, 1935. DOI: 10.1039/JR9350000527.

[4.36] G. Taylor. Deposition of a viscous fluid on the wall of a tube. *J. Fluid Mech.*, 10(2):161–165, 1961. DOI: 10.1017/S0022112061000159.

[4.37] J.-D. Chen. Measuring the film thickness surrounding a bubble inside a capillary. *J. Colloid Interf. Sci.*, 109(2):341–349, 1986. DOI: 10.1016/0021-9797(86)90313-9.

[4.38] L. Schwartz, H. Princen, and A. Kiss. On the motion of bubbles in capillary tubes. *J. Fluid Mech.*, 172:259–275, 1986. DOI: 10.1017/S0022112086001738.

[4.39] P. Aussillous and D. Quéré. Quick deposition of a fluid on the wall of a tube. *Phys. Fluids*, 12(10):2367–2371, 2000. DOI: 10.1063/1.1289396.

[4.40] Y. Han and N. Shikazono. Measurement of the liquid film thickness in micro tube slug flow. *Int. J. Heat Fluid Flow*, 30(5):842–853, 2009. DOI: j.ijheatfluidflow.2009.02.019.

[4.41] I. Beresnev, W. Gaul, and R. Dennis Vigil. Thickness of residual wetting film in liquid-liquid displacement. *Phys. Rev. E*, 84(2):026327–026335, 2011. DOI: 10.1103/PhysRevE.84.026327.

[4.42] H. Chen, Z. Li, and J. Li. Thin-film profile around long bubbles in square microchannels measured by chromatic interference method. *Appl. Phys. Lett.*, 109:041604, 2016. DOI: 10.1063/1.4959791.

[4.43] M. Matin and S. Moghaddam. Thin liquid film formation and evaporation mechanisms around elongated bubbles in rectangular cross-section microchannels. *Int. J. Heat Fluid Flow*, 163:120474, 2020. DOI: 10.1016/j.ijheatmasstransfer.2020.120474.

[4.44] C.-E. Wu, H.-W. Du, J. Qin, E.-Q. Li, and P. Gao. Experiment on bubble formation through dynamic wetting transition in a square capillary. *AIP Advances*, 11:075107, 2021. DOI: 10.1063/5.0057296.

[4.45] D. Reinelt and P. Saffman. The penetration of a finger into a viscous fluid in a channel and tube. *SIAM J. Sci. Stat. Comput.*, 6(3):542–561, 1985. DOI: 10.1137/0906038.

[4.46] H. Westborg and O. Hassager. Creeping motion of long bubbles and drops in capillary tubes. *J. Colloid Interf. Sci.*, 133(1):135–147, 1989. DOI: 10.1016/0021-9797(89)90287-7.

[4.47] H. Wong, C. Radke, and S. Morris. The motion of long bubbles in polygonal capillaries. Part 1. Thin films. *J. Fluid Mech.*, 292:71–94, 1995. DOI: 10.1017/S0022112095001443.

[4.48] H. Wong, C. Radke, and S. Morris. The motion of long bubbles in polygonal capillaries. Part 2. Drag, fluid pressure and fluid flow. *J. Fluid Mech.*, 292:95–110, 1995. DOI: 10.1017/S0022112095001455.

[4.49] M. Giavedoni and F. Saita. The axisymmetric and plane cases of a gas phase steadily displacing a Newtonian liquid—a simultaneous solution of the governing equations. *Phys. Fluids*, 9(8):2420–2428, 1997. DOI: 10.1063/1.869360.

[4.50] M. Heil. Finite Reynolds number effects in the Bretherton problem. *Phys. Fluids*, 13(9):2517–2521, 2001. DOI: 10.1063/1.1389861.

[4.51] A. Hazel and M. Heil. The steady propagation of a semi-infinite bubble into a tube of elliptical or rectangular cross-section. *J. Fluid Mech.*, 470:91–114, 2002. DOI: 10.1017/S0022112002001830.

[4.52] S. Hodges, O. Jensen, and J. Rallison. The motion of a viscous drop through a cylindrical tube. *J. Fluid Mech.*, 501:279–301, 2004. DOI: 10.1017/S0022112003007213.

[4.53] J. Feng. Steady axisymmetric motion of a small bubble in a tube with flowing liquid. *Proc. R. Soc. A*, 466:549–562, 2010. DOI: 10.1098/rspa.2009.0288.

[4.54] D. Langewisch and J. Buongiorno. Prediction of film thickness, bubble velocity, and pressure drop for capillary slug flow using a CFD-generated database. *Int. J. Heat Fluid Flow*, 54:250–257, 2015. DOI: 10.1016/j.ijheatfluidflow.2015.06.005.

[4.55] M. Dzikowski, L. Laniewski-Wollk, and J. Rokicki. Single component multiphase lattice Boltzmann method for Taylor/Bretherton bubble train flow simulations. *Commun. Comput. Phys.*, 19(4):1042–1066, 2016. DOI: 10.4208/cicp.220115.110915a.

[4.56] M. Magnini and O. Matar. Morphology of long gas bubbles propagation in square capillaries. *Int. J. Multiphas. Flow*, 129:103353, 2020. DOI: 10.1016/j.ijmultiphaseflow.2020.103353.

[4.57] D. Langewisch. *Application of the polynomial chaos expansion to multiphase CFD: a study of rising bubbles and slug flow*. PhD thesis, Massachusetts Institute of Technology, 2004.

[4.58] E. Klaseboer, R. Gupta, and R. Manica. An extended Bretherton model for long Taylor bubbles at moderate capillary numbers. *Phys. Fluids*, 26:032107, 2014. DOI: 10.1063/1.4868257.

[4.59] G. Balestra, L. Zhu, and F. Gallaire. Viscous Taylor droplets in axisymmetric and planar tubes: From Bretherton's theory to empirical models. *Microfluid Nanofluid*, 22(6):67, 2018. DOI: 10.1007/s10404-018-2084-y.

[4.60] G. Hirasaki and J. Lawson. Mechanisms of foam flow in porous media: apparent viscosity in smooth capillaries. *Soc. Pet. Eng. J.*, 25(02):176–190, 1985. DOI: 10.2118/12129-PA.

[4.61] N. Denkov, V. Subramanian, D. Gurovich, and A. Lips. Wall slip and viscous dissipation in sheared foams: effect of surface mobility. *Colloids Surf. A*, 263(1):129–145, 2005. DOI: 10.1016/j.colsurfa.2005.02.038.

[4.62] G. Ginley and C. Radke. Influence of soluble surfactants on the flow of long bubbles through a cylindrical capillary. In J. Borchardt and T. Yen, editors, *Oil-field chemistry. Enhanced recovery and production stimulation*, chapter 26, pages 480–501. 1989. DOI: 10.1021/bk-1989-0396.ch026.

[4.63] J. Ratulowski and H.-C. Chang. Marangoni effects of trace impurities on the motion of long gas bubbles in capillaries. *J. Fluid Mech.*, 210:303–328, 1990. DOI: 10.1017/S0022112090001306.

[4.64] C.-W. Park. Influence of soluble surfactants on the motion of a finite bubble in a capillary tube. *Phys. Fluids A*, 4(11):2335–2347, 1992. DOI: 10.1063/1.858475.

[4.65] F. Wassmuth, W. Laidlaw, and D. Coombe. Calculation of interfacial flows and surfactant redistribution as a gas/liquid interface moves between two parallel plates. *Phys. Fluids A*, 5(7):1533–1548, 1993. DOI: 10.1063/1.858831.

[4.66] K. Stebe and D. Barthès-Biesel. Marangoni effects of adsorption-desorption controlled surfactants on the leading end of an infinitely long bubble in a capillary. *J. Fluid Mech.*, 286:25–48, 1995. DOI: 10.1017/S0022112095000632.

[4.67] S. Ghadiali and D. Gaver. The influence of non-equilibrium surfactant dynamics on the flow of a semi-infinite bubble in a rigid cylindrical capillary tube. *J. Fluid Mech.*, 478:165–196, 2003. DOI: 10.1017/S002211200200335X.

[4.68] R. Johnson and A. Borhan. Pressure-driven motion of surfactant-laden drops through cylindrical capillaries: effect of surfactant solubility. *J. Colloid Interf. Sci.*, 261(2):529–541, 2003. DOI: 10.1016/S0021-9797(03)00031-6.

[4.69] M. Severino, A. Giavedoni, and F. Saita. A gas phase displacing a liquid with soluble surfactants out of a small conduit: the plane case. *Phys. Fluids*, 15(10):2961–2972, 2003. DOI: 10.1063/1.1605424.

[4.70] P. Dapira and G. Paşa. The effect of surfactant on the motion of long bubbles in horizontal capillary tubes. *J. Stat. Mech.*, 2010(2):L02002, 2010. DOI: 10.1088/1742-5468/2010/02/l02002.

[4.71] T. Swaminathan, K. Mukundakrishnan, P. Ayyaswamy, and D. Eckmann. Effect of a soluble surfactant on a finite-sized bubble motion in a blood vessel. *J. Fluid Mech.*, 642:509–539, 2010. DOI: 10.1017/S0022112009992692.

[4.72] U. Olgac and M. Muradoglu. Effects of surfactant on liquid film thickness in the Bretherton problem. *Int. J. Multiphas. Flow*, 48:58—-70, 2013. DOI: 10.1016/j.ijmultiphaseflow.2012.08.007.

[4.73] Y. Cui and N. Gupta. Numerical study of surfactant effects on the buoyancy-driven motion of a drop in a tube. *Chem. Eng. Sci.*, 144:48–57, 2016. DOI: 10.1016/j.ces.2016.01.020.

[4.74] N. Hammoud, P. Trinh, P. Howell, and H. Stone. Influence of van der Waals forces on a bubble moving in a tube. *Phys. Rev. Fluids*, 2(6):063601, 2017. DOI: 10.1103/PhysRevFluids.2.063601.

[4.75] H. Cho, A. Nikolov, and D. Wasan. Step-wise velocity of an air bubble rising in a vertical tube filled with a liquid dispersion of nanoparticles. *Langmuir*, 33(11):2920–2928, 2017. DOI: 10.1021/acs.langmuir.6b04489.

[4.76] H. Cho, A. Nikolov, and D. Wasan. Estimation of structural film viscosity based on the bubble rise method in a nanofluid. *J. Colloid Interf. Sci.*, 516:312–316, 2018. DOI: 10.1016/j.jcis.2018.01.066.

[4.77] H. Cho, A. Nikolov, and D. Wasan. Prediction of the rate of the rise of an air bubble in nanofluids in a vertical tube. *J. Colloid Interf. Sci.*, 525:115–118, 2018. DOI: 10.1016/j.jcis.2018.04.062.

[4.78] C. Madec, B. Collin, J. Jerome, and S. Joubaud. Puzzling bubble rise speed increase in dense granular suspensions. *Phys. Rev. Lett.*, 125(6):078004, 2020. DOI: 10.1103/PhysRevLett.125.078004.

[4.79] Y.-C. Li, Y.-C. Liao, T.-C. Wen, and H.-H. Wei. Breakdown of the Bretherton law due to wall slippage. *J. Fluid Mech.*, 741:200–227, 2014. DOI: 10.1017/jfm.2013.562.

[4.80] J. Ratulowski and H.-C. Chang. Transport of gas bubbles in capillaries. *Phys. Fluids A - Fluid*, 1(10):1642–1655, 1989. DOI: 10.1063/1.857530.

[4.81] W. Kolb and R. Cerro. The motion of long bubbles in tubes of square cross section. *Phys. Fluids A - Fluid*, 5(7):1549–1567, 1993. DOI: 10.1063/1.858832.

[4.82] Z.-S. Mao and A. Dukler. The motion of Taylor bubbles in vertical tubes. I. A numerical simulation for the shape and rise velocity of Taylor bubbles in stagnant and flowing liquid. *J. Comput. Phys.*, 91(1):132–160, 1990. DOI: 10.1016/0021-9991(90)90008-O.

[4.83] A. Borhan and J. Pallinti. Pressure-driven motion of drops and bubbles through cylindrical capillaries: Effect of buoyancy. *Ind. Eng. Chem. Res.*, 37(9):3748–3759, 1998. DOI: 10.1021/ie980087l.

[4.84] M. Magnini, S. Khodaparast, O. Matar, H. Stone, and J. Thome. Dynamics of long gas bubbles rising in a vertical tube in a cocurrent liquid flow. *Phys. Rev. Fluids*, 4(2):023601, 2019. DOI: 10.1103/PhysRevFluids.4.023601.

[4.85] Y. Yu, M. Magnini, L. Zhu, S. Shim, and H. Stone. Non-unique bubble dynamics in a vertical capillary with an external flow. *J. Fluid Mech.*, 911:A34, 2021. DOI: 10.1017/jfm.2020.1027.

[4.86] R. Manica, E. Klaseboer, and D. Chan. The hydrodynamics of bubble rise and impact with solid surfaces. *Adv. Colloid Interfac.*, 235:214–232, 2016. DOI: 10.1016/j.cis.2016.06.010.

[4.87] G. Lyutskanova, K. Mihaylov, and V. Kolev. Axisymmetric drop shape analysis. In *Proceedings of Preparatory Modelling Week*, Sofia, Bulgaria, 2015. URL: `http://pmw2015.fmi.uni-sofia.bg/Documents/Problem_2_Report.pdf`.

[4.88] T. Feagin. A tenth-order Runge-Kutta method with error estimate. In A. Avidan, editor, *Proceedings of the IAENG Conf. on Scientific Computing*, volume 1, page 1, Hong Kong, 2007. URL: `https://sce.uhcl.edu/feagin/courses/rk10.pdf`.

Chapter 5

Conclusions and main contributions

5.1 General conclusions

A complex fluid (three-dimensional phase) is fluid, which is not Newtonian or the surface tension on its material interfaces (two-dimensional phases) is not constant. Examples for complex fluids are foams, emulsions, melts, biological cells, tissues and liquids, etc., which have applications in the chemical, pharmaceutical and oil industry, everyday life and medicine. In continuum mechanics, a complex fluid is modelled by the mass, momentum and energy balance equations, which are not closed. To close the physicochemical models and to introduce a mathematical formulation of the respective problems, the natural scientists assume different semi-empirical laws (linear or nonlinear) to relate the stress and strain tensors. Even in the simplest linear rheological case of Newtonian fluids, the Navier–Stokes equations for incompressible fluids become of a fourth order (the elimination of the pressure leads to nonlinear partial differential equations, which contain bi-Laplacian of the velocity vector). For typical applications, the bulk fluids are incompressible but the material interfaces are not — they can deform, take different complex shapes and have considerably different rheological behavior, which is affected by the adsorbed surfactants, polymers or particles, by the properties of the biological membranes, etc. Generally, the appearance of interfaces leads to complex boundary value problems. To construct adequate rheological models, the experimentalists need simplified mathematical models and fast numerical procedures to fit the obtained data and to extract information about the rheological parameters (e.g. the surface dilatational and shear viscosity and elasticity, yield stress, etc.).

In the thesis, we consider three different applications of the boundary value problems in the case of linear or strongly nonlinear models of the second or higher orders. The first problem (Chapter 2) is related to the interaction between large protein molecules and colloid particles (particles of micron or submicron sizes), both of which are attached to the interface between two fluids. For small sizes (below 3 microns), the proteins and colloids (termed as particles) interact with van der Waals, electrostatic and capillary forces. Except for the van der Waals interactions, the electrostatic and capillary forces arise because of the surface charge density of particles and their three-phase contact angles. Due to the small particle volumes, the gravity is negligible and, therefore, the deformation of the interface is

a result of the electrostatic pressure distribution along the interface and related to it electro-dipping force. The strategy for computer modeling is to solve the respective problem for flat interface, to calculate the electrostatic pressure distribution and the electro-dipping force; to use the calculated distribution in the normal stress boundary condition in order to compute the interfacial deformation; etc. From experimental viewpoint, the first two steps are the most important.

In the literature [5.1, 5.2], the problem for the electrostatic distribution is solved numerically and analytically (in the terms of Mehler–Fock integral transform) in the case of one fully conductive bulk phase (water). This simplification leads to the Dirichlet boundary conditions at the particle–water and dielectric phase–water boundaries (the electrostatic potential at these boundaries is equal to zero). The estimation of the part of the electro-dipping force, arising from the water phase, shows that the contribution from the water phase is not negligible and one should account for all dielectric phases simultaneously. In Chapter 2, the Laplace equations for the electrostatic potentials in all three domains (spherical particle, upper and lower dielectric phases) are solved with the boundary conditions at all three dividing surfaces (continuity of the electrostatic potentials and balance of surface charges). The numerical solution of this generalized (in fact more realistic) problem gives the answer to the question for the role of water phase on the electrostatic potential distribution. In the most cases, some of the physical quantities have weak singularities at the three-phase contact line (in our case, the derivative of the electrostatic potential that is the electric field vector). Physically, a weak singularity means that the integral of the respective force, containing these quantities, over the surface has a well-defined finite value. The isolation of the weak singularity, transformation of the complex numerical domains into rectangles, using toroidal coordinates, and the application of fast and precise numerical methods become of a crucial importance for the adequate solution of the problem, described in Chapter 2.

The second problem (Chapter 3) is a part of two very complex tasks. The first one is to predict the two-dimensional ordering of a large number of molecules and colloidal particles, which float at the surface between two fluids, and the drag forces, which act on them due to their Brownian motion under the action of van der Waals, electrostatic and capillary forces. The second task is related to the fact that there is no direct microscopic method to measure the value of the three-phase contact angle. The recently developed optical trap method uses laser beams to manipulate colloidal particles at the interfaces and biological membranes. From the lateral velocity of a particle and the applied optical tweezer force, the experimentalists measure the drag force of the colloidal particle (tracer). Thus, one needs a fast and precise numerical method to calculate the drag force for a given three-phase contact angle and to use this procedure for fitting of experimental data in order to obtain the most probable value of the three-phase contact angle. From a physical viewpoint, the formulation of the model in Chapter 3 is quite clear: Stokes equation in each of the incompressible fluid phases; continuity of the velocity and tangential stresses at the flat dividing surface between them; given translational velocity of the spherical colloidal particle, attached to the interface, with a fixed three-phase contact angle. One possible numerical approach to solve the problem is the two-vorticities-one-velocity formulation [5.3]. The reported method is of a second-order in the three-dimensional domains (with respect to the Stokes equations) but of a first-order in the two-dimensional domains (with respect to the boundary conditions). As a result, the method is slow and not convenient for multitask applications. The problem has also an analytical solution in terms of the Mehler–Fock integral transform for negligible viscosity of one of the fluids (e.g. water–air interface) and contact angles $\leq 90^\circ$ [5.4]. In fact, this particular case is not realistic and with a quite restricted application. Nevertheless, the

only way to check the validity of a numerical method and its precision is to use this exact solution of the problem. The main reason for the difficulties in numerical computations in [5.3] and for the restricted validity of the analytical solution (contact angles $\leq 90°$) [5.4] is the weak singularity of the pressure function at the three-phase contact line.

Our approach in Chapter 3 is based on the gauge reformulation of the Stokes problem, which introduces vector and scalar potentials of the velocity and pressure distributions; the reduction of the three-dimensional problem in the two-dimensional one for the first Fourier modes with respect to the polar angle; the transformation of the complex domains into rectangles, using a modification of the standard toroidal coordinates. As a result, the original problem for the bulk fluids is reduced to a system of four partial differential equations of a second-order for each of the phases. These systems are interrelated with the boundary conditions at the dividing surfaces. The main difficulty in the gauge formulation is to introduce self-consistent boundary conditions for the vector and scalar potentials. The introduced in Chapter 3, new type of boundary conditions resolves this problem and gives possibility to construct an efficient second-order ADI-type scheme for the numerical solution, which is fast enough and gives good precision. The asymptotic analysis of the weak singularity at the three-phase contact line shows the regions of regular and singular pressure distributions and improves the precision of the calculation for the drag force.

One of the most difficult problems in physicochemical and biological modeling is to obtain the shape of material interfaces in static and dynamic regimes. The complex shapes, the stability and instability of interfaces and their interactions with other material objects are of general importance for the description of their physicochemical properties. One example is considered in Chapter 4 — a motion of a long bubble through a cylindrical capillary under the action of pressure gradients (Poiseuille flow) and gravity. The bubble surface can be: free, i.e. tangentially mobile interface — classical formulation; tangentially immobile but deformable, e.g. the model of biological membranes, surfactant laden interfaces, etc. The analytical solutions of the classical problems (free surfaces) for the gravity- and for the pressure-driven motion in the case of very small bubble velocity are known as the Bretherton problems [5.5]. The only formulas that extend the validity of the Bretherton formulas and are applicable in the case of bubble with a free surface under the action of pressure, are published in Refs. [5.6, 5.7]. Again, this problem is a part of more complex computations, e.g. a motion of drops and bubbles in a rock porous medium in the oil recovery problems or the motion of biological inclusions in the human veins. Due to the fact that the available numerical calculations are very time consumable, it is difficult (and in the most cases impossible) these calculations to be generalized to complex fluids and material interfaces.

In Chapter 4, we combine the Bretherton idea with the approach in [5.6] and solve the hydrodynamic problem for the lubrication approximation not only for the zero-order but also for the first-order approximation of the fluid velocity and pressure. As it can be expected, this increases the precision of the used approximation solution. One advantage of this analytical method is its validity for an arbitrary smooth shape of the interface. As a result, the analytical expressions for the flow characteristics in the case of tangentially mobile and immobile interfaces are obtained. The normal stress boundary condition, in which the lubrication approximation solution is substituted, defines the shape of bubble. The obtained numerical problem is a system of four nonlinear differential equations with one adjustable parameter, which has to be varied in order to calculate a close capillary profile. From mathematical and numerical viewpoint, the obtained problem is analogous to the method known as an axisymmetric drop shape analysis, which is incorporated in many commercial

apparatuses for measurement of the surface tension and the contact angle. The obtained numerical results describe excellently the available experimental data; expand the validity of the semi-analytical model by at least two orders of magnitude to moderate capillary and Bond numbers; explain the complex behavior of the simultaneous action of gravity and pressure-driven flow; show the principle difference between mobile and immobile interfaces.

5.2 Main contributions

1. The problem for distribution of electrostatic potentials in dielectric media (two immiscible fluid phases and a spherical colloidal particle, attached to the flat interface between them) consists of Laplace equations for the functions in the three-dimensional domains, continuity of these functions and conditions for their normal derivatives at the known two-dimensional boundaries. The problem is solved numerically, using the developed for this purpose fast and efficient algorithm. The strategy of computations is based on: the transformation of the complex domains into rectangles, using appropriate toroidal coordinates; analytical computation of the weak singularity at the three-phase contact line; implementation of a self-consistent second-order ADI-type numerical scheme. The results generalize the idealized case in [5.1], in which the water permeability is assumed to be infinite. In the present study, we take into account its finite value as well as the simultaneous effect of all dielectric phases.

2. The problem for the translational motion of a spherical colloidal particle, attached to a flat interface between two incompressible fluids, consists of Stokes equations for the velocity vector and the pressure (in fact bi-Laplacian of the velocity vector is equal to zero) in the three-dimensional domains, continuity of the velocity and the tangential stresses at the two-dimensional fluid–fluid interface and a known velocity vector at the particle surface. The problem is solved numerically from 10 to 1000 times faster than by the proposed method in method [5.3]. The strategy of computations is based on: the gauge formulation in terms of vector and scalar potentials of velocity and pressure; transformation of the three-dimensional problem into the two-dimensional one for the first Fourier mode with respect to the polar angle; transformation of the complex domains into rectangles, using modified toroidal coordinates; construction of a second-order ADI-type numerical scheme, taking into account the original formulation of the two-dimensional boundary conditions; the analytical calculation of the weak singularity at the three-phase contact line and the isolation of the pressure singularity, which increases the precision of the drag force calculations.

3. The problem for the gravity- and pressure-driven motion of a long bubble with tangentially mobile (classical case) or immobile interface (biological membrane, surfactant laden interface, etc.) through a cylindrical capillary is solved semi-analytically. The problem consists of: Stokes equations in the three-dimensional domain; known Poiseuille velocity profile at large distances from the bubble; no-slip boundary condition at the capillary wall; tangential and normal stress boundary conditions at the deformable bubble surface. The strategy of computations is based on: the exact analytical solution of the Stokes problem for small slopes of the tangent to the bubble shape, which leads to zero- and first-order approximations at an arbitrary smooth bubble shape; substitution of the obtained solutions in the normal stress boundary condition, from which it follows a system of four first order nonlinear differential equations with respect to the arc length with one adjustable parameter (the capillary pressure at the bubble apex); the efficient numerical scheme for calculating the fourth-order boundary value problem for the shape by fitting the adjustable parameter

in order to obtain a closed capillary profile. As a result, the obtained method describes excellently the available experimental data, increases more than two orders of magnitude the range of the applicability of the analytical approaches known in the literature, and explain the complex physical picture of the simultaneous action of gravity and pressure-driven flows for classical and tangentially immobile interfaces.

References

[5.1] K. Danov and P. Kralchevsky. Electric forces induced by a charged colloid particle attached to the water–nonpolar fluid interface. *J. Colloid Interface Sci.*, 298(1):213–231, 2006. DOI: 10.1016/j.jcis.2005.12.037.

[5.2] P. Petkov, K. Danov, and P. Kralchevsky. Monolayers of charged particles in a langmuir trough: Could particle aggregation increase the surface pressure? *Journal of Colloid and Interface Science*, 462:223–234, 2015. DOI: 10.1016/j.jcis.2015.09.075.

[5.3] K. Danov, R. Dimova, and B. Pouligny. Viscous drag of a solid sphere straddling a spherical or flat surface. *Phys. Fluids*, 12:2711–2722, 2000. DOI: 10.1063/1.1289692.

[5.4] M. Zabarankin. Asymmetric three-dimensional stokes flows about two fused equal spheres. *Proc. R. Soc. A*, 463(2085):2329–2349, 2007. DOI: 10.1098/rspa.2007.1872.

[5.5] F. Bretherton. The motion of long bubbles in tubes. *J. Fluid Mech.*, 10(2):166–188, 1961. DOI: 10.1017/S0022112061000160.

[5.6] J. Ratulowski and H.-C. Chang. Transport of gas bubbles in capillaries. *Phys. Fluids A - Fluid*, 1(10):1642–1655, 1989. DOI: 10.1063/1.857530.

[5.7] W. Kolb and R. Cerro. The motion of long bubbles in tubes of square cross section. *Phys. Fluids A - Fluid*, 5(7):1549–1567, 1993. DOI: 10.1063/1.858832.

Appendix A

Drag force coefficient

The net drag force $\mathbf{F}$ on a particle of radius R, attached on the interface between two viscous fluids, is calculated by integrating the stress tensor $\mathbf{P}$ over the particle volume or as a surface integral of the normal component of the stress tensor over the particle surface S_p (divergence theorem), i.e.

$$\mathbf{F} = \iint_{S_p} \mathbf{P} \cdot \mathbf{n} \; dS_p, \tag{A.1}$$

where $\mathbf{n}$ is the unit normal vector to the surface S_p, pointing to the fluid phases (see Fig. 3.1). Due to the fact that the drag force depends on fluid 1 at the upper part of the particle S_{p1} and on fluid 2 — at the lower part S_{p2}, we obtain

$$\mathbf{F} = \iint_{S_{1\mathrm{p}}} \mathbf{P}_1 \cdot \mathbf{n} \; dS_{1\mathrm{p}} + \iint_{S_{2\mathrm{p}}} \mathbf{P}_2 \cdot \mathbf{n} \; dS_{2\mathrm{p}}, \tag{A.2}$$

where $\mathbf{P}_1$ denotes the stress tensor at the upper part of the particle surface and $\mathbf{P}_2$ — at lower part. The stress tensor $\mathbf{P}_m$ of the viscous fluid phase m is computed as

$$\mathbf{P}_m = -p_m \mathbf{I} + \eta_m \left[\nabla \mathbf{v} + (\nabla \mathbf{v})^T \right], \tag{A.3}$$

where p_m is the pressure and η_m is the viscosity of phase m, see Eq. (U.64) in the Supplementary file U.

Next, we parametrize the spherical particle (x_s, y_s, z_s) by using spherical coordinates

$$x_s = R \cos\varphi \sin\theta, \tag{A.4}$$
$$y_s = R \sin\varphi \sin\theta, \tag{A.5}$$
$$z_s = R \cos\theta + R \cos\alpha, \tag{A.6}$$

where $\varphi \in [0, 2\pi)$ is the azimuth angle and $\theta \in [0, \pi)$ is the polar angle. Then, the polar angle changes from 0 to $\pi - \alpha$ ($0 \leq \theta \leq \pi - \alpha$) along the upper part of the particle surface and from $\pi - \alpha$ to π ($\pi - \alpha \leq \theta \leq \pi$) along the lower one. Therefore, one represents the

expression for the drag force (A.2) in the following form:

$$\begin{aligned}\mathbf{F} &= \int_0^{2\pi}\int_0^{\pi-\alpha} (\mathbf{P}_1\cdot\mathbf{n})|\mathbf{n}|d\theta d\varphi + \int_0^{2\pi}\int_{\pi-\alpha}^{\pi} (\mathbf{P}_2\cdot\mathbf{n})|\mathbf{n}|d\theta d\varphi \\ &= R^2\int_0^{2\pi}\int_0^{\pi-\alpha} (\mathbf{P}_1\cdot\mathbf{n})\sin\theta d\theta d\varphi + R^2\int_0^{2\pi}\int_{\pi-\alpha}^{\pi} (\mathbf{P}_2\cdot\mathbf{n})\sin\theta d\theta d\varphi, \qquad (A.7)\end{aligned}$$

by calculating the length of $\mathbf{n}$:

$$\begin{aligned}|\mathbf{n}| &= |\,(-R\sin\varphi\sin\theta\mathbf{e}_x + R\cos\varphi\sin\theta\mathbf{e}_y) \\ &\quad\times (R\cos\varphi\cos\theta\mathbf{e}_x - R\sin\varphi\cos\theta\mathbf{e}_y - R\sin\theta\mathbf{e}_z)\,| \\ &= |-R^2\left(\cos\varphi\sin^2\theta\mathbf{e}_x + \sin\varphi\sin^2\theta\mathbf{e}_y + \sin\theta\cos\theta\mathbf{e}_z\right)| \qquad (A.8)\\ &= R^2\sin\theta. \qquad (A.9)\end{aligned}$$

Due to the fact that most of the computations in Chapter 3 are done in cylindrical coordinates (r,φ,z), we use cylindrical coordinates in order to simplify the expression under the integral sign. Taking into account that the particle surface is parameterised by spherical coordinates, we use the transformation between the standard cylindrical coordinates and spherical ones:

$$r = \rho\sin\theta,\ \varphi = \varphi,\ z = \rho\cos\theta + R\cos\alpha, \qquad (A.10)$$

where ρ is the radial distance. Then, the parametrization of the sphere in cylindrical coordinates is

$$r = R\sin\theta,\ \varphi = \varphi,\ z = R\cos\theta + R\cos\alpha \qquad (A.11)$$

and the unit normal $\mathbf{n}$ has the following coordinate form:

$$\mathbf{n} = \frac{(R\cos\theta\mathbf{e}_r - R\sin\theta\mathbf{e}_z)\times\mathbf{e}_\varphi}{|\,(R\cos\theta\mathbf{e}_r - R\sin\theta\mathbf{e}_z)\times\mathbf{e}_\varphi|} = \sin\theta\mathbf{e}_r + \cos\theta\mathbf{e}_z, \qquad (A.12)$$

where $\mathbf{e}_r$, $\mathbf{e}_\varphi$ and $\mathbf{e}_z$ are the standard basis vectors of the cylindrical coordinate system. Using the expression for the normal vector, one obtains the components of stress tensor:

$$(\mathbf{P}_m\cdot\mathbf{n})_r = P_{mrr}\sin\theta + P_{mrz}\cos\theta,\ m = 1,2, \qquad (A.13)$$
$$(\mathbf{P}_m\cdot\mathbf{n})_\varphi = P_{m\varphi r}\sin\theta + P_{m\varphi z}\cos\theta,\ m = 1,2, \qquad (A.14)$$
$$(\mathbf{P}_m\cdot\mathbf{n})_z = P_{mzr}\sin\theta + P_{mzz}\cos\theta,\ m = 1,2. \qquad (A.15)$$

Note that the drag force has y-component F_y, which is calculated from the stress tensor:

$$(\mathbf{P}_m\cdot\mathbf{n})_y = (\mathbf{P}_m\cdot\mathbf{n})_r\sin\varphi + (\mathbf{P}_m\cdot\mathbf{n})_\varphi\cos\varphi,\ m = 1,2, \qquad (A.16)$$

see Eq. (S.346). Using formulas (A.7) and (A.16), one gets the formula for drag force

component F_y

$$\begin{aligned} F_y = R^2 \int_0^{2\pi} \int_0^{\pi-\alpha} & [(P_{1rr}\sin\theta + P_{1rz}\cos\theta)\sin\varphi \\ & + (P_{1\varphi r}\sin\theta + P_{1\varphi z}\cos\theta)\cos\varphi]\sin\theta d\theta d\varphi \\ + R^2 \int_0^{2\pi} \int_{\pi-\alpha}^{\pi} & [(P_{2rr}\sin\theta + P_{2rz}\cos\theta)\sin\varphi \\ & + (P_{2\varphi r}\sin\theta + P_{2\varphi z}\cos\theta)\cos\varphi]\sin\theta d\theta d\varphi, \end{aligned} \tag{A.17}$$

where the cylindrical coordinates of the stress tensor are computed as follows:

$$P_{mrr} = -p_m + 2\eta_m \frac{\partial v_{mr}}{\partial r},\ m = 1, 2, \tag{A.18}$$

$$P_{mrz} = \eta_m \left(\frac{\partial v_{mr}}{\partial z} + \frac{\partial v_{mz}}{\partial r} \right),\ m = 1, 2, \tag{A.19}$$

$$P_{m\varphi r} = \eta_m \left(\frac{\partial v_{m\varphi}}{\partial r} - \frac{v_{m\varphi}}{r} + \frac{1}{r}\frac{\partial v_{mr}}{\partial \varphi} \right),\ m = 1, 2 \tag{A.20}$$

$$P_{m\varphi z} = \eta_m \left(\frac{\partial v_{m\varphi}}{\partial z} + \frac{1}{r}\frac{\partial v_{mz}}{\partial \varphi} \right),\ m = 1, 2. \tag{A.21}$$

see Eqs. (A.3) and (S.349). Next, we nondimensionalize the variables, using Eqs. (3.22), (3.23) and

$$\overline{F}_y = \frac{r_c F_y}{(\eta_1 + \eta_2) R^2 V},\ \overline{\mathbf{P}}_m = \frac{r_c \mathbf{P}_m}{V \eta_m},\ \overline{\rho} = \frac{\rho}{r_c}. \tag{A.22}$$

Then, we obtain the following formula for the component $\overline{F}_y$;

$$\begin{aligned} \overline{F}_y = \mu_1 \int_0^{2\pi} \int_0^{\pi-\alpha} & \left[\left(\overline{P}_{1rr}\sin\theta + \overline{P}_{1rz}\cos\theta\right)\sin\varphi \right. \\ & \left. + \left(\overline{P}_{1\varphi r}\sin\theta + \overline{P}_{1\varphi z}\cos\theta\right)\cos\varphi \right] \sin\theta d\theta d\varphi \\ + \mu_2 \int_0^{2\pi} \int_{\pi-\alpha}^{\pi} & \left[\left(\overline{P}_{2rr}\sin\theta + \overline{P}_{2rz}\cos\theta\right)\sin\varphi \right. \\ & \left. + \left(\overline{P}_{2\varphi r}\sin\theta + \overline{P}_{2\varphi z}\cos\theta\right)\cos\varphi \right] \sin\theta d\theta d\varphi, \end{aligned} \tag{A.23}$$

where

$$\overline{P}_{mrr} = -\overline{p}_m + 2\frac{\partial \overline{v}_{mr}}{\partial \overline{r}},\ m = 1, 2, \tag{A.24}$$

$$\overline{P}_{mrz} = \frac{\partial \overline{v}_{mr}}{\partial \overline{z}} + \frac{\partial \overline{v}_{mz}}{\partial \overline{r}},\ m = 1, 2, \tag{A.25}$$

$$\overline{P}_{m\varphi r} = \frac{\partial \overline{v}_{m\varphi}}{\partial \overline{r}} - \frac{\overline{v}_{m\varphi}}{\overline{r}} + \frac{1}{\overline{r}}\frac{\partial \overline{v}_{mr}}{\partial \varphi},\ m = 1, 2 \tag{A.26}$$

$$\overline{P}_{m\varphi z} = \frac{\partial \overline{v}_{m\varphi}}{\partial \overline{z}} + \frac{1}{\overline{r}}\frac{\partial \overline{v}_{mz}}{\partial \varphi},\ m = 1, 2. \tag{A.27}$$

For notional convenience, we shall skip the bars for all non-dimensional variables except F_y and ρ for the rest of this chapter. Then, in the gauge formulation, we have

$$\begin{aligned} P_{mrr} &= \nabla \cdot \mathbf{w}_m + 2\frac{\partial \overline{v}_{mr}}{\partial \overline{r}} \\ &= 3\frac{\partial w_{mr}}{\partial r} + \frac{w_{mr}}{r} + \frac{1}{r}\frac{\partial w_{m\varphi}}{\partial \varphi} + \frac{\partial w_{mz}}{\partial z} - 2\frac{\partial^2 \xi_m}{\partial r^2},\ m = 1, 2, \end{aligned} \tag{A.28}$$

$$P_{mrz} = \frac{\partial w_{mr}}{\partial z} + \frac{\partial w_{mz}}{\partial r} - 2\frac{\partial^2 \xi_m}{\partial r \partial z},\ m = 1, 2, \tag{A.29}$$

$$P_{m\varphi r} = \frac{\partial w_{m\varphi}}{\partial r} - \frac{w_{m\varphi}}{r} + \frac{1}{r}\frac{\partial w_{mr}}{\partial \varphi} + \frac{2}{r^2}\frac{\partial \xi_m}{\partial \varphi} - \frac{2}{r}\frac{\partial^2 \xi_m}{\partial r \partial \varphi},\ m = 1, 2, \tag{A.30}$$

$$P_{m\varphi z} = \frac{\partial w_{m\varphi}}{\partial z} + \frac{1}{r}\frac{\partial w_{mz}}{\partial \varphi} - \frac{2}{r}\frac{\partial^2 \xi_m}{\partial \varphi \partial z},\ m = 1, 2, \tag{A.31}$$

see equations (3.30), (3.31), (3.34), (S.348) and (S.350). Using the Fourier amplitudes (3.54) and (3.55), one simplifies these expressions as follows:

$$P_{mrr} = \left(3\frac{\partial a_{mr}}{\partial r} + \frac{a_{mr}}{r} - \frac{a_{m\varphi}}{r} + \frac{\partial a_{mz}}{\partial z} - 2\frac{\partial^2 b_m}{\partial r^2}\right)\sin\varphi,\ m = 1, 2, \tag{A.32}$$

$$P_{mrz} = \left(\frac{\partial a_{mr}}{\partial z} + \frac{\partial a_{mz}}{\partial r} - 2\frac{\partial^2 b_m}{\partial r \partial z}\right)\sin\varphi,\ m = 1, 2, \tag{A.33}$$

$$P_{m\varphi r} = \left(\frac{\partial a_{m\varphi}}{\partial r} - \frac{a_{m\varphi}}{r} + \frac{a_{mr}}{r} + \frac{2b_m}{r^2} - \frac{2}{r}\frac{\partial b_m}{\partial r}\right)\cos\varphi,\ m = 1, 2, \tag{A.34}$$

$$P_{m\varphi z} = \left(\frac{\partial a_{m\varphi}}{\partial z} + \frac{a_{mz}}{r} - \frac{2}{r}\frac{\partial b_m}{\partial z}\right)\cos\varphi,\ m = 1, 2. \tag{A.35}$$

We substitute the expressions (A.32)–(A.35) into the integrals in the right-hand side of equation (A.23) for the calculation of the drag force and obtain

$$\overline{F}_y = \pi(\mu_1 \overline{f}_1 + \mu_2 \overline{f}_2), \tag{A.36}$$

where the drag force coefficients $\overline{f}_1$ and $\overline{f}_2$ correspond to the contributions of the upper and lower parts of the particle:

$$\begin{aligned} \overline{f}_1 = \int_0^{\pi-\alpha} \Bigg[&\left(3\frac{\partial a_{1r}}{\partial r} + \frac{2a_{1r}}{r} - \frac{2a_{1\varphi}}{r} + \frac{\partial a_{1z}}{\partial z} - 2\frac{\partial^2 b_1}{\partial r^2} + \frac{\partial a_{1\varphi}}{\partial r} + \frac{2b_1}{r^2} - \frac{2}{r}\frac{\partial b_1}{\partial r}\right)\sin\theta \\ &+ \left(\frac{\partial a_{1r}}{\partial z} + \frac{\partial a_{1z}}{\partial r} - 2\frac{\partial^2 b_1}{\partial r \partial z} + \frac{\partial a_{1\varphi}}{\partial z} + \frac{a_{1z}}{r} - \frac{2}{r}\frac{\partial b_1}{\partial z}\right)\cos\theta \Bigg] \sin\theta d\theta, \end{aligned} \tag{A.37}$$

$$\begin{aligned} \overline{f}_2 = \int_{\pi-\alpha}^{\pi} \Bigg[&\left(3\frac{\partial a_{2r}}{\partial r} + \frac{2a_{2r}}{r} - \frac{2a_{2\varphi}}{r} + \frac{\partial a_{2z}}{\partial z} - 2\frac{\partial^2 b_2}{\partial r^2} + \frac{\partial a_{2\varphi}}{\partial r} + \frac{2b_2}{r^2} - \frac{2}{r}\frac{\partial b_2}{\partial r}\right)\sin\theta \\ &+ \left(\frac{\partial a_{2r}}{\partial z} + \frac{\partial a_{2z}}{\partial r} - 2\frac{\partial^2 b_2}{\partial r \partial z} + \frac{\partial a_{2\varphi}}{\partial z} + \frac{a_{2z}}{r} - \frac{2}{r}\frac{\partial b_2}{\partial z}\right)\cos\theta \Bigg] \sin\theta d\theta. \end{aligned} \tag{A.38}$$

Below, we simplify the integrals for the drag force coefficients. From boundary conditions

(3.60) and (3.61), one concludes

$$\begin{aligned}\overline{f}_1 = &\int_0^{\pi-\alpha}\Bigg[\left(3\frac{\partial a_{1r}}{\partial r}+\frac{\partial a_{1z}}{\partial z}-2\frac{\partial^2 b_1}{\partial r^2}+\frac{\partial a_{1\varphi}}{\partial r}+\frac{2b_1}{r^2}\right)\sin\theta\\ &+\left(\frac{\partial a_{1r}}{\partial z}+\frac{\partial a_{1z}}{\partial r}-2\frac{\partial^2 b_1}{\partial r\partial z}+\frac{\partial a_{1\varphi}}{\partial z}+\frac{a_{1z}}{r}-\frac{2}{r}\frac{\partial b_1}{\partial z}\right)\cos\theta\Bigg]\sin\theta d\theta\\ = &\int_0^{\pi-\alpha}\Bigg[\left(3\frac{\partial a_{1r}}{\partial r}+3\frac{\partial a_{1z}}{\partial z}+\frac{\partial a_{1\varphi}}{\partial r}-2\frac{\partial^2 b_1}{\partial z^2}-2\frac{\partial^2 b_1}{\partial r^2}+\frac{2b_1}{r^2}\right)\sin\theta\\ &+\left(\frac{\partial a_{1r}}{\partial z}-\frac{\partial a_{1z}}{\partial r}+\frac{\partial a_{1\varphi}}{\partial z}+\frac{a_{1z}}{r}-\frac{2}{r}\frac{\partial b_1}{\partial z}\right)\cos\theta\Bigg]\sin\theta d\theta\\ = &\int_0^{\pi-\alpha}\Bigg[\left(3\frac{\partial a_{1r}}{\partial r}+3\frac{\partial a_{1z}}{\partial z}+\frac{\partial a_{1\varphi}}{\partial r}-2\frac{\partial^2 b_1}{\partial z^2}-2\frac{\partial^2 b_1}{\partial r^2}+\frac{2b_1}{r^2}\right)\sin\theta\\ &+\left(\frac{\partial a_{1r}}{\partial z}+\frac{\partial a_{1\varphi}}{\partial z}-\frac{\partial a_{1z}}{\partial r}-\frac{a_{1z}}{r}\right)\cos\theta\Bigg]\sin\theta d\theta. \end{aligned}\tag{A.39}$$

Further, one uses equation (3.59) to eliminate b_1 from Eq. (A.39):

$$\begin{aligned}\overline{f}_1 = &\int_0^{\pi-\alpha}\Bigg[\left(\frac{\partial a_{1r}}{\partial r}+\frac{\partial a_{1z}}{\partial z}+\frac{\partial a_{1\varphi}}{\partial r}+\frac{2}{r}\frac{\partial b_1}{\partial r}-\frac{2a_{1r}}{r}+\frac{2a_{1\varphi}}{r}\right)\sin\theta\\ &+\left(\frac{\partial a_{1r}}{\partial z}+\frac{\partial a_{1\varphi}}{\partial z}-\frac{\partial a_{1z}}{\partial r}-\frac{a_{1z}}{r}\right)\cos\theta\Bigg]\sin\theta d\theta. \end{aligned}\tag{A.40}$$

Taking into account boundary conditions (3.60) and (3.61), we obtain

$$\begin{aligned}\overline{f}_1 = &\int_0^{\pi-\alpha}\Bigg[\left(\frac{\partial a_{1r}}{\partial r}+\frac{\partial a_{1\varphi}}{\partial r}+\frac{\partial a_{1z}}{\partial z}\right)\sin\theta\\ &+\left(\frac{\partial a_{1r}}{\partial z}+\frac{\partial a_{1\varphi}}{\partial z}-\frac{\partial a_{1z}}{\partial r}-\frac{a_{1z}}{r}\right)\cos\theta\Bigg]\sin\theta d\theta. \end{aligned}\tag{A.41}$$

Substituting the definitions of the numerical functions (3.75) into the right-hand side of equation (A.41) leads to

$$\overline{f}_1 = 2\int_0^{\pi-\alpha}\left[\left(2\frac{\partial u_{10}}{\partial r}+\frac{\partial u_{11}}{\partial z}\right)\sin\theta+\left(2\frac{\partial u_{10}}{\partial z}-\frac{\partial u_{11}}{\partial r}-\frac{u_{11}}{r}\right)\cos\theta\right]\sin\theta d\theta. \tag{A.42}$$

Next, using the nondimensionalized form of transformation (A.10), i.e.

$$r=\overline{\rho}\sin\theta,\ \varphi=\varphi,\ z=\overline{\rho}\cos\theta+\frac{R}{r_c}\cos\alpha, \tag{A.43}$$

we obtain the following relations:

$$\frac{\partial}{\partial\overline{\rho}}=\sin\theta\frac{\partial}{\partial r}+\cos\theta\frac{\partial}{\partial z} \tag{A.44}$$

$$\frac{\partial}{\partial\theta}=\overline{\rho}\cos\theta\frac{\partial}{\partial r}-\overline{\rho}\sin\theta\frac{\partial}{\partial z}. \tag{A.45}$$

Due to the fact that we parametrized the surface of the particle, using Eq. (A.10), the function under the integral sign is evaluated for $\overline{\rho} = R/r_c$. Therefore, the equation (A.42) is simplified as follows:

$$\begin{aligned}
\overline{f}_1 &= 2\int_0^{\pi-\alpha}\left(2\frac{\partial u_{10}}{\partial\overline{\rho}}\sin\theta - \frac{r_c}{R}\frac{\partial u_{11}}{\partial\theta}\sin\theta - \frac{r_c u_{11}}{R}\cos\theta\right)d\theta \\
&= 2\left(2\int_0^{\pi-\alpha}\frac{\partial u_{10}}{\partial\overline{\rho}}\sin\theta d\theta - \frac{r_c}{R}\int_0^{\pi-\alpha}\sin\theta du_{11} - \int_0^{\pi-\alpha}\frac{r_c u_{11}}{R}\cos\theta d\theta\right) \\
&= 4\int_0^{\pi-\alpha}\frac{\partial u_{10}}{\partial\overline{\rho}}\sin\theta d\theta - \left.\frac{2r_c u_{11}\sin\theta}{R}\right|_{\theta=0}^{\pi-\alpha} \\
&= 4\int_0^{\pi-\alpha}\frac{\partial u_{10}}{\partial\overline{\rho}}\sin\theta d\theta - \frac{2r_c u_{11}(\pi-\alpha)\sin\alpha}{R}.
\end{aligned} \tag{A.46}$$

Analogously, we obtain for the drag force coefficient of the lower part of the particle

$$\overline{f}_2 = 4\int_{\pi-\alpha}^{\pi}\frac{\partial u_{20}}{\partial\overline{\rho}}\sin\theta d\theta + \frac{2r_c u_{21}(\pi-\alpha)\sin\alpha}{R}. \tag{A.47}$$

Then, F_y is computed as

$$\begin{aligned}
F_y = 4\pi R^2 V&\left(\eta_1\int_0^{\pi-\alpha}\frac{\partial u_{10}}{\partial\rho}\sin\theta d\theta + \eta_2\int_{\pi-\alpha}^{\pi}\frac{\partial u_{20}}{\partial\rho}\sin\theta d\theta\right) \\
&+ 2\pi V R\sin\alpha\left[\eta_2 u_{21}(\pi-\alpha) - \eta_1 u_{11}(\pi-\alpha)\right],
\end{aligned} \tag{A.48}$$

see Eqs. (A.22), (A.36), (A.46) and (A.47). Finally, changing variables ρ and θ to the toroidal coordinates σ and τ, defined by (3.92), we conclude that

$$\begin{aligned}
F_y = -4\pi V R\sin\alpha&\left(\eta_1\int_0^{1}\frac{\partial u_{10}}{\partial\sigma}\cdot\frac{1-\tau^2}{\tau h}d\tau + \eta_2\int_0^{1}\frac{\partial u_{20}}{\partial\sigma}\cdot\frac{1-\tau^2}{\tau h}d\tau\right) \\
&+ 2\pi V R\sin\alpha\left[\eta_2 u_{21}(\pi-\alpha) - \eta_1 u_{11}(\pi-\alpha)\right].
\end{aligned} \tag{A.49}$$

List of all references, sorted alphabetically

[1] P. Aussillous and D. Quéré. Quick deposition of a fluid on the wall of a tube. *Phys. Fluids*, 12(10):2367–2371, 2000. DOI: 10.1063/1.1289396.

[2] R. Aveyard, B. Binks, J. Clint, P. Fletcher, T. Horozov, B. Neumann, V. Paunov, J. Annesley, S. Botchway, D. Nees, A. Parker, A. Ward, and A. Burgess. Measurement of long-range repulsive forces between charged particles at an oil-water interface. *Phys. Rev. Lett.*, 88:246102–246106, 2002. DOI: 10.1103/PhysRevLett.88.246102.

[3] R. Azadi and D. Nobes. Local flow dynamics in the motion of slug bubbles in a flowing mini square channels. *Int. J. Heat Mass Transf.*, 178:121588, 2021. DOI: 10.1016/j.ijheatmasstransfer.2021.121588.

[4] G. Balestra, L. Zhu, and F. Gallaire. Viscous Taylor droplets in axisymmetric and planar tubes: From Bretherton's theory to empirical models. *Microfluid Nanofluid*, 22(6):67, 2018. DOI: 10.1007/s10404-018-2084-y.

[5] H.A. Barnes, J.F. Hutton, and K. Walters. *An Introduction to Rheology*. Elsevier, Amsterdam, 1989.

[6] C. Baroud, S. Tsikata, and M. Heil. The propagation of low viscosity fingers into fluid-filled branching network. *J. Fluid Mech.*, 546:285–294, 2006. DOI: 10.1017/S0022112005007287.

[7] G. Barr. XXXI. The air-bubble viscometer. *Lond. Edinb. Dubl. Phil. Mag.*, 1(2):395–405, 1926. DOI: 10.1080/14786442608633640.

[8] K. Baryshnikova, M. Petrov, V. Babicheva, and P. Belov. Plasmonic and silicon spherical nanoparticle anti-reflective coatings. *Scientific Reports*, 6, 08 2015. DOI: 10.1038/srep22136.

[9] G.K. Batchelor. *An Introduction of Fluid Mechanics*. Cambridge Univ. Press, London, 1967.

[10] K. Bendiksen. On the motion of long bubbles in vertical tubes. *Int. J. Multiphas. Flow*, 11(6):797–812, 1985. DOI: 10.1016/0301-9322(85)90025-4.

[11] I. Beresnev, W. Gaul, and R. Dennis Vigil. Thickness of residual wetting film in liquid-liquid displacement. *Phys. Rev. E*, 84(2):026327–026335, 2011. DOI: 10.1103/PhysRevE.84.026327.

[12] A. Borhan and J. Pallinti. Pressure-driven motion of drops and bubbles through cylindrical capillaries: Effect of buoyancy. *Ind. Eng. Chem. Res.*, 37(9):3748–3759, 1998. DOI: 10.1021/ie980087l.

[13] F. Bretherton. The motion of long bubbles in tubes. *J. Fluid Mech.*, 10(2):166–188, 1961. DOI: 10.1017/S0022112061000160.

[14] D. Brown, R. Cortez, and M. Minion. Accurate projection methods for the incompressible navier-–stokes equations. *Journal of Computational Physics*, 168(2):464–499, 2001. DOI: 10.1006/jcph.2001.6715.

[15] J. Bugg, K. Mack, and K. Rezkallah. A numerical model of Taylor bubbles rising through stagnant liquids in vertical tubes. *Int. J. Multiphas. Flow*, 24(2):271–281, 1998. DOI: 10.1016/S0301-9322(97)00047-5.

[16] J. Bugg and G. Saad. The velocity field around a Taylor bubble rising in a stagnant viscous fluid: numerical and experimental results. *Int. J. Multiphas. Flow*, 28(5):791–803, 2002. DOI: 10.1016/S0301-9322(02)00002-2.

[17] O. Cayre and V. Paunov. Fabrication of microlens arrays by gel trapping of self-assembled particle monolayers at the decane-water interface. *Journal of Materials Chemistry*, 14, 2004. DOI: 10.1039/b413361g.

[18] C. Chao, X. Jin, and X. Fan. Evolution of thin-liquid films surrounding bubbles in microfluidics and their impact on the pressure drop and fluid movement. *Langmuir*, 36(49):15102–15111, 2020. DOI: 10.1021/acs.langmuir.0c02679.

[19] H. Chen, Z. Li, and J. Li. Thin-film profile around long bubbles in square microchannels measured by chromatic interference method. *Appl. Phys. Lett.*, 109:041604, 2016. DOI: 10.1063/1.4959791.

[20] J.-D. Chen. Measuring the film thickness surrounding a bubble inside a capillary. *J. Colloid Interf. Sci.*, 109(2):341–349, 1986. DOI: 10.1016/0021-9797(86)90313-9.

[21] H. Cho, A. Nikolov, and D. Wasan. Step-wise velocity of an air bubble rising in a vertical tube filled with a liquid dispersion of nanoparticles. *Langmuir*, 33(11):2920–2928, 2017. DOI: 10.1021/acs.langmuir.6b04489.

[22] H. Cho, A. Nikolov, and D. Wasan. Prediction of the rate of the rise of an air bubble in nanofluids in a vertical tube. *J. Colloid Interf. Sci.*, 525:115–118, 2018. DOI: 10.1016/j.jcis.2018.04.062.

[23] H. Cho, A. Nikolov, and D. Wasan. Estimation of structural film viscosity based on the bubble rise method in a nanofluid. *J. Colloid Interf. Sci.*, 516:312–316, 2018. DOI: 10.1016/j.jcis.2018.01.066.

[24] C. Clanet, P. Heraud, and G. Searby. On the motion of bubbles in vertical tubes of arbitrary cross-sections: some complements to the Dumitrescu–Taylor problem. *J. Fluid Mech.*, 519:359–376, 2004. DOI: 10.1017/S0022112004001296.

[25] Y. Cui and N. Gupta. Numerical study of surfactant effects on the buoyancy-driven motion of a drop in a tube. *Chem. Eng. Sci.*, 144:48–57, 2016. DOI: 10.1016/j.ces.2016.01.020.

[26] A. Dani, G. Keiser, M. Yeganeh, and C. Maldarelli. Hydrodynamics of particles at an oil–water interface. *Langmuir*, 31:13290–13302, 2015. DOI:10.1021/acs.langmuir.5b02146.

[27] K. Danov, R. Dimova, and B. Pouligny. Viscous drag of a solid sphere straddling a spherical or flat surface. *Phys. Fluids*, 12:2711–2722, 2000. DOI: 10.1063/1.1289692.

[28] K. Danov and P. Kralchevsky. Electric forces induced by a charged colloid particle attached to the water–nonpolar fluid interface. *J. Colloid Interface Sci.*, 298(1):213–231, 2006. DOI: 10.1016/j.jcis.2005.12.037.

[29] K. Danov and P. Kralchevsky. Forces acting on dielectric colloidal spheres at a water/nonpolar fluid interface in an external electric field. 2. charged particles. *Journal of colloid and interface science*, 405:269–277, 2013. DOI: 10.1016/j.jcis.2013.05.015.

[30] K. Danov, P. Kralchevsky, and M. Boneva. Electrodipping force acting on solid particles at a fluid interface. *Langmuir*, 20(15):6139–6151, 2004. DOI: 10.1021/la0497090.

[31] P. Dapira and G. Paşa. The effect of surfactant on the motion of long bubbles in horizontal capillary tubes. *J. Stat. Mech.*, 2010(2):L02002, 2010. DOI: 10.1088/1742-5468/2010/02/l02002.

[32] R. Davies and G. Taylor. The mechanics of large bubbles rising through extended liquids and through liquids in tubes. *Proc. R. Soc. Lond. A*, 200:375–390, 1950. DOI: 10.1098/rspa.1950.0023.

[33] N. Denkov, V. Subramanian, D. Gurovich, and A. Lips. Wall slip and viscous dissipation in sheared foams: effect of surface mobility. *Colloids Surf. A*, 263(1):129–145, 2005. DOI: 10.1016/j.colsurfa.2005.02.038.

[34] W. Dhaouadi and J. Kolinski. Bretherton's buoyant bubble. *Phys. Rev. Fluids*, 4(12):123601–123611, 2019. DOI: 10.1103/PhysRevFluids.4.123601.

[35] E. Dickinson. Food emulsions and foams: Stabilization by particles. *Current Opinion in Colloid & Interface Science*, 15(1):40–49, 2010. DOI: j.cocis.2009.11.001.

[36] S. Dimova, T. Chernogorova, and A. Jotova. *Numerical methods for partial differential equations (in Bulgarian)*. University of Sofia "St. Kliment Ohridski", 2010.

[37] A. Dorr, S. Hardt, H. Masoud, and H. Stone. Drag and diffusion coefficients of a spherical particle attached to a fluid-fluid interface. *J. Fluid Mech.*, 790:607–618, 2016. DOI: 10.1017/jfm.2016.41.

[38] D. T. Dumitrescu. Strömung an einer Luftblase im senkrechten Rohr. *Z. Angew. Math. Mech.*, 23(3):139–149, 1943. DOI: 10.1002/zamm.19430230303.

[39] Y. D'Yakonov. Difference schemes with a "disintegrating" operator for multidimensional problems. *USSR Computational Mathematics and Mathematical Physics*, 2(4):581–607, 1963. DOI: 10.1016/0041-5553(63)90531-7.

[40] M. Dzikowski, L. Laniewski-Wollk, and J. Rokicki. Single component multiphase lattice Boltzmann method for Taylor/Bretherton bubble train flow simulations. *Commun. Comput. Phys.*, 19(4):1042–1066, 2016. DOI: 10.4208/cicp.220115.110915a.

[41] W. E and J.-G. Liu. Gauge method for viscous incompressible flows. *Comm. Math. Sci.*, 1(2):317–332, 2003. DOI: 10.4310/CMS.2003.v1.n2.a6.

[42] D.A. Edwards, H. Brenner, and D.T. Wasan. *Interfacial Transport Processes and Rheology*. Butterworth-Heinemann, Boston, 1991.

[43] S. Ezrahi, E. Tuval, A. Aserin, and N. Garti. Daily applications of systems with wormlike micelles. In R. Zana and E.W. Kaler, editors, *Giant Micelles. Properties and Applications*, pages 515–544. Taylor and Francis, New York, 2007. DOI: 10.1201/9781420007121-18.

[44] F. Fairbrother and A. Stubbs. 119. Studies in electro-endosmosis. Part VI. The bubble-tube method of measurement. *J. Chem. Soc.*, (0):527–529, 1935. DOI: 10.1039/JR9350000527.

[45] T. Feagin. A tenth-order Runge-Kutta method with error estimate. In A. Avidan, editor, *Proceedings of the IAENG Conf. on Scientific Computing*, volume 1, page 1, Hong Kong, 2007. URL: `https://sce.uhcl.edu/feagin/courses/rk10.pdf`.

[46] J. Feng. Steady axisymmetric motion of a small bubble in a tube with flowing liquid. *Proc. R. Soc. A*, 466:549–562, 2010. DOI: 10.1098/rspa.2009.0288.

[47] R. Finn. *Equilibrium Capillary Surface*. Springer-Verlag, New York, 1986.

[48] D. Gaver, D. Halpern, O. Jensen, and J. Grotberg. The steady motion of a semi-infinite bubble through a flexible-walled channel. *J. Fluid Mech.*, 319:25–65, 1996. DOI: 10.1017/S0022112096007240.

[49] C. Gerald and P. Wheatley. *Applied numerical analysis*. Pearson College Div, 7 edition, 2004.

[50] S. Ghadiali and D. Gaver. The influence of non-equilibrium surfactant dynamics on the flow of a semi-infinite bubble in a rigid cylindrical capillary tube. *J. Fluid Mech.*, 478:165–196, 2003. DOI: 10.1017/S002211200200335X.

[51] M. Giavedoni and F. Saita. The axisymmetric and plane cases of a gas phase steadily displacing a Newtonian liquid—a simultaneous solution of the governing equations. *Phys. Fluids*, 9(8):2420–2428, 1997. DOI: 10.1063/1.869360.

[52] A. Gibson. LXXXIV. On the motion of long air-bubbles in a vertical tube. *Lond. Edinb. Dubl. Phil. Mag.*, 26(156):952–965, 1913. DOI: 10.1080/14786441308635043.

[53] G. Ginley and C. Radke. Influence of soluble surfactants on the flow of long bubbles through a cylindrical capillary. In J. Borchardt and T. Yen, editors, *Oil-field chemistry. Enhanced recovery and production stimulation*, chapter 26, pages 480–501. 1989. DOI: 10.1021/bk-1989-0396.ch026.

[54] H. Goldsmith and S. Mason. The movement of single large bubbles in closed vertical tubes. *J. Fluid Mech.*, 14(1):42–58, 1962. DOI: 10.1017/S0022112062001068.

[55] P. Grassia. Motion of an oil droplet through a capillary with charged surfaces. *J. Fluid Mech.*, 866:721–758, 2019. DOI: 10.1017/jfm.2019.126.

[56] D. Halpern and T. Secomb. The squeezing of red blood cells through capillaries with near-minimal diameters. *J. Fluid Mech.*, 203:381–400, 1989. DOI: 10.1017/S0022112089001503.

[57] N. Hammoud, P. Trinh, P. Howell, and H. Stone. Influence of van der Waals forces on a bubble moving in a tube. *Phys. Rev. Fluids*, 2(6):063601, 2017. DOI: 10.1103/PhysRevFluids.2.063601.

[58] Y. Han and N. Shikazono. Measurement of the liquid film thickness in micro tube slug flow. *Int. J. Heat Fluid Flow*, 30(5):842–853, 2009. DOI: j.ijheatfluidflow.2009.02.019.

[59] J. Happel and H. Brenner. *Low Reynolds Number Hydrodynamics with Special Applications to Particulate Media*. Prentice-Hall, Englewood Cliffs, New York, 1965.

[60] T. Harmathy. Velocity of large drops and bubbles in media of infinite or restricted extent. *AIChE J.*, 6(2):281–288, 1960. DOI: 10.1002/aic.690060222.

[61] A. Hazel and M. Heil. The steady propagation of a semi-infinite bubble into a tube of elliptical or rectangular cross-section. *J. Fluid Mech.*, 470:91–114, 2002. DOI: 10.1017/S0022112002001830.

[62] M. Heil. Finite Reynolds number effects in the Bretherton problem. *Phys. Fluids*, 13(9):2517–2521, 2001. DOI: 10.1063/1.1389861.

[63] M. Heil. The Bretherton problem in elastic-walled channels: finite Reynolds number effects. In A. King and Y. Shikhmurzaev, editors, *IUTAM symposium on free surface flows. Fluid mechanics and its application*, volume 62, pages 113–120, Dordrecht, 2001. Springer. DOI: 10.1007/978-94-010-0796-2_14.

[64] G. Hirasaki and J. Lawson. Mechanisms of foam flow in porous media: apparent viscosity in smooth capillaries. *Soc. Pet. Eng. J.*, 25(02):176–190, 1985. DOI: 10.2118/12129-PA.

[65] S. Hodges, O. Jensen, and J. Rallison. The motion of a viscous drop through a cylindrical tube. *J. Fluid Mech.*, 501:279–301, 2004. DOI: 10.1017/S0022112003007213.

[66] M. Hoorfar and A. Neumann. Recent progress in axisymmetric drop shape analysis (ADSA). *Adv. Colloid Interfac. Sci.*, 121(1):25–49, 2006. DOI: 10.1016/j.cis.2006.06.001.

[67] T. Horozov, R. Aveyard, B. Binks, and J. Clint. Structure and stability of silica particle monolayers at horizontal and vertical octane-water interfaces. *Langmuir*, 21(16):7405–7412, 2005. DOI: 10.1021/la050923d.

[68] T. Horozov, R. Aveyard, J. Clint, and B. Binks. Order-disorder transition in monolayers of modified monodisperse silica particles at the octane-water interface. *Langmuir*, 19(7):2822–2829, 2003. DOI: 10.1021/la020858x.

[69] M. Hsu, M. Nikolaides, A. Dinsmore, A. Bausch, V. Gordon, X. Chen, J. Hutchinson, D. Weitz, and M. Marquez. Self-assembled shells composed of colloidal particles: fabrication and characterization. *Langmuir*, 21(7):2963–2970, 2005. DOI: 10.1021/la0472394j.

[70] T. Hu, X. Mei, Y. Wang, X. Weng, R. Liang, and M. Wei. Two-dimensional nanomaterials: fascinating materials in biomedical field. *Science Bulletin*, 64(22):1707–1727, 2019. DOI: 10.1016/j.scib.2019.09.021.

[71] H. Jiang, Y. Sheng, and T. Ngai. Pickering emulsions: Versatility of colloidal particles and recent applications. *Current Opinion in Colloid & Interface Science*, 49:1–15, 2020. DOI: 10.1016/j.cocis.2020.04.017.

[72] R. Johnson and A. Borhan. Pressure-driven motion of surfactant-laden drops through cylindrical capillaries: effect of surfactant solubility. *J. Colloid Interf. Sci.*, 261(2):529–541, 2003. DOI: 10.1016/S0021-9797(03)00031-6.

[73] E. Klaseboer, R. Gupta, and R. Manica. An extended Bretherton model for long Taylor bubbles at moderate capillary numbers. *Phys. Fluids*, 26:032107, 2014. DOI: 10.1063/1.4868257.

[74] W. Kolb and R. Cerro. The motion of long bubbles in tubes of square cross section. *Phys. Fluids A - Fluid*, 5(7):1549–1567, 1993. DOI: 10.1063/1.858832.

[75] P. Kralchevsky and K. Nagayama. *Particles at Fluid Interfaces and Membranes: Attachment of Colloid Particles and Proteins to Interfaces and Formation of Two-Dimensional Areas*. Elsevier Science, 2001.

[76] M. Kreutzer, F. Kapteijn, J. Moulijn, C. Kleijn, and J. Heiszwolf. Inertial and interfacial effects on pressure drop of taylor flow in capillaries. *AIChE J.*, 51(9):2428–2440, 2005. DOI: 10.1002/aic.10495.

[77] D. Kwak and C. Kiris. Methods for solving viscous incompressible flow problems. 01 2011. DOI: 10.1007/978-94-007-0193-9_2.

[78] C. Lamstaes and J. Eggers. Arrested bubble rise in a narrow tube. *J. Stat. Phys.*, 167(3):656–682, 2017. DOI: 10.1007/s10955-016-1559-z.

[79] L.D. Landau and E.M. Lifshitz. *Fluid Mechanics*. Pergamon Press, Oxford, 1984.

[80] L.D. Landau, E.M. Lifshitz, and L.P. Pitaevskii. *Electrodynamics of Continuous Media*. Elsevier Butterworth-Heinemann, Oxford, 2004.

[81] D. Langewisch. *Application of the polynomial chaos expansion to multiphase CFD: a study of rising bubbles and slug flow*. PhD thesis, Massachusetts Institute of Technology, 2004.

[82] D. Langewisch and J. Buongiorno. Prediction of film thickness, bubble velocity, and pressure drop for capillary slug flow using a CFD-generated database. *Int. J. Heat Fluid Flow*, 54:250–257, 2015. DOI: 10.1016/j.ijheatfluidflow.2015.06.005.

[83] H. Langtangen, K. Mardal, and R. Winther. Numerical methods for incompressible viscous flow. *Advances in Water Resources*, 25(8):1125–1146, 2002. DOI: 10.1016/S0309-1708(02)00052-0.

[84] V. Levich. *Physicochemical Hydrodynamics*. Prentice-Hall, Englewood Cliffs, New York, 1962.

[85] Y.-C. Li, Y.-C. Liao, T.-C. Wen, and H.-H. Wei. Breakdown of the Bretherton law due to wall slippage. *J. Fluid Mech.*, 741:200–227, 2014. DOI: 10.1017/jfm.2013.562.

[86] Z. Li, L. Wang, J. Li, and H. Chen. Drainage and lubrication film around stuck bubbles in vertical capillaries. *Appl. Phys. Lett.*, 115:111601, 2019. DOI: 10.1063/1.5112055.

[87] V. Lotito and T. Zambelli. Approaches to self-assembly of colloidal monolayers: A guide to nanotechnologists. *Adv. Colloid Interfac. Sci.*, 246:217–274, 2017. DOI: 10.1016/j.cis.2017.04.003.

[88] G. Lyutskanova, K. Mihaylov, and V. Kolev. Axisymmetric drop shape analysis. In *Proceedings of Preparatory Modelling Week*, Sofia, Bulgaria, 2015. URL: `http://pmw2015.fmi.uni-sofia.bg/Documents/Problem_2_Report.pdf`.

[89] C. Madec, B. Collin, J. Jerome, and S. Joubaud. Puzzling bubble rise speed increase in dense granular suspensions. *Phys. Rev. Lett.*, 125(6):078004, 2020. DOI: 10.1103/PhysRevLett.125.078004.

[90] M. Magnini, S. Khodaparast, O. Matar, H. Stone, and J. Thome. Dynamics of long gas bubbles rising in a vertical tube in a cocurrent liquid flow. *Phys. Rev. Fluids*, 4(2):023601, 2019. DOI: 10.1103/PhysRevFluids.4.023601.

[91] M. Magnini and O. Matar. Morphology of long gas bubbles propagation in square capillaries. *Int. J. Multiphas. Flow*, 129:103353, 2020. DOI: 10.1016/j.ijmultiphaseflow.2020.103353.

[92] T. Majeed, M. Kamal, X. Zhou, and T. Solling. A review of foam stabilizers for enhanced oil recovery. *Energy Fuels*, 35(7):5594–5612, 2021. DOI: 10.1021/acs.energyfuels.1c00035.

[93] R. Manica, E. Klaseboer, and D. Chan. The hydrodynamics of bubble rise and impact with solid surfaces. *Adv. Colloid Interfac.*, 235:214–232, 2016. DOI: 10.1016/j.cis.2016.06.010.

[94] Z.-S. Mao and A. Dukler. The motion of Taylor bubbles in vertical tubes. I. A numerical simulation for the shape and rise velocity of Taylor bubbles in stagnant and flowing liquid. *J. Comput. Phys.*, 91(1):132–160, 1990. DOI: 10.1016/0021-9991(90)90008-O.

[95] Z.-S. Mao and A. Dukler. The motion of Taylor bubbles in vertical tubes – II. Experimental data and simulations for laminar and turbulent flow. *Chem. Eng. Sci.*, 46(8):2055–2064, 1991. DOI: 10.1016/0009-2509(91)80164-T.

[96] M. Matin and S. Moghaddam. Thin liquid film formation and evaporation mechanisms around elongated bubbles in rectangular cross-section microchannels. *Int. J. Heat Fluid Flow*, 163:120474, 2020. DOI: 10.1016/j.ijheatmasstransfer.2020.120474.

[97] A. Morgado, J. Miranda, J. Araújo, and J. Campos. Review on vertical gas-liquid slug flow. *Int. J. Multiphas. Flow*, 85:348–368, 2016. DOI: 10.1016/j.ijmultiphaseflow.2016.07.002.

[98] L. Nicolas-Morgantini. Giant micelles and shampoos. In R. Zana and E.W. Kaler, editors, *Giant Micelles. Properties and Applications*, pages 493–514. Taylor and Francis, New York, 2007. DOI: 10.1201/9781420007121.

[99] U. Olgac and M. Muradoglu. Effects of surfactant on liquid film thickness in the Bretherton problem. *Int. J. Multiphas. Flow*, 48:58—-70, 2013. DOI: 10.1016/j.ijmultiphaseflow.2012.08.007.

[100] C.-W. Park. Influence of soluble surfactants on the motion of a finite bubble in a capillary tube. *Phys. Fluids A*, 4(11):2335–2347, 1992. DOI: 10.1063/1.858475.

[101] D. Peaceman and J. Rachford. The numerical solution of parabolic and elliptic differential equations. *Journal of the Society for Industrial and Applied Mathematics*, 3(1):28–41, 1955. DOI: 10.1137/0103003.

[102] P. Petkov, K. Danov, and P. Kralchevsky. Monolayers of charged particles in a langmuir trough: Could particle aggregation increase the surface pressure? *Journal of Colloid and Interface Science*, 462:223–234, 2015. DOI: 10.1016/j.jcis.2015.09.075.

[103] D. Picchi, A. Ullmann, N. Brauner, and P. Poesio. Motion of a confined bubble in a shear-thinning liquid. *J. Fluid Mech.*, 918:A7, 2021. DOI: 10.1017/jfm.2021.321.

[104] K. Rahul and S. Bhattacharyya. One-sided finite-difference approximations suitable for use with richardson extrapolation. *Journal of Computational Physics*, 219(1):13–20, 2006. DOI: 10.1016/j.jcp.2006.05.035.

[105] J. Ratulowski and H.-C. Chang. Transport of gas bubbles in capillaries. *Phys. Fluids A - Fluid*, 1(10):1642–1655, 1989. DOI: 10.1063/1.857530.

[106] J. Ratulowski and H.-C. Chang. Marangoni effects of trace impurities on the motion of long gas bubbles in capillaries. *J. Fluid Mech.*, 210:303–328, 1990. DOI: 10.1017/S0022112090001306.

[107] D. Reinelt and P. Saffman. The penetration of a finger into a viscous fluid in a channel and tube. *SIAM J. Sci. Stat. Comput.*, 6(3):542–561, 1985. DOI: 10.1137/0906038.

[108] T. Savin, M. Bandi, and L. Mahadevan. Pressure-driven occlusive flow of a confined red blood cell. *Soft Matter*, 12(2):562–573, 2016. DOI: 10.1039/C5SM01282A.

[109] L. Schwartz, H. Princen, and A. Kiss. On the motion of bubbles in capillary tubes. *J. Fluid Mech.*, 172:259–275, 1986. DOI: 10.1017/S0022112086001738.

[110] M. Severino, A. Giavedoni, and F. Saita. A gas phase displacing a liquid with soluble surfactants out of a small conduit: the plane case. *Phys. Fluids*, 15(10):2961–2972, 2003. DOI: 10.1063/1.1605424.

[111] N. Shanmugam, R. Pugazhendhi, R. Elavarasan, K. Pitchandi, and N. Das. Anti-reflective coating materials: A holistic review from pv perspective. *Energies*, 13:2631, 05 2020. DOI: 10.3390/en13102631.

[112] J.C. Slattery. *Momentum, Energy, and Mass Transfer in Continua.* Krieger, Huntington, New York, 1978.

[113] J.C. Slattery. *Interfacial Transport Phenomena*. Springer-Verlag, New York, 1990. DOI: 10.1007/978-0-387-38442-9.

[114] H. Son, H. Kim, G. Lee, J. Kim, and W. Sung. Enhanced oil recovery using nanoparticle-stabilized oil/water emulsions. *Korean J. Chem. Eng.*, 31:338–342, 2014. DOI: 10.1007/s11814-013-0214-5.

[115] J. Stark and M. Manga. The motion of long bubbles in a network of tubes. *Transport in Porous Media*, 40:201–218, 2000. DOI: 10.1023/A:1006697532629.

[116] K. Stebe and D. Barthès-Biesel. Marangoni effects of adsorption-desorption controlled surfactants on the leading end of an infinitely long bubble in a capillary. *J. Fluid Mech.*, 286:25–48, 1995. DOI: 10.1017/S0022112095000632.

[117] G. Stokes. On the effect of the internal friction of fluids on the motion of pendulums. *Trans. Camb. Phil. Soc.*, 9:8–106, 1851. DOI: 10.1017/CBO9780511702266.002.

[118] A. Studart, U. Gonzenbach, I. Akartuna, E. Tervoort, and L. Gauckler. Materials from foams and emulsions stabilized by colloidal particles. *Journal of materials chemistry*, 31:3283–3289, 2007. DOI: 10.1039/B703255B.

[119] P.F. Sullivan, M.K.R. Panda, and V. Laffite. Applications of wormlike micelles in oilfield industry. In C.A. Dreiss and Y. Feng, editors, *Wormlike Micelles. Advances in Systems, Characterization and Applications*, pages 330–352. RSC, 2017. DOI: 10.1039/9781782629788-00330.

[120] Q. Sun, J. Chen, and A. Routh. Coated colloidosomes as novel drug delivery carriers. *Expert Opinion on Drug Delivery*, 16(9):903–906, 2019. DOI: 10.1080/17425247.2019.1652594.

[121] T. Swaminathan, K. Mukundakrishnan, P. Ayyaswamy, and D. Eckmann. Effect of a soluble surfactant on a finite-sized bubble motion in a blood vessel. *J. Fluid Mech.*, 642:509–539, 2010. DOI: 10.1017/S0022112009992692.

[122] G. Taylor. Deposition of a viscous fluid on the wall of a tube. *J. Fluid Mech.*, 10(2):161–165, 1961. DOI: 10.1017/S0022112061000159.

[123] J. Thomas. *Numerical Partial Differential Equations: Finite Difference Methods*. Springer New York, 1995. DOI: 10.1007/978-1-4899-7278-1.

[124] K. Thompson, M. Williams, and S. Armes. Colloidosomes: Synthesis, properties and applications. *Journal of Colloid and Interface Science*, 447:217–228, 2014. DOI: 10.1016/j.jcis.2014.11.058.

[125] T. Tran, M. Ahmad, P. Neogi, and B. Bai. A single pore model for displacement of heavy crude oil with carbon dioxide. *SPE J.*, 21(03):0864—-0872, 2016. DOI: 10.2118/178425-PA.

[126] R. van Hout, A. Gulitski, D. Barnea, and L. Shemer. Experimental investigation of the velocity field induced by a Taylor bubble rising in stagnant water. *Int. J. Multiphas. Flow*, 28(4):579–596, 2002. DOI: 10.1016/S0301-9322(01)00082-9.

[127] D. Venkataramani, A. Tsulaia, and S. Amin. Fundamentals and applications of particle stabilized emulsions in cosmetic formulations. *Advances in Colloid and Interface Science*, 283:102234, 2020. DOI: 10.1016/j.cis.2020.102234.

[128] B. Wang, B. Ke, B. Chen, R. Li, and R. Tian. A technical review of research progress on thin liquid film thickness. *Exp. Comput. Multiph. Flow*, 2:199–211, 2020. DOI: 10.1007/s42757-019-0051-9.

[129] Y.-M. Wang and T. Wang. A compact adi method and its extrapolation for time fractional sub-diffusion equations with nonhomogeneous neumann boundary conditions. *Computers and Mathematics with Applications*, 75(3):721–739, 2018. DOI: 10.1016/j.camwa.2017.10.002.

[130] F. Wassmuth, W. Laidlaw, and D. Coombe. Calculation of interfacial flows and surfactant redistribution as a gas/liquid interface moves between two parallel plates. *Phys. Fluids A*, 5(7):1533–1548, 1993. DOI: 10.1063/1.858831.

[131] H. Westborg and O. Hassager. Creeping motion of long bubbles and drops in capillary tubes. *J. Colloid Interf. Sci.*, 133(1):135–147, 1989. DOI: 10.1016/0021-9797(89)90287-7.

[132] E. White and R. Beardmore. The velocity of rise of single cylindrical air bubbles through liquids contained in vertical tubes. *Chem. Eng. Sci.*, 17:351–361, 1962. DOI: 10.1016/0009-2509(62)80036-0.

[133] H. Wong, C. Radke, and S. Morris. The motion of long bubbles in polygonal capillaries. Part 1. Thin films. *J. Fluid Mech.*, 292:71–94, 1995. DOI: 10.1017/S0022112095001443.

[134] H. Wong, C. Radke, and S. Morris. The motion of long bubbles in polygonal capillaries. Part 2. Drag, fluid pressure and fluid flow. *J. Fluid Mech.*, 292:95–110, 1995. DOI: 10.1017/S0022112095001455.

[135] C.-E. Wu, H.-W. Du, J. Qin, E.-Q. Li, and P. Gao. Experiment on bubble formation through dynamic wetting transition in a square capillary. *AIP Advances*, 11:075107, 2021. DOI: 10.1063/5.0057296.

[136] J. Wu and G.-H. Ma. Recent studies of pickering emulsions: Particles make the difference. *Small*, 12(34):4633–4648, 2016. DOI: 10.1002/smll.201600877.

[137] X. Xing, M. Chen, Y. Gong, Z. Lv, S. Han, and Y. Zhou. Building memory devices from biocomposite electronic material. *Sci Technol Adv Mater.*, 21(1):100–121, 2020. DOI: 10.1080/14686996.2020.1725395.

[138] N. Yanenko. *The Method of Fractional Steps, the Solution of Problems of Mathematical Physics in Several Variables*. Springer Berlin, Heidelberg, 1971. DOI: 10.1007/978-3-642-65108-3.

[139] Y. Yu, M. Magnini, L. Zhu, S. Shim, and H. Stone. Non-unique bubble dynamics in a vertical capillary with an external flow. *J. Fluid Mech.*, 911:A34, 2021. DOI: 10.1017/jfm.2020.1027.

[140] M. Zabarankin. Asymmetric three-dimensional stokes flows about two fused equal spheres. *Proc. R. Soc. A*, 463(2085):2329–2349, 2007. DOI: 10.1098/rspa.2007.1872.

[141] J. Zakin, A. Maxson, T. Saeki, and P. Sullivan. Turbulent drag-reduction applications of surfactant solutions. In C.A. Dreiss and Y. Feng, editors, *Wormlike Micelles. Advances in Systems, Characterization and Applications*, pages 353–378. RSC, 2017. DOI: 10.1039/9781782629788-00353.

[142] E. Zukoski. Influence of the viscosity, surface tension, and inclination angle on motion of long bubbles in closed tubes. *J. Fluid Mech.*, 25(4):821–837, 1966. DOI: 10.1017/S0022112066000442.